Assessment of chloride corrosion in steel fibre reinforced cementitious composites

DOCTORAL THESIS

Doctoral thesis by:

Mylene de Melo Vieira

Thesis directors:

Antonio Aguado De Cea

Sergio Henrique Pialarissi Cavalaro

Doctoral programme:

Construction Engineering

Barcelona, October 2018

UNIVERSITAT POLITÈCNICA DE CATALUNYA
BARCELONATECH
Departamento de Ingeniería Civil y Ambiental

To my beloved parents, Arcanjo and Mirleide, who gave me my two most precious gifts: my life and my faith.

AKNOWLEDGEMENTS

"Indeed a good angel will go with him and he will have a successful journey!" (Tb. 5, 22). With this word and promise of God I started this journey! Praise and gratitude to my God who always sends His angels to accompany His friends along the way! I also recognize so many other "angels" who supported me during this PhD journey and I would like to express my gratitude!

I would like to thank my supervisors Professor Antonio Aguado De Cea and Professor Sergio Henrique Pialarissi Cavalaro for all support and trust in my potential during all this project. Professor Antonio thank you for guiding me with your strong academic experience. Professor Sergio, the words are very poor to express how grateful I am for so many talks over this doctoral journey, for always being available to help me with the work and specially for considering me not only a student but a person.

I would like to express my deepest gratitude to so many friends that I met during this time in the PhD: Razmik, Liau, Amin, Amir, Tai, Rubén, Carlos, Tina, Fran, Francesco, Jorge, Cesar, Lidiane and Debora. In special, Andressa, Eduardo, Jannil, Renan, Talita, Luis Montoya, Helen and Ricardo. How good is to be together with friends!

I am really grateful to all laboratory technicians: Tomás Garcia, Camilo Bernard, Jordi Cabrerizo, Robert Micheal, Carlos Hurtado, Jordi Lafuente and Patrícia Muñoz. It would be impossible to perform such a long experimental programme without your support. I also would like to thanks the ESCOFET company, specially to Gerard for the production of the specimens for the experimental programme.

Thanks are extended to Doctors Ignacio Segura, Renan Pícolo, Celia Varga and Diego Aponte for supporting me with the SEM and EDS experiments and analysis.

I also thank two undergraduate students: Xinzhi Tang and James Sweetnam, for your important contribution in this work.

I would like to thanks my dear friend Bruno for helping me with the draws of the thesis and as I usually sing to you: "you are simply the best!".

Also, I would like to thanks all my flatmates during this stay in Barcelona, specially Daniela who more than a flatmate became a friend. From so many nationalities and cultures it was an amazing experience to share this time with you.

I would like to thank CAPES (CAPES Foundation, Ministry of Education of Brazil, process 13177/13-00) for the scholarship granted.

I am very grateful to my brothers and sisters from Shalom Catholic Community in London for your presence and prayers. We are a family!

Finally, I want to express my gratitude to my beloved family for your love, care and prayers. You all are my greatest treasure! My parents, Arcanjo e Mirleide, my sisters Arleide, Adriana and Mychelle, my brother Daniel, all my dear nieces, nephews, my sister in law Marina and my brothers in law.

Through the intersection of the Virgin Mary and Saint Joseph, God bless you all!

SUMMARY

High performance steel fibre reinforced cementitious composites (HPSFRCCs) show enhanced structural performance and durability. The improved properties favour its use in aggressive conditions (such as marine environment) prone to corrosion. Despite the remarkable advances in the knowledge about corrosion of conventional reinforced concrete structures, questions still remain about its effects on the durability of HPSFRCC. The governing mechanisms of corrosion, the presence of cracks, the high steel fibre content, and the long-term chloride exposure still need to be properly evaluated.

Given the increased application of HPSFRCC with structural responsibility and the high steel fibre content commonly used in the mixes, it is of great importance to understand the main mechanisms governing the chloride corrosion and its effects on the durability of the real-scale structures constructed with the material. To overcome these barriers and the uncertainty mentioned, this doctoral thesis addresses the following key issues: the effect of chlorides in uncracked HPSFRCCs under constant conditions; the influence of chloride corrosion in uncracked HPSFRCCs under wet-dry cycles with chlorides; the effect of corrosion in pre-cracked HPSFRCCs subjected to the same cycles and the proposal of a simplified model to consider the structural effects of corrosion.

The first subject concerns the assessment of chloride corrosion on the aesthetic aspect and on the mechanical behaviour of HPSFRCCs by means of an accelerated test. For that, HPSFRCCs specimens with and without chlorides added to the mixes and with different fibre contents were tested. The preliminary experimental programme shows that, in general, the chlorides produce a level of surface corrosion with aesthetic consequences but have small influence on the mechanical performance. In the second subject, the influence of cycles was assessed in accelerated tests with uncracked HPSFRCCs prisms. The results reveal that, for uncracked HPSFRCCs elements, the corrosion affects the surface aspect but has no influence on the post-cracking response.

The third subject focuses on the analysis of pre-cracked HPSFRCCs prisms under cyclic chloride exposure, considering different pre-crack widths and fibre contents. The study shows that the corrosion affects significantly the mechanical behaviour of the fibres for all specimens. The last subject covers a proposal of a simplified model to consider the effect of corrosion in the ULS design of HPSFRCC elements under cyclic chloride exposure. The model proposed was capable of reproducing the influence of the corrosion process over the cycles, being compatible with the current philosophy proposed in codes for the design of HPSFRCC structures.

RESUMEN

Los compuestos cementicios de alta resistencia reforzados con fibra de acero (CCARRFA) muestran un mayor rendimiento estructural y durabilidad. Las mejoras en las propiedades del CCARRFA debido a la inclusión de fibras de acero favorecen su uso en condiciones agresivas (tales como el ambiente marino) propensas a la corrosión. A pesar de los notables avances en el estudio de la corrosión de estructuras de hormigón armado, aún quedan cuestiones sin resolver respecto a sus efectos en la durabilidad del CCARRFA. En relación a ello, los mecanismos que gobiernan la corrosión, la presencia de fisuras, el alto contenido de fibra de acero y la exposición prolongada a los cloruros deben ser evaluados adecuadamente.

Dado el aumento de la utilización de CCARRFA con responsabilidad estructural y el alto contenido de fibra de acero comúnmente utilizado en las mezclas, resulta de gran importancia comprender los principales mecanismos que gobiernan la corrosión, así como sus efectos en la durabilidad de estructuras a escala real construidas con este material. Para superar estas barreras y las incertidumbres mencionadas, esta tesis doctoral tratará los siguientes aspectos clave: el efecto de los cloruros en CCARRFA no fisurado en condiciones constantes; la influencia de la corrosión por cloruros en CCARRFA no fisurado sometido a ciclos de mojado y secado con cloruros; el efecto de la corrosión en CCARRFA fisurados sometidos a los mismos ciclos y una propuesta de modelo simplificado para considerar los efectos estructurales de la corrosión.

El primer aspecto aborda la evaluación de la corrosión por cloruros desde un punto de vista estético y del comportamiento mecánico del CCARRFA mediante un ensayo acelerado. Para ellos, se han ensayado probetas de CCARRFA con y sin cloruros añadidos a las mezclas con diferentes contenidos de fibra. La campaña experimental preliminar mostró que, en general, los cloruros producen un nivel de corrosión superficial con consecuencias estéticas, pero con poca influencia en el comportamiento mecánico. En el segundo aspecto, se evaluó la influencia de los ciclos en ensayos acelerados en probetas de CCARRFA no fisuradas. Los resultados revelaron que en los elementos de CCARRFA no fisurados la corrosión afecta al aspecto superficial pero no influye en la respuesta post-fisuración.

El tercer aspecto trata el análisis de probetas de CCARRFA fisuradas con diferentes anchos de fisura y contenidos de fibra sometidas a una exposición cíclica de cloruros. El estudio muestra que la corrosión afecta significativamente al comportamiento mecánico de las fibras de todas las probetas. El último aspecto se centra en la propuesta de uno modelo simplificado que considera el efecto de la corrosión en el diseño en ELU de elementos de CCARRFA bajo una exposición cíclica de cloruros. El modelo propuesto es capaz de reproducir el efecto del proceso de la corrosión a lo largo de los ciclos, siendo compatible con la actual filosofía propuesta en códigos para el diseño de estructuras de CCARRFA.

TABLE OF CONTENTS

LIST OF FIGURES

LIST OF TABLES

1. INTRODUCTION

1.1. BACKGROUND AND CONTEXT

Fibre reinforced concrete (FRC) saw its first patent in 1874, but for all practical purposes, progress in FRC was almost at a standstill for more than 100 years, and picked up at an exceptional pace only during 1960s (Naaman 2007). This structural material also known as fibre reinforced cementitious composite (FRCC) is generally defined as composite made of fibre and cementitious matrix. According to Naaman (2007), the increased interest may be partly due to fundamental research, better understanding of the reinforcing mechanisms of FRCCs, the need for materials with particular properties, developments in advanced materials, economic competitiveness, and tecnical circumstances.

Advanced composites such as high-performance fibre reinforced cementitious composites (HPFRCCs) are a result of the effort made towards the development of FRCCs with improved performance. Guerrini (2000) highlights that the most interesting properties of HPFRCCs are strength, ductility, toughness, durability, stiffness and thermal resistance. The development of these advanced materials according to Guerrini (2000) was due to improvements such as the development of high performance cement-based matrices with improved microstructural properties in terms of strength and durability, the development of adequate processing techniques (including controlling chemical reactions) that enable high toughness and low porosity and the optimization of fibre-matrix adhesion properties.

Particular applications of HPFRCCs may include bridge decks and special structures such as offshore platforms, spacecraft launching platforms, super high-rise structures, high-end structures, light structural elements, precast elements, repair and rehabilitation among others. In Figure 1.1, some examples of this type of structures and the great versatility of applications are illustrated. It is precisely due to this broad variety of applications that HPFRCCs are often exposed to extremely severe conditions (e.g., marine environment, freeze-thaw cycles, etc.).

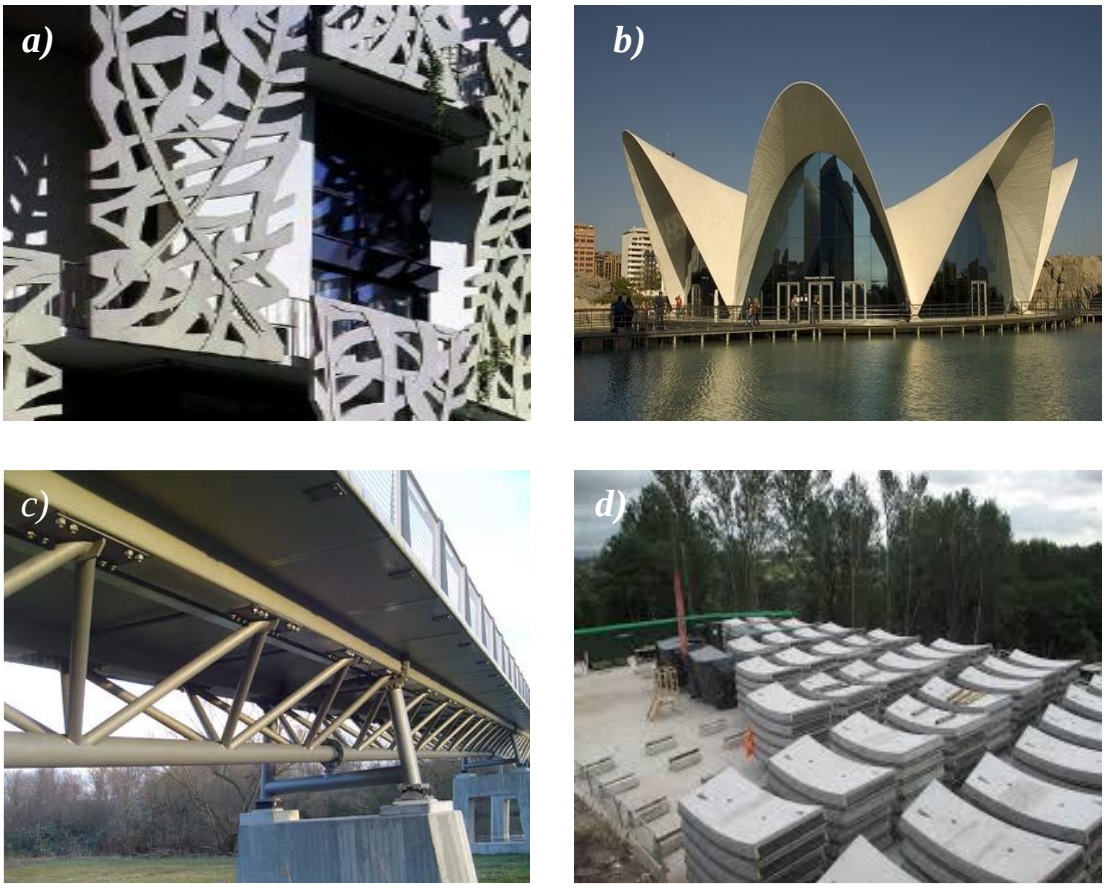

Figure 1.1 – Field applications of HPFRCCs: a) façades panels, b) shell roof, c) high performance deck glued to a 3-D steel truss and d) precast elements.

According to Trüb (2011), fibres are the key component of FRCCs, used in many shapes and sizes. The broad variety of field applications, growing urbanization and improving construction industry worldwide has driven the SFRC market. According to Zion Research analysis (2016), among the different types of fibres for concrete reinforcement, steel fibres dominated the market with over 45% of the market share in 2014. (see Figure 1.2).

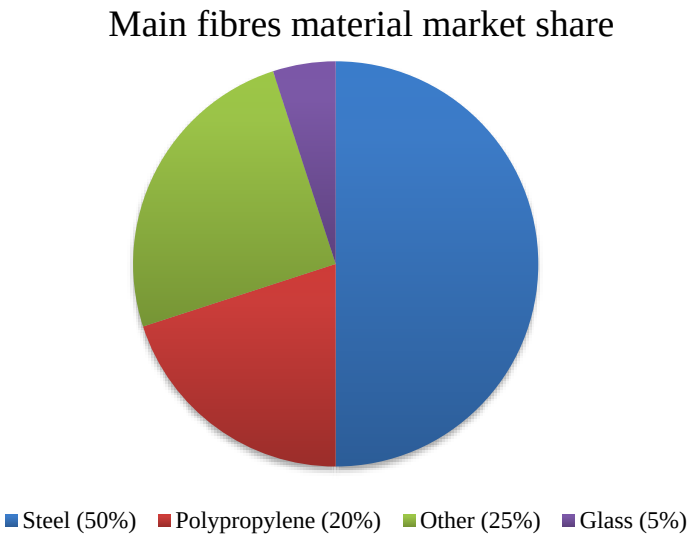

Figure 1.2 – Fibres market share (Zion Research analysis 2016).

The use of steel fibres in these structures could raise questions regarding its resistance to corrosion and durability. The fact that the fibres do not receive any special treatment to avoid corrosion means that their durability depends on the confinement in the alkaline environment of the concrete (pH around 12.5) where it will remain passivated (Figueiredo 2000). Considering that the chloride induced corrosion is the greatest threat to the durability and integrity of steel-reinforced concrete structures, adequate design may consider durability requirements in order to the avoid damage due to corrosion.

According to Hoobs (2001), in the past 30 years, the emphasis of concrete research has been increasingly focused on durability because:

- some deterioration processes have become more common;
- previously unknown deterioration processes have been identified (e.g., alkali-silica reaction, delayed ettringite formation, and thaumasite formation by external sulphate attack);
- the understanding of the deterioration processes is incomplete;
- new ranges of binders and combinations have been introduced with varying proportions of Portland cement being replaced by ground granulated blast furnace slag, fly ash, silica fume, and selected ground limestone.

According to Marcos-Meson *et al*. (2018), nowadays, international standards and guidelines are not consistent regarding the durability consideration of steel fibres in structural elements exposed to aggressive environment, hampering the development of civil infrastructure built with SFRC. In particular, long-term chloride exposure and its effects in the residual tensile strength is still unclear. Academics and regulators agree that steel fibres in uncracked SFRCCs exposed to chlorides show higher durability than conventional steel rebar. However, questions still remain regarding the aesthetics and the

mechanical performance of high performance steel fibre reinforced cementitious composites (HPSFRCCs) subject to chlorides.

The effects of chloride corrosion on cracked HPSFRCCs involving the main mechanisms governing the corrosion of carbon steel fibres bridging the cracks and the consequent structural impact still require further studies. This gains more importance as the industry applies SFRC with structural responsibilities (Blanco 2013). Studies of Abbas (2014) and Schnütgen (2003) present new perspectives of use the steel fibres as partial or total replacement of conventional reinforcement bars for prefabricated segmental tunnel linings. Investigations by Marcos-Meson *et al*. (2018) suggest that the elimination of the conventional steel reinforcement will remain controversial until the durability of SFRC under severe chloride and carbon dioxide exposure is addressed.

Figure 1.3 presents the number of published papers obtained with page Scopus using search words "corrosion and reinforced concrete", "corrosion and steel fibre reinforced concrete" and "corrosion and high-performance steel fibre reinforced concrete", from 1987 to 2017. Most of the publications are related to corrosion of the steel reinforcement or how the presence of fibres might affect the corrosion of the steel reinforcement. Just a few researchers focused on the steel fibre corrosion in HPSFRCCs.

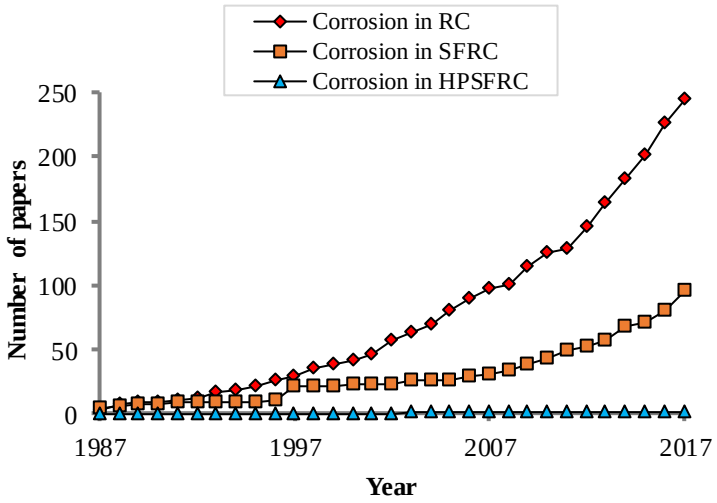

Figure 1.3 – Number of papers published over the years.

Several subjects need to be addressed to achieve deeper understanding on chloride corrosion for HPSFRCCs. Some of these subjects, which are contemplated in this doctoral thesis, are described subsequently:

- Bearing that in mind that concrete structure might crack, should the presence of cracks lead to a significant damage regarding corrosion and affecting the predicted residual response of the fibres? For example, in the case of structures subjected to cyclic chloride exposure, how the fibre degradation increase over time? Should a reduced structural response be expected depending on the crack width and the fibre content?

- High steel fibres contents may be used in HPSFRCCs. Therefore, more fibres are expected close to the structure surface. In spite of the very dense matrix of these materials, the ingress of detrimental agents such as chlorides may occur. In this regard, the study of the effects of chloride corrosion on the aesthetic aspect and of the mechanisms of steel fibres degradation would be of great interest.

- So far, the design procedures present recommendations regarding durability, mainly focussed on the crack width limitations in design according to the class of environment exposure of the structure, which were conceived for traditionally reinforced concrete. This remains an unexplored subject in the case of SFRC. Another subject yet to be included in codes and guideline is the consideration of corrosion damage factors which may predict a reduction in the structural performance of the elements. In this sense, experimental and numerical studies are required to fully understand the effects of corrosion in SRFC and to develop formulations able to predict the structural response of structures subjected to chlorides.

Aiming to gain more insight to answer the abovementioned subjects, this work developed an extensive experimental programme in order to generate more knowledge and contribute to the improvement of codes and engineering practice.

1.2. OBJECTIVES

Taking that into account, four general objectives that correspond to the main subjects addressed in this doctoral thesis are defined as follows.

- Study the influence of chlorides in uncracked HPSFRCCs by means of an accelerated test.

- Identify the main governing mechanisms involved in chloride-induced corrosion for uncracked and cracked HPSFRCCs under wet-dry cycles with chloride.

- Study the influence of chloride corrosion on the aesthetic and the mechanical behaviour of cracked and uncracked HPSFRCCs.

- Propose an analytical model to predict the influence of chloride corrosion in the residual tensile strength in cracked HPSFRCCs considered in the ULS design.

In order to achieve these main goals, several specific objectives are set. Table 1.1 shows the main specific goals for each subject treated in the thesis.

Table 1.1 – Specific objectives.

Subject	Specific objectives
Preliminary experimental programme	• Assess in a short time the effects of chlorides on the aesthetic aspect of uncracked HPSFRCCs under constant conditions. • Analyse the influence of chloride corrosion on the mechanical behaviour of HPSFRCCs specimens. • Provide data for the elaboration of a specific experimental programme for uncracked and pre-cracked HPSFRCCs under chloride exposure.
Specific experimental programme uncracked section	• Analyse the evolution of surface corrosion. • Identify the main mechanisms that influence the chloride corrosion for uncracked HPSFRCCs under wet-dry cycles with chlorides. • Establish a conceptual model taking into account the main mechanisms involved in surface corrosion of uncracked section. • Evaluate the effects of corrosion on the mechanical response of uncracked HPSFRCCs under chloride cyclic exposure.
Specific experimental programme pre-cracked section	• Analyse the ingress of chlorides into the crack depending on fibre content, crack width and number of cycles. • Elucidate the main mechanisms that govern the chloride corrosion for cracked HPSFRCCs under wet-dry cycles with chlorides. • Identify the depth and level of fibre corrosion in cracked section. • Evaluate the effects of corrosion on the residual strength of steel fibres. • Analyse the corrosion process in cracked section by means a microstructural analysis over cycles. • Provide data for an analytical model regarding corrosion in pre-cracked HPSFRCCs under wet-dry chloride exposure.
Simplified model	• Identify the main variables obtained by means the specific experimental programme that influences the residual response. • Propose an analytical model to provide an initial estimation of the reduction of the residual tensile response due to corrosion.

1.3. METHODOLOGY

In order to achieve the proposed general and specific objectives, the thesis is divided in four parts as shown in Figure 1.4. Part I describes the motivations of the thesis and is composed by Chapters 1 and 2. Chapter 1 is the introduction, where the background, objectives, scope and general overview of research methodology are presented. Chapter 2 is the literature review, which covered the fundamental knowledge to identify the motivations for this work and the current knowledge on the subject. This knowledge includes the background of the main mechanisms involved in chloride corrosion in steel fibre reinforced concrete. Furthermore, experimental programmes and models from the literature to predict the chloride corrosion and its influence in cracked and uncracked HPSFRCCs are presented.

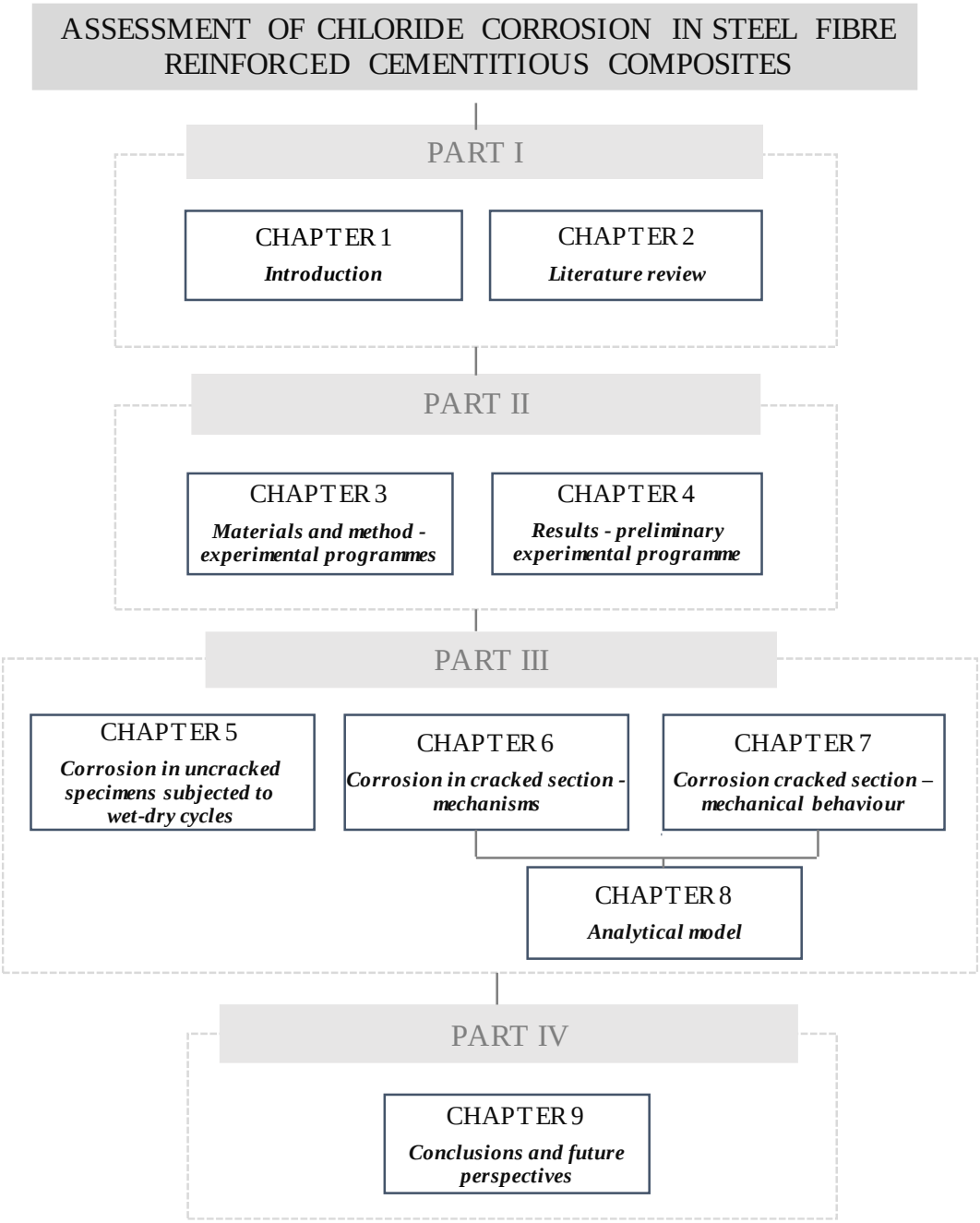

Figure 1.4 – Outline of the thesis.

Part II deals with the experimental programme and the analysis of the results of the preliminary experimental programme. These subjects are subdivided into two Chapters (3 and 4). In Chapter 3 the experimental programme conducted in two distinct parts is presented (see Figure 1.5). The first part consists of a preliminary experimental programme where an accelerated method of chloride attacks was performed in order to analyse in a short time the effects of chlorides corrosion in HPSFRCCs. In Chapter 4 the results and analysis of the preliminary experimental programme are presented. The mechanisms of chloride corrosion and its influence on the aesthetic aspect and mechanical response for uncracked HPSFRCCs are analysed for mixes with different fibre contents.

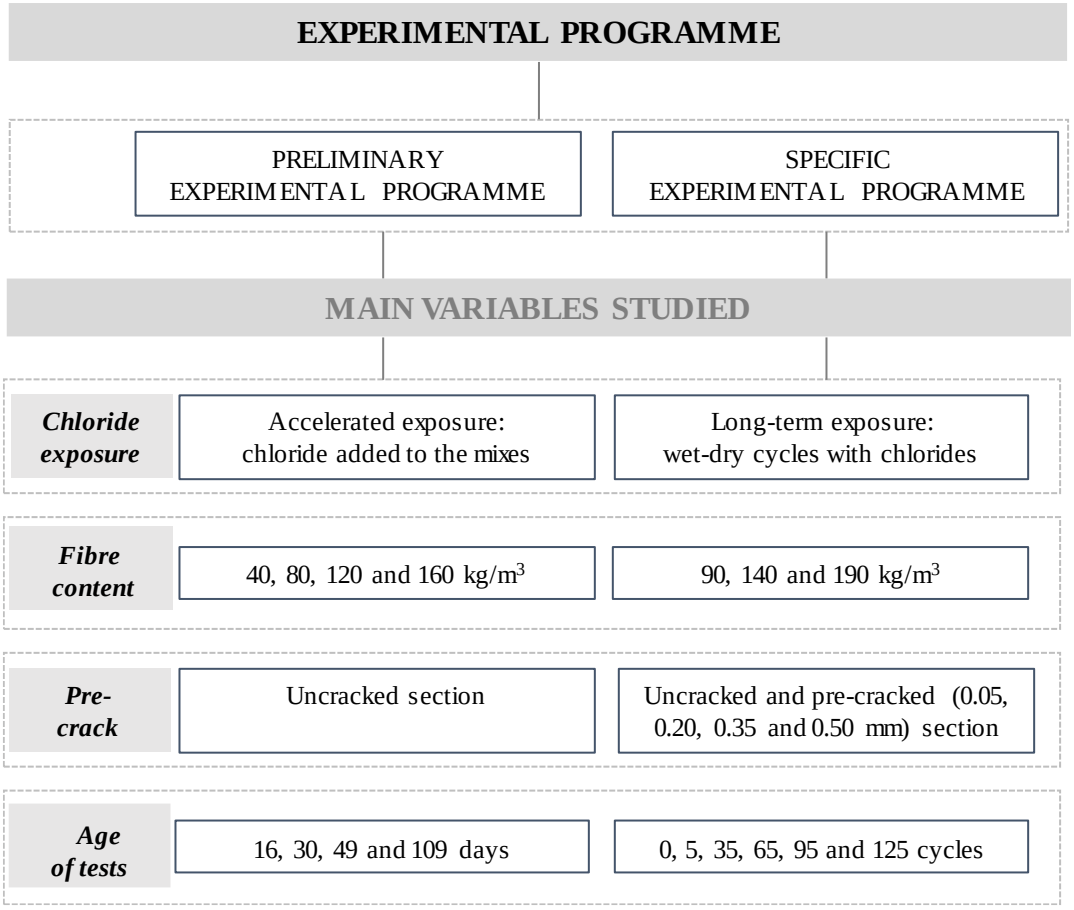

Figure 1.5 – Overview of the experimental programme.

In Part III, the results of the specific experimental programme are presented and discussed and an analytical model for cracked section is proposed. These subjects are addressed in Chapters 5, 6, 7 and 8. In Chapter 5, the effects of chloride corrosion in uncracked section of HPSFRCCs under long-term exposure are analysed regarding the aspects of surface corrosion and post-cracking behaviour. Additionally, a conceptual model involving the main mechanisms of surface corrosion in HPSFRCCs is proposed. Chapter 6 covers the analysis of the results obtained for pre-cracked HPSFRCCs in terms of the ingress of chlorides in cracks, the level and depth of corrosion of steel fibres in cracks and the microstructural analysis of the crack surface.

In Chapter 7 the main results of the effects of corrosion on the mechanical behaviour for pre-cracked HPSFRCCs with regard the influence of crack width, fibre content and number of cycles are presented. Then, in Chapter 8, an analytical model is proposed to enable the consideration of corrosion in the structural design of SFRC elements in ULS. The model considers the influence of parameters such as crack width, fibre content and number of chloride cycles. Finally, Part IV describes the conclusions of each of the subjects addressed in this thesis and presents the future perspectives of research in Chapter 9.

2. LITERATURE REVIEW

2.1. INTRODUCTION

Durability is considered one of the main requirement considered in the design of structures, imposing new requirements also on cement-based materials used in their production (Brandt 2008). High performance steel fibre reinforced cementitious composites (HPSFRCCs) are special structural materials with improved mechanical properties and durability, becoming of great interest for civil engineering applications.

According to Brandt (2008), the corrosive environment in which bridges, dams and marine structures are constructed, loads varying with the service life of the buildings, the impacts and thermal actions imposed on industrial structures and buildings facades, degradation due to intensive traffic, freezing and thawing of roads, highways and runways are only some examples of situations found around the world. Furthermore, corrosion due to chloride present in marine environment is the most important degradation process among all, according to Odriozola and Gutiérrez (2008).

In the case of HPSFRCCs, despite its increased applications in civil structures, inconsistencies among international standards and guidelines regarding the consideration of steel fibres for the structural verification when exposed to corrosive environments were observed by Marcos-Meson *et al*. (2018). Steel fibre corrosion may affect the aesthetic aspect leading to undesirable surface damage with the formation of rust stains as well as influence on the residual mechanical response. The unavoidable formation of cracks may lead to reduced structural performance of the steel fibres despite of the very dense matrix. These phenomena are still unclear. The objectives of this literature review are to identify the knowledge gaps regarding corrosion in HPSFRCCs to justify this thesis and to briefly cover the literature concerning several subjects that will be addressed in this work.

2.2. FIBRE REINFORCED CEMENTITIOUS COMPOSITE (FRCC)

Fibre reinforced cementitious composites is a term commonly used for a broad class of materials with optimized combination of properties. Every FRCC consists of two basic components: a cementitious base material called matrix, which is reinforced by steel of synthetic fibres (Trüb 2011). According to Naaman (2007), while the cementitious matrix may itself be considered a composite with several components, it is generally assumed to represent the first main component of the FRC composite whereas the fibre represents the second main component. Fibres are the key component and assumed to be discontinuous, randomly oriented and distributed within the volume of the composite.

The main purpose behind the addition of fibres to concrete is to better control the fracture process by bridging discrete cracks (Berrocal 2017). The addition of fibres leads to improved properties such as enhanced durability, increased fracture energy, toughness and ductility. The post-cracking behaviour of FRCCs is influenced by the microstructure at the interface between the fibre and the matrix (ITZ) (Löfgren 2005). Moreover, according to Bentur and Mindess (2007), the characteristics of the ITZ fibre-matrix exerts several affects specially with to fibre-matrix bond, and the debonding process across the interface.

Cracking occur when a tensile load is applied to a FRCCs, so that the matrix will transfer part of the load to the fibre (Löfgren 2005). The fibre-matrix bond may ensure a level of transference of load from the matrix to the fibres before the initiation of micro-cracks. In the post-cracking stage, after initiation of the first crack, the SFRCC should not present a brittle behaviour. The phenomenon is governed by the mechanisms of the fibres debonding, post-debonding friction between fibre and matrix (fibre slipping and pull-out), fibre fracture, fibre abrasion and plastic deformation (or yielding).

The improved mechanical properties of FRCCs increased the use of such materials in structural engineering applications. Such outcome also increased the research on SFRC about four decades ago. The various types of steel fibres developed (see Figure 2.1) have different mechanical properties in terms of tensile strength, grade of mechanical anchorage and capability of stress distribution and absorption (Holschemacher *et al*. 2010). Fibres play a key role in reaching a certain load bearing capacity after the matrix fracture, depending on allocation, orientation and embedded length (Holschemacher *et al*. 2010). Regarding orientation, a clear example is the walls of the formwork, which clearly limit the possible directions that fibres might assume (Cavalaro and Aguado 2015).

Figure 2.1 –Types of steel fibres.

Short steel fibres of various aspect ratios and strength were usually incorporated in high and ultra-high cementitious composites with various contents (more or equal 2%) to achieve muiti-cracking behaviours and increases ductility (up to 1%) (Habel *et al*. 2006; Kim and Parra-Montesinos 2003). According to Naaman and Reinhardt (1995), high performance fibre reinforced cementitious composite (HPFRCC) is considered as

high-performance if the stress-strain curves shows a quasi-strain hardening (or pseudo hardening) behaviour (i.e. a post-cracking strength larger than the cracking strength, or elastic-plastic response). Pseudo-strain hardening behaviour exhibit multiple-cracking in the post-cracking stage, reaching loads higher than the that of first cracking. Figure 2.2 illustrates the tensile strength classification of FRCCs.

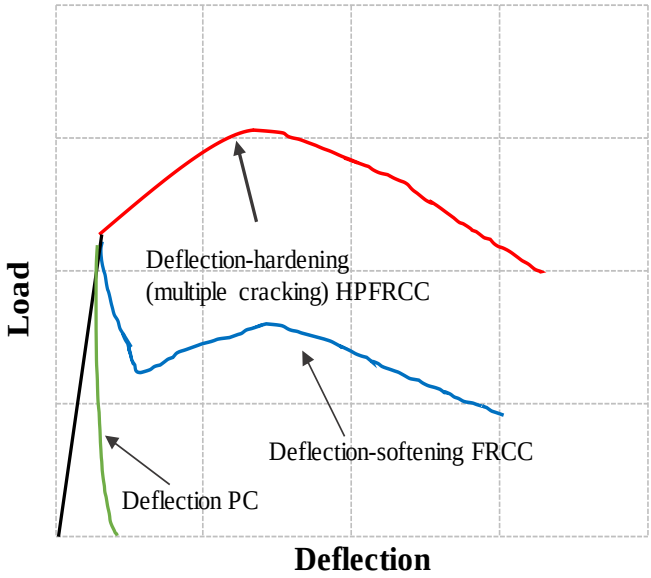

Figure 2.2 – Classification of fibre reinforced cementitious materials (Naaman and Reinhardt 2006).

Considering the high quality control required needed for the production of HPFRCCs, its application has been prolific in the pre-cast concrete industry. According to Marković (2006), in most cases, the pre-cast elements made of HPFRCC are prestressed, without conventional steel reinforcement. Possibilities applications include medium and long span girders, plates and shells, structures where a high durability is required, heavily loaded elements (e.g. columns in high-rise buildings, connections between pre-cast concrete elements) and steel-concrete fibre-matrix structures.

Applications of HPFRCC in hot-water storage tank (Reineck 2002), in strengthening of existing bridges (Walter *et al.* 2003), pre-cast concrete elements with long span by (Aljeboury (2005), for widening of existing bridges and viaducts by Van Blokland (1997) are reported in the literature. Hurk (2014) investigated design for slender box girders with less stirrups by applying HPSFRCC. Applications of HPFRCCs to enhance seismic performance in precast bridge piers, low-rise walls (Kim and Parra-Montesinos 2003), precast infill damper elements for seismic upgrading of steel structures (Xia and Naaman 2002) and in deficient structures (Yoon and Billinton 2002, Dogan and Krstulovic-Opara 2003; Kesner and Billinton 2004) are also reported. An extensive overview of studies and applications of HPFRCCs in earthquake-resistant structures is presented by Parra-Montesinos (2005).

2.3. CORROSION OF STEEL IN CONCRETE

Iron is the major component of steel and can comprise up to 80% of some special steel types. According to Figueiredo and Meira (2013), the concrete offers steel a physical protection - separating it from direct contact with the external environment - and a chemical protection - assured by the high pH of concrete which promotes the formation of a passive film around the steel element. The pH of the pore solution of concrete is a key parameter for the durability of reinforced concrete structures, being strongly related with the hydration phases present in the concrete (Plusquellec *et al*. 2017).

The study of the passivity of iron appears first in the research by Schoenbein (1836) and Faraday´s subsequent experiments. Schoenbien was the first to use the term passivity to describe the peculiar electrical state, giving rise to the decreased reactivity of iron surfaces (Davenport *et al*. 2000). According to Broomfield (2007), the passive layer is a dense, impenetrable film, which, if fully established and maintained, prevents further corrosion. MacDonald (1999) suggests that the passive films form as bilayer structure, consisting of a defective oxide (the barrier layer) adjacent to the metal and the outer layer that from the reaction of metal cations with species in the solution (including the solvent). From the investigation of MacDonald (1992), species in the solution phase may be incorporated in the outer layer, but not in the inner layer, whereas alloying elements from the substrate alloy may be incorporated in both layers.

Regarding the iron on aqueous environment, previous analysis conducted by Nagayama and Cohen (1962), mention that the passive film is a bilayer formation consisting in an inner layer Fe_3O_4 (at the iron/film interface) and an outer layer γ–Fe_2O_3 (at film solution interface). The study of Ohtsuka (2012) reveals that the passive oxide is probably composed of spinel type oxides Fe_3O_4 and γ–Fe_2O_3. The outer hydrated layer is formed in the case that ferrous ions exists in electrolyte. The oxidized inner layer is more stable, dense, with a ratio of Fe/O between 0.5 and 0.7 (Kitowski and Wheat 1997), whereas the outer layer is composed mainly of Ca and K and sometimes iron being more porous than the metal side layer.

Another model of passive film known as the hydrated amorphous oxide model was proposed by Murphy (1992). According to Prucner (2001), the main concept is that the bonded water keeps the thin film amorphous, and the incorporated water molecules hold together the ‘iron oxides chains’ in an amorphous structure like a binder, blocking diffusion of Fe^{2+} ions from the metal base beneath the film to the hydration sites at the passive film/solution interface. Results from Schroeder and Devine (1999) also suggest that the passive film is a multilayer film, with an inner spinel layer of Fe_3O_4 or γ–Fe_2O_3 defected with Fe^{2+} whereas the outer layer is a mixture of a small amount of a phase that resembles Fe_3O_4 or γ–Fe_2O_3 and an ferric oxide, hydroxide, or oxyhydroxide), as shown in Figure 2.3.

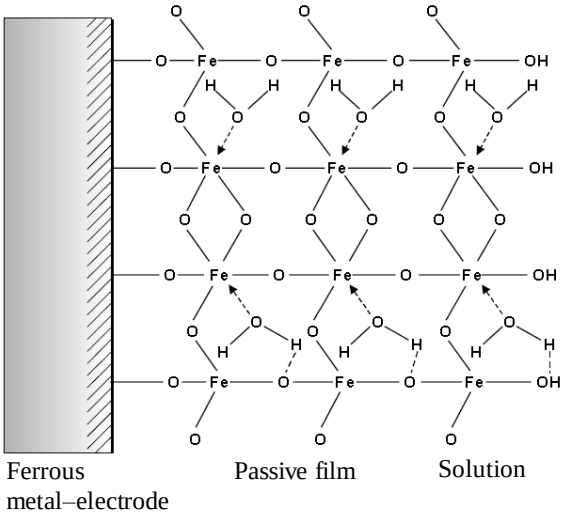

Figure 2.3 – Schematic representation of the hydrated passive film (Murphy 1992; Dauberschmidt 2006).

The breakdown of the passivity of various metals and their alloys occurs in the presence of so called aggressive anions (Strehblow 1984). Figure 2.4 shows the mechanisms of breakdown of the passive film suggested by Jayalakshmi and Muraliharan (1996). The model considers three main steps: adsorption of the aggressive ions on the oxide scale, penetration of the aggressive ions into the oxide and formation of complexes by aggressive ions.

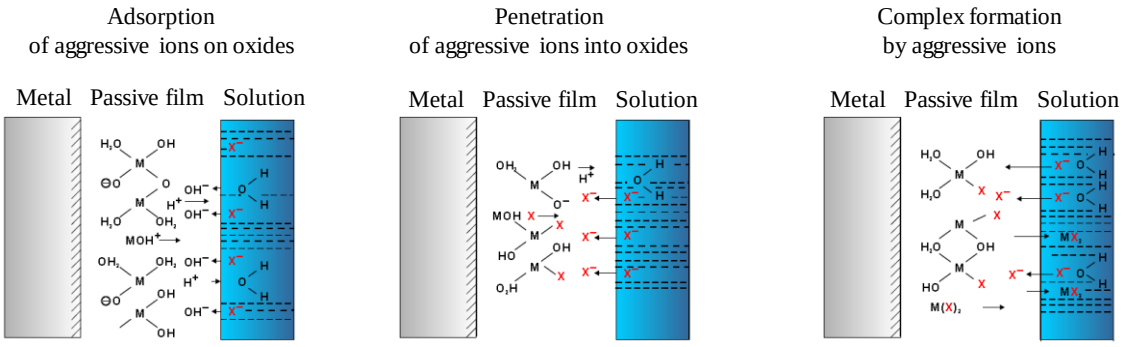

Figure 2.4 – Breakdown of the passive film by incorporation of aggressive ions (Jayalakshmi and Muraliharan 1996; Dauberschmidt 2006).

Corrosion is a phenomenon that, for the most part, has an electrochemical nature, implying the formation and movement of charged particles in the presence of a conducting electrolyte. Steel corrosion in concrete is a process in which iron is solubilised at the anode and oxygen is reduced at the cathode, with electrons flowing through the steel between the anode and cathode. The electrochemical process characterized by oxidation half-reaction (anode) cell at a certain location on steel surface in equation (2.1).

$$Fe \rightarrow Fe^{2+} + 2e^{-} \qquad (2.1)$$

The two electrons ($2e^-$) created in the anodic reaction must be consumed elsewhere on the steel surface to preserve the electrical neutrality (Broomfield 2007). Another chemical reaction to consume the electrons occurs (cathodic reaction) consuming also water and oxygen, as shown in equation (2.2).

$$2e^- + H_2O + \frac{1}{2}O_2 \rightarrow 2OH^- \tag{2.2}$$

The process of steel corrosion also needs an electrolyte, which is a medium capable of conducting electric current by ionic current flow (in concrete, the pore solution). In addition to that, a metallic path which acts as a connection between the cathode and anode, allowing the return of the current and completing the circuit (steel). Figure 2.5 illustrates de anodic and cathodic reactions.

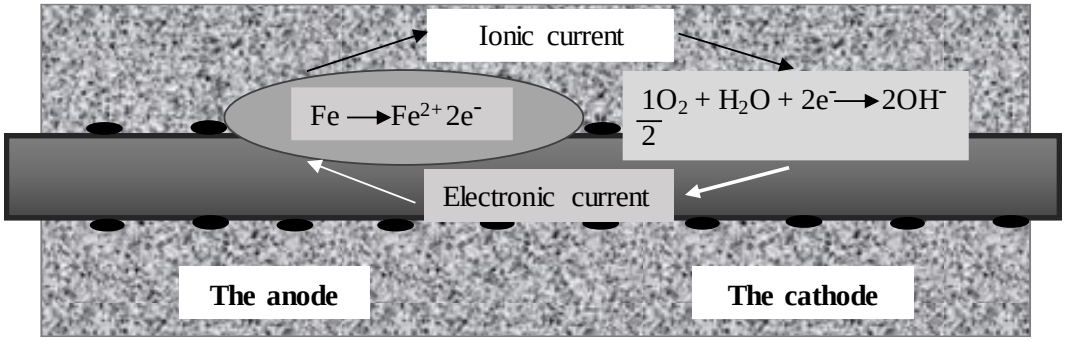

Figure 2.5 – Anodic and cathodic reactions (Broomfield 2007).

Several more reactions must occur to form 'rust'. The hydroxyl ions move through the pore solution and combine with the ferrous ions to form ferrous hydroxide which may also become hydrated ferric oxide (rust) by further oxidation. The chemical processes form products such as: ferrous hydroxide, ferric hydroxide and hydrated ferric oxide through equations (2.3), (2.4) and (2.5), respectively.

$$Fe^{2+} + 2OH^- \rightarrow Fe(OH)_2 \tag{2.3}$$

$$4Fe(OH)_2 + O_2 + 2H_2O \rightarrow 4Fe(OH)_3 \tag{2.4}$$

$$2Fe(OH)_3 \rightarrow Fe_2O_3.H_2O + 2H_2O \tag{2.5}$$

Two conditions (carbonation and chloride attack) can break down the passivating environment without attacking the concrete first (Broomfield 2007). Penetration of chlorides in through concrete is one of the factors which aims to the depassivation of reinforcing bars and therefore, may shorten the life of the structure (Andrade 1993). Differences of electrochemical potential can occur from distinct concentrations of chloride ions in the vicinity of the steel. When a sufficient amount of chloride ions reaches the steel surface, they break down the passive film locally to form an anode, while the

passivated surface acts as a cathode (Šavija 2014). The amount of chloride is commonly referred to as *the chloride threshold value* or *the critical chloride content*.

The chloride induced corrosion tends to be highly localized in a small anode with a formation of a corrosion pit. The soluble iron chloride ($FeCl_2$) increases the acidity of the pit (anode) by lowering the pH value, which favours further oxidation of the iron. Several reactions are involved in the process (such as equations (2.6) and (2.7), according to Richardson (2003) and Neville (1995).

$$Fe^{2+} + 2Cl^{-} \rightarrow FeCl_2 \tag{2.6}$$

$$FeCl_2 + 2H_2O \rightarrow Fe(OH)_2 + 2HCl \tag{2.7}$$

The entry of aggressive ions into the passive film occurs at points of local disturbances (Dauberschmidt 2006). According to Sato (1971), there is a critical thickness above which mechanical deformation or breakdown of the oxide film could occur, so anion adsorption lowers the surface tension and decreases the critical thickness for breakdown. In the adsorption mechanism, the addition of aggressive ions to the passive film surface occurs with an exchange with the OH^- and O^- ions of the passive film, which can lead to a perforation of the oxide layer (Dauberschmidt 2006). The breakdown of the passive layer by a formation of complex ions represents the continuation of the adsorption of anions at preferred surface sites, forming soluble complexes with metal ions from the oxide, as observed by Jayalakshmi and Muraliharan (1996). Such phenomenon leads to the thinning of the film by the increased dissolution of the iron (Heusler and Fischer 1973; Jayalakshmi and Muraliharan 1996).

Another explanation of the breakdown of the passive film is attributed to internal stresses. Effects of electrostriction and interfacial tension and other stress sources such as defects and impurities produce internal mechanical stresses which affect the film pressure (Sato 1971). The surface tension is of particular importance because it stabilizes the passive film (Dauberschmidt 2006). According to Strehblow (1984), the breakdown film may induce pitting in stationary conditions whereas a stationary passive film will be more susceptible to the adsorption mechanism.

Figure 2.6 shows the breakdown of the passive film by adsorption (Strehblow 1984; Sato 1971). A pitting is observed in the passive layer after the depassivation of the steel by chlorides, whereas the remaining surface remains unaffected. The pitting phenomenon of steel in concrete containing chloride, may produce a volume of products of corrosion up to 6 times larger than the original volume of the iron depending on the oxidation state reached. Figure 2.7 illustrates the relative volume of iron and its oxides according to Mansfeld (1981).

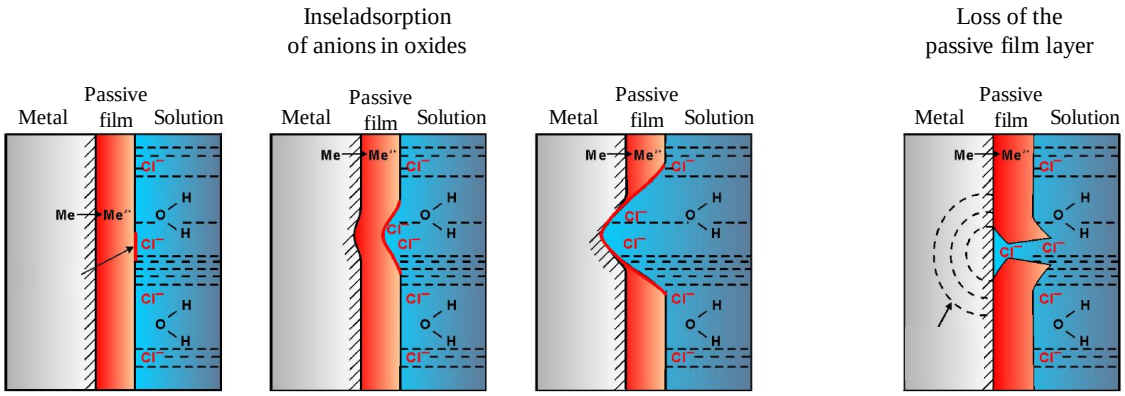

Figure 2.6 – Breakdown of the passive film by adsorption (Strehblow 1984; Sato 1971; Dauberschmidt 2006).

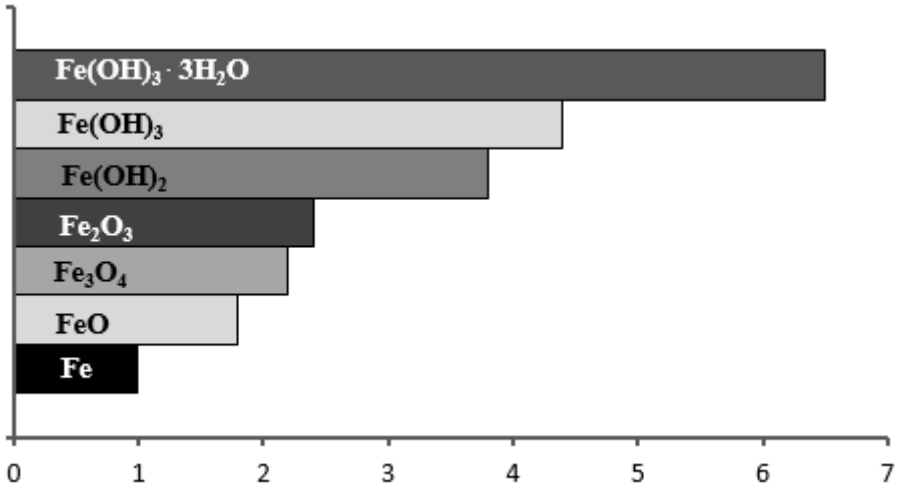

Figure 2.7 – Relative volume of iron and its oxides (Mansfeld 1981).

2.4. MECHANISMS OF CHLORIDE INDUCED CORROSION IN SFRC

According to Marcos-Meson *et al*. (2018), the main design variables influencing the durability of SFRC exposed to chlorides are fibre type; type of steel and coatings and fibre dimensions (i.e. length and diameter). Studies from Nordström (2000) and Frazão *et al*. (2015) observed presence of corrosion and reduction of fibre diameter in SFRC with cold-draw steel wire under chloride exposure. More recently, Dauberschmidt (2006) demonstrated that the cold-draw steel fibres with hooked ends suffered chloride induced corrosion due to the un-machined cold-draw steel wire. Such phenomenon was characterized by early initiation of pitting corrosion at micro-flaws at the bended regions of the fibres. According to the authors, during fibre production, the surface of the thicker initial wire is transformed in a thinner steel fibre. As a result, sharp cuts in the fibre surface are formed. Moreover, a lubricant is also used for the production and part of this material remains at the fibre surface filling the micro-flaws. The presence of the lubricant may lead to an 'incomplete passivation' of the region of the micro-flaws, favouring the corrosion.

The phenomena causing degradation of steel fibre in concrete structures are largely dependent on the mechanisms that allow the ingress of humidity, oxygen and detrimental agents, such as chloride ions. According to Salomon and Helene (2004), aggressive agents in the environment surrounding the concrete structure can percolate, diffuse, and penetrate across the pores of the concrete. Steel fibre in concrete without the presence of deleterious substances may remain passivated due to the high alkalinity of the concrete. The ingress and build-up of chloride ions into the matrix surrounding the steel disrupt the passive layer and reduces locally the pH at the steel surface, initiating pitting-corrosion (Bertolini *et al*. 2013).

Chlorides penetrate in concrete mainly through a system of capillary pores, voids, defects, and cracks. Various physical and chemical transport mechanisms contribute to chloride ingress, which depend on the concrete pore structure, (micro) environmental conditions, temperature, moisture content in the concrete, among others factors (Šavija 2014). Transport mechanisms are usually divided into the following groups (Poulsen and Mejlbro 2005; Šavija 2014):

- *Capillary suction*- the transport of chloride is driven by a difference in moisture content (pressure). In non-saturated concrete, water containing chloride ions moves toward zones with lower moisture content due to surface tension in the capillary pores.

- *Diffusion*- the transport of chloride is driven by the difference of the concentration of chlorides in various zones. Chloride ions move from zones with higher concentration to zones with lower concentration.

- *Permeation*- the transport of chloride is driven by a difference of hydraulic pressure in various zones. Chloride ions move into zones with smaller hydraulic pressure.

- *Migration*, where the transport of chloride ions is driven by a difference in electrical potential. Chloride ions migrate to zones with lower electrical potential. This is typical of accelerated tests, such as NT Build 492 (1999).

Notice that, in practise any of these mechanisms (or their combined action) can govern the ingress of chloride ions into concrete (Šavija 2014).

2.4.1. Chloride induced corrosion in uncracked SFRC

The transport properties of uncracked SFRC have been proven similar to the properties of unreinforced concrete (Marcos-Meson *et al*. 2018). The transport properties are closely related to the microstructure of the cementitious composite which may involve the bulk matrix, the aggregate and the interfacial transition zones (aggregate-matrix and steel fibre-matrix). The ITZ between the fibre and the matrix does not provide a

preferential path for the ingress of chlorides according to Berrocal *et al*. (2015), Abbas *et al*. (2014) and Mangat and Gurusamy (1987a).

In the case of uncracked SFRC exposed to chlorides, the steel fibres present more resistance to corrosion if compared to conventional steel reinforcement rebars. Studies from Dauberschmidt (2006); Nordström (2005); Mangat and Molloy (2000); Weydert and Schiessl (1996), revealed a limited corrosion for uncracked SFRC exposed to chlorides. This may be attributed to characteristics such as the discontinuous nature of the fibres, the uniform steel fibre surface due to the process of production, the dense and uniform ITZ fibre-matrix, and the small dimension of the fibres.

The discontinuous nature of fibres leads to smaller potential difference along the steel surface and greater anode/cathode ratios, thereby potentially limiting the formation of distinct cathode regions (Dauberschmidt 2006; Nordström 2005). The microstructure of the ITZ plays an important role in controlling the overall properties of FRC (Bentur *et al*. 1995). The fibre dispersed in the cementitious matrix as a result of casting conditions, favours a more uniform and dense ITZ of ~10 µm, rich in $Ca(OH)_2$ (Page 1982; Bentur *et al*. 1985). The analysis revealed a presence of a thin duplex film in direct contact with the steel surface, made majority of CH. The ITZ also includes regions with porous mass of C-S-H, ettringite and individual CH crystals in contact with the duplex film.

The solid hydration products on the steel surface protect the steel, both by acting as a physical barrier and by buffering the pH in the pore solution at the steel surface (Angst 2011). Figure 2.8 shows the formation of the fibre-cementitious ITZ which starts from the accumulation of a layer of water around the fibres as they are dispersed in fresh concrete. Calcium hydroxide grows in this layer during hardening (Dauberschmidt 2006).

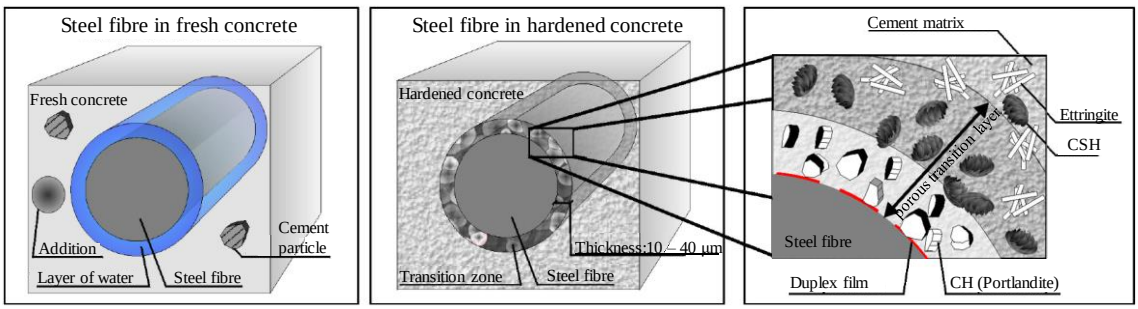

Figure 2.8 – ITZ in SFRC: a) fibre with a layer of water in fresh concrete, b) formation of contact zone in hardened concrete and c) close detail of the ITZ (Dauberschmidt 2006).

A fibre, being electrically discontinuous, in not capable of giving rise to galvanic corrosion (Sadeghi-Pouya *et al*. 2013). The small volume of the fibre is insufficient to create the bursting stresses associated with the corrosion of larger diameter reinforcement bars and therefore, for well compacted concrete, corrosion of fibres is restricted to the surface of the concrete (Lambrechts 2003). The short length of the steel fibres impedes large potential differences along the fibre and limits the formation of anode and cathode regions.

Researchers reported that fibre corrosion is less active if compared to that of steel bar reinforcement (King and Adler 2001; Sadeghi-Pouya *et al*. 2013). Janotka *et al*. (1989) assessed the behaviour of cement mortar containing steel fibre and steel bar, with addition of 0%, 2%, 6% and 10% of $CaCl_2$ by weight of cement. The results revealed that the steel bars presented signs of corrosion with 2% of $CaCl_2$ whereas the steel fibres did not indicate significant corrosion until chloride contents of 6% and 10%. Dauberschmidt (2006) studied the mechanisms of the increased corrosion resistance of steel fibres compared to conventional reinforcing steel bars.

Figure 2.9 compares the microstructures of the rebar-matrix ITZ and the fibre-matrix ITZ. A larger and more uniform calcium hydroxide (CH) layer is observed around the fibre, protecting against chloride and oxygen ingress (Marcos-Meson *et al*. 2018). By contrast, a more porous layer was observed for the rebar-matrix ITZ. The improved fibre-matrix ITZ when compared to rebar-matrix ITZ is responsible for the increased corrosion resistance of steel fibres, leading to a higher critical chloride threshold.

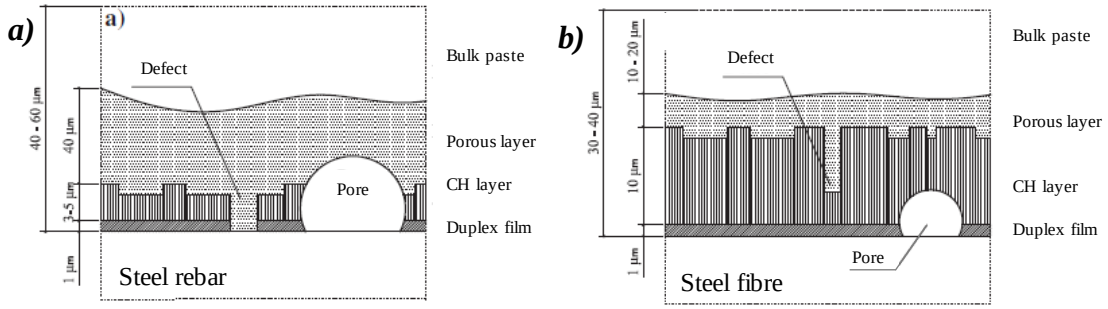

Figure 2.9 – Microstructure of a) rebar-matrix ITZ (Poole and Sims 2015) and b) fibre-matrix ITZ (Bentur *et al.* 1985; Marcos-Meson *et al*. 2018).

2.4.2. Effects of chloride corrosion in uncracked SFRC

Surface corrosion

Studies reveal that for uncracked SFRC, the corrosion of steel fibre is limited to fibres localized within approximately 5 mm from the exposed surface. In a study by Balouch *et al*. (2010), uncracked specimens of SFRC subjected to chloride cycles presented formation of corrosion spots on the surface. The results demonstrated that fibres located less than 1 mm (for mixes with water/cement ratio of 0.78) and 0.1-0.2 mm (for mixes with water/cement ratio of 0.50) from the surface are susceptible to corrosion, leading to deposition of corrosion products at the surface. Mangat and Gurusamy (1988) observed that SFRC specimens with low carbon fibres subjected to cycles of marine exposure showed extensive deposition of corrosion products at the surface at 150 cycles. No sign of deeper corrosion (beyond a superficial layer) was observed until 2000 cycles (1250 days).

Corinaldesi and Moriconi (2003), studied fibre reinforced self-compacting concrete subjected to 1 month of immersion in 10% sodium chloride aqueous solution. The results revealed that the steel fibres located 2 mm away from the external surface presented a slight evidence of corrosion whereas fibre placed at 30 mm from its edge remained sound. SFRC with recycled steel fibres and with new steel fibres subjected to chloride wet-dry cycles were investigated by Graef *et al*. (2009). More severe corrosion was observed after curing in the specimens with recycled fibres. After 5 months of cycles, specimens with recycled fibres presented a higher level of surface corrosion then those with new steel fibre. In both cases, corrosion was only found close to the surface.

Serna and Arango (2008) studied the performance of white steel fibre reinforced concrete (WSFRC). Cut sheet fibres and cold-drawn fibres, galvanized and non-galvanized were analysed. Uncracked specimens subjected to sea water immersion and drying cycles presented corrosion at a layer no deeper than 2 mm from the surface after 12 months of cycles. Besides that, a lower level of corrosion was observed in specimens with galvanized fibres. Abbas (2014) studied UHPC with steel fibres subjected to chloride attack (salt ponding and salt immersion tests). A limited corrosion on the surface and no evidence of corrosion on the fibres deeper than 3 mm from the surface was detected. Such behaviour is attributed to the low porosity of UHPC which controls the ingress of chloride ions, moisture and oxygen required for the onset of corrosion.

Granju and Balouch (2005) found that steel fibres at a depth of 2-3 mm from the surface presented a severe level of corrosion in SFRC specimens exposed to marine-like environment during 1 year. Rider and Heidersbach (1978) studied several different types of steel fibres in SFRC exposed to partial immersion in sea water. A depth of 6.4 mm of corrosion was observed after 6 months of exposure. Lankard and Walker (1978) studied SFRC subjected to weekly salt applications (0.2 Kg/m^2 of NaCl). The corrosion of the fibres after 5 years of exposure was limited to 1.6 mm from the surface. Hannant and Edgington (1975) observed a severe corrosion (depth of 6.4 mm from the surface) in SFRC specimens after 57 months in coastal environment exposure.

The experimental programme performed by Aitcin *et al*. (1985) on SFRC under salt fog exposure (salt solution with 5 % $CaCl_2$ in de-ionized water) showed corrosion up to a depth of 3.2 mm after 67 days of exposure. Kim *et al*. (2011) tested SFRC in two severe environments (salt-water immersion and salt-water wet-dry cycles) in a long-term test exposure (21 months). Specimens subjected to immersion presented no sign of corrosion, whereas specimens under cycles showed a severe corrosion of the steel fibres localized at the surface.

Steel fibre reinforced lightweight concrete was tested at field exposure in tidal zone by Schupack (1985). After 10 years of marine environment exposure, the corrosion of the fibres was limited to the surface. Sadeghi-Pouya *et al*. (2013) analysed high performance steel fibre reinforced concrete under accelerated chloride corrosion for one month (equivalent to approximately 50-60 years' life of a typical bridge exposed to de-

icing salts). The visual analysis after exposure a minor surface rust stain. According to Hoff (1987), uncracked fibre reinforced concrete generally experiences no adverse corrosion effects from a marine environment, showing corrosion limited to those fibres immediately at the surface.

Mechanical behaviour

Studies by Mangat and Gurusamy (1987b) with SFRC under prolonged marine exposure (1200 marine spray cycles) showed slight reductions of the load-deflection curves of specimens with the cycles. Such outcome indicate that the chloride exposure did not reduce the embedded fibres cross section and the failure occurred due to debonding and gradual pull-out of fibres from the matrix. Graef *et al*. (2009) observed no changes on the post-cracking behaviour of a corroded SFRC specimen compared to a no-corroded one after 5 months of wet-dry cycles.

Alizade *et al*. (2016) noticed a reduction in the post-peak response of uncracked SFRC subjected to chloride cycles. Compared to control specimens cured at air, the peak stress and toughness of specimens saturated in salt solution for 2 months increased by 30%. Such behaviour may be attributed to long term curing conditions and the early effect of corrosion, which improve the bond strength at the fibre-matrix ITZ. On the contrary, the specimens saturated for 6 months showed a reduction of 30% in the peak stress and toughness be due to the intensive effect of corrosion on the steel fibres.

A study by Mantegazza and Gatti (2004) revealed that SFRC under chloride wetting and drying cycles had a reduction in the mechanical performance after the cycles. Abbas (2014) showed that specimens of UHPFRC subjected to various corrosive environments (salt ponding, immersion in 3% and 10% of chloride solution) presented no reduction in the mechanical properties after long-term tests. Such outcome may be attributed to the dense microstructure and good quality of the fibre-matrix ITZ. This agrees with the findings by Sadeghi-Pouya *et al*. (2013), who showed that HPSFRC under long-term accelerated corrosion (3% of NaCl per weight of cement added in the mixes and then the samples submerged in 3% of chloride salt solution) experienced almost no reduction in the flexural and tensile behaviour after the attack. By contrast, SFRC specimens subjected to corrosive environment (submerged in 3.5% NaCl solution) for 60 days showed a slight loss of flexural strength and flexural toughness, according to Carrillo *et al*. (2017).

Kim *et al*. (2011) studied SFRC subjected to two severe environments (salt-water immersion and salt-water wet-dry cycles) during a long-term test exposure (21 months). The results revealed that the average residual strength was not affected for the specimens under immersion whereas a slight increment was observed for uncracked specimens subjected to chloride cycles.

2.4.3. Chloride induced corrosion in cracked SFRC

Steel fibres are often used for crack control due to their high elastic modulus and good resistance to the alkalinity of concrete (Berrocal 2017). Crack width is considered the most important factor governing the ingress of deleterious substances in concrete. Some researchers (Abbas 2014; Nordström 2005; Mangat and Gurusamy 1987c) concluded that a mitigating mechanism of fibre corrosion may occur for a critical crack width ($w < 0.20$ mm) due to the limited ingress of chlorides and oxygen. The authors also observed autogenous (self)-healing and that products of corrosion block the crack and limit the evolution of corrosion into the crack.

According to Marcos-Meson *et al*. (2018), the damage at ITZ in cracked SFRC due to the strain at the fibres bridging the crack may induce corrosion at the weakest regions, according to the mechanism illustrated in Figure 2.10.

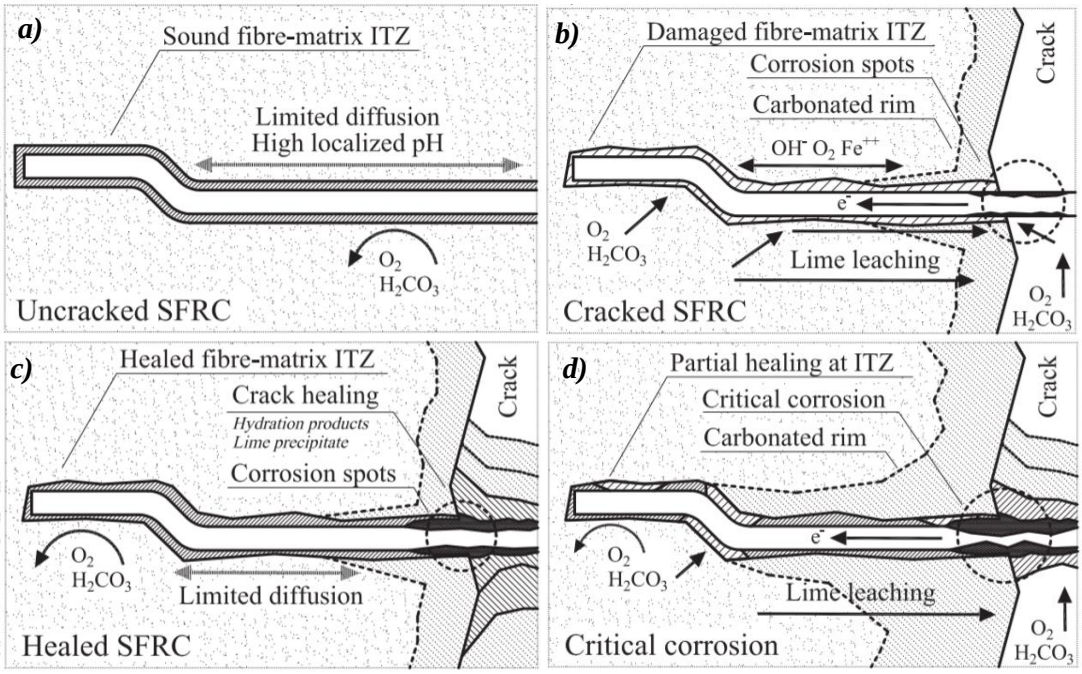

Figure 2.10 – Corrosion mechanisms: a) uncracked SFRC, b) cracked SFRC at an early stage, c) cracked SFRC after autogenous healing and d) cracked SFRC with critical corrosion (Marcos-Meson *et al*. 2018).

In uncracked condition, the dense and uniform steel-matrix ITZ acts as a protective coating (see Figure 2.10-a) preventing the access of aggressive agents (e.g. oxygen, chlorides) and limiting the contact of the steel surface with the electrolyte (i.e. limiting ionic diffusion along the steel surface). When cracks appear, the bond between fibre and matrix is activated, favouring the damage of the ITZ. The extent of this damage is directly related to the strain (i.e. larger cracks induce greater damage at the ITZ) and the shape of the fibres (Granju and Balouch (2005); Nemegeer *et al*. (2000) observed localized corrosion damage at the hook). The damaged ITZ would provide a preferential path for diffusion of chlorides and oxygen, promoting corrosion (see Figure 2.10-b). For small damage levels, the steel fibre-matrix ITZ rich in CH may eventually repassivate the

fibre (see Figure 2.10-c). A combination of un-hydrated cement, lime leaching, corrosion products and salt crystal would eventually seal the crack, limiting the ingress of chlorides and oxygen. The fibres bridging the cracks may serve as preferential surface for deposition of these compounds (Homma *et al*. 2009).

Large damage levels at the fibre-matrix ITZ (i.e. due to larger strain) can lead to a delayed or defective healing at the ITZ at the regions more affected by the damage (e.g. deformed regions, fibre-crack intersection). This can produce progressive and localized reduction of the fibre cross-section due to corrosion, potentially changing the failure mode of the SFRC from fibre pull-out to fibre yield or breakage. Consequently, the residual tensile strength would decrease (Figure 2.10-d), as observed by Batson (1977); Bernard (2004); Kosa and Naaman (1990) and Nordström (2005).

2.4.4. Effects of chloride corrosion in cracked SFRC

Influence of exposure conditions and time

Studies by Mangat and Gurusamy (1987b); Morse and Williamson (1977); Bernard (2004); and Nemegeer (2003) revealed that SFRC specimens with crack widths smaller than 0.25 mm exposed to laboratory marine spray cycles, wet-dry salt water environment, submerged coastal environment showed a limited damage after the cycles. According to Nordström (2005), SFRC specimens exposed to long-term (5 years) aggressive conditions (de-icing-salts). The results indicated that the chloride content increased close to the crack mouth and a stabilization of reduction in the mechanical behaviour after 1 year.

According to Nordström (2005), there are two major techniques to estimate long-term behaviour during degradation: either by measurements of the degrading process under near-field conditions or by increasing the severity of the exposure in accelerated tests. The use of wet-dry cycles is an effective method to accelerate the corrosion-induced damage in SFRC (Marcos-Meson *et al*. 2018). The wetting increases the concentration of ions such chlorides and the drying helps to increase the availability of oxygen required for steel corrosion, as oxygen has a substantially lower diffusion coefficient in saturated concrete (Hong 1998).

Tests in SFRC specimens with crack widths smaller than 0.2 mm under short exposure (up to 6 months) subjected to wetting and drying cycles with chlorides (3.5-5 wt.% NaCl and $CaCl_2$) revealed contradictory results regarding the mechanical behaviour after a period of aggressive exposure. Nordström (2005) observed negligible loss of steel fibre diameter. The study of Frazão *et al*. (2015) revealed that the corrosion of the steel fibres induced to micro cracks and a consequent decrease of tensile strength. Results showing a significant reduction of the mechanical response was observed by several researchers. Alizade *et al*. (2016) identified a reduction of peak stress and toughness;

Anandan *et al*. (2014) found a reduced flexural strength; Mantegazza and Gatti (2004) observed weak mechanical performance due to corrosion under application of load.

Several studies do not find evident loss in mechanical performance in case of SFRC specimens with cracks widths smaller than 0.2 mm subjected to extended exposure (from 6 months to 3 years) to wet-dry cycles with chlorides (3-5 wt.% NaCl). Abbas (2014) noticed an increment in the flexural strength attributed to the self-healing of micro crack with products of corrosion and the increased friction bond between fibre and cementitious matrix for low levels of corrosion. Roque *et al*. (2009) noticed no degradation and even a modest improvement in mechanical properties. Kim *et al*. (2011) found similar results for cracked and uncracked SFRC. By contrast, for crack widths bigger than 0.2 mm, a significant loss of residual tensile strength due to corrosion was observed by Serna and Arango (2008); Schiessl and Weydert (1998).

The investigation conducted by Kim *et al*. (2011) with SFRC under 21-month exposure in two environments (immersion in salt-water and salt-water wet-dry cycles) revealed that pre-cracked specimens subjected to chloride immersion presented no reduction in the average residual strength whereas the samples under chloride cycles presented a reduction due to the corrosion.

Influence of crack width

Despite the enhanced resistance to corrosion of the fibres in uncracked concrete, steel fibres bridging the cracks are susceptible to degradation under chloride exposures. The durability of cracked SFRC subjected to chlorides is a controversial subject that may be analysed according to three ranges of crack width (w_k): $w_k < 0.5$ mm; narrow cracks $0.5 \text{ mm} \geq w_k > 0.2$ mm; hairline cracks: $w_k \geq 0.2$ mm (Marcos-Meson *et al*. 2018).

According to Marcos-Meson *et al*. (2018), there is a general consensus regarding the high probability of corrosion of carbon-fibres bridging if cracks widths bigger than 0.5 mm are present in elements subjected to an aggressive environment. Mangat and Gurusamy (1987d) suggest a permissible crack width value of 0.15 mm in order to provide a satisfactory margin of safety against corrosion for SFRC. Frazão *et al*. (2015) observed that for steel fibre reinforced self-compacting concrete (SFRSCC) in extreme conditions allowed the corrosion of steel fibres, which led to the formation of micro-cracks in surrounding concrete.

2.4.5. Previous models to consider the effect of corrosion in SFRC

Most of the existing studies from the literature focus on the analysis of corrosion in conventional reinforced concrete or the corrosion of steel rebars in a steel fibre reinforced concrete. The crack control mechanisms provided by the fibres in traditionally reinforced concrete may delay the initiation of corrosion in the rebar (Berrocal *et al*. 2015; Blunt 2008). Table 2.1 summarizes previous models that try to model chloride corrosion

in SFRC with and without traditional reinforcement. Notice that most of these models focus on the assessment of the corrosion process in rebars embedded in a SFRC, ignoring the potential negative impact of the fibre corrosion in the structural performance.

Table 2.1 – Models to assess chloride corrosion.

References	Concrete	Model	Study
Nordström 2005	SFRC	Analytical model	load bearing capacity
Dauberschmidt 2006	SFRC	Numerical model	corrosion kinetics
Rafiee 2012	RC-UHPSRC	Numerical model	loss of cross section
Solgaard 2013	RC-SFRC	Numerical model	steel fibres; cracks
Paul 2015	RC-SHCC	Analytical model	time to corrosion
Berrocal 2017	RC-SFRC	Analytical and numerical models	steel fibres; cracks
Carrillo *et al*. 2017	SFRC	Analytical model	flexural properties

2.5. DISCUSSION

The first part of this chapter reviewed some basic concepts of the main mechanisms regarding the corrosion in steel. Then, the mechanisms involving the corrosion process of steel fibres in SFRC when subjected to chloride attacks were also described. Fibres show a significant resistance to corrosion due to characteristics such as small diameter, short length, smooth surface and enhanced fibre-matrix ITZ. Even so, fibre depassivation and corrosion may still occur under aggressive environments.

Several studies focussed on cracked and uncracked SFRC and the effects of corrosion on the surface aspect and residual strength. The main mechanisms involved in the corrosion process and its effects considering parameters as crack width, time and exposure condition on the level of damage in SFRC were identified. Results from the studies reveal controversial conclusions regarding the durability of SFRC. Different critical crack width, depth of corrosion, formation of surface rust stains, level of mechanical damage was also observed in the data from the existing literature.

The review of the literature provided knowledge about the gaps related to the mechanisms governing chloride corrosion of high carbon steel fibres in cracked and uncracked HPSFRCCs. It also highlighted the need of further research regarding the influence of fibres corrosion on the aesthetic aspect and residual strength considering parameters such as crack width, fibre content in a long-term cyclic chloride exposure. Furthermore, simplified tools to estimate the consequences of corrosion in the mechanical performance of HPSFRCCs are still required. Most of the existing models focus on predicting the corrosion of steel rebars embedded in the SFRC.

3. MATERIALS AND METHOD OF THE EXPERIMENTAL PROGRAMMES

3.1. INTRODUCTION

High performance steel fibre reinforced cement composites (HPSFRCCs) are materials developed with optimized mixture consisting of a dense matrix and fibres. The high performance of these materials is closely related to the excellent mechanical and durability properties. Due to the enhanced properties, one of the preferred areas of applications are structures subjected to aggressive environments.

Chapter 2 showed several types of external and internal degradation processes that might affect durability of the real-scale structures constructed with HPSFRCCs. Chapter 2 also revealed a concerning lack of studies about the influence of corrosion in elements made with HPSFRCCs, despite the high importance of the fibres for the structural performance of structures.

The **objective** of this chapter is to describe the two experimental programmes conducted in this thesis to overcome this lack of knowledge and their specific objectives. The preliminary experimental programme (section 3.2) was conducted to analyse the effect of chlorides in uncracked HPSFRCC specimens under constant conditions. The specific experimental programme (section 3.3) was performed to go deeper on the influence of corrosion in pre-cracked and uncracked HPSFRCC specimens under cyclic conditions.

3.2. PRELIMINARY EXPERIMENTAL PROGRAMME

The following specific objectives were defined for the preliminary experimental programme:

- Investigate the effect of chlorides on the aesthetic of HPSFRCC specimens under constant conditions;
- Assess the influence of corrosion in the post-cracking behaviour of the steel fibres;
- Provide data for the proposal of the specific experimental programme focusing on pre-cracked and uncracked sections under cyclic conditions.

3.2.1. Materials and mixes

Two main variables were defined in the study: fibre content and ages of tests. The definition of the materials and compositions was based on the ultra-high performance steel fibre reinforced concrete mixes proposed by Klein and Aguado (2010). To ensuring good workability and avoid the influence of the compaction process in the fibre orientation of mixes with different fibre contexts, self-compacting mixes were used.

All mixes contain Portland Cement CEM I 42,5R (without additions), limestone sand with particle size distribution between of 0-5 mm, limestone sand with diameter of 0-2 mm and limestone filer. Potable water from the public network of Barcelona was used for the mixes as it is acceptable according to the recommendations of the Spanish code EHE-08 (CPH 2008) for structural concrete. The density and the water absorption of the aggregates were determined according to UNE-EN 1097-6:2001 (AENOR 2001) and considered to correct water-cement ratio. The total quantity of water (W_T) was calculated with equation (3.1) taking into account the water absorption of the aggregates (W_{abs}), the theoretical water cement ratio ($W_{w/c}$), the water of the superplasticizer (W_s), the water of the retarding admixture (W_r) and the water due to humidity of the aggregates (W_h).

$$W_T = W_{w/c} + W_{abs} - W_s - W_r - W_h \tag{3.1}$$

Mixes were produced with fibre contents of 40, 80, 120 and 160 kg/m³, added in substitution of the equivalent volume of sand. A short straight steel fibre of type Dramix® OL13/.20 (13 mm in length and 0.2 mm in diameter) with a high percentage of carbon and copper coating was selected. Further characteristics of fibres are presented in Table 3.1.

Table 3.1 – Characteristics of fibres used (provided by the manufacturer).

Characteristic	Unit	Value	
Length (L)	mm	13	
Diameter (d)	mm	0.2	
Aspect ratio (L/d)	-	62	
Tensile strength (f_y)	MPa	2600	
Modulus of elasticity (E)	GPa	200	

To accelerate the access of the chloride to the fibres and the corrosion process, 179.50 g of anhydrous sodium chloride was added per litre of the mixing water. This value corresponds to half the saturation point of sodium chloride. Equivalent mixes without chloride were also produced as reference.

To compensate for variations of workability of the mixes with the addition of fibre and chloride, two approaches are possible: the modification of the water content and the modification of the superplasticizer content. The first option was discarded as it would imply a modification of the porosity and of the mechanical properties of different mixes. Therefore, to ensure similar workability, the amount of superplasticizer of type Glenium C303 SCC was modified. A retarding admixture (Basf Pozzolith 111R) was also added to control the set acceleration effect due to the inclusion of sodium chloride.

Trials were conducted to adjust the dosage of superplasticizer and retarder that ensured a flow extent of 210 ± 10 mm, measured according to UNE-EN 12350-5:2009 (AENOR 2009) without applying any blow at the table. All mixes were produced with amounts of superplasticizer ranging from 2 to 5% by cement weight (bcw) and retarder ranging from 0.30 to 1% bcw until the target flow extent was achieved (see Figure 3.1).

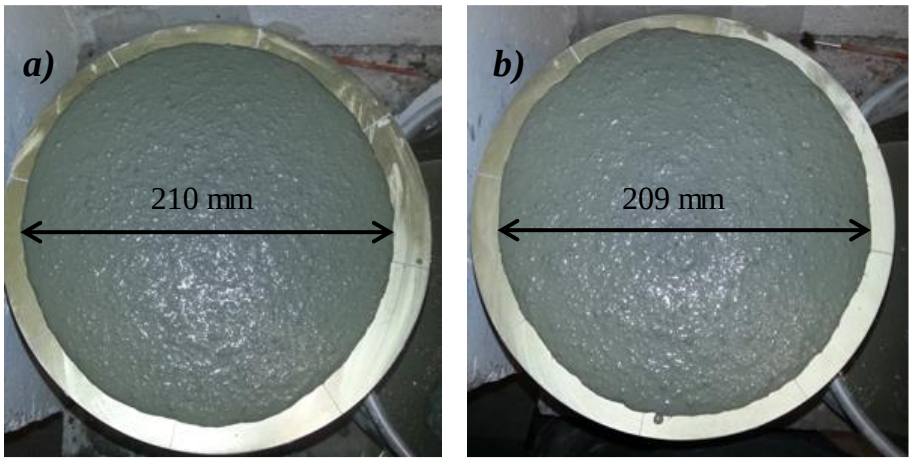

Figure 3.1 – Flow stent test: a) mix without chlorides and b) mix with chlorides.

For the experimental programme eight mixes were designed. Table 3.2 shows the final composition of the mixes defined after the trials. Notice that the amount of past remained constant for all mixes, whereas the amount of sand reduced with the increase of the fibre content.

Table 3.2 - Composition of the HPSFRCC mixes for the preliminary experimental programme.

Components	Characteristics	Content (kg/m³)							
Cement	CEM I 42.5 R	700	700	700	700	700	700	700	700
Filer	Limestone	255	255	255	255	255	255	255	255
Sand (0/2 mm)	Limestone	631.6	623	608.6	594.3	631.6	623	608.6	594.3
Sand (0/5 mm)	Limestone	340.1	335.4	327.7	320	340.1	335.4	327.7	320
Water	-	213.5	213.6	210.9	208.2	213.5	213.6	210.9	208.2
Superplasticizer	Glenium C303 SCC	31.5	31.5	35	38.5	31.5	31.5	35	38.5
Retarding admixture	Pozzolith 111R	2.1	2.1	2.1	2.1	2.1	2.1	2.1	2.1
Fibres	Steel fibre OL 13/0.20	40	80	120	160	40	80	120	160
Chloride	Sodium chloride	-	-	-	-	44	44	44	44
Slump flow test (mm)		209	213	215	210	209	210	211	209

3.2.2. Specimens preparation

A mixer with 8-L capacity was used to produce the HPSFRCC specimens. First, water and cement were mixed during 60 seconds (with a speed of 110 rpm). Then the superplasticizer was added, and the materials were further mixed for 60 seconds keeping the same speed. After that, the retarding admixture was added and mixed during the same time and speed in order to ensure a proper homogenization of all components. The sand and the filler were gradually added and mixed for additional 60 seconds.

Next, to avoid accumulation of materials at the walls of the mixing bowl, the mixer was stopped for 90 seconds. The material accumulated at the lateral surface of the mixing bowl was incorporated again with a spatula. Then, materials were mixed for 60 seconds more. Fibres were added carefully and mixed for one minute and a half with a speed of 188 rpm. Finally, the chloride was added (in the mixes with chlorides) and mixed for 90 seconds with a speed of 188 rpm.

After that (see Figure 3.2-a), the material was placed into metallic moulds (see Figure 3.2-b) according to the UNE-EN 196-1:2005 without additional compaction process. In total, 36 prisms of 40 x 40 x 160 mm were produced per mix. The moulds were covered with a plastic sheet to avoid water loss by evaporation and kept in a controlled room at 24 °C. Specimens were removed from the moulds within 24 hours of casting and identified.

Then, they were kept in a wet room at 20 °C and up to 90% of relative humidity for 44 days (see Figure 3.2-c). After that, specimens were placed in a climatic room at

controlled temperature (20 °C) and between 45% to 55% of relative humidity until the date of tests and analyses (see Figure 3.2-d). The degree of humidity affects the diffusion rate of oxygen enhancing the corrosion rate. In theory, in a saturated condition, almost no oxygen is available to enable the corrosion process. On the contrary, for lower relative humidity, oxygen is available and might lead to corrosion.

Figure 3.2 – Specimens preparation: a) mix prepared, b) mixes placed into metallic moulds, c) curing in the wet room and d) curing in the climatic room.

3.2.3. Characterization tests

In an effort to characterize the effects of chlorides in the specimens over time regarding aesthetic aspect and mechanical response, three experimental tests were performed. Visual inspection of the surface was performed to detect deposition of corrosion products that might affect the aesthetics of the specimens. Three-pointing bending test was performed to assess the influence of corrosion in the mechanical behaviour. A visual inspection of cut cross-sections was conducted after the bending test to identify the corrosion profile.

Visual inspection of the surface

The aspect of the surface and the signs of corrosion were monitored from the demoulding until the age of mechanical testing. Prisms were turned 90° from the casting

surface and one of the faces was chosen for the analysis. The number of corrosion spots on the surface of the specimen (see Figure 3.3) was assessed and the criteria in Table 3.3 was used to classify the level of corrosion.

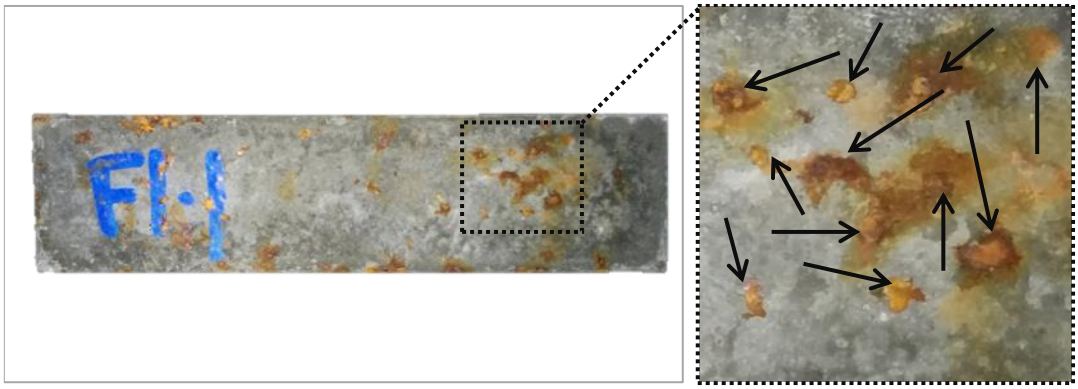

Figure 3.3 – Corrosion spots on the surface of the specimen.

Table 3.3 – Classification of levels of corrosion.

Level	Number of corrosion spots
Low	< 10
Medium	10 - 20
High	> 20

3-point bending test

In order to investigate the mechanical response of HPSFRCCs, 3-point bending tests were performed according to a modification of the UNE-EN 196-1:2005. An Ibertest MEH 3000 kN press and a bending apparatus were used. A displacement control of the relative movement of the plates of the press was used. For that, a LVDT was installed, as shown in Figure 3.4. For each age and mix, four specimens were tested to obtain the first crack load, the maximum load and the residual loads.

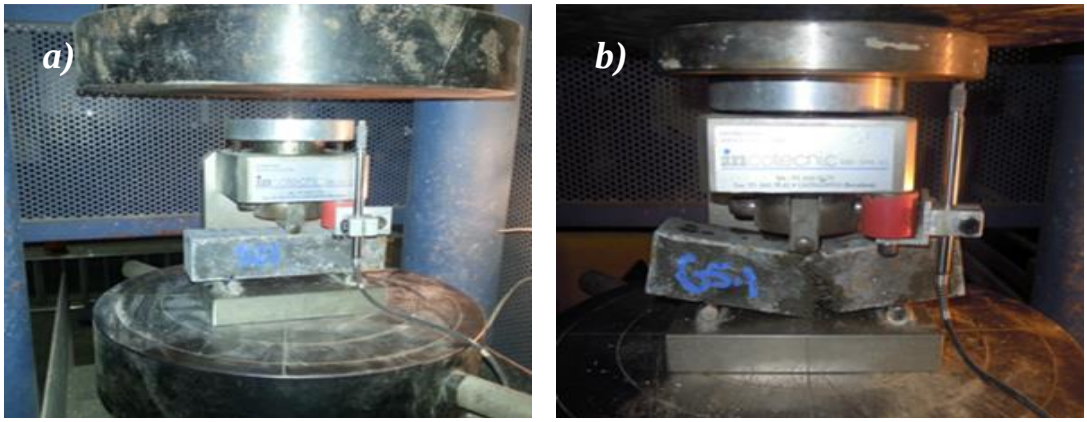

Figure 3.4 – 3-point bending test: a) specimen in the apparatus for the test and b) specimen failure after the test.

Visual inspection of the cross section after bending test

After the mechanical tests, 2 slices with 1 cm of thickness were cut from each specimen perpendicular to the length of the specimen (see Figure 3.5-a). Then the dust generated by cutting was cleaned to allow adequate inspection of the cross-section (see Figure 3.5-b). Finally, the cross-sections were inspected with a Stereo Microscope.

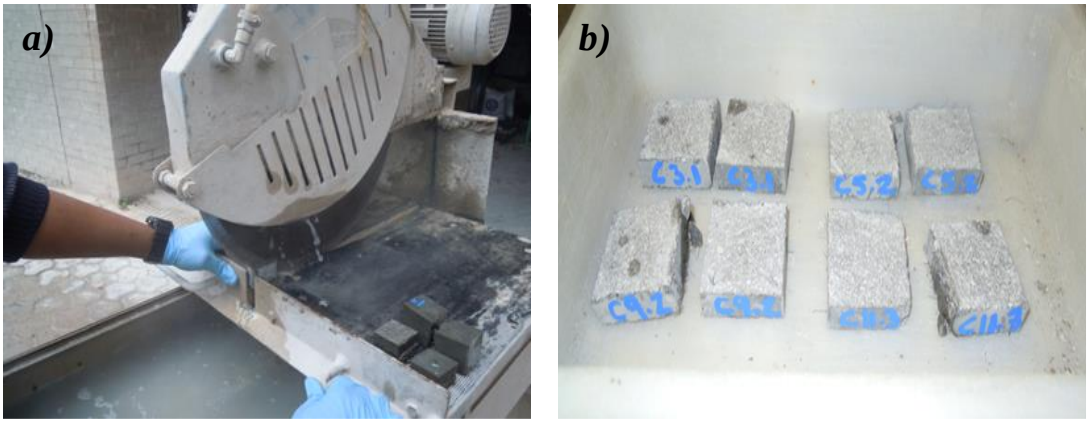

Figure 3.5 – Preparation of the specimens: a) cutting of the 1-cm thick slices and b) 2 pieces of each specimen for the inspection.

3.3. SPECIFIC EXPERIMENTAL PROGRAMME

A specific experimental programme was performed to assess the effect of chloride corrosion in pre-cracked and uncracked HPSFRCC specimens under cyclic conditions. The following specific objectives are defined:

- Investigate the effects of chlorides regarding the aesthetic aspect;
- Investigate the influence of corrosion in the post-cracking behaviour of pre-cracked and uncracked specimens;
- Analyse the level and depth of corrosion of the fibres in specimens over the cycles.

3.3.1. Materials and mixes

Portland Cement CEM I 52,5R (without additions), silica sand with 0.3-0.4 mm size, potable water from the public network were used. The amount of water added was corrected following the same procedure described in section 3.2.1. Mixes with Dramix® OL13/.20 (see Table 3.1) steel fibres in contents of 0, 90, 140 and 190 kg/m^3 were produced. An amorphous nanosilica suspension of type Meyco MS 685 and ultrafine calcium carbonate of type Betoflow were used to improve the density and mechanical properties of the paste. A superplasticizer of type Glenium ACE 425 was added in different to ensure similar workability and to reduce the water-cement ratio.

Table 3.4 shows the composition of the mixes used, which represent an improvement in relation to those characterized in the preliminary experimental programme. Notice that the superplasticizer content remained constant for mixes with the same w/c, regardless of the fibre content. All of them were self-compacting and did not require any vibration during the production of the specimens. Mixes with all fibre contents were produced with a w/c of 0.23. Mixes with fibre contents of 90 and 190 kg/m³ were also produced with w/c of 0.28 to assess the influence of the w/c in the corrosion.

Table 3.4 – Mix composition for the specific experimental programme.

Materials		**Mixes**					
		1	**2**	**3**	**4**	**5**	**6**
Cement I 52.5R	kg/m³	800	800	800	800	800	800
Silica sand 0.3-0.4 mm	kg/m³	1161	1131	1108	1098	1129	1098
Water	kg/m³	129	129	129	129	184.6	184.6
Superplasticizers	l/m³	32	32	32	32	15.4	15.4
Nano silica	l/m³	40	40	40	40	40	40
Calcium carbonate	kg/m³	200	200	200	200	200	200
Steel fibre OL 13/0.20	kg/m³	0	90	140	190	90	190
w/c	-	0.23	0.23	0.23	0.23	0.28	0.28

3.3.2. Specimens preparation

Due to the large number of specimens needed per composition, the production process was performed at the facilities of the company ESCOFET S.A., which has extensive experience in manufacturing HPSFRCCs and UHPSFRCCs elements. Table 3.5 shows the sizes and number of specimens produced.

Table 3.5 – Size and quantity of the specimens.

Specimens size (mm)	**Quantity for each mix (unit)**	**Total quantity (unit)**
Cylinder 100 x 200	10	66
Prism 40 x 40 x 160	200	1200

Cylinders for control tests were cast in metallic moulds and prims for the durability test were cast in disposable moulds due the large number of specimens per mix. The first step of the production process was to organize the metallic moulds (Figure 3.6-a). Then, one layer of a de-moulding agent was sprayed in the metallic moulds.

A 1000 litres vertical axis mixer (see Figure 3.6-b) was used to produce 1 batching volume per composition. Initially, the dried components (cement, silica sand and calcium carbonate, in this order) were weighed and placed by means of a conveyor belt into the

mixer and mixed for one minute. Subsequently, water, nanosilica and steel fibres were added manually and mixed for approximately four minutes.

Figure 3.6 – Preparation of the specimens: a) moulds and b) vertical axis mixer.

Small amounts of material was extracted from the mixer to assess the flow extent according to the procedure described in the preliminary experimental programme (see Figure 3.7). The test also allowed a qualitative evaluation of the material stability by analysing signs of fibre segregation, such as the formation of lumps and irregular distribution of fibres. Once approved, mixes were placed in a skip with straight outlet that was transported over the moulds and opened to cast the specimens (see Figure 3.8-a). The excess of materials over the moulds was removed manually (Figure 3.8-b).

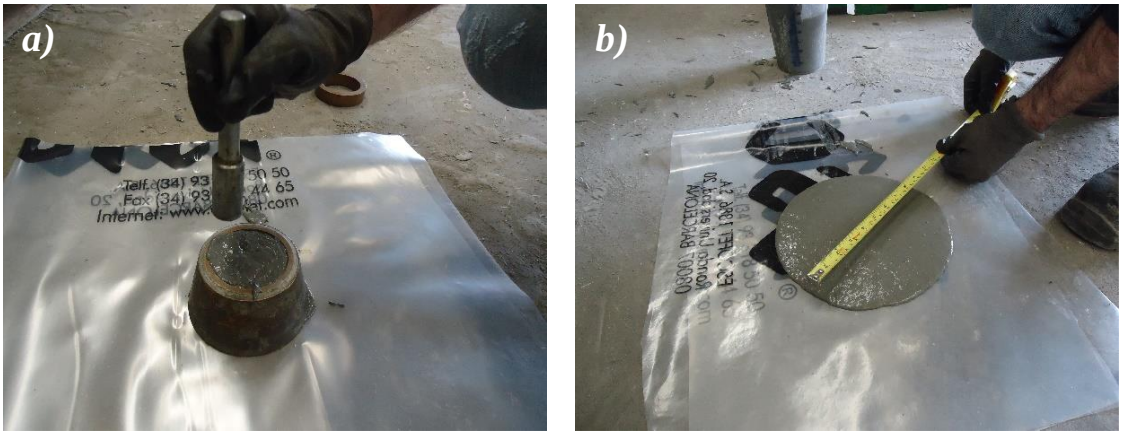

Figure 3.7 – Flow extent test.

Figure 3.8 – Casting process: a) filling the moulds and b) final aspect of moulds after removing excess.

Finally, a curing film was sprayed (Figure 3.9-a) over the samples to reduce the loss of water by evaporation (see Figure 3.9-b). Specimens were removed from the moulds within 24 hours of casting, identified by number and arranged on a pallet (see Figure 3.10-a). Then, they were packed with a plastic sheet (Figure 3.10-b) and stored at the company. Subsequently, they were transported to the Laboratory of Structure Technology Luis Agulló at the UPC and stored at ambient temperature.

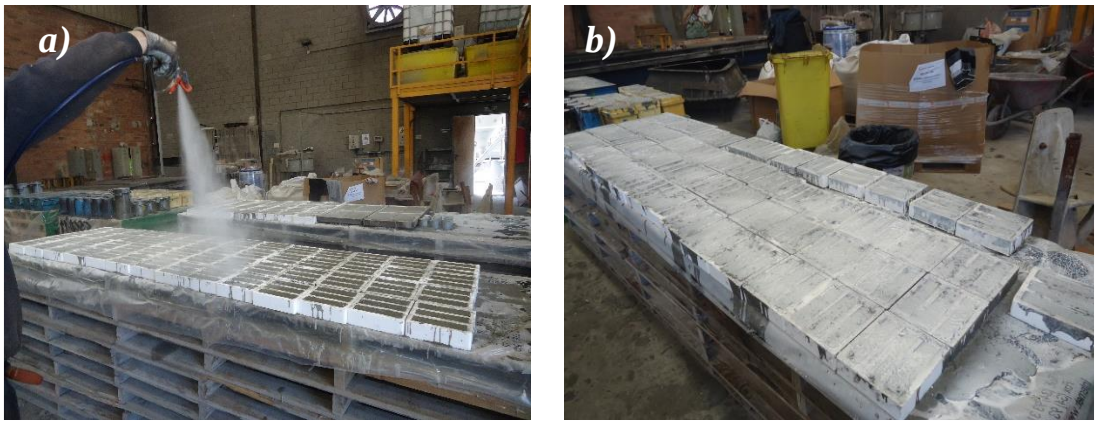

Figure 3.9 – Detail of: a) spraying the curing film and b) specimens with a layer of curing film.

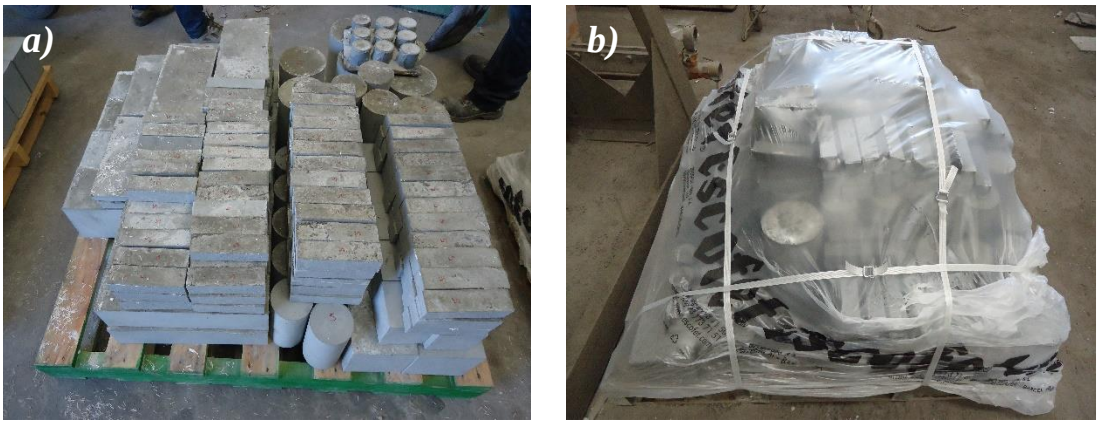

Figure 3.10 – Transport of the specimens: a) samples organized in a pallet and b) packed with a plastic sheet.

3.3.3. Procedures for the durability tests

Several activities were conducted to prepare the prism for the durability tests after production and curing. In this section, these activities are described following the order of execution.

Inductive method

To identify outlier specimens prior to the durability test, the inductive method (Cavalaro *et al*. 2015; Cavalaro *et al.* 2016) was applied. The method allows the assessment of the amount and orientation of steel fibre in the specimens. The apparatus for the test consists of a coil acting as a sensor and an inductance measurer. When the specimen is placed inside the coil, the magnetic field around it is affected by the fibres and the inductance value changes (see Figure 3.11-a). Each specimen is measured 3 times: with the axes x, y and z (see Figure 3.11-b) aligned with the axis of the coil. The sum of the measurements in the three directions provides information about the content of fibres in the specimen. The relative values in each axis provide information about the orientation of the fibres in the specimen. Figure 3.11-c and d show the inductive test set up performed for all specimens.

The biggest increase of inductance was observed along the x-axis of the specimen due to the preferential fibre alignment caused by the wall-effect of the moulds and the casting procedure. Therefore, the inductance in the x-axis was considered for the detection of outliers. Specimens with inductance out of the outlier limits were discarded from the study.

Mixes 03 (with w/c of 0.23 and 140 kg of fibre) and 04 (with w/c of 0.23 and 190 kg of fibre) had 1.30% and 6.70 % of the specimens discarded, respectively. Others mixes had no specimens discarded. Specimens not discarded were grouped in subsets corresponding to an initial condition (uncracked or pre-cracked) and 6 testing ages according to their x-axis induction. The aim of this grouping process was to guarantee that all sets have nearly the same average x-axis induction to reduce the influence of the scatter of the fibre content and distribution in the test results.

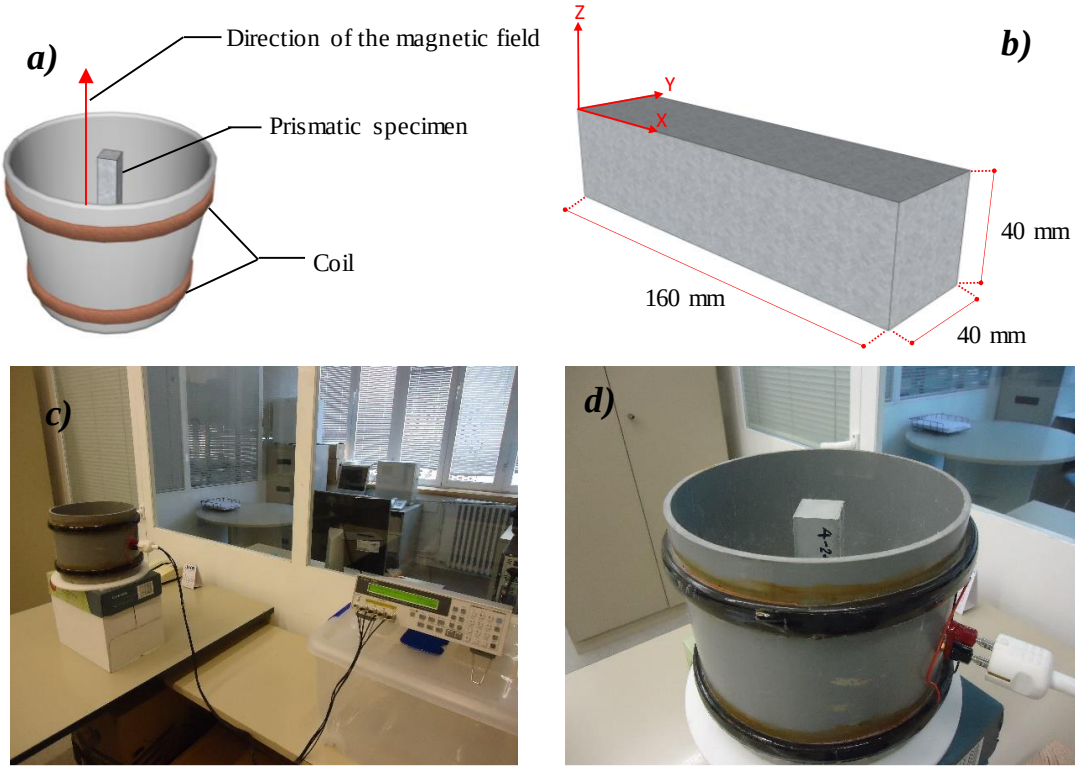

Figure 3.11 – Inductive method: a) apparatus for the test, b) directions of measurements, c) test set up with coil and inductance analyser and d) specimen placed into the apparatus.

Pre-cracking the prisms

To ensure that pre-cracking occurs at the centre of the prisms, all specimens were notched with the use of dry saw (see Figure 3.12-a). Prisms were turned 90° with the casting direction and sawn through of the width of the samples at midspan. The notch (see Figure 3.12-b) had width and the depth of 2 mm and 6.5 mm, respectively.

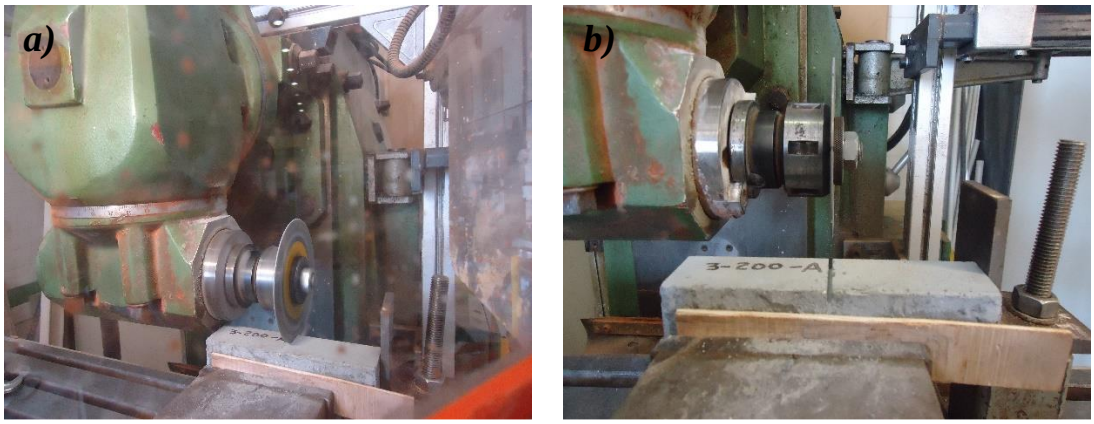

Figure 3.12 – Notching: a) dry sawing starting the notch and b) notch in the centre of the specimen.

Once notched, prisms were pre-cracked in a 3-point bending setup with a free span of 133 mm and loading at midspan. A clip gauge located at the tip of the crack controlled the CMOD during the pre-cracking stage (see Figure 3.13-a). Four different pre-crack

openings were defined for the tests: 0.05, 0.20, 0.35 and 0.50 mm. To ensure the pre-crack opening desired at the tip of the notch, trials were conducted with discarded specimens. After achieving a certain CMOD (see Figure 3.13-b), specimens were unloaded and examined by means of a stereo microscope with increase of 80x to assess the crack opening (see Figure 3.13-c and d).

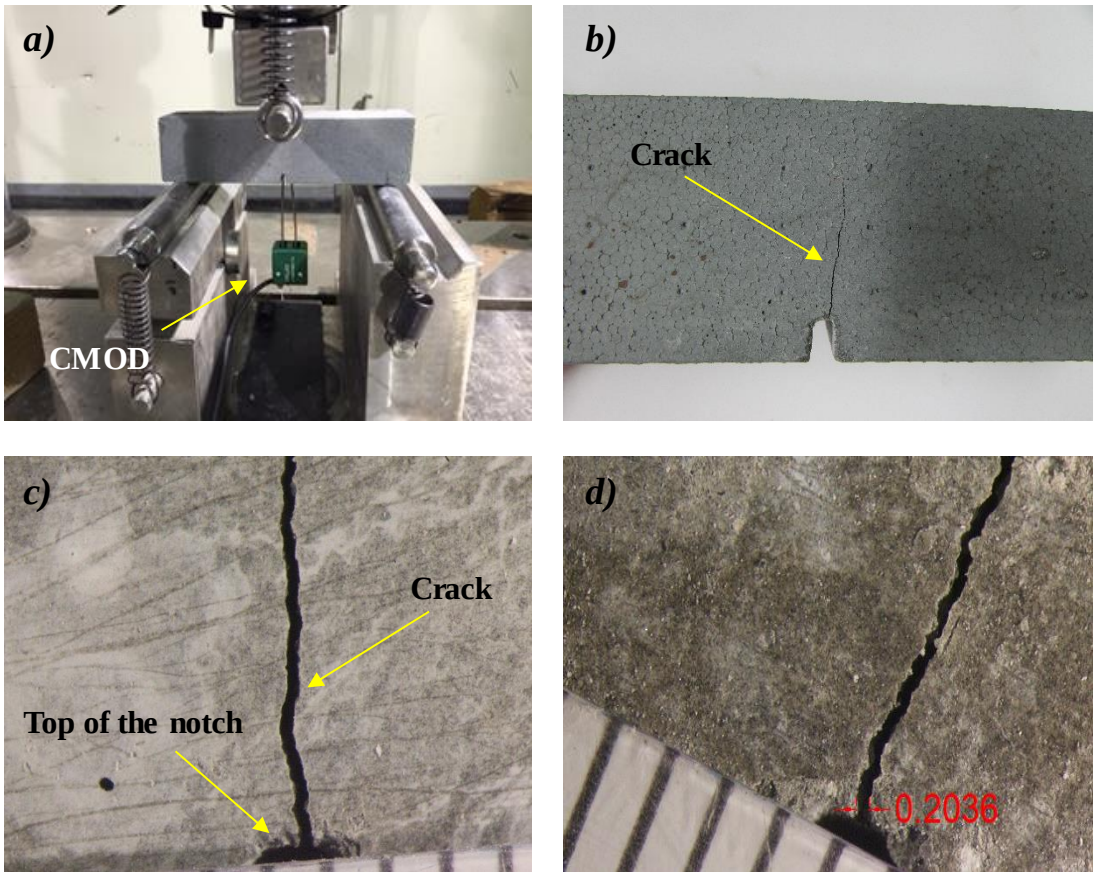

Figure 3.13 – Pre-cracking of the specimens: a) 3-point bending set up and b) crack generated on the surface, c) picture of crack from in the stereo microscope and d) measurement of the crack opening.

The same procedure was repeated until the target pre-crack opening was achieved. Then, the corresponding CMOD was fixed. In order to assure the desired crack opening for each mix, the same process of measurement was conducted for 10 samples of each mix and crack opening. Notice that for each fibre content the CMOD value fixed to achieve the pre-crack opening desired was different due to the variations induced in the CMOD recovery in the unloading stage. Figure 3.14 shows the Load-CMOD curves for crack openings of 0.05, 0.20, 0.35 and 0.50 mm for samples with 90 kg/m^3 of steel fibre. The fixed values of CMOD for each fibre content and crack opening are also summarized.

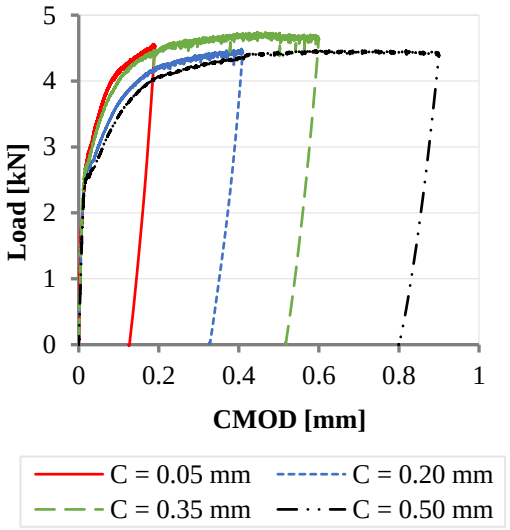

Code	CMOD [mm]
F90_C0.05	0.19
F90_C0.20	0.41
F90_C0.35	0.69
F90_C0.50	0.90
F140_C0.05	0.20
F140_C0.20	0.43
F140_C0.35	0.72
F140_C0.50	0.92
F190_C0.05	0.20
F190_C0.20	0.47
F190_C0.35	0.75
F190_C0.50	0.96

Figure 3.14 – Load-CMOD curves for pre-crack openings for 90 kg/m^3 of fibre and CMOD values for all pre-cracking openings and fibre contents.

Waterproofing of the surfaces

In order to allow the ingress of chlorides in only one direction, five faces of each specimen were waterproofed. A flexible water-based epoxy membrane resistant to high humidity and medium chemical attack (including salt water) was used. The epoxy membrane was applied with a brush to the faces of specimens in two coats (see Figure 3.15-a) with interval of 24 hours between them according to the producer's instructions. Afterwards the specimens were maintained stored for 7 days at ambient temperature for curing (Figure 3.15-b). To avoid the penetration of the product into the pre-cracks, an adhesive tape was placed over the face with the notch before the waterproofing. The adhesive tape was removed after the curing process.

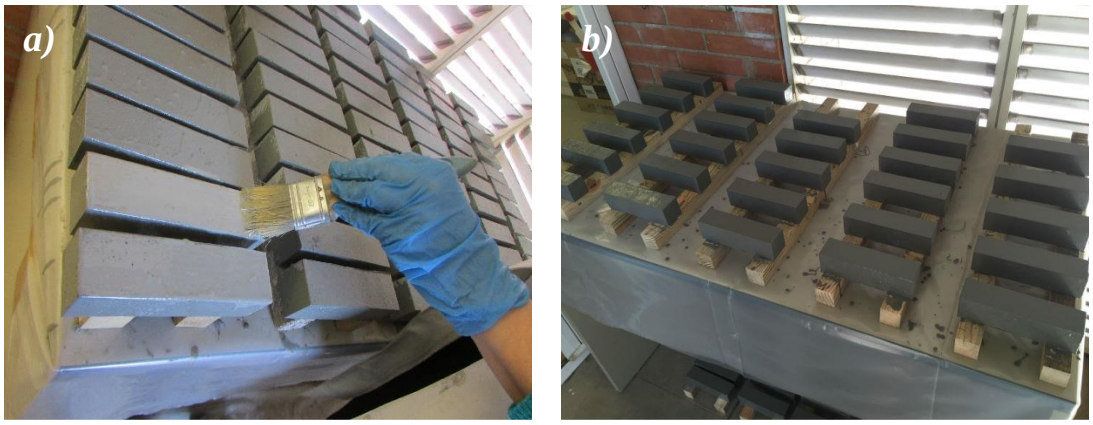

Figure 3.15 – Waterproofing the specimens: a) applying the epoxy membrane and b) curing of samples.

Wetting and drying cycles

After all preparation, specimens for the wetting and drying cycles were stored in plastic boxes and organized by each mix (Figure 3.16-a). Specimens were exposed to two wet (48 hours submerged in distilled water) and dry (48 hours at ambient temperature) cycles before being exposed to the aggressive environment. This ensured a similar saturation of the specimens in the beginning and during the cycles. If this procedure was not adopted, a more significant chloride ingress would occur in the first cycles due to the lower humidity of the specimen. Figure 3.16-b shows the first cycles of the samples with distilled water.

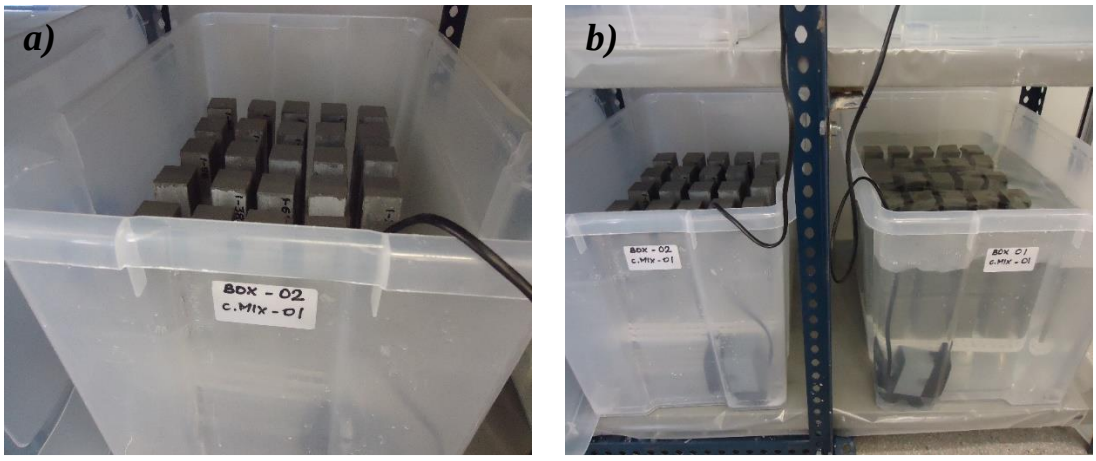

Figure 3.16 – Wetting and drying cycles with distilled water: a) specimens organized in the boxes and b) set up of the cycles.

After the two cycles, chloride (5% NaCl) was added to the same distilled water and the specimens were exposed to cycles of wetting and drying (Figure 3.17-a). This amount of sodium chloride was selected with the purpose of accelerating the corrosion. The complete cycle consisted of 48 hours submerged in salt water (wetting) and 48 hours at ambient temperature (drying). A circulation pump was used during wetting stage to circulate the salt water and avoid concentration variations with the depth. After two days of the wetting cycle, a suction pump extracted the salt water out of the box to start the two days of drying cycle (see Figure 3.17-b). Boxes were closed during the wetting cycles and opened during the drying cycles. The laboratory temperature was monitored kept almost constant during the time of exposure.

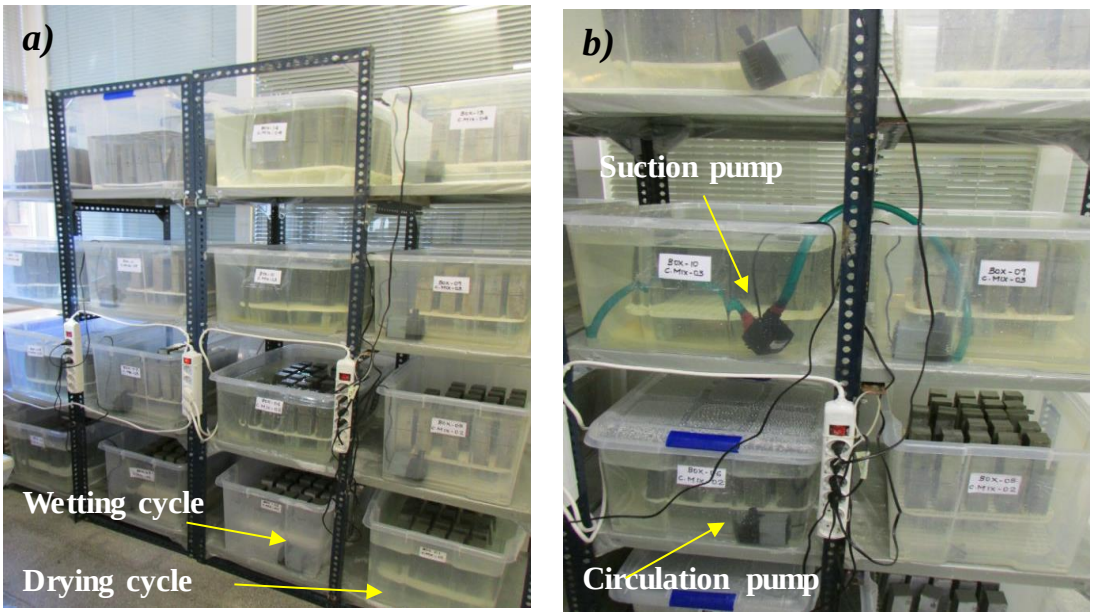

Figure 3.17 – Cycles: a) wetting and drying cycles and b) detail of pumping system.

The water level was controlled every cycle and the chloride content was adjusted monthly to guarantee similar conditions throughout the cycles (see Figure 3.18-a). The method to assess the chloride content consisted of taking a 1-ml sample of the solution of each box and adding silver nitrate (Figure 3.18-b). Then with the value of the free chloride content obtained from the measurer (Titrator micro TT 2050), the NaCl content in the adjusted when necessary in each box.

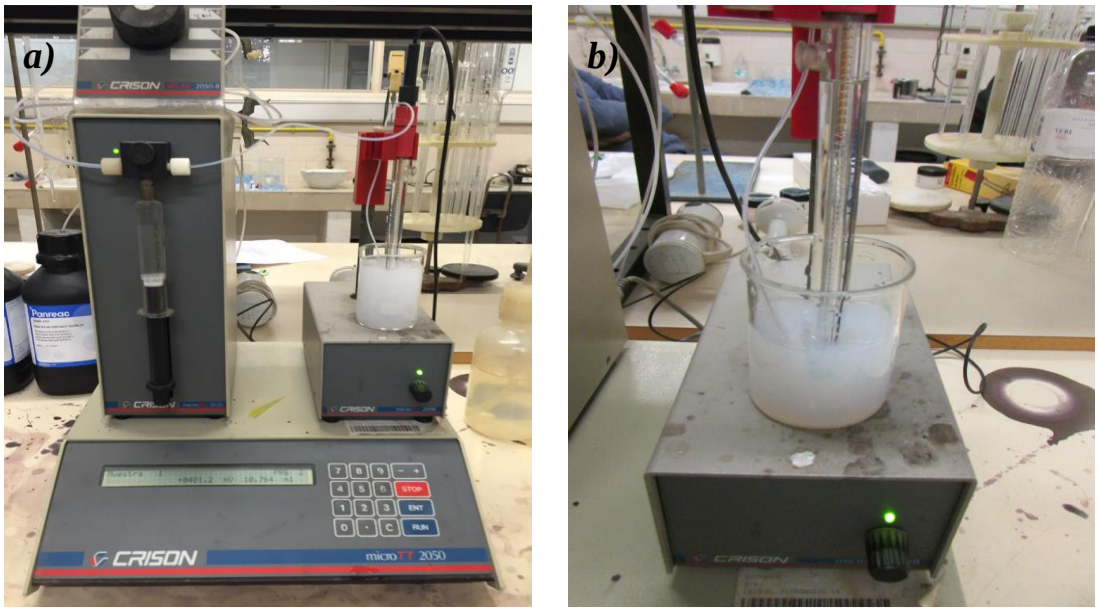

Figure 3.18 – Chloride content control: a) free chloride content test set up and b) silver nitrate and salt water.

3.3.4. Mechanical tests

3-point bending test

The assessment of the post-cracking behaviour of fibres after the cycles were conducted following the 3-point bending setup described in section 3.2 using a Instrom 5569 press with displacement control. Tests were performed at six different ages (0, 5, 35, 65, 95 and 125 cycles) in 4 prisms of each mix with uncracked section and 4 prisms with pre-cracked section (openings of 0.05, 0.20, 0.35 and 0.50 mm). The CMOD (Crack mouth opening displacement) gauge with length of 5 mm was placed at the crack mouth to measure the CMOD. The test was finished for CMOD = initial CMOD + 4 mm (see Figure 3.19).

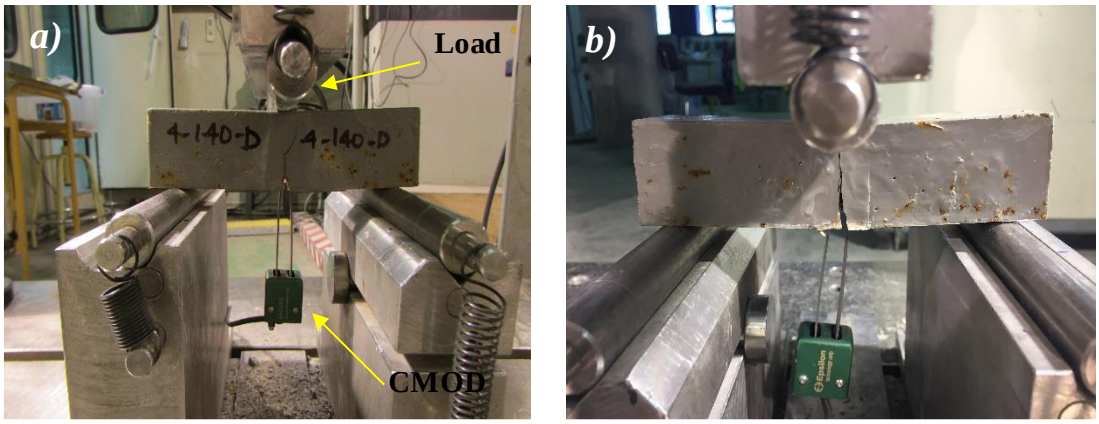

Figure 3.19 – Specimen for the mechanical test: a) set up and b) end of the test.

Analysis of the corrosion in the cracked section

The evolution of the corrosion was analysed throughout the cycles at each age of the mechanical tests. The level and depth of fibre corrosion in the cross section were assessed in the both cracked surfaces. For this, after the 3-point bending tests, the 2 parts of the same prism were completely separated and carefully analysed in a stereo microscope.

Tree different level of fibres corrosion were defined for the analysis: low corrosion for a very superficial corrosion of the fibres (see Figure 3.20-a); medium corrosion for a deeper corrosion that produces a slight loss of fibres cross-section (see Figure 3.20-b) and a high corrosion for a severe corrosion resulting in fibre breakage (see Figure 3.20-c) or complete loss of fibre cross-section (see Figure 3.20-d).

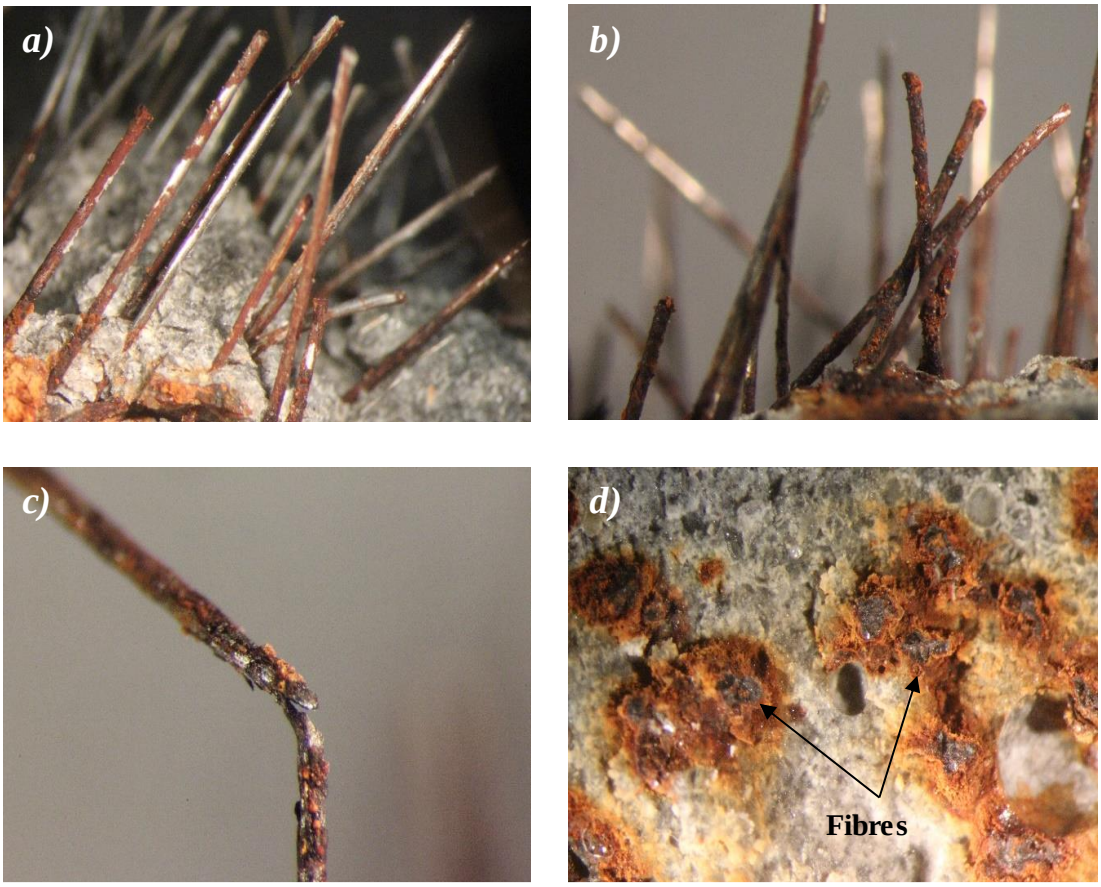

Figure 3.20 – Level of fibre corrosion: a) low, b) medium, c) high with breakage of the fibre and d) high with complete loss of cross section.

Finally, pictures were taken of both sides of the cracked section and the depth of each level of corrosion was measured from the top of the notch. Figure 3.21 shows an example of the depth and level of corrosion along the cracked section of both sides of one specimen. The average depth of both sides for the four specimens tested at each age was assessed.

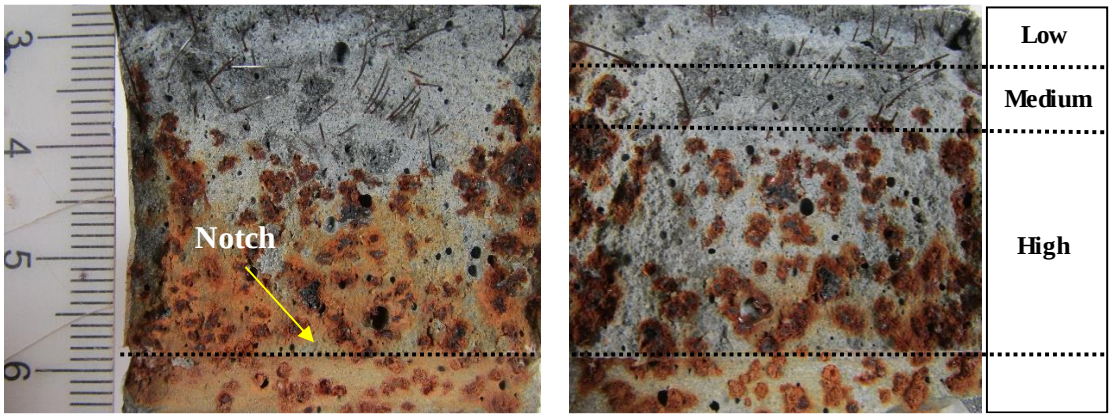

Figure 3.21 – Depth and level of the fibre corrosion along cracked section.

Analysis of chloride ingress in the cross section

The ingress of chlorides in the cross section was studied for uncracked section only. After the tests, 5 slices were cut from each specimen and sprayed with 0.1M silver nitrate solution. Then a picture of the sprayed section was taken (see Figure 3.22-a) and the depth of penetration of chloride was measured as a change in the colour. The presence of corroded fibres was studied over cycles with a stereo microscope (see Figure 3.22-b).

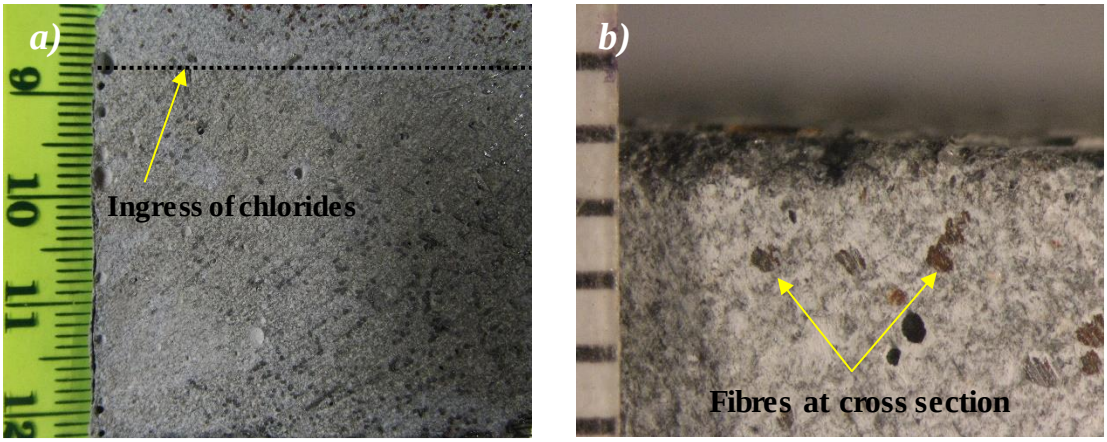

Figure 3.22 – Analysis of the cross section: a) depth of ingress of chlorides measured with colorimeter method and b) corroded fibres at the cross-section.

Analysis of the corrosion on the surface

The effect of steel fibres corrosion in the aesthetic aspect of HPSFRCC specimens was also investigated. For that, a group of 10 specimens of each mix was prepared with the same process as the samples for the mechanical tests and exposed to the same wetting and drying cycles. Every 10 cycles, pictures were taken of the surface of the specimens not coated with a water-based epoxy membrane. After that, the corroded area on the surface of each sample were analysed. To identify the evolution of the area with corrosion, an algorithm was developed and implemented in Matlab® using the HSV (Human Visual System) colour model. The first step was to transform the image from RGB (Red, Green and Blue) to HVS and decompose it into three layers that represent the model: hue (H), saturation (S) and brightness value (V).

For each of the layers the interest range is indicated by the histograms: for the hue, the pixels are separated with values from 0 (zero) to the threshold, for the saturation and brightness the pixels with values greater than the threshold are selected. Next, pixels that appear simultaneously in the range of interest of the three layers are identified as corrosion stains. The relation between the identified pixels and the total quantity of pixels of the image (resolution) defines the percentage of area with corrosion stains. Figure 3.23 shows a picture of a specimen before and after the image analysis.

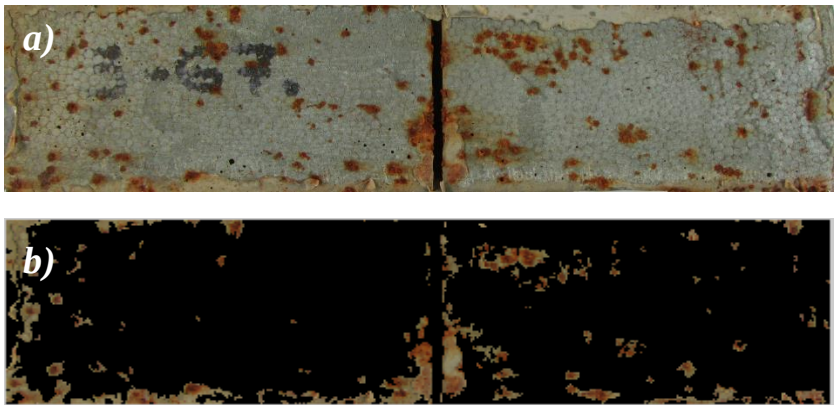

Figure 3.23 – Analysis of corrosion stains: a) before and b) after image analysis.

SEM and EDS microanalysis of the cross section

Scanning electron microscopy was used to evaluate how the ingress of chlorides influences the microstructure of the cement composites in cracked section. Tests were executed in a JEOL JSM 7100F microscope at the voltage of 20 kV. Regions were also analysed by EDS to obtain the relative intensity of the elements. For the tests the samples were coated with carbon.

The microanalysis of the walls of the cracked section was analysed at four ages (0, 35, 65 and 95 cycles). The fibre-matrix interface, the surface of the steel fibre, the phases deposited on the fibre surface, the holes produced after the fibres pull-out, the distribution of oxides in the cement matrix and the damage of fibre-matrix interface after fibre pull-out were analysed in each sample. The microanalysis of fibres without corrosion at 5 and 125 cycles was also performed.

4. RESULTS - PRELIMINARY EXPERIMENTAL PROGRAMME

4.1. INTRODUCTION

Chapter 3 of the thesis presented a preliminary experimental programme performed with the aim of investigating the effects of chlorides in uncracked HPSFRCC specimens. The short length of steel fibres and the improved interfacial transition zone between the fibre and the cementitious matrix (in the case of high performance concretes) are factors that may render the steel fibres less vulnerable to corrosion if compared to conventional reinforcement.

Studies from the literature show limited superficial damage of uncracked SFRC elements exposed to chlorides (Balouch *et al*. 2010; Serna and Arango 2008; Abbas 2014). However, more information is still required regarding durability of HPSFRCC given the high fibre content typically used in the mixes. Furthermore, the main mechanisms involving the chloride corrosion of high carbon steel fibres and its effects on the aesthetic and the post-cracking residual response are still unclear.

The **general objective** of this chapter is to present and discuss the results of the preliminary experimental programme performed to assess the effects of chlorides in HPSFRCCs in terms of aesthetic aspect and the mechanical response. For that, the following **specific objectives** are defined:

- Analyse the evolution of the level of corrosion stains deposited at the surface of the specimens;
- Evaluate the influence of the corrosion on the structural behaviour of the steel fibres over time;
- Identify the mechanisms according which the corrosion might affect the aesthetic and the mechanical response.

In section 4.2, the results of visual analysis of the surface is presented and analysed in terms of the influence of chlorides, time, curing condition and fibre content. In section 4.3, the results of the mechanical tests are presented and studied in terms of the load-deflection curves, first crack, maximum load and residual loads. Subsequently, in section

4.4, the visual analysis of the cross section conducted to investigate the level of fibres corrosion. Finally, in section 4.5, the main conclusions of the study are highlighted.

4.2. VISUAL ANALISYS OF SURFACE

4.2.1. Analysis of the influence of chlorides

Figure 4.1 presents the low and high levels of surface corrosion in one of the specimens with chlorides. The average number of corrosion spots and the level of corrosion (see section 3.2.3) for all fibre contents and age of tests for the samples without and with chlorides are summarized in Table 4.1.

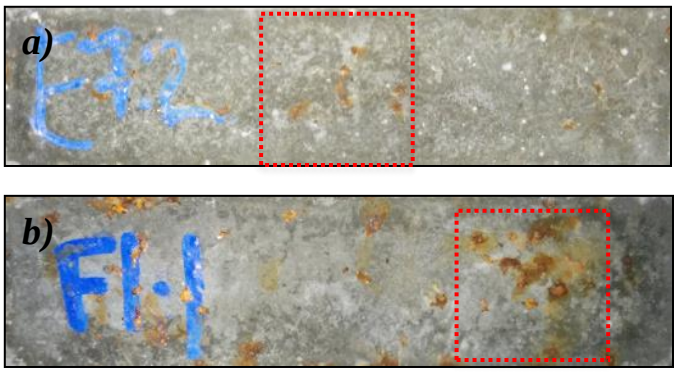

Figure 4.1 – Surface corrosion: a) low level and b) high level.

The results in Table 4.1 show that for all specimens without chlorides no sign of corrosion was observed at any of the ages evaluated. Despite the availability of humidity and oxygen over time, fibres remained protected by the alkaline matrix. Under alkalinity conditions, a very thin, dense and stable iron-oxide film is formed on the surface of the steel (Ghods 2010). This film is a passive layer which reduces greatly the mobility of ions between the steel and the surrounding cementitious matrix. Besides that, the lack of chlorides in the cementitious matrix did not induce corrosion initiation.

Surface corrosion was observed in all specimens with chlorides. The corrosion spots observed at the surface may be attributed to two main phenomena: the chloride induced corrosion of the steel fibre and the mobilization of the products of corrosion to the surface. The hole process includes the dissolution and oxidation of the of the iron and the precipitation of the ferric oxides (see equations (2.1 – 2.5)). The mechanisms of steel fibre corrosion involve the breakage of the passive layer due to the presence of chlorides, the dissolution of iron and production of the ferrous hydroxide ($Fe(OH)_2$) and of the insoluble ferric oxide (Fe_2O_3) as described in section 2.3. For fibres close to the surface, the process of corrosion is more expressive. The proximity to the surface favours the exchange of oxygen and humidity, increasing the corrosion rate and the mobility of compounds that are subsequently deposited at surface.

Table 4.1 – Number of corrosion spots and level of corrosion.

Nomenclature	Fibre content (kg/m^3)	Cure condition	Age of tests (days)	Average number of corrosion spots		Level of corrosion (specimens with chlorides)
				Without chlorides	With chlorides	
F40_R1_16	40	wet room	16	0	6.0	low
F40_R1_30	40	wet room	30	0	8.0	low
F40_R2_49	40	wet and climatic room	49	0	9.0	low
F40_R2_109	40	wet and climatic room	109	0	9.0	low
F80_R1_16	80	wet room	16	0	12.0	medium
F80_R1_30	80	wet room	30	0	14.0	medium
F80_R2_49	80	wet and climatic room	49	0	16.0	medium
F80_R2_109	80	wet and climatic room	109	0	19.0	medium
F120_R1_16	120	wet room	16	0	16.0	medium
F120_R1_30	120	wet room	30	0	19.0	medium
F120_R2_49	120	wet and climatic room	49	0	26.0	high
F120_R2_109	120	wet and climatic room	109	0	31.0	high
F160_R1_16	160	wet room	16	0	17.0	high
F160_R1_30	160	wet room	30	0	20.0	high
F160_R2_49	160	wet and climatic room	49	0	28.0	high
F160_R2_109	160	wet and climatic room	109	0	35.0	high

4.2.2. Analysis of the influence of time and curing condition

For the analysis of the influence of time and curing condition in the surface corrosion, the mechanisms during the curing should be highlighted. Over time the specimens were subjected to two different exposure conditions which favoured the process of corrosion. In the first condition (R1), after one day of production, samples had been subjected to 44 days under wet room and in the second condition (R2) specimens continued in climatic room until the age of the tests.

Figure 4.2 illustrates the mechanisms during the exposures conditions R1 and R2. The corrosion of the steel is an electrochemical process. In the case of the specimens with chlorides into the matrix, such presence provides thermodynamic conditions to induce corrosion. However, the kinetics of the process depends on the presence of oxygen and water which also controls its velocity. The electrochemical corrosion is impossible

without the simultaneous presence oxygen and water. According to Rodriguez (2001), the corrosive process occurs with the consumption of water and oxygen at the same time.

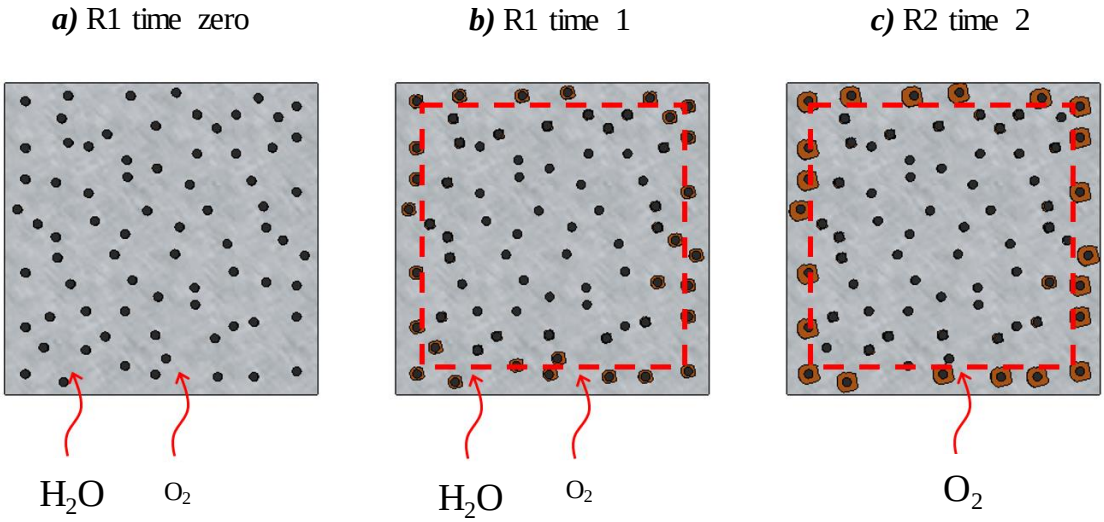

Figure 4.2 – Exposure to oxygen and humidity at both curing conditions over time.

In the first curing condition (R1) and time zero (see Figure 4.2-a), specimens had a high saturation level (due to the 90% relative humidity at wet room), and a limited amount of oxygen coming from outside. The chlorides in the matrix allows the corrosion initiation close to the surface that consumes most of the oxygen available. The presence of abundant water facilitates the movement of corrosion products that may reach the surface causing the first stain points. Over time and until 45 days (see Figure 4.2-b), corrosion progresses at slow rates due to the limited amount of oxygen available. Consequently, the rate of corrosion and of formation of corrosion spots reduces.

After 45 days (see Figure 4.2-c), the change of curing condition to R2 (under climatic room with relative humidity between 45% to 55%) reduces the availability of water and increases drastically the availability of oxygen close to the surface. This accelerates the rate of corrosion of fibres near the surface in an initial stage. The excess of water inside the specimens tends to move to the outside in order to reach an equilibrium with the new external environment. In the process, water brings ferric oxides to the surface, also accelerating the formation of corrosion spots. The rate of corrosion and of formation of corrosion spots should reduce again as the amount of water available at the surface reduces.

Based on the mechanisms of corrosion mentioned above, the influence of the time and curing condition are analysed for the samples with chlorides. For that, a velocity of formation of corrosion spots at surface and the number of corrosion spots detected with the tests were considered. Figure 4.3-a shows the curves of the velocity of formation of corrosion spots at surface for each fibre content and Figure 4.3-b presents the number of corrosion spots over time. The dashed lines in the graphs indicate the change of curing condition from R1 to R2 at 45 days.

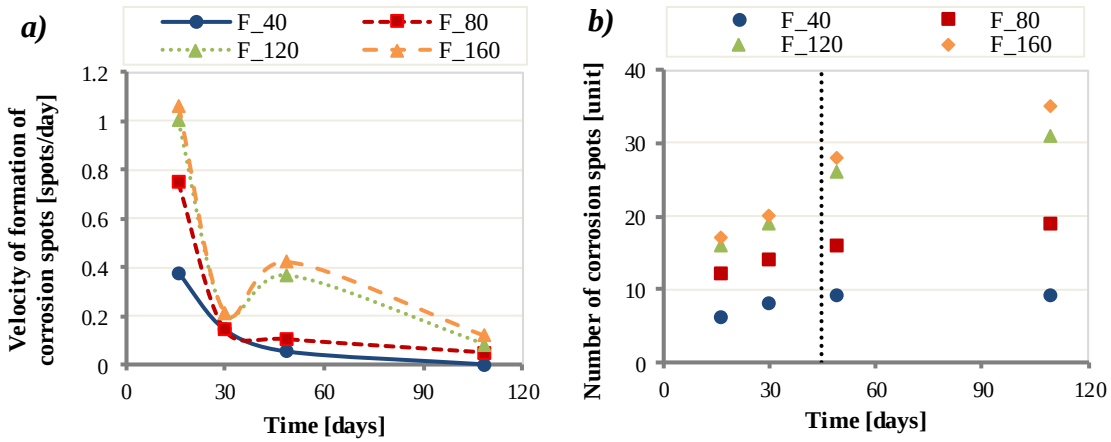

Figure 4.3 – Evolution of the surface corrosion: a) velocity of formation of corrosion spots and b) absolute number of corrosion spots at surface over time.

Figure 4.3-a shows that the first curing condition (R1) at 16 days presents the greatest velocity of formation of spots at the surface. This confirms the mechanism described previously, suggesting the oxygen available is consumed. Moreover, the presence of chlorides into the matrix and the fibres with only a very thin covering allow the corrosion. The condition R1 at 30 days presents an expressive reduction of velocities of formation of corrosion spots when compared to 16 days due to the consumption of the oxygen available. Such phenomenon may be expected since the corrosion occurs by means a cathodic reaction with the reduction of oxygen simultaneously with anodic reaction of dissolution of the iron. The ingress of oxygen is limited by the high saturation of the specimens.

At 49 days, the curing condition R2 (climatic room) provides a considerable increment of oxygen available. Mixes with higher fibre content showed an increase in the rate of formation of corrosion spots, whereas those with lower contents show smaller rates despite the change in the environment. Mixes with higher fibre content have bigger volume of steel close to the surface, which have reached lower levels of corrosion in the curing stage R1 since the limited oxygen available had to be shared by a bigger number of fibres. When the amount oxygen increased in curing R2, corrosion was reactivated, leading to an increase of formation of spots at the surface. By contrast, mixes with smaller fibre content might have reached a higher degree of corrosion in R1. The increment in terms of corrosions spots due to change of environment was significantly smaller in this case as most of the spots had already been formed in R1.

The condition R2 at 109 days presents the lowest velocities of formation of corrosion spots. Although the availability of oxygen is high, at this age the degree of saturation of the surface should have reduced considerably, limiting the progress of the corrosion process and the mobility of the corrosion products towards the surface. In addition to that, most of the fibres had already been affected in previous ages, meaning that additional spots did not form.

4.2.3. Analysis of the influence of fibre content

The influence of the fibre content in the surface corrosion is studied for 16, 49 and 109 days for all samples with chlorides. Figure 4.4 presents the percentage of increment of corrosion spots at the surface for the fibre contents 80, 120 and 160 kg/m^3, considering the mix 40 kg/m^3 as a reference (100%). In all cases, an increase in the fibre content leads to a bigger number of corrosion spots at the surface of the specimen. This outcome is attributed to the bigger number of fibres located closer to the surface. The low water-cement ratio of the mixes creates a matrix with low diffusion coefficient. Consequently, only fibres close to the surface have access to oxygen and water in the proportion needed to unchain corrosion and enable the movement of corrosion products to the surface.

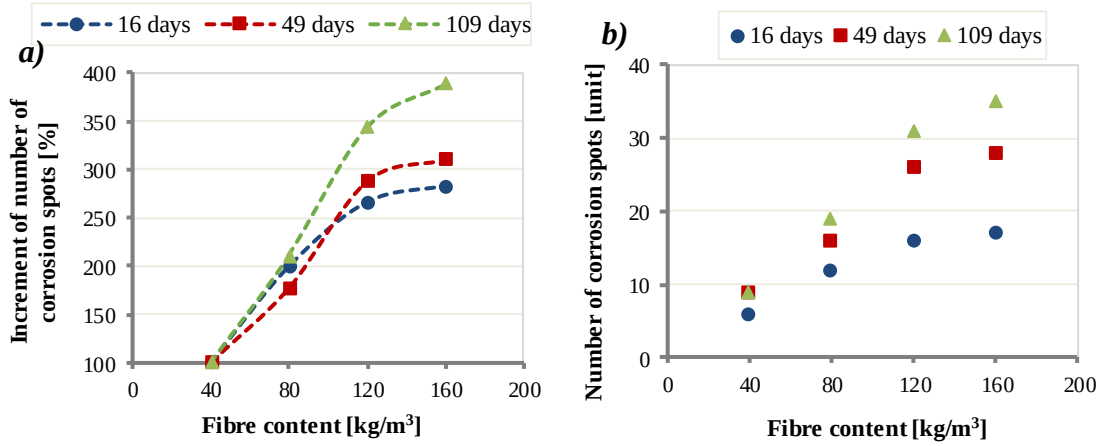

Figure 4.4 – Influence of the fibre content: a) relative increment of number of corrosion spots and b) number of corrosion spots.

Figure 4.4-a also reveals an almost linear increase (in %) of the number of corrosion spots with the fibre content for mixes with 80 kg/m^3 and 120 kg/m^3 of fibres Interestingly, the linear increment does not hold true for mixes with 160 kg/m^3. A possible explanation is that due to the high content, fibres near the surface are located close to each other, creating a superposition effect in which the deposition of the corrosion products of one fibre overlaps with that of other fibres. Consequently, the contribution of the corrosion of multiple fibres might be counted towards the formation of the same corrosion spots. On the contrary, for smaller contents, fibres near the surface are located farther from each other, enhancing the likelihood of formation of independent corrosion spots. Another possible explanation is that the degree of corrosion of individual fibres are lower in mixes with higher fibre contents since the oxygen and the water have to be shared between a bigger number of fibres.

4.3. 3-POINT BENDING TEST

The flexural response of specimens without and with chlorides were tested at 16, 30, 49 and 109 days. Figure 4.5 illustrates the main parameters extracted from the results of the test, which are the first crack load, the peak load and the residual loads L_{R3}, L_{R5} and

L_{R7} (residual loads at the distance of 3, 5 and 7 mm from the first crack deflection, respectively). In addition to those, the shape of the load-deflection curves was also studied. The influence of the corrosion was analysed for the variables: presence of chlorides, the time and curing condition and the fibre content.

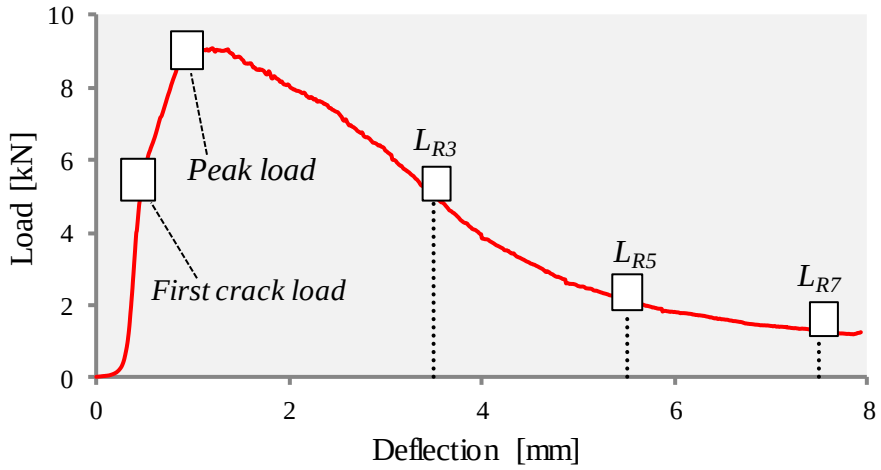

Figure 4.5 – Parameters of the load-deflection curve.

4.3.1. Load-deflection curves

Figure 4.6 presents the average load-deflection curves of specimens without and with chlorides at for all fibre contents at different ages. A general overview reveals that the shape of the curves of mixes with chloride is similar to that found in specimens without chloride. Although the presence of chlorides in the matrix may affects the hydration of cement phases modifying their quality and cause corrosion, it did not affect the shape of the curves.

In general, specimens show a stiff behaviour with high increase of load for low increments in deflection until the first cracks appear. Until this moment, the matrix is the main responsible for bearing the stresses in the cross section and the contribution of the fibres is limited. After that, an increase of both load and displacement is observed as fibres become active and bridge multiple cracks, leading to a strain hardening behaviour in flexion. Once the peak load is reach, a localization of cracking takes place, leading to a reduction of the load resisted.

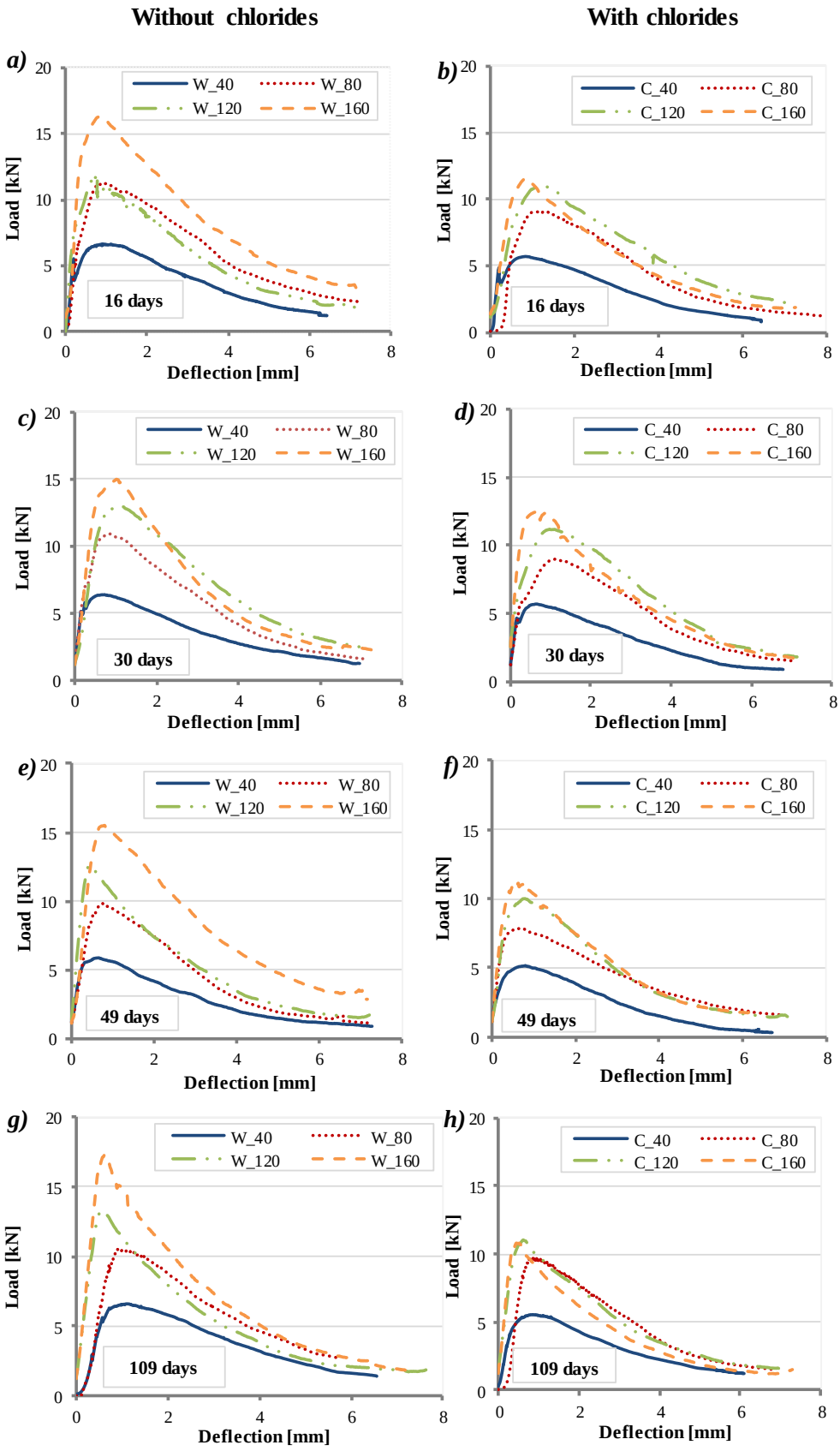

Figure 4.6 - Load-deflection curves for different ages and fibre content.

4.3.2. First crack

In addition to remaining dissolved in water and unbound, chlorides directly added to the matrix can be bound to the hydrated cement products through several processes that affect the strength, chemical composition, surface area, morphology, and the pore characteristics of the hydration products (Ramachandran 1971). The binding capacity is particularly affected by the contents of tricalcium aluminate (C_3A) and tetra calcium aluminaferrite (C_4AF) (Dousti *et al*. 2011). The chemical reaction with C_3A produces the calcium chloroaluminate hydrate ($C_3A.CaCl_2.10H_2O$), also known as Friedel's salt. Similar reaction between C_4AF and chlorides produce calcium chloroferrite ($C_3F.CaCl_2.10H_2O$). The fast reactions with aluminates tends to accelerate setting and increase the strength at initial ages. The accelerated crystals formed have different morphology, with less homogeneity, producing a less resistant matrix. Moreover, the compounds formed fill the porous of the matrix reducing space for posterior hydrated phases, such as the silicates.

According to Ramachandran (1971), chlorides also interact with C-S-H. They can create a chemisorbed layer over the C-S-H, penetrate in the C-S-H interlayer spaces, or be intimately bound to the C-S-H lattice. Chlorides are known to promote the formation of porous C-S-H and the leaching of $Ca(OH)_2$, compromising the long-term strength gain (Lee *et al*. 2000). Furthermore, the chloroaluminates produced might cause deterioration by decalcifications that are more noticeable at later days.

Figure 4.7 shows first crack load measured at 16, 30, 49 and 109 days for samples with and without chlorides with 40, 80 and 160 kg/m^3 of fibre. Graphs depicting the absolute and relative difference between equivalent mixes with and without chloride are also included. The first crack load is mainly determined by the properties of the cementitious matrix. Figure 4.7–a and Figure 4.7–b reveal that, the addition of chlorides reduces the stress bearing capacity of the matrix. Specimens without chlorides present slightly higher values of first crack load in comparison with equivalent specimens with chlorides. This may be a consequence of the change in cement hydration induced by the chlorides, as described previously. No clear trend on how the difference varies with the age, curing condition or fibre content is observed.

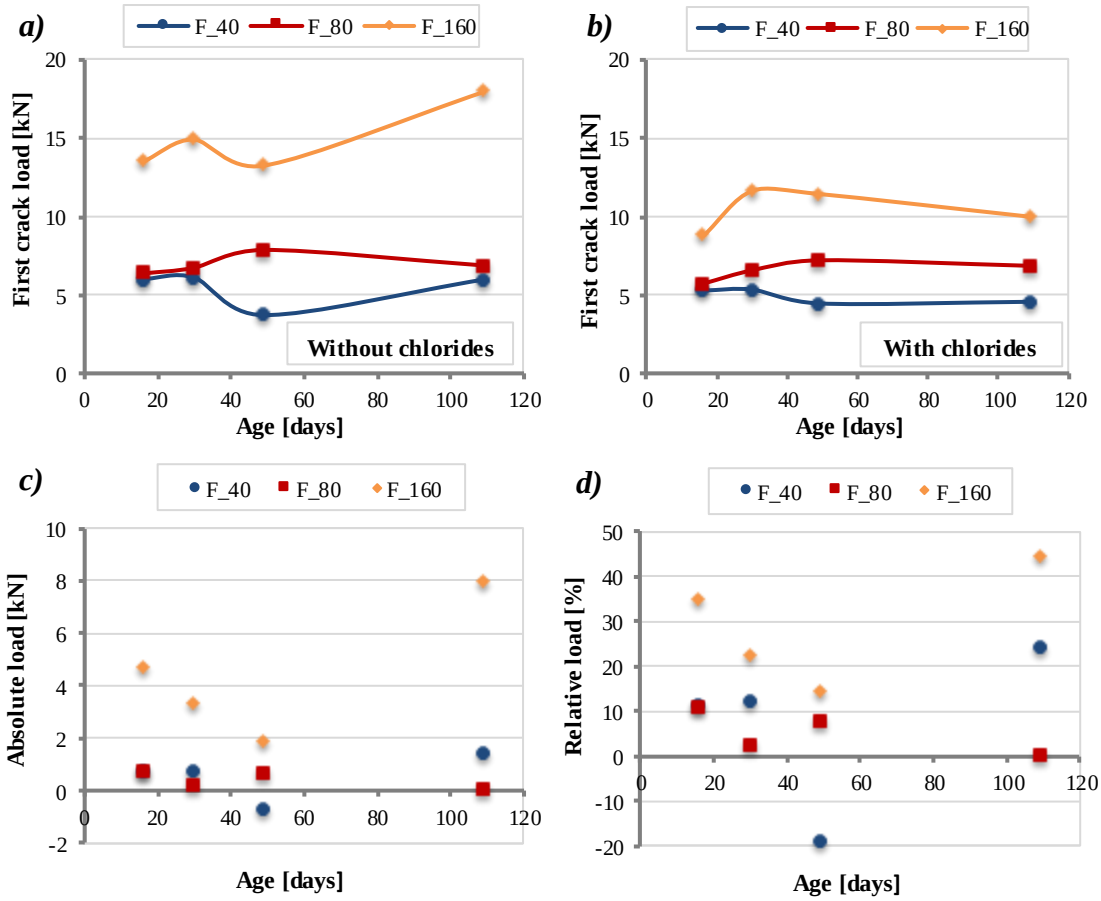

Figure 4.7 – First crack load: a) specimens without chlorides, b) specimens with chlorides, c) absolute and d) relative difference.

4.3.3. Maximum load

Figure 4.8 shows the curves of the maximum load and the graphs of the absolute and the relative load at 16, 30, 49 and 109 days for samples with and without chlorides for 40, 80, and 120 kg/m^3 of fibre. The maximum load is reached after a phenomenon of formation of multiple cracks. At this stage, the main mechanism affecting load reached is the bond between fibre and matrix.

The absolute and the relative values are the difference between the specimens without and with chlorides. As in the case of the first crack load, the inclusion of chlorides produces a consequent reduction of the resistant capacity. The level of reduction could be attributed to the influence of chloride in the normal hydration and to the corrosion of the fibres.

The percentage of reduction observed for the maximum load is similar to that observed for the first crack load and does not seem to increase with the age. Should the corrosion be the main cause, over time, the load resisted would reduce and the difference between mixes with and without chloride would increase. This contradicts the results of Figure 4.8, suggesting that the main cause of the difference is the influence of the

chlorides in the hydration process. The influence of fibre content and curing condition is not clear.

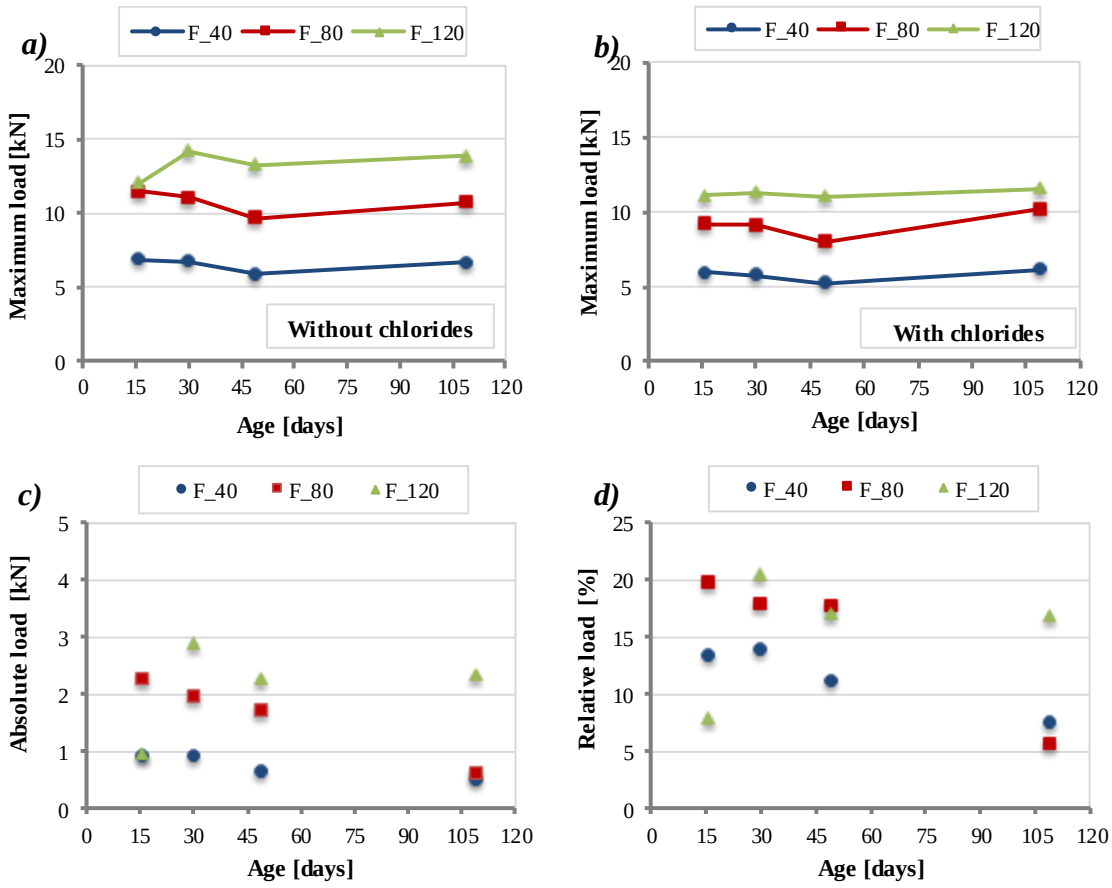

Figure 4.8 – Maximum load for 40, 80 and 120 kg/m^3 of fibre: a) specimens without chlorides, b) specimens with chlorides, c) absolute and d) relative differences between specimens with and without chlorides.

In the specimens studied, the corrosion affects a small number of fibres located in a thin layer close to the surface while in the interior region of the cross sectional the fibres remain almost unaffected. The fact that no decrease in maximum load is observed over time despite the increase in number of corrosion spots suggests that the corrosion of the fibres is not enough to compromise the maximum load. The dense matrix produced due to the low w/c and high cement content limits the diffusion of ions and elements needed to activate the corrosion. Therefore, despite the presence of chlorides, very limited corrosion was observed in the cross-section.

4.3.4. Residual load

Figure 4.9 shows the residual load for samples without and with chlorides for mixes with 40, 80 and 160 kg/m^3 of fibre measured at 16 and 109 days. In this case, the results correspond to the residual loads L_{R3} *and* L_{R5} (at the distance of 3 and 5 mm from the first crack deflection, respectively). The absolute and the relative difference between specimens with and without chloride are also presented. L_{R3} *and* L_{R5} are observed after

the peak-load, indicating a progressive crack opening characterized by the sliding of the fibres.

The residual load decreases with time, whereas the difference between specimens with and without chlorides increases with time. Moreover, the relative reduction is bigger than the observed for the first crack load. Such trend is more evident in mixes with higher fibre content. This suggests a possible influence of the corrosion process in the results, although definitive conclusions may not be drawn due to the influence of the chlorides in the hydration process.

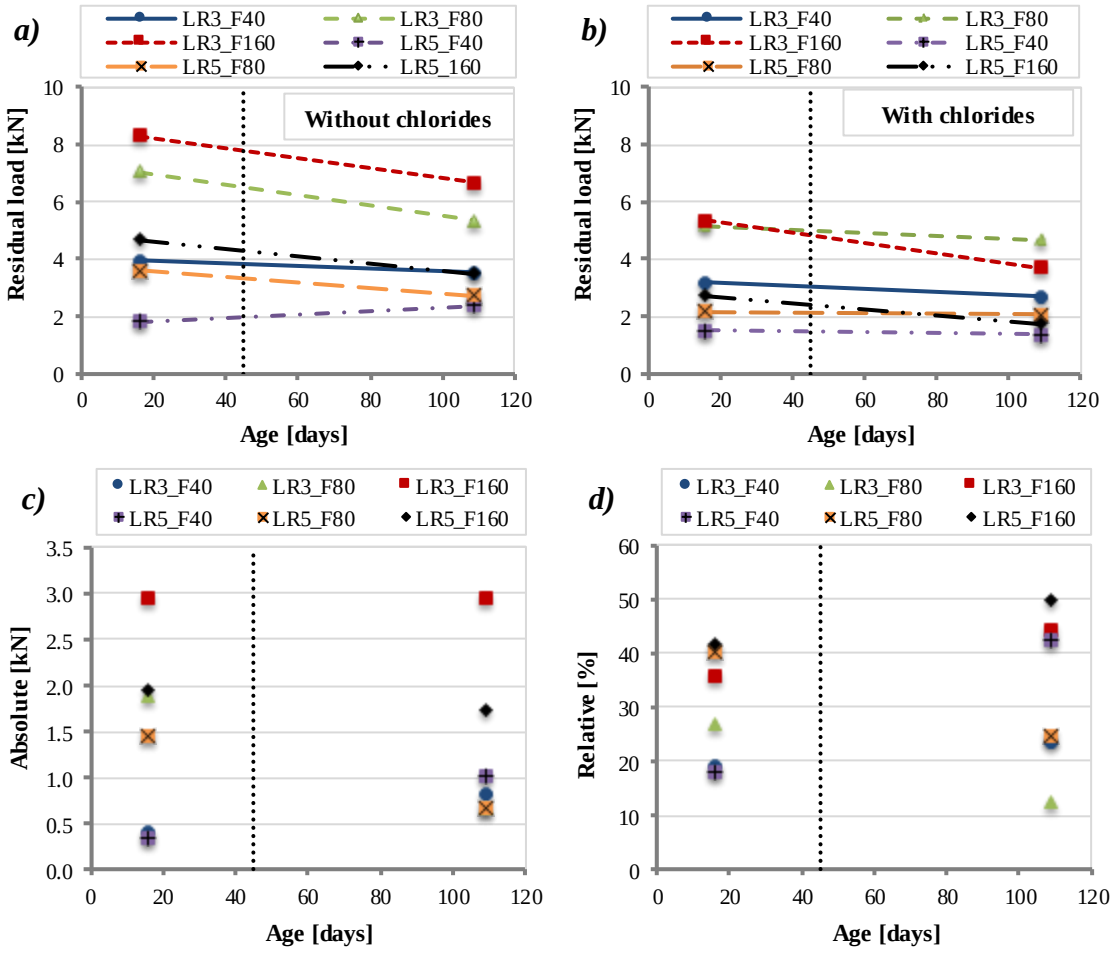

Figure 4.9 – Residual load for 40, 80 and 160 kg/m^3 of fibre: a) specimens without chlorides, b) specimens with chlorides, c) absolute and d) relative difference between mixes with and without chlorides.

4.4. ANALISYS OF THE FIBRES AT CROSS SECTION

4.4.1. Visual inspection immediately after the 3-point bending test

In order to analyse the corrosion of fibres, a visual inspection was performed immediately after the 3-point bending tests of all specimens. Figure 4.10 shows an example of a cross section of one specimen with chlorides. The high density of the matrix

does not allow deeper movement of water and oxygen in the specimen, contributing for a very superficial corrosion.

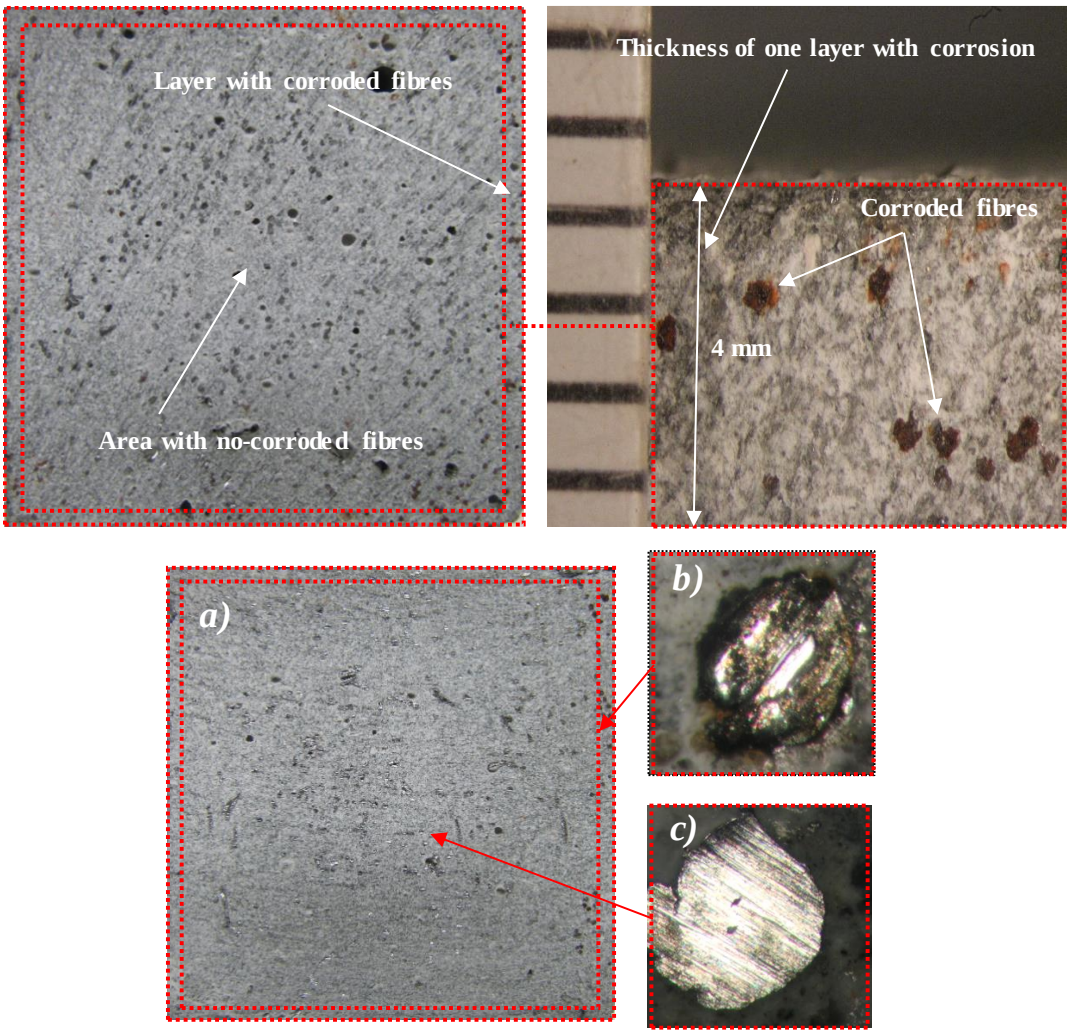

Figure 4.10 – Cross section of one specimen with chlorides: a) complete view of the cross section; b) corroded steel fibre from the border and c) no-corroded steel fibre from the centre.

The visual inspection indicated that only fibres at the surface presented signs of corrosion. On the contrary, fibres in the interior region of the cross section showed no sign of corrosion. Such result was expected since in the interior of the samples, the ingress of external water and oxygen to react with chlorides and the iron of the fibres may be very reduced. Although a high chloride content was added to the cementitious matrix, the process of corrosion depends on the availability of water and oxygen. No corrosion was observed in specimens without chlorides.

4.4.2. Visual inspection after exposure at climatic room

After the visual inspection immediately after the 3-PBT, slices were stored in the environment R2 for 7 days. Figure 4.11 shows a montage with the slices extracted from specimens with 40, 80, 120 and 160 kg/m^3 of fibre at 16, 30, 49 and 109 days. Images in

Figure 4.11-a was taken immediately after the 3-PBT and those in Figure 4.11-b was taken 7 days after, being kept in environment R2.

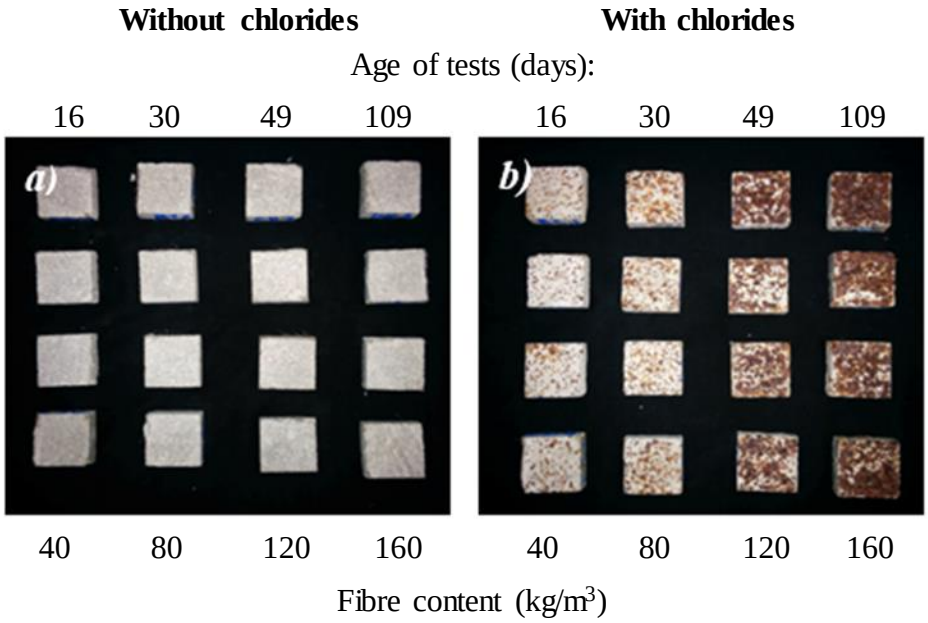

Figure 4.11 – Pictures of slices a) immediately after the 3-PBT and b) after additional storage in R2.

The cutting process used to produce the slices exposed areas from the inside of the specimen that had limited access to oxygen and water. In this condition, chloride present in the matrix enabled the rapid corrosion of the fibres. This confirms that free chloride was left to react with the fibres, which was not possible only due to the limited availability of oxygen and water attributed to the low diffusion coefficient of such a dense matrix. As expected, the area covered by corrosion products increases significantly with the fibre content.

4.5. CONCLUDING REMARKS

The preliminary experimental programme involved two types of analysis: the influence of chlorides in the aesthetic aspect and in the mechanical response. The following conclusions may be derived from the results of the tests performed:

- The presence of chlorides in the mixes led to the deposition of corrosion spots in the surface of specimens with chloride, whereas no spots were found in specimens without chloride. This corrosion is restricted to a thin layer close to the surface. The phenomena may be attributed to the ingress of external water and oxygen that reacted with the chlorides and the iron of the fibres to generate corrosion products that were later mobilized to the surface. The increase in the formation of corrosion spots increases almost linearly with the fibre content. This has to be taken into account in elements with high aesthetic requirements.

- A decrease in the first crack load and maximum load values was observed for the specimens with chlorides. This does not seem the result of the corrosion of the fibres. Despite the advance of the corrosion over time confirmed by the formation of spots at the surface of the specimens over time, the difference between the load of specimens with and without chloride remain constant. The most probable cause is the influence of the chlorides in the normal hydration of the cement phases.

- A decrease is also observed in the residual load. In this case, however, the reduction becomes more evident over time. The influence of the corrosion may not be discarded, requiring additional studies.

- The visual inspections of cut specimens after the 3-PBT confirm that the corrosion occurred only in fibres located in a small layer close to the surface. By contrast, most of the cross section showed no sign of corrosion, despite the high chloride content. This confirms that the low diffusion coefficient of the matrix limits the availability of oxygen and water required to activate the corrosion, thus protecting the fibres. The small thickness of the layer affected is responsible for the lack of clear influence of the corrosion process in the mechanical response of HPSFRCC specimens.

5. CORROSION IN UNCRACKED SPECIMENS SUBJECTED TO WET-DRY CYCLES

5.1. INTRODUCTION

Chapter 4 showed that the presence of chlorides in HPSFRCC affects the aesthetics of specimens, leading to the formation of corrosion spots at the surface. Results from Chapter 4 suggest a small influence on the mechanical performance of uncracked sections, although further investigation is required on this matter. Some authors (Dauberschmidt 2006; Mangat and Molloy 2000; Nordström 2005) highlighted the limited corrosion on uncracked steel fibre reinforced concrete (SFRC) mainly attributed to the discontinuous nature of the fibres, the reduced surface roughness due to their manufacturing process and the dense and uniform fibre-matrix interfacial transition zone (ITZ). International standards and guidelines are unclear about the consideration of the fibre corrosion in HPSFRCC subjected to aggressive environments.

The use of wet-dry cycles has been an effective method to accelerate the corrosion-induced damage of SFRC (Marcos-Meson *et al*. 2018). Results on SFRC under cyclic chloride wetting and drying exposure (Serna and Arango 2008; Anandan *et al*. 2014) revealed a damage limited to stains at surface suggesting an early stabilization of the deterioration of the steel fibres. In the case of the structural response of uncracked specimens, sources report negligible loss (Anandan *et al*. 2014) and significant reduction (Anandan *et al*. 2014; Alizade *et al*. 2016) of the flexural strength (Anandan *et al*. 2014).

In this sense, a study regarding the effects of chloride corrosion on the surface aspect and on the structural behaviour for uncracked HPSFRCC specimens subjected to wetting and drying cycles may be of great interest in order to identify the level of damage in the case of a dense matrix with high fibre content.

In view of the exposed, the **general objective** of this chapter is to present and discuss the results of the specific experimental programme performed with the aim to study the effects of chlorides corrosion in HPSFRCCs in terms of aesthetic aspect and of mechanical response for uncracked specimens. For that, the following **specific objectives** are defined:

- Analyse the evolution of the area of corrosion at the surface over time;

- Identify the mechanisms that lead to formation of surface depositions due to chloride corrosion;

- Evaluate the influence of the corrosion on the structural behaviour for uncracked specimens.

Section 5.2 presents the evolution of the surface corrosion is presented and analysed in terms of the influence of time, fibre content and water-cement ratio (w/c). Section 5.3 discuss the results of the depth of ingress of chlorides and the rate of chloride penetration. Subsequently, section 5.4 address the visual analysis performed on the surface and on the cross section. Section 5.5 analyses the SEM-EDS analysis of the cross section, of the fibres and of the surface. The conceptual model of mechanisms of corrosion in HPSFRCCs is presented in section 5.6. Then, the results of the mechanical tests for uncracked section are presented and discussed in section 5.7. Finally, section 5.8 highlights the main conclusions of the study.

5.2. ANALISYS OF SURFACE CORROSION

In order to evaluate the effects of steel fibre corrosion in the aesthetic, 4 HPSFRCC mixes were exposed to wetting and drying cycles with and without chloride (see section 3.3.4). Pictures of the surface of the specimen were taken from 5 to 95 cycles, at every 10 cycles. Then, the pictures were analysed by means of an image analysis algorithm that quantified the percentage of surface covered by corrosion depositions. The so called “corroded area” represents the average value of 10 specimens tested for each cycle and mix.

The corrosion at the surface in structures under cyclic wet-dry condition is related to several transport mechanisms. Capillary absorption occurs when the concrete surface is not saturated and becomes exposed to a chloride solution. The capillary tension will drive the chloride into the concrete (Hooton and McGrath 1995). The pores will be filled by the solution until saturation and a level of concentration of chlorides will remain in the matrix. When the layers become saturated, the ingress of ions is governed by diffusion, seeking to attain equilibrium of the pore solution with the outside.

When the external environment dries, the pure water will evaporate from the pores, and the salts that were originally in the solution may precipitate in the pores close to the surface. Such movement generates a high concentration of chlorides, particularly in pores close to the surface of the sample. The drying of the concrete also helps to increase the availability of the oxygen required for steel corrosion, as oxygen has a substantially lower diffusion coefficient in saturated concrete (Hong 1998).

The surface corrosion in cyclic exposure is mainly affected by the rate at which the chlorides penetrate in the sample. The duration of the wetting and drying periods play the main role in the rate of chloride ingress. According to Hong (1998), if the wetting

period is short, the entry by absorption will carry the salts into the interior and be further concentrated during drying. Then, in presence of a level of humidity in the pores, the salts may enter deeper into the sample through diffusion.

Due to the dense HPSFRCC matrix, corrosion should be more significant for the fibres close to the surface. The proximity with the surface allows the reaction between the iron of the steel fibre, the chlorides, the water from the salt solution and the oxygen. Moreover, the movement of the oxidized compounds during the reactions and the flow of humidity enables mobilization of corrosion products and consequently deposition on the surface.

5.2.1. Influence of number of cycles

Figure 5.1 shows the pictures of the exposed surface and the corroded areas detected of a specimen with 90 kg/m^3 of fibre and w/c of 0.23. The figure illustrates the evolution of corrosion at 5, 35, 65 and 95 cycles. The graphs of the average percentage area of the corroded surface from cycles 5 to 95 and the relative increment related to cycle 5 (considered as 100%) are presented in Figure 5.2.

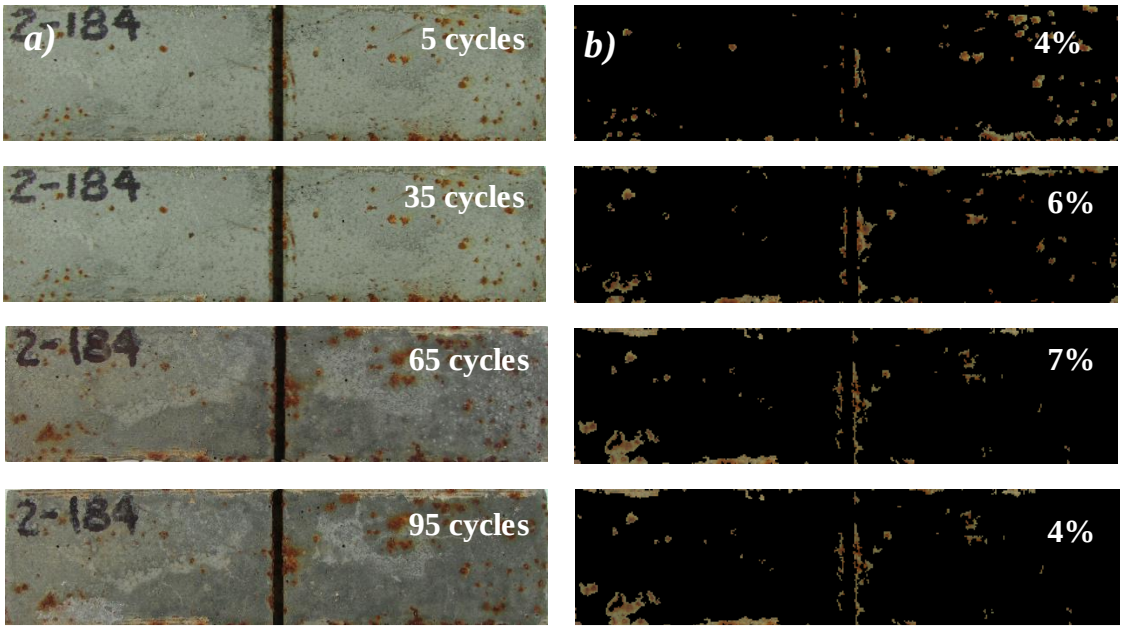

Figure 5.1 – Surface corrosion for specimen with 90 kg/m^3 of fibre and w/c of 0.23: a) pictures of the surfaces and b) corroded areas detected.

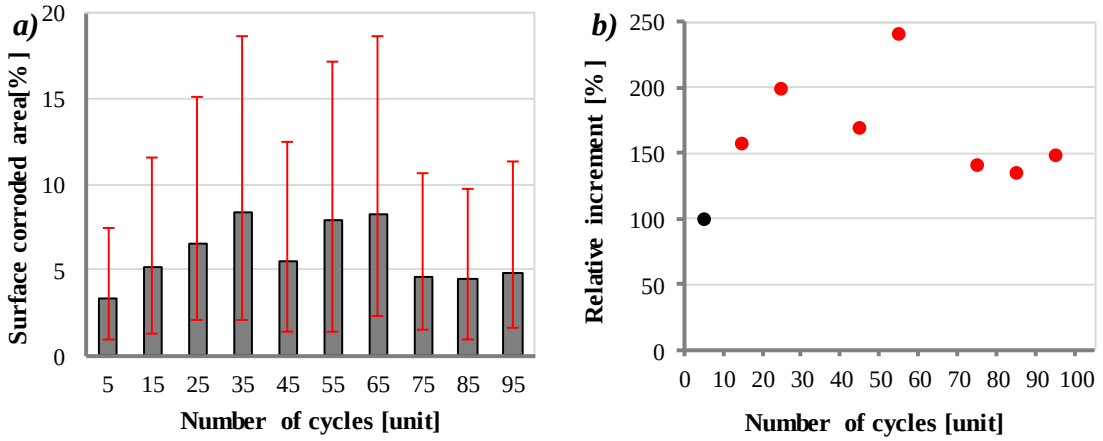

Figure 5.2 – a) Percentage of corroded area and b) relative increment of corroded area for specimen with 90 kg/m^3 of fibre and w/c of 0.23.

The results reveal that the number of wetting and drying cycles in salt solution influences the formation of surface corrosion. Surface corrosion is observed since cycle 5, increasing gradually until cycle 35. The ingress of water, chlorides and oxygen during the cycles induces the corrosion of the fibres placed close to the surface. The presence of water also facilitates the mobilization of the ferric oxides in the pores and their deposition over the surface.

After cycle 35, a decrease or stability in the corroded area is observed. This suggests a stabilization of the deterioration of the steel fibres which might be attributed to the absence of available fibre close to the surface to be corroded. Another explanation is the leaching of corrosion products. During the wetting period, the specimens submerged in salt solution may have the products close to the surface leached by the solution, which could be accelerated by the constant movement of liquids induced by the pumping system.

In order to detect the leaching process of iron oxides and hydroxides over cycles, the solids deposited at the bottom of the containers during the cycles were collected and analysed by SEM-EDS. Figure 5.3 presents the SEM images and the results of the microanalysis, which revealed the presence of ferric oxides. This confirms that the products of corrosion were leached from the surfaces of the specimens during the cycles. In addition to that, a level of leaching of calcium from the cementitious matrix was observed. Such result suggests a reduction of the pH close to the surface of the specimen, which may further favour the corrosion process at this layer.

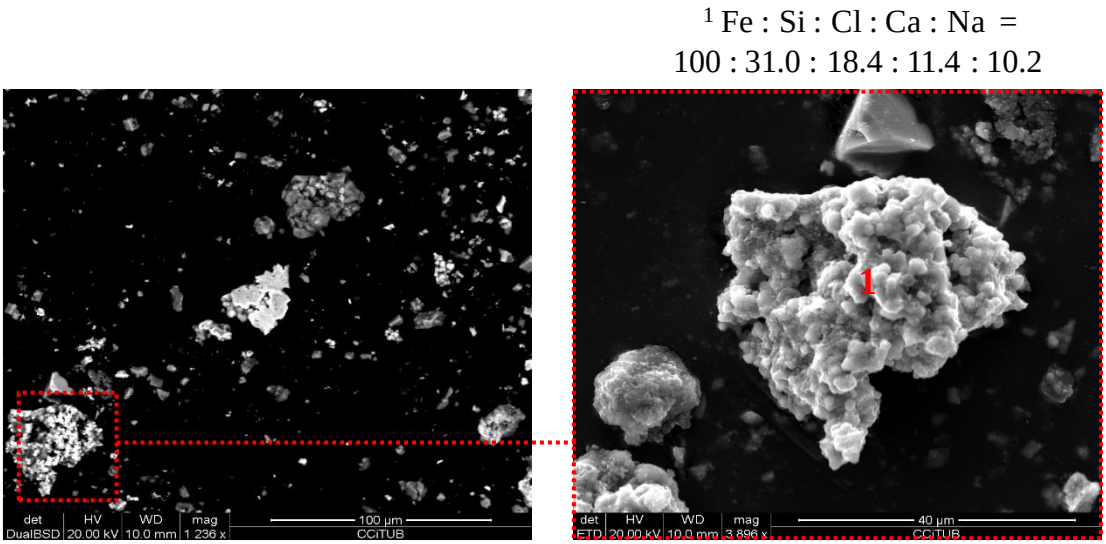

Figure 5.3 – SEM analysis and corresponding EDS spectra of Solids extracted from the bottom of containers.

The evolution of the surface corrosion and the corroded areas detected of one specimen with 190 kg/m^3 of fibre, and w/c 0.23 are presented in Figure 5.4. Figure 5.5 shows the graphs of the percentage of corroded surface area from cycle 5 to 95 and the relative increment relative to cycle 5 (considered as 100%).

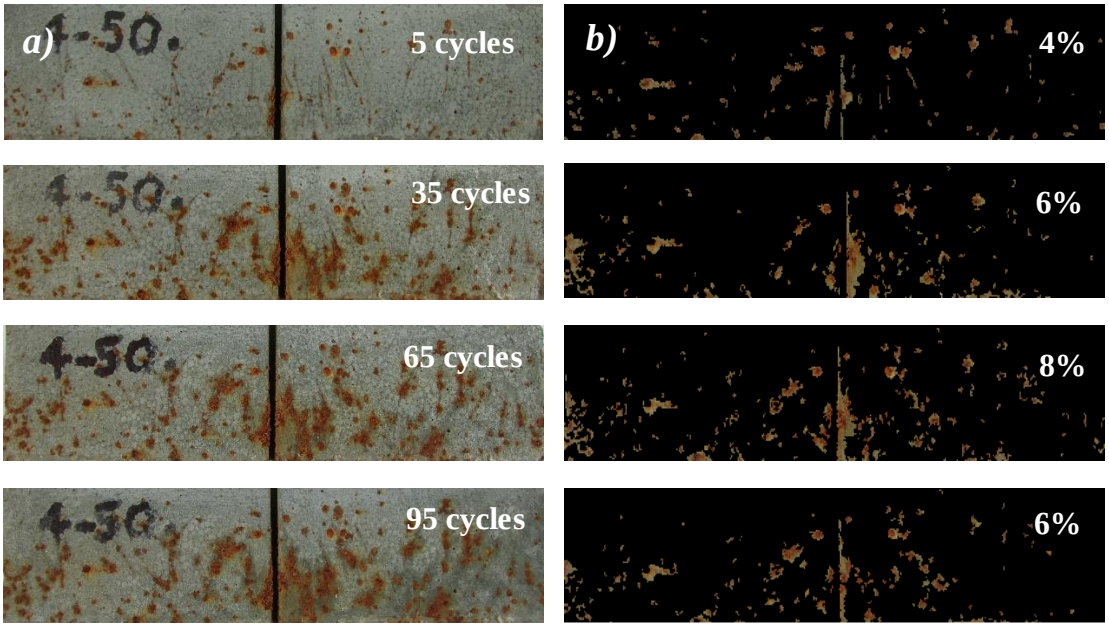

Figure 5.4 – Surface corrosion for specimen with 190 kg/m^3 of fibre and w/c of 0.23: a) pictures of the surfaces and b) corroded areas detected.

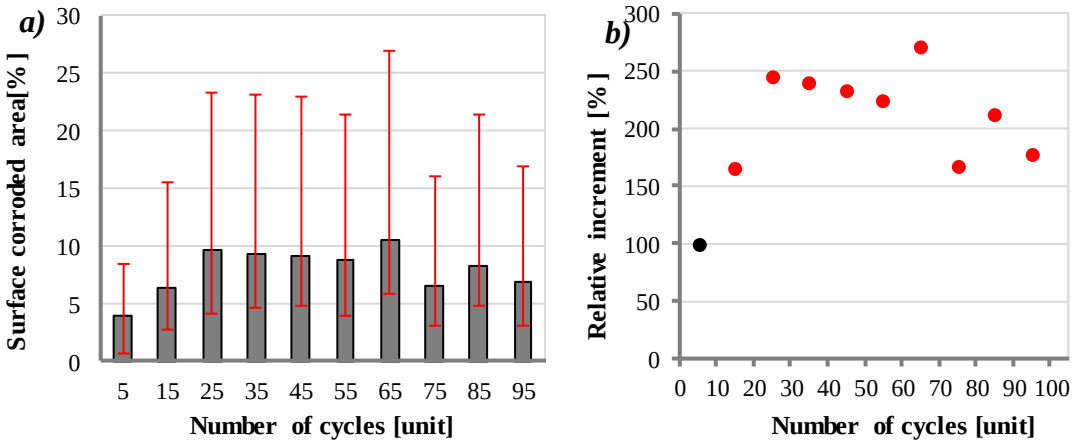

Figure 5.5 – a) Percentage of corroded area and b) relative increment of corroded area for specimen with 190 kg/m^3 of fibre and w/c of 0.23.

The same trend described for the specimens with 90 kg/m³ of fibres is observed here. Again, surface corrosion is observed since cycle 5, increasing until cycle 35. After that, a stability is reached. As mentioned previously, this stability is caused by the limited number of fibre generating corrosion products and the leaching effect of the solution during the wetting stage that removes some of the corrosion products from the surface.

Figure 5.6 presents the evolution of surface corrosion and the corroded areas detected of a specimen at 5, 35, 65 and 95 cycles with 190 kg/m^3 of fibre and w/c of 0.28. Graphs of the average percentage of corroded area from cycle 5 to 95 and the relative increment related to 5 cycles are presented in Figure 5.7.

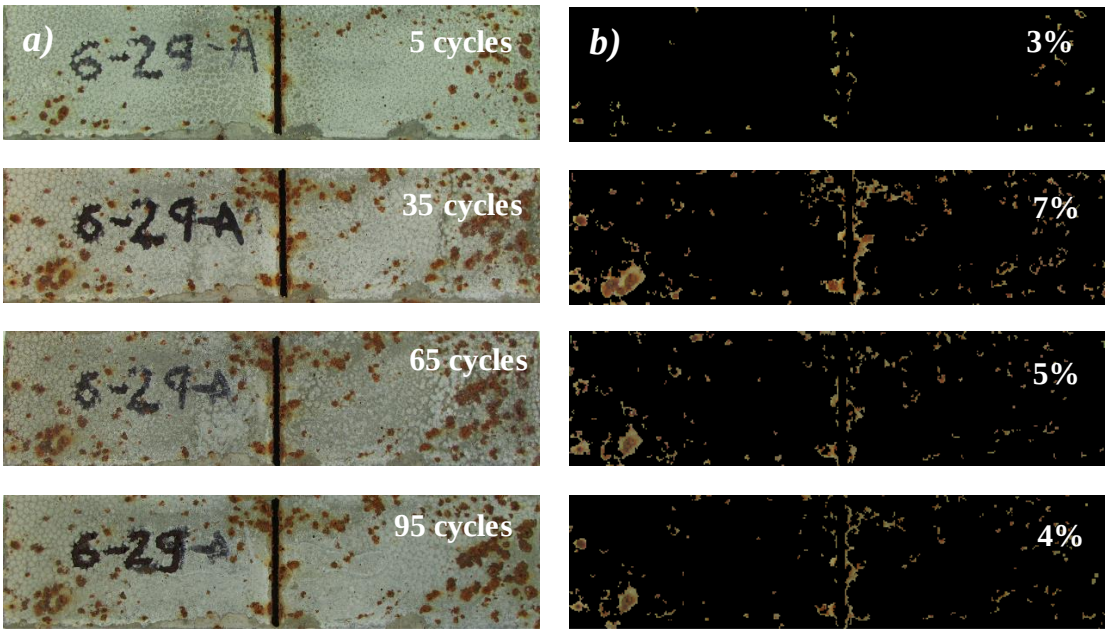

Figure 5.6 – Surface corrosion for specimen with 190 kg/m^3 of fibre and w/c of 0.28: a) pictures of the surfaces and b) corroded areas detected.

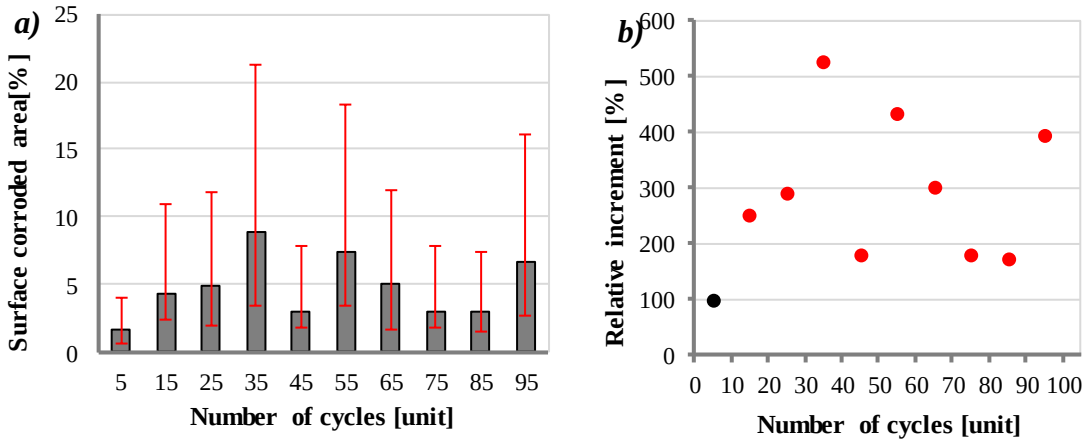

Figure 5.7 – a) Percentage of corroded area and b) relative increment of corroded area for specimen with 190 kg/m^3 of fibre and w/c of 0.28.

The same general behaviour regarding the deposition of corrosion products is observed for the mix with w/c 0.28. Interestingly, however, these mixes show a reduction in the surface area with deposition of corrosion products in comparison with equivalent mixes with w/c 0.23. This trend is further analysed in section 5.2.3.

5.2.2. Influence of fibre content

The evolution of the surface corrosion is analysed in terms of fibre content, for 90 and 190 kg/m^3 of fibre, and w/c of 0.23. Figure 5.8 presents the graphs of the average percentage of corroded area from cycles 5 to 95 and the relative increment of surface corrosion for 190 kg/m^3 of fibre when compared to 90 kg/m^3 (considered 100%).

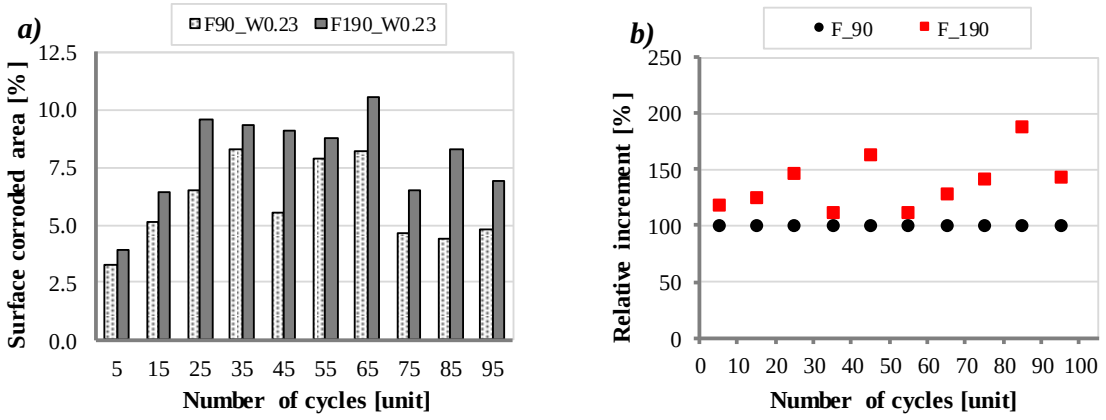

Figure 5.8 – Surface corrosion for 90 and 190 kg/m^3 of fibre: a) percentage of corroded area and b) relative increment of corroded area.

Figure 5.8 reveals that samples with 190 kg/m^3 of fibre presented bigger surface corrosion than those with 90 kg/m^3. Nevertheless, the increment is not directly proportional to the increase of fibre content. Despite nearly doubling the fibre content, a maximum difference of only 5% of the corroded surface is assessed. The same was observed in the preliminary experimental programme (Chapter 4) for the highest fibre

contents. As in that case, this outcome may be attributed to a superposing effect. According to this effect, the deposition of corrosion products of 2 fibres close to each other might occur at nearly the same area on the surface. Consequently, the area affected is not doubled, being only slightly increased.

5.2.3. Influence of w/c

The influence of water/cement ratio in the surface corrosion is studied for 90 kg/m^3 of fibre. Figure 5.9 presents the graphs of the average percentage of corroded area from cycles 5 to 95 and the relative increment of surface corrosion of mix with w/c 0.28 when compared to the equivalent one with w/c 0.23 (considered 100%).

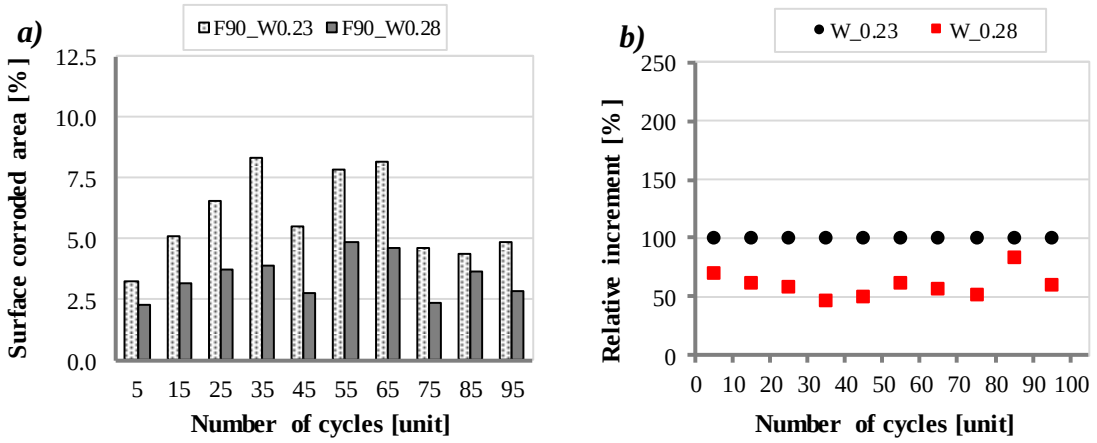

Figure 5.9 – Surface corroded area for 90 kg/m^3 of fibre: a) percentage of corroded area for w/c 0.23 and 0.28 and b) relative increment of corroded area.

Figure 5.9 reveals that the increment of the w/c for the fibre content of 90 kg/m^3 decreased the corrosion at the surface at all cycles. An identical trend is also observed for mixes with 90 kg/m³. Such trend contradicts the initial expectation that the increase of the w/c would increase the porosity of the matrix and facilitate the movement of ions, thus enabling more advanced corrosion states and the deposition of more corrosion products at the surface. Although a definitive explanation is not feasible with the information at hand, a possible explanation is that the higher porosity of the surface also facilitates the leaching of corrosion products, avoiding further accumulation at the surface.

5.3. ANALYSIS OF THE PENETRATION DEPTH OF CHLORIDES

Figure 5.10 shows the cross section of specimens tested for the depth of chloride penetration. Measurements were performed at cycles 5, 35, 65,95 and 125 (corresponding to 20, 140, 260, 380 and 500 days, respectively). The penetration rate and the total penetration depth of chloride for mixes with 90, 140 and 190 kg/m^3 of fibre are presented in Figure 5.11.

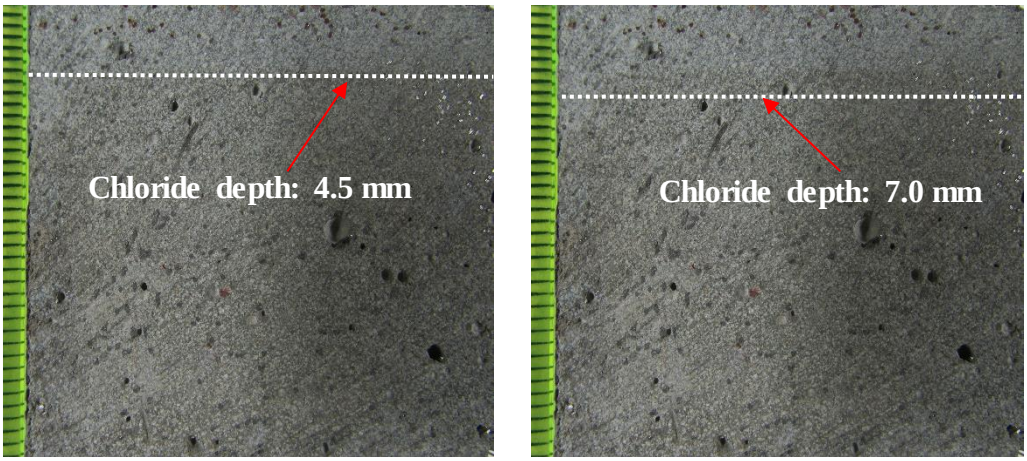

Figure 5.10 – Penetration depth of chlorides in the cross section.

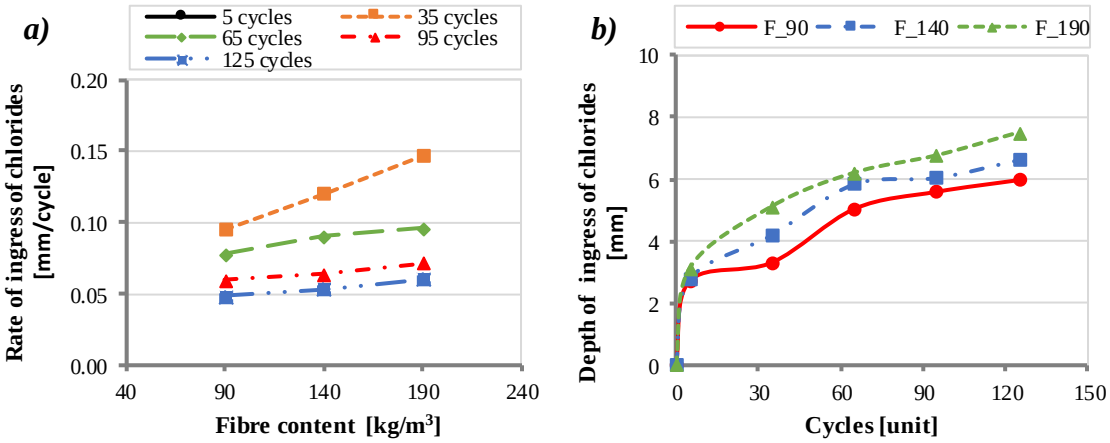

Figure 5.11 – Chlorides a) penetration rate and b) total penetration depth in the cross section.

Figure 5.11-a shows that the highest penetration rate is observed for cycle 5. Such outcome may be attributed to the capillary suction of the salt solution during the first cycles. It should be remarked that the specimens were first subjected to two wetting (submerged in distilled water) and drying (at environment temperature) to ensure the same condition in the begin of the chloride cycles. However, the surface of the specimens may be easier dried than the bulk of the matrix allowing faster ingress of substances.

According to Hong (1998), during the wetting cycles, the dry or partially dry surface exposed to salt water absorbs the salt solution until saturation and the concentration of chlorides increases in the pores near the surface. During the drying, the pure water evaporates and the salts in the solution precipitate out of these deeper pores and remain into the pores nearer to the surface.

Such movement of the salt solution develop a gradient of chlorides in the pores. Given the low permeability of the matrix, the capillary absorption is limited to a small layer close to the surface. In the first cycles, a considerable ingress of chlorides occurs in this layer. As the cycles progress, an equilibrium between the external chloride content and the chloride concentration in the pore solution of the surface layer is achieved, so that

the penetration rate decreases. Further chloride entrance beyond this layer is governed mostly by a diffusion process, which produce a slower chloride ingress than the caused by the capillary absorption. This reduces the chloride penetration rate in comparison with the first cycles, explaining the trend observed in Figure 5.11.

The increment of fibre content increases the penetration rates of chloride at all cycles. The result suggests that the addition of fibres alter properties of the composites such as porosity and permeability. An increment of the volume of capillary pores as well as the permeability in cementitious grouts with the addition of fibres was observed by Toutanji (1999). The fibre-matrix ITZ might also act as a channel facilitating the movement of the chlorides inside the matrix.

5.4. VISUAL INSPECTION OF CORROSION

5.4.1. Analysis of the cross section

Figure 5.12 shows images of the fibres after the 3-PBT in specimens exposed to 0 (before the attack), 5, 95 and 125 cycles. The analysis of the fibres at before the attack (see Figure 5.12-a) reveals no sign of corrosion, indicating that they still are protected by the passive film. Figure 5.12-b shows that a low level of pits of corrosion is formed at the surface of some fibres close to the surface at cycle 5. Fibres maintain their original diameter with no significant loss of cross sectional area. Such small level of corrosion may be a consequence of the low permeability of the matrix and the low porosity around the fibres. Researchers such as Nemegeer *et al*. (2003); Mangat and Gurusamy, (1988) and, Dauberschmidt (2006), highlighted higher chloride threshold values for steel fibres compared to conventional steel bars. The moisture exchange over the cycles may mobilize the products of corrosion to the surface due to the short distance between fibre and the surface of the specimen.

At 95 cycles (see Figure 5.12-c) the fibres close to the surface presents an increased level of corrosion. Some regions of the fibres show localized accumulation of rust, i.e. products (including various iron oxides and hydroxides) with relatively lower density that occupy much more volume than the original iron (Chen and Mahadevan 2008). This may indicate that the corrosion occurs with different speeds along the length of the fibre, being partially governed by the steel composition, the distribution of the matrix porosity and the variation in the concentration of chlorides, among other factors. As corrosion progress, rust products spread filling the pores of the ITZ. The porous matrix surrounding the fibre can to some extent absorb the higher volume of the rust products. Alternatively, the corrosion products may be driven through the pore system to the surface.

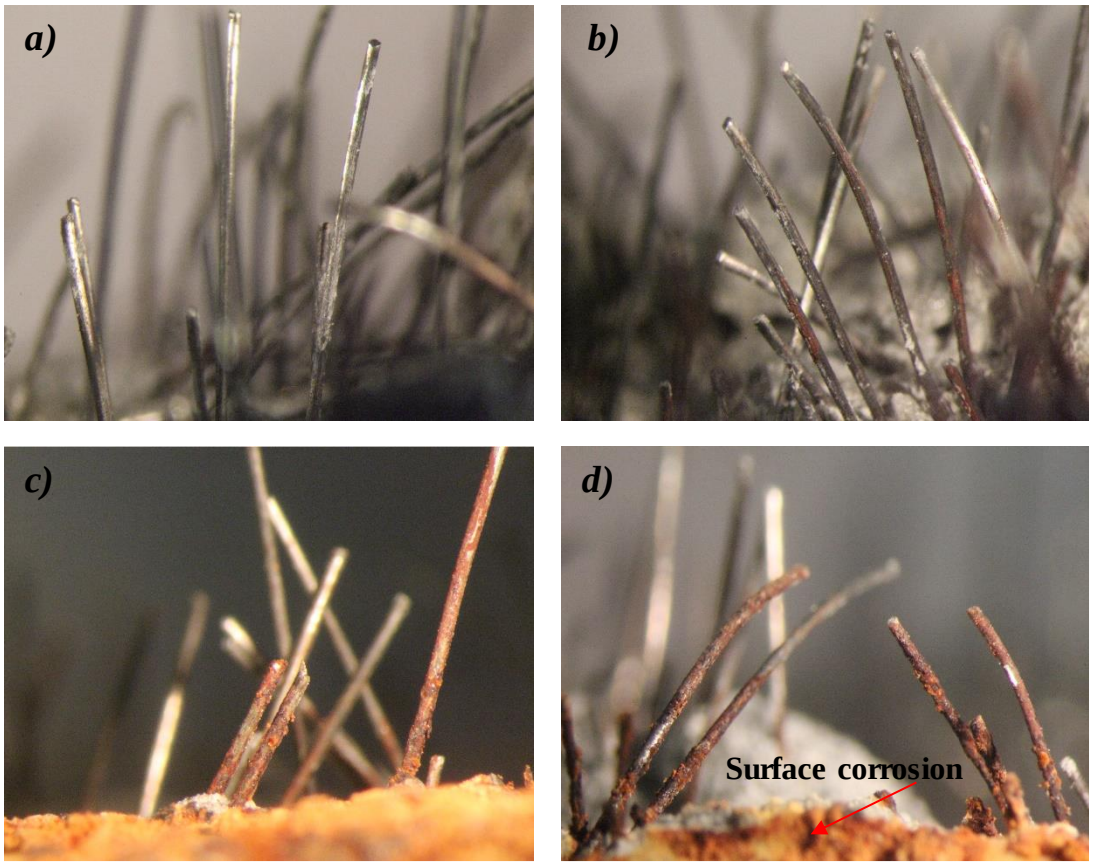

Figure 5.12 – Corrosion of the fibres close to the surface at cycles a) 0, b) 5, c) 95 and d) 125.

The corrosion does not affect all fibres close to the surface of the specimen. In fact, some of them still show no sign of corrosion. The corrosion resistance of such fibres may be explained by a combination of factors. The short length and discontinuous nature of fibres impedes large potential differences over the fibre surface, thereby potentially limiting the formation of anode and cathode regions (Dauberschmidt 2006). Another factor is related to a well-defined interfacial layer rich in $Ca(OH)_2$ in direct contact with the steel fibres, which is more uniform and presents less defects than that found around conventional rebars (Page 1982; Bentur *et al*. 1985). A third factor is the high density of the matrix that might "encapsulate" some fibres, blocking the contact with the chlorides.

At 125 cycles, fibres in the layer close to the surface of the specimen (see Figure 5.12-d) show significant corrosion with loss of cross section. On the contrary, fibres in deeper layer of the specimen but very close to the surface as well show no sign of corrosion. This may be a consequence of the limited penetration of chlorides or the limited availability of oxygen and/or water inside the specimen.

Figure 5.13 shows a layer of the cross section close to the surface of specimens at 5, 35, 95 and 125 cycles.

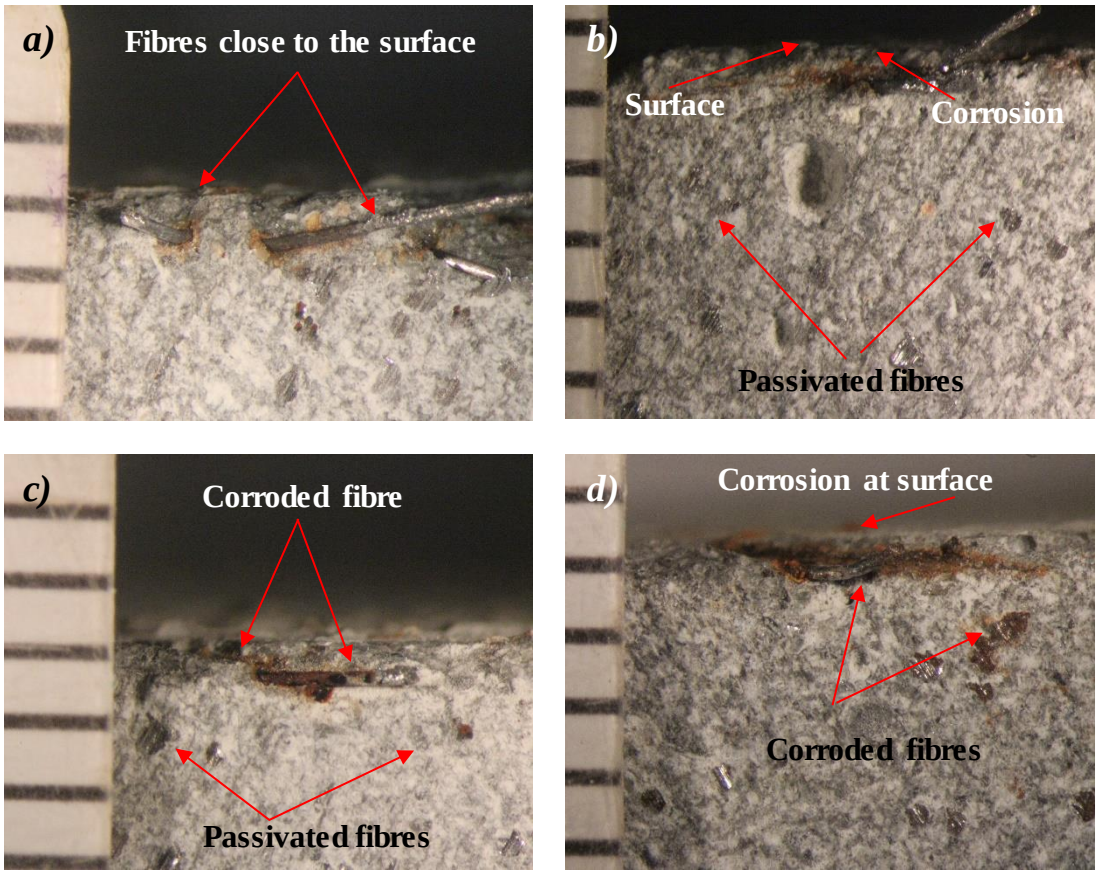

Figure 5.13 – Corrosion at cross section close to the surface at cycles a) 5, b) 35, c) 95 and d) 125.

At 5 cycles (see Figure 5.13-a), fibres located in a layer close to the surface of the specimen (between 0.4 and 0.5 mm) present a very low level of corrosion. The products of corrosion filling the pores appear in a very thin region surrounding the fibres. Passive fibres close to the surface can be clearly identified. No significant presence of iron oxides and hydroxides is observed in the bulk matrix of the superficial region of the sample.

In Figure 5.13-b, the layer close to the surface presents an increment of products of corrosion but most of the fibres still remain unaffected, despite of higher concentration of chlorides in the pores of this region. In cycle 95 (see Figure 5.13-c), an enhanced level of corrosion is observed in the fibres close to the surface. The matrix in this region shows no significant presence of ferrous oxides and hydroxides, thus suggesting that the density of the matrix limits the corrosion and the mobilization of the rust to the surface.

The evolution of corrosion in the layer close to the surface is analysed at 125 cycles (see Figure 5.13-d). The results reveal that the products of corrosion are occupying the pores in a region surrounding the corroded fibre. Such outcome may indicate that the volume of rust generated from the reactions fills the pores in a limited region close to the fibres. The matrix above the corroded fibre presents a clean aspect with no oxidation products, which were contained around the fibre.

5.4.2. Analysis of the surface of the specimen

Figure 5.14 illustrates the presence of fibres and of the products of corrosion at the surface of the specimen. The visual analysis reveals that the stains of corrosion at surface are related to the presence of fibres in a very superficial layer with almost no cover.

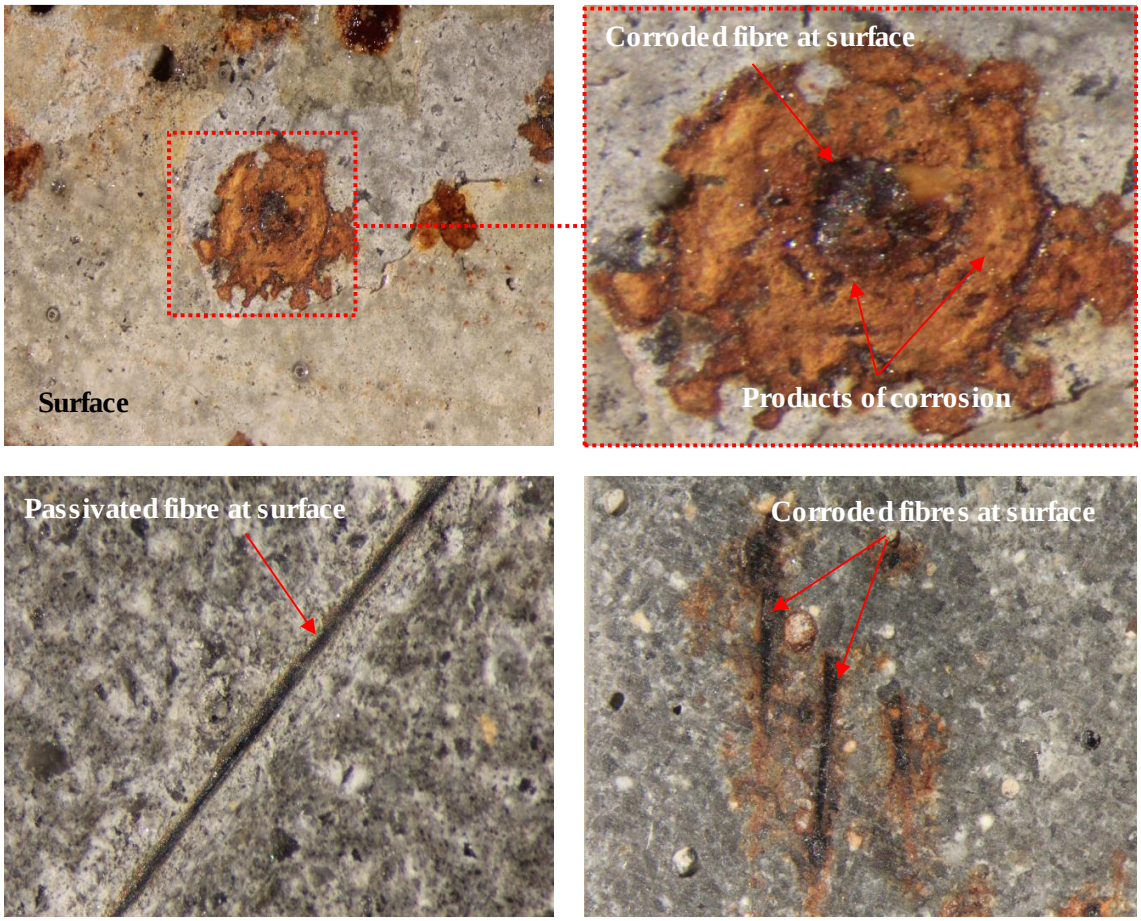

Figure 5.14 – Fibres and products of corrosion at the surface of the specimen.

The visual analysis (see Figure 5.14) reveals the presence of corroded fibres and products of corrosion that could be Fe_2O_3 (black colour), $Fe(OH)_2$ (white colour), $Fe(OH)_3$ (brown colour) and $Fe(OH)_3{,}3H_2$ (yellow colour). According to Thoft-Christensen (2001), the expanded volume of these products represent 2.1, 3.8, 4.2 and 6.4 cm^3 to 1 cm^3 of iron, respectively. So, as the volume of rust products is much greater than the volume of the iron, a small amount of corroded fibres close to the surface may generate a significant stain.

5.5. SEM AND EDS MICROANALYSIS

A microanalysis was performed to study the mechanisms of corrosion at the surface of the specimen. A scanning electron microscopy was conducted after the mechanical tests and regions were analysed by EDS to identify the elements present. EDS

spectra are represented as the relative intensities of each element, located above each image. Ca, Si, Fe Na, Cl and O peaks were considered, corresponding to the energies of 3.6, 1.8, 6.3, 0.9, 2.7 and 0.5 keV, respectively.

5.5.1. Chloride corrosion of the surface of the fibre

Figure 5.15 shows a representation of the steel fibre surface and SEM images of the fibre without corrosion and with corrosion at 5 and 125 cycles. Fibre surface without corrosion (see Figure 5.15-a, b and c) show micro-flaws aligned with the length of the fibre as a result of the production process. The micro-flaws are filled with the lubricant applied for the production of the fibre. The presence of the lubricant may lead to an incomplete or absent passivation in these regions that facilitate corrosion initiation (Dauberschmidt 2006).

Figure 5.15-d and e illustrate the SEM images of the fibre surface at 5 cycles of chloride attack. The microanalysis reveals the formation of products of corrosion aligned to the micro-flaws at fibre surface. This may be a consequence of the unstable passive region which favours the iron corrosion leading to deposition of ferric oxides and hydroxides. Notice that the deposition of the corrosion products follows the direction of the micro-flaws.

At 125 cycles, the fibre surface is completely covered by products of corrosion (see Figure 5.15-f and g). Fibre present a greater diameter due to the accumulation of expansive corrosion products around the fibre surface, indicating an accelerated process of corrosion. According to de la Fuente *et al*. (2016), the rust layers formed present heavy cracking, tending to exfoliate and become partly or completely detached from the base steel, which in turn presents heavy pitting with very deep pits. The exfoliated rust layer occurs under high concentration of chlorides and moisture.

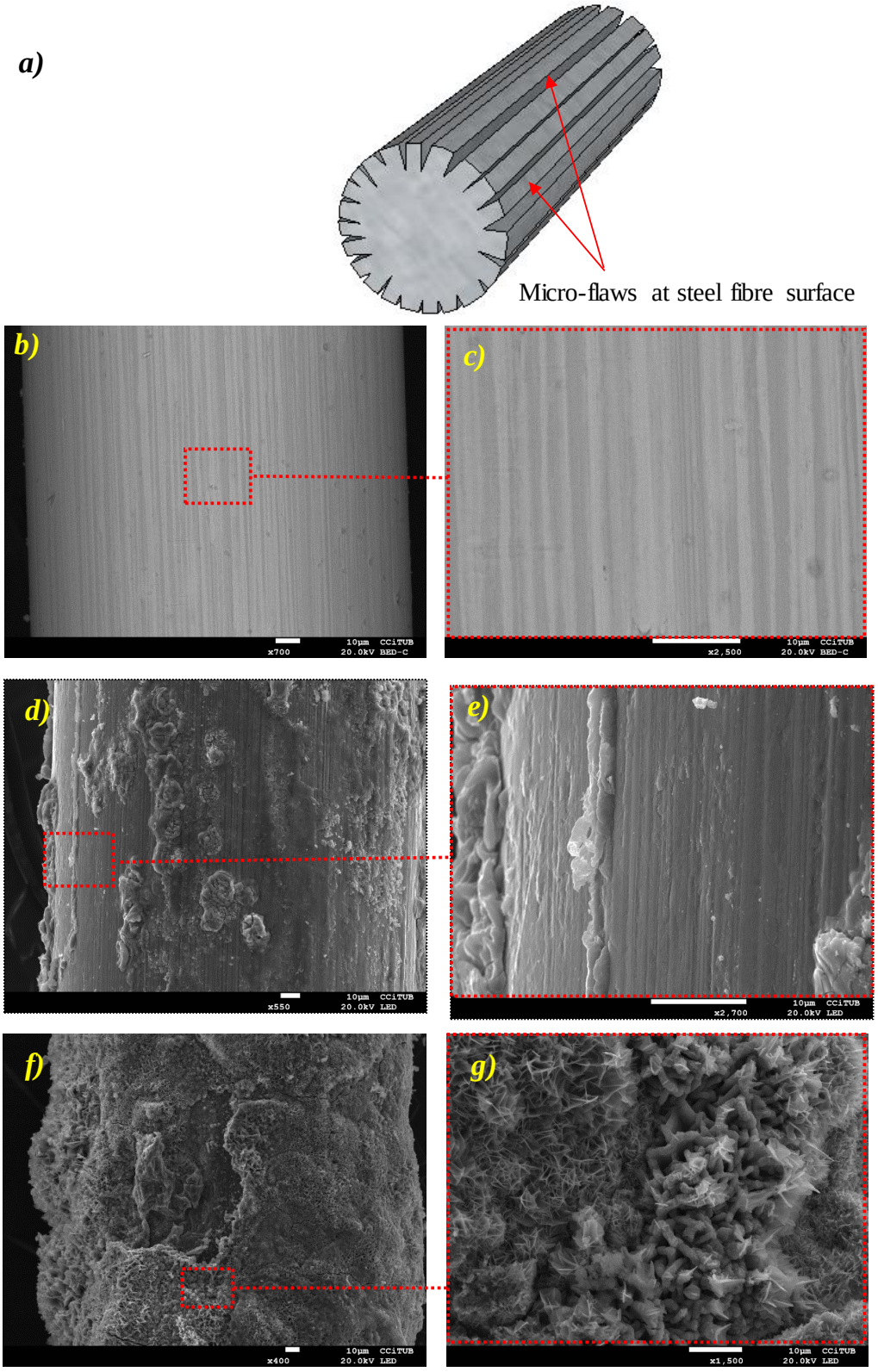

Figure 5.15 – Steel fibre degradation: a) representation of steel fibre surface; b and c) SEM image of fibre without corrosion; d and e) SEM image of corrosion at 5 cycles; f and g) SEM image of the corrosion at 125 cycles.

5.5.2. Microanalysis of the cross section of the specimen

Figure 5.16 presents the SEM-EDS microanalysis of the cross section of several fibres from specimens exposed to 0 and 125 cycles.

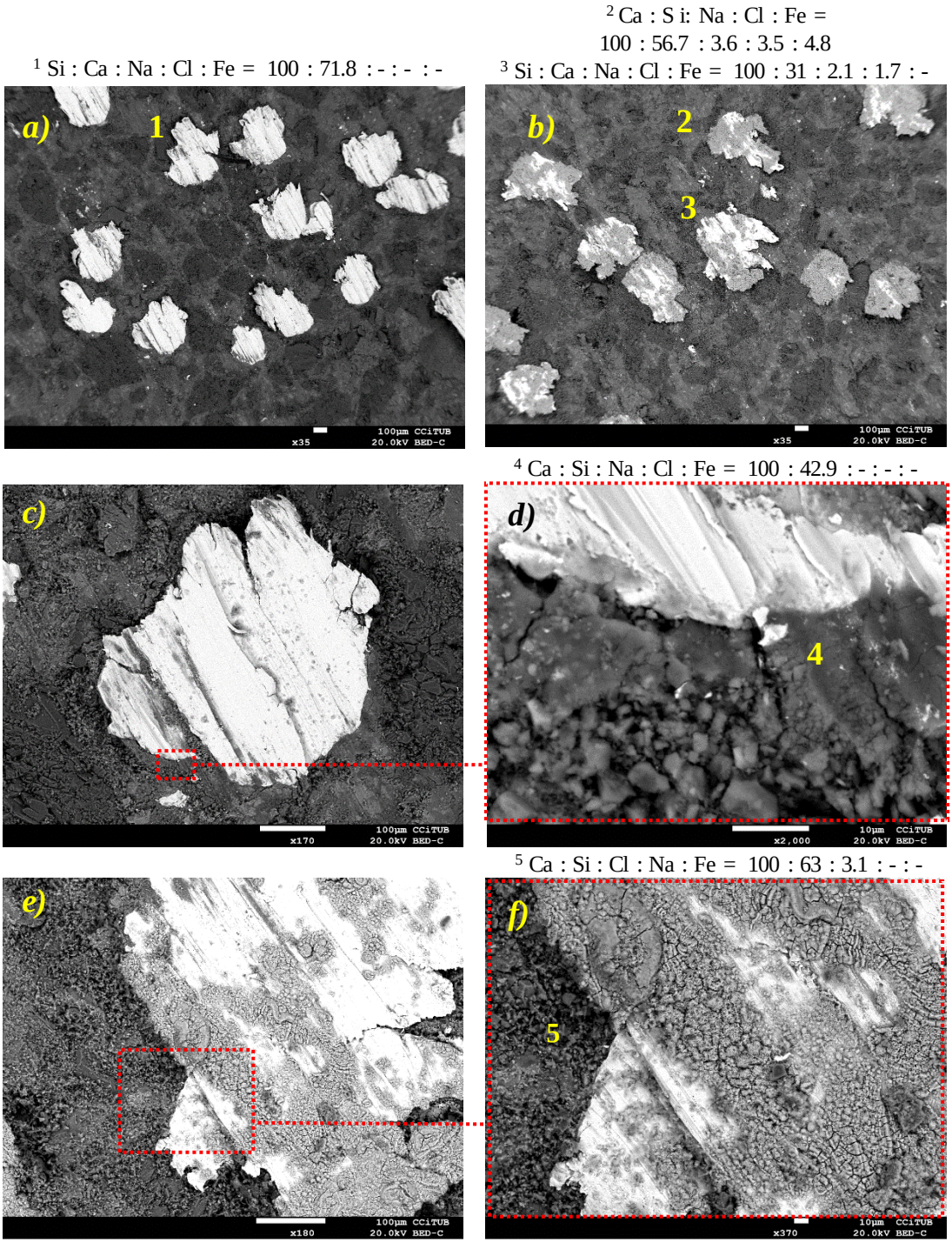

Figure 5.16 – SEM images of the cross section: a) at 0 cycles, b) at 125 cycles; c and d) detail of one fibre and matrix at 0 cycles; e and f) detail of one fibre and matrix at 125 cycles.

Figure 5.16-a reveals a dense matrix with low porosity around and between fibres. This is attributed to the low w/c and high content of fines (cement, Nano-silica and

calcium carbonate) in the mix. The analysis of the cross section area close to the surface at 125 cycles (see Figure 5.16-b) reveals a level of chlorides in the matrix. However, the presence of iron oxides was only observed in a thin layer close to the surface. The SEM images in Figure 5.16-c and d at 0 cycles, show the good bond between fibre and matrix. The contact zone fibre-matrix is formed for a dense layer rich in calcium and with a percentage of silica. According to Bentur *et al*. (1996), a water filled space tends to build up around the fibre, which is mainly filled by C-H hydrated products. In particular, Dauberschmidt (2006) discussed the presence of a large and more uniform calcium hydroxide (C-H) layer around the fibre, creating an increased protection of fibres against chloride and oxygen ingress (Marcos-Meson *et al*. 2018).

At 125 cycles (see Figure 5.16-e and f), a dense layer with a low percentage of chlorides is observed around the fibre. This may be a consequence of the ingress of salt solution over the cycles which penetrates the pores of the cementitious matrix in the layer close to the surface. Notice that oxides formed and mobilized through the pores were not observed. This may be a consequence of the high density of the ITZ fibre-matrix with a low porosity controlling the dissolution and release of iron from the passive fibre surface.

5.5.3. Microanalysis of the surface of the specimen

Figure 5.17 presents the SEM images of the products of corrosion deposited at surface of the specimens at cycles 5 and 125. The surface of the specimens exposed to chlorides at 5 cycles (see Figure 5.17-a and b), presents a deposition of iron oxides and hydroxides. According to de la Fuente *et al*. (2016), the corrosion mechanisms that act on the steel exposed to a very severe marine condition may accelerate the corrosive process. The rust layer formed is easily detachable from the base of the steel fibre. The analysis shows that products of corrosion generated at the fibres localized in the layer very close to the surface can be easily mobilized to the surface through the pores over the cycles.

SEM images of the surface at 5 cycles (see Figure 5.17-c and d) suggests the formation of iron oxides dendrites. The dendrite develops with a typical multi-branching three-like form. According to Swartzlow (1934), the most common types of dendrites are those formed in cracks and joint plates where the dendritic materials are carried through short distances and are usually composed of insoluble oxides. The ferrous oxides formed with the fibre corrosion are mobilized to the surface by means of the flow of the moisture and the dendrite formation is influenced by the surface tension upon evaporation of the salt water.

The microstructure of the surface at 125 cycles (see Figure 5.17-e and f) indicates the formation of iron oxides and hydroxides deposited at surface. The SEM images show that the products of corrosion occur in some regions of the surface while other regions present no sign of rust. It may be a consequence of the controlled process of surface corrosion limited by the dense matrix and the available iron of the fibres in a very thin layer close to the surface.

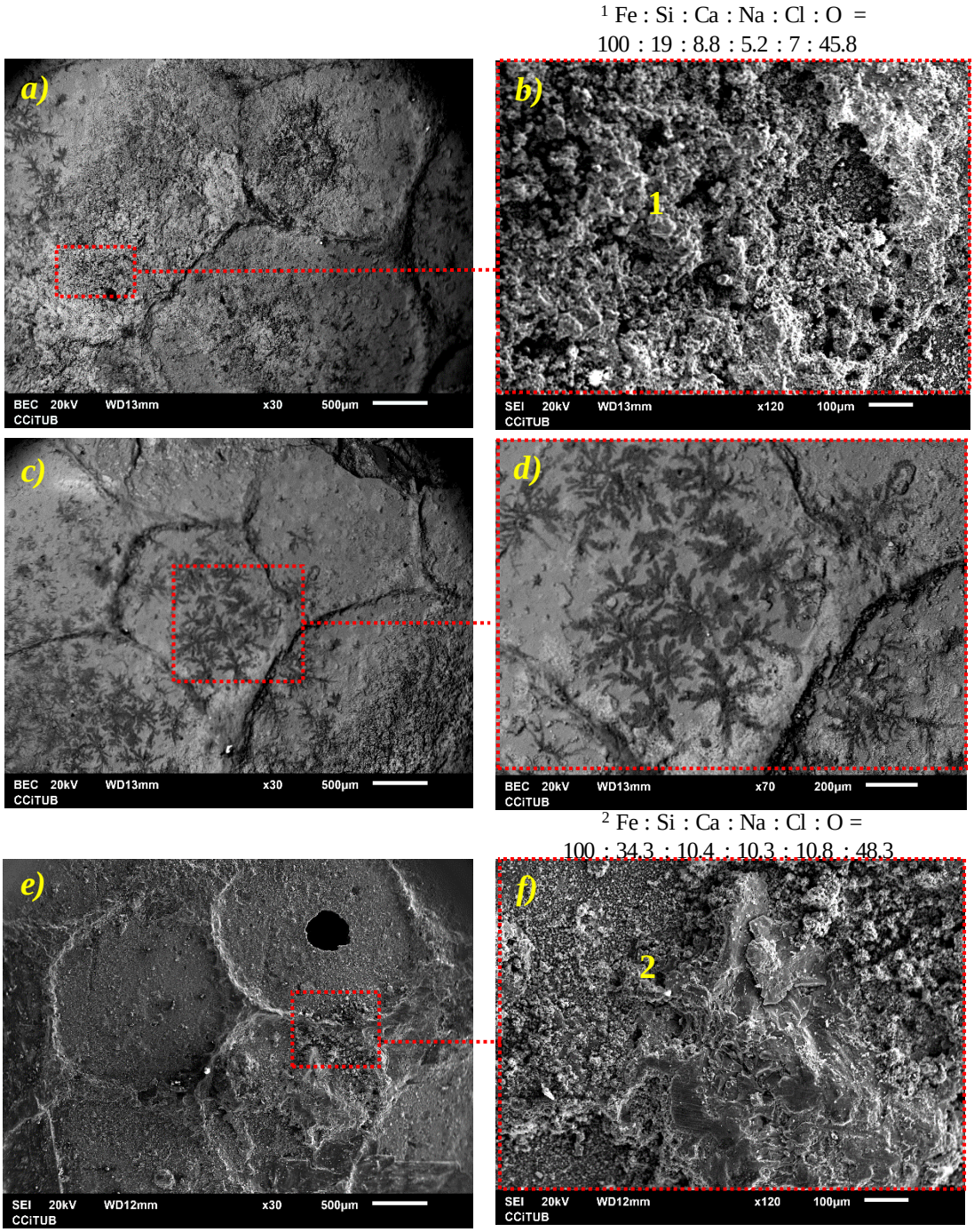

Figure 5.17 – SEM images of the surface: a) at 5 cycles, b) detail of products of corrosion at 5 cycles, c) formation of dendrites of iron oxides at 5 cycles, d) detail of the dendrite formation, e) surface at 125 cycles and f) products of corrosion at 125 cycles.

5.6. CONCEPTUAL MODEL OF SURFACE CORROSION

A conceptual model was developed based on the literature and the results from the specific experimental programme included in this chapter. The model represents the evolution of the corrosion mechanism considering three stages: induction (Figure 5.18), acceleration (Figure 5.19) and deceleration (Figure 5.20).

Before the wetting and drying cycles, all fibres (see Figure 5.18-a) are protected by the alkalinity of the cementitious matrix that form a passive film. The film may be considered a bilayer usually composed by a stable Fe_2O_3 and a soluble Fe_2O_3. H_2O (Szklarska-Smialowska 1986; Nishimura and Sato 1983). The stable Fe_2O_3 reduces the ion mobility between the steel and the surrounding ITZ and inhibits the diffusion in the passive regions of fibre surface.

During the cycles, the mechanism of capillary absorption and diffusion enables the penetration of chlorides that reach the fibres close to the surface (see Figure 5.18-b). Micro-flaws at the surface of the fibres (produced during the manufacturing process) act as cavities that can potentially hold different concentration of ions compared with the surrounding surface of the fibre. This favours the formation of anodes and cathodes over the surface of the fibre. When the chloride threshold is exceeded, the corrosion is activated. The chlorides are not consumed in the process, further compromising the passivate film and enhancing the corrosion process.

By contrast, an increment of concentration of free chloride ions and oxygen occur in the layer close to the surface over the cycles (see Figure 5.18-c), accelerating the formation of corrosion products, such as $Fe(OH)_2$, $Fe(OH)_3$ and Fe_2O_3 (see Figure 5.19). These products have a high volume and may expand by about 4-6 times the original volume of the iron (Chen and Mahadevan 2008) consumed in the reactions. Consequently, they move to the border of the cavities and spread into the pores of the ITZ and of the matrix. The exchange of moisture during the cycles favours the mobility of the expanded rust products towards more superficial pores of the matrix. Due to the movement of the salt solution during the wetting cycles, a level of leaching can be also observed removing the ferric oxides and hydroxides from the surface.

In the phase of deceleration, the fibres in the layer very close to the surface (see Figure 5.20) present advanced corrosion and only small amounts of new product of the corrosion are generated due to the lack of iron to be consumed by the reactions. A level of gradual reduction of the corrosion at surface is observed over the cycles. This may also be a consequence of the process of leaching at the surface of the specimen during the wetting cycles, removing partially these products from the surface. The movement of chloride, water and oxygen towards deeper layers from the surface is limited by the density of the matrix and of the ITZ, thus maintaining deeper fibre in a passive state or with very low levels of corrosion.

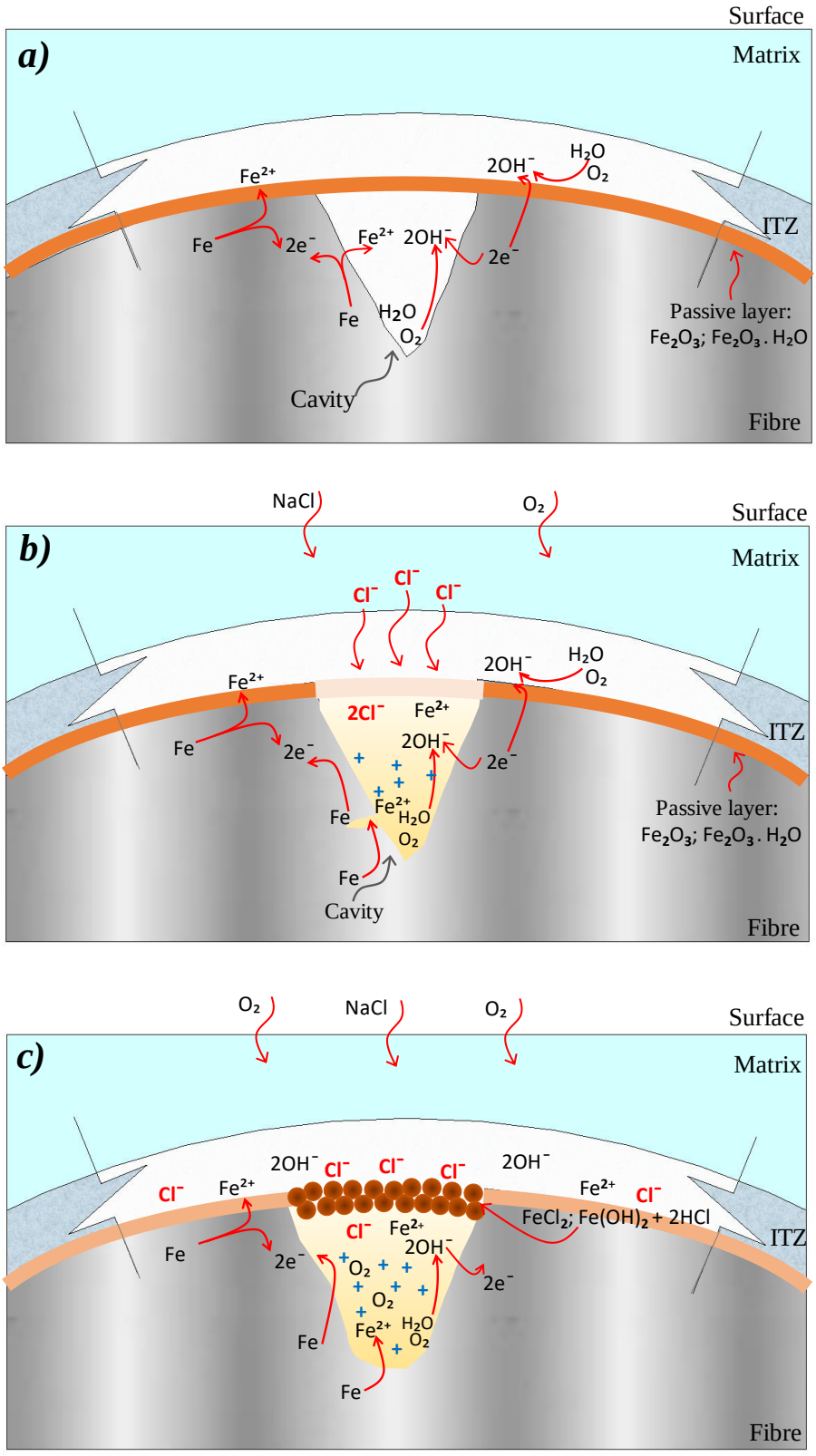

Figure 5.18 – Conceptual model for the surface corrosion in HPSFRCCs - Induction.

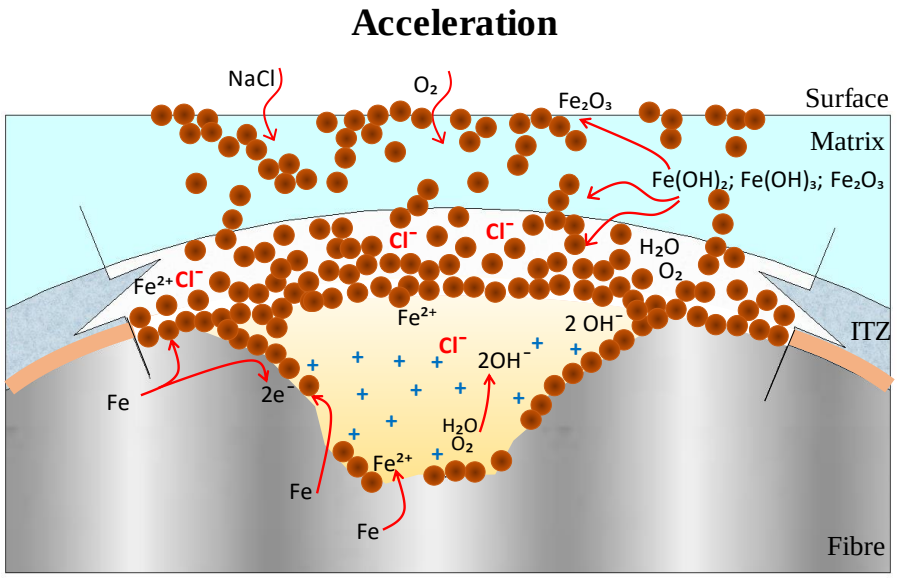

Figure 5.19 – Conceptual model for the surface corrosion in HPSFRCCs - Acceleration.

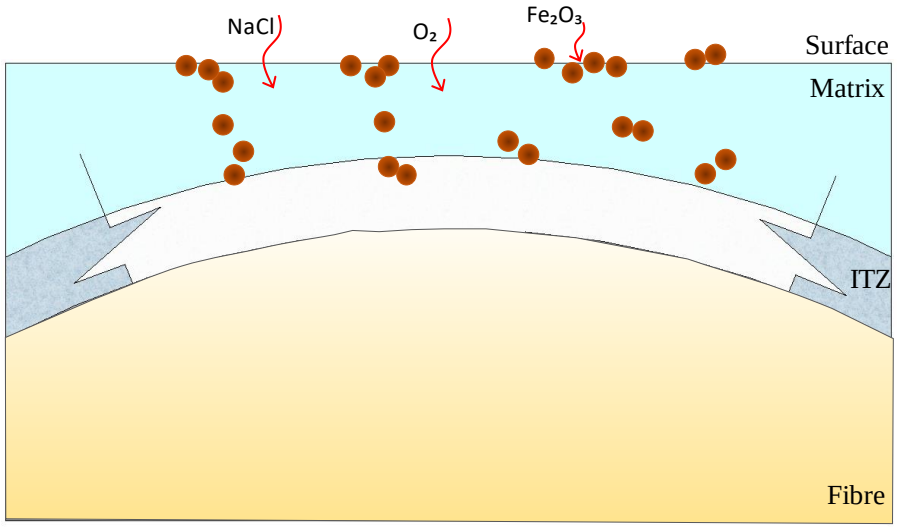

Figure 5.20 – Conceptual model for the surface corrosion in HPSFRCCs - Deceleration.

5.7. EFFECTS OF THE CORROSION IN THE MECHANICAL PERFORMANCE OF UNCRACKED SPECIMENS

In order to study the effects of corrosion in the uncracked section, the 3-point bending tests were performed at 0, 5, 35, 65, 95 and 125 cycles. Given that the tendencies are similar, Figure 5.21 presents the average load-deflection curves obtained for the specimens with 90, 140 and 190 kg/m^3 of fibre and w/c of 0.23. A general overview of the curves reveals that the ingress of chlorides over the cycles has no significant influence on the shape of the curves and the values reached, regardless of the CMOD.

Such result is expected given the limited penetration of chlorides and the corrosion restricted to a small layer close to the surface of the specimen. This corrosion is not enough to compromise the mechanical performance of the uncracked specimens subjected to the wet-dry cycles. This result is consisted to that obtained in Chapter 3 for the preliminary experimental programme, which showed no clear evidence that the corrosion induced due to the chlorides affect the mechanical performance of HPSFRCC specimens.

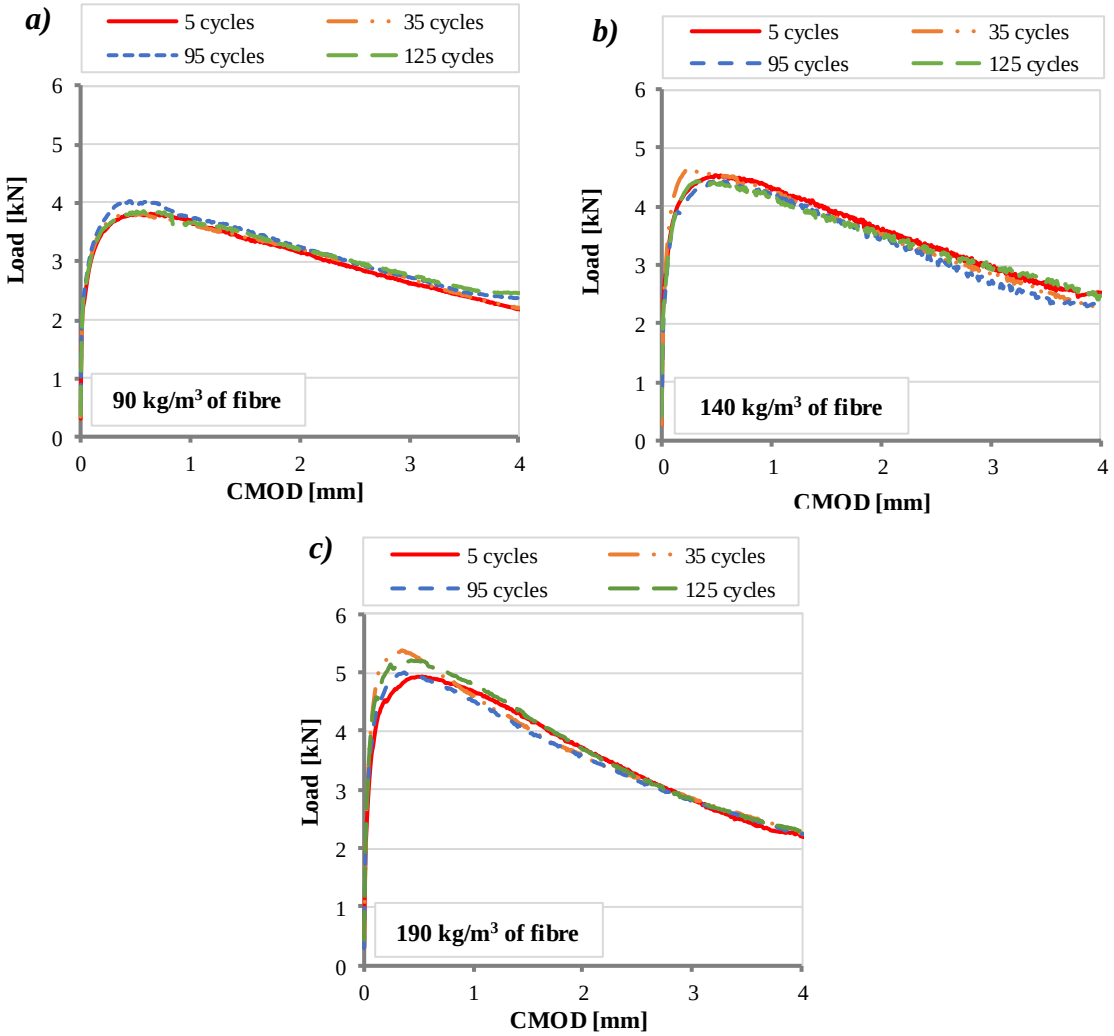

Figure 5.21 - Load-deflection curves for uncracked sections at 5, 35, 95 and 125 cycles of specimens with: a) 90 kg/m^3, b) 140 kg/m^3 and c) 190 kg/m^3 of fibre.

5.8. CONCLUDING REMARKS

Chapter 5 analysed the influence of wet-dry cycles with chloride solution in the aesthetics and the mechanical performance of uncracked HPSFRCC specimens. The following conclusions may be derived from the analysis of the experimental results:

- The surface corrosion of specimens under cyclic chloride exposure shows three main stages: induction, acceleration and deceleration. Chloride ions penetrate a thin matrix layer close to the surface, compromising the passive film around the fibres and initiating corrosion. The increase in chloride concentration accelerates the corrosion of these fibres. Finally, a decrease in the corrosion takes place due to lack of fibre to be corroded in the very superficial layer of the specimen. The dense matrix hinders deeper chloride penetration and the corrosion of fibres located in the inner portion of the cross-section, which remain unaltered.

- The formation of corrosion stains at surface of the specimen is a consequence of the corrosion of the steel fibres located in a layer smaller than 5 mm from the surface of the sample. The area of the surface of the specimen with deposition of corrosion products increases until cycle 35, stabilizing after that. This stability is attributed to the reduction of the formation of corrosion products (due to the deceleration mention previously) combined with the leaching of the corrosion products at the surface during the cycles. The dense ITZ and matrix act as a protective barrier against fibres corrosion and the mobility of corrosion products from deeper within the cross section of the specimen.

- The uncracked HPSFRCC specimens exposed to chloride presented no reduction in the flexural tensile response over cycles. Such result was expected since the ingress of chlorides is limited to a thin layer close to the surface, not significantly affecting the overall structural contribution of the fibres in the cross section. This confirms that the influence of chloride in the mechanical performance of HPSFRCC will be small in case no cracking has occurred.

6. CORROSION IN CRACKED SECTION - MECHANISMS

6.1. INTRODUCTION

Chapter 5 revealed that the presence of chlorides in uncracked section brings a level of damage regarding the aesthetic while the structural behaviour is not affected over the wetting and drying cycles. However, concrete structures frequently present cracks due to different causes such as, mechanical loads, shrinkage, thermal effects and physical weathering as freezing and thawing. In this context, cracks in concrete may act as a preferential path for the penetration of deleterious substances such as chlorides.

The build-up of chlorides in cracks due to wet-dry cycles, evaporation, and limited wash-out, increases the chloride concentration at the crack (Marcos-Meson *et al*. 2018). According to Hansen *et al*. (1999), this phenomenon may lead to high concentrations of chlorides at the crack surfaces similarly as occur in external exposed surfaces. Studies in chloride-induced corrosion in cracks are mainly focussed on the deterioration of the steel rebar reinforcement (Berrocal 2017; Jaffer and Hansson 2008; Blagogević 2016; Otieno 2008).

The effects of chloride degradation of crack-bridging steel fibres and the main mechanisms that govern the process of corrosion are not fully investigated yet. Further research on the effects and on the main mechanisms of chloride corrosion of pre-cracked HPSFRCC considering different variables is required. Therefore, studies to identify the levels of damage according to the fibre content, the crack width and time of accelerated chloride exposure should be conducted.

In light of exposed, the **general objective** pursued in this chapter is to present and discuss the results of the specific experimental program performed to study the effects of chlorides in pre-cracked HPSFRCC specimens. To achieve this goal, the following **specific objectives** are defined:

- Assess the ingress of chlorides into the crack and level of fibre corrosion depending on the fibre content, crack width and number of cycles;
- Analyse the effect of chlorides in the microstructure of the fibres and of the crack surfaces;

- Identify the deterioration mechanisms that govern the chloride corrosion in cracked specimens under wetting and drying cycles;

Initially, in section 6.2, the ingress of chlorides into the cracks is presented and analysed. Subsequently, in section 6.3, the level and depth of the fibre corrosion is presented and analysed depending on the fibre content, of crack width and of number of wetting and drying cycles. In section 6.4, the results of the depth and the rate corrosion in cracked section is presented and studied over the cycles. The results of the microanalysis performed to investigate the effects of chlorides in cracked surface presented and analysed in section 6.5. Finally, in section 6.6, the main conclusions of the study are highlighted.

6.2. INGRESS OF CHLORIDES IN CRACKS

The presence of chlorides, the level and depth of corrosion were analysed in the cracked surfaces of the specimens after the 3-PBT. Figure 6.1 shows the depth of ingress of chlorides in the cracked section of the specimens with 90 kg/m^3 of fibre, tested at 95 wetting and drying cycles for the crack openings of 0.05 and 0.50 mm.

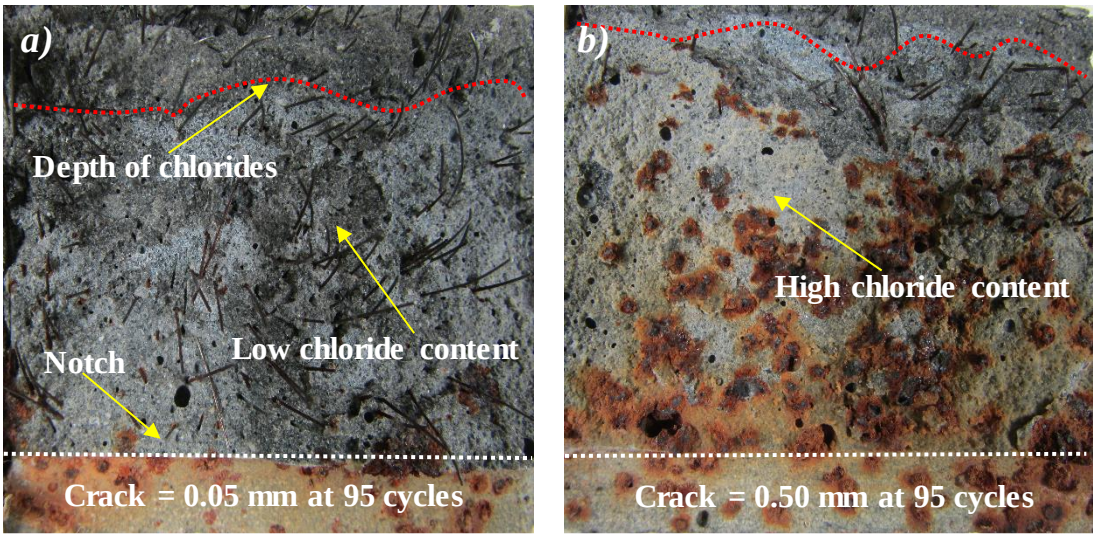

Figure 6.1 – Chlorides and corrosion in the cracks at 95 cycles for specimens with crack width a) 0.05 mm and b) 0.50 mm.

The process of chloride transport in cracked cementitious composites under wetting and drying cycles is mainly governed by 3 mechanisms: free movement, capillary suction and diffusion. The free movement occurs mainly in the wider portions of the crack openings being characterized by the direct entrance of water inside the crack. During the wetting, the chlorides also penetrates the crack by capillary suction being driven inside by the surface tension, particularly in zones with small crack openings. The mechanism of diffusion may also occur due to differences of chloride concentration along the crack surface during the wetting and the drying, if a minimum humidity is left in the microstructure. The chloride ion penetration due to diffusion tends to be significantly

slower than the penetration due to the other mechanisms. The increase of the crack opening provides more freedom of movement to the chloride ions, enabling bigger penetration and higher concentration, which increases the damage due to corrosion. According to Šavija (2014), crack width is the most important factor governing the ingress of deleterious substances in cracked concrete.

In line with this explanation, Figure 6.1 shows that specimens with crack opening of 0.05 mm presents corrosion until a smaller depth and a smaller level of damage of individual fibres in comparison with specimens with crack openings of 0.50 mm. The analysis reveals that the level and depth of corrosion increases significantly with the crack width as a result of a bigger depth and concentration of chlorides. The same finding was observed for all specimens analysed.

The influence of the number of wet-dry cycles in the chloride depth and content at the crack surface is studied for the crack width of 0.35 mm. Figure 6.2 illustrates the level of chlorides in the cracked section of the specimens with 90 kg/m^3 of fibre, tested at 5 and 95 cycles. The increment of chlorides in the crack surface is observed with the increase of number of cycles. This indicates that longer test duration leads to deeper chloride penetration and more advanced corrosion, as observed by Win *et al*. (2004).

Chloride already reach most part of the cracked surface in cycle 5 (see Figure 6.2-a), suggesting a rapid penetration through the crack. Variations in the penetration depth of the same specimen may be attributed to the tortuosity and roughness of the crack surface. Although the penetration depth at 95 cycles (see Figure 6.2-b) increases slightly, the main difference seems to be the concentration of chlorides, showing a gradient greater at the tip of the notch and smaller at the top of the crack. Such outcome may be a consequence of the mobilization of chlorides during the drying which tend to move from inside to outside of the sample, accumulating close to the mouth of the crack. In addition to that, the condition and duration of the exposure influences the chloride transports in cracks. The high concentration of chlorides in the solution (5% of NaCl) may contribute to deeper penetration and high content over the cycles.

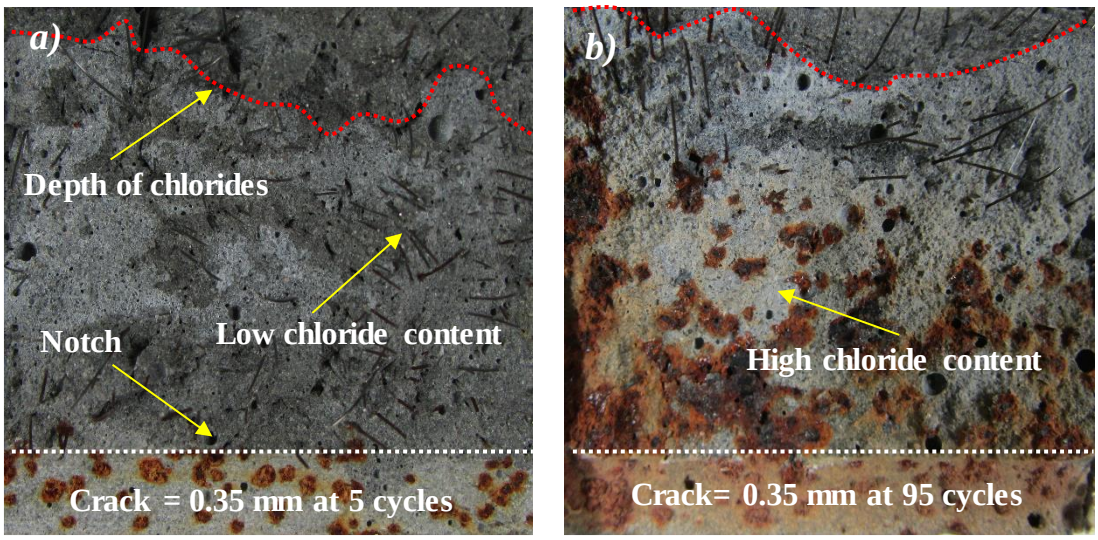

Figure 6.2 – Chlorides in specimen with crack width 0.35 mm at: a) 5 and b) 95 cycles.

While the water in the cracks evaporates during the drying, chlorides are left behind, thereby creating a concentration gradient at the outer part and the inner, still-water-filled part of the crack (Hansen *et al*. 1999). According to Hansen *et al*. (1999), such concentration of chlorides increases until the solution eventually becomes saturated with chlorides and the salt begins to crystalize. The build-up of chlorides leads to similar chloride concentrations at the crack faces compared to external exposed surfaces (Marcos-Meson *et al*. 2018).

The presence of chlorides in the crack surface is analysed in terms of the influence of the fibre content. Figure 6.3 illustrates the crack surface of specimens with 90 kg/m^3 and 190 kg/m^3 of fibre, tested at 95 wetting and drying cycles. The sample with of 90 kg/m^3 of fibre (see Figure 6.3-a) presents high concentration of chlorides along the crack surface and a distribution of corroded fibres along most of the cracked section. By contrast, specimens with 190 kg/m^3 of fibre tend to present smaller penetration depths, less concentration of chlorides and a considerably bigger number of fibres corroded near the crack mouth.

This analysis reveals that the increase of the fibre content reduces the ingress of chlorides into the cracks. One explanation is that bigger volume of fibre bridging the crack create a more tortuous path that limits the penetration of chlorides into the cracks. Besides, the products of corrosion generated into the cracks throughout the cycles fill part of the space originally available, creating an additional barrier to the ingress of salt solution – an effect that becomes more evident as the fibre content increases.

A third factor that explains the trend observed is related to the dependence of the chloride for the oxidation to take place. Chlorides break down the passive film and extract iron atoms from the fibres. This means that chloride ions might be momentarily retained near the surface of the fibre during the reactions. The increase of fibre content also increases the surface of iron able to momentarily retain chloride ions for the corrosion,

impeding some of them to proceed deeper into the crack. Such phenomena may result in less mobilization of chlorides to the deeper region of crack surface and justifies the more severe degree of corrosion located closer to the crack mouth in the case of mixes with higher fibre content.

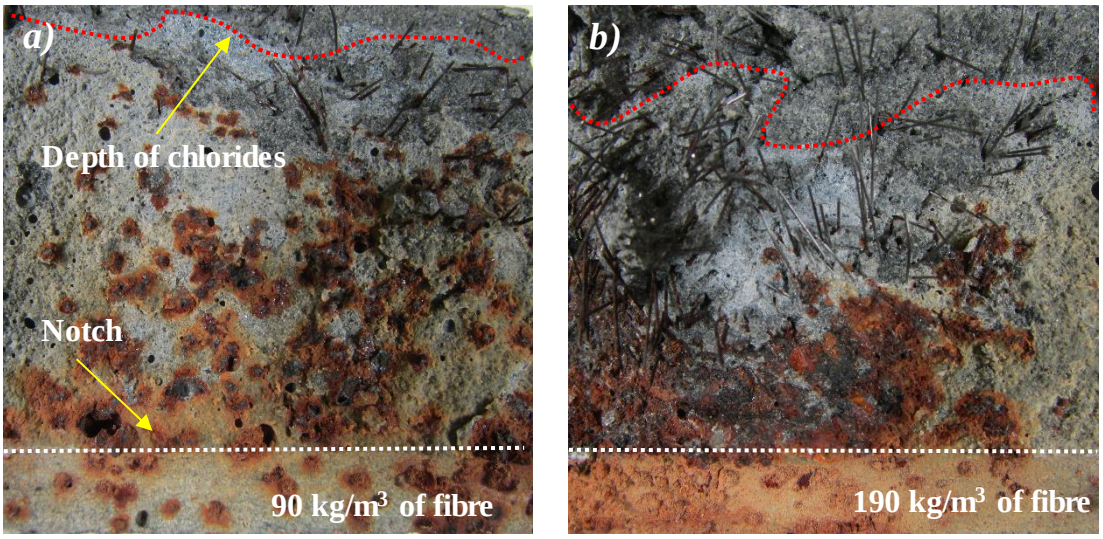

Figure 6.3 – Chlorides in specimens with crack width 0.50 mm at 95 cycles: fibre contents of a) 90 kg/m^3 and b) 190 kg/m^3.

6.3. FIBRE CORROSION IN CRACKS

The mechanisms of corrosion in steel fibre is an electrochemical process which occurs when the iron is exposed to corrosive environment. In the case of cracked section, the steel fibres crossing the cracks are directly in contact with the salt solution. During the chloride wet-dry cycles, a continuous supply of water, chlorides ions and oxygen into the crack increases the process of corrosion. Figure 6.4 illustrates the two main corrosion mechanisms that can be distinguished along the fibre bridging the cracks.

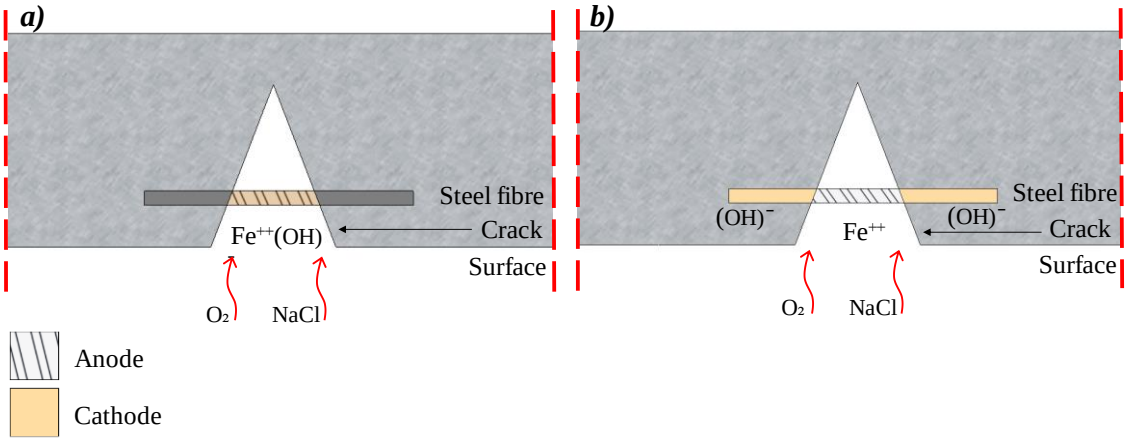

Figure 6.4 – Mechanisms of fibre corrosion into the cracks.

The part of the steel fibre that shows a negative potential behaves as an anode, while the reminder acts as a cathode (Blagojević 2016). The corrosion occurs in the anodic part from which current flows to the cathodic site where the release of hydroxyl ions OH^- takes place. The cathode is connected to the anode by the electrolyte (solution in the pores of the composite or in the crack) which conduct the current. To complete the electric circuit, the current come back through the steel fibre surface.

Based on a conceptual model of Schiessl (1997), two different mechanisms of fibre corrosion can occur in the cracked zone or in the surrounding area: microcell corrosion and macrocell corrosion. In the mechanism of microcell corrosion (see Figure 6.4-a), the corrosion takes place in the region of the fibre crossing the crack, and both cathodic and anodic processes occur side by side, where the oxygen can easily penetrate from outside through the crack. In the case of the macrocell corrosion (see Figure 6.4-b), the region of the fibre in the cracked zone acts as an anode while the passive region of the fibre into the cementitious matrix acts as a cathode.

The study of the corrosion over the cycles in cracked specimens was performed by means of a visual inspection of the crack surfaces using the criterion for classification of level of corrosion described in section 3.3.4. Figure 6.5 shows the level and depth of corrosion of specimens with 90 and 190 kg/m^3 of fibre (pre-crack width of 0.35 mm) at cycle 65. Figure 6.6 summarizes the average depth affected by each level of corrosion.

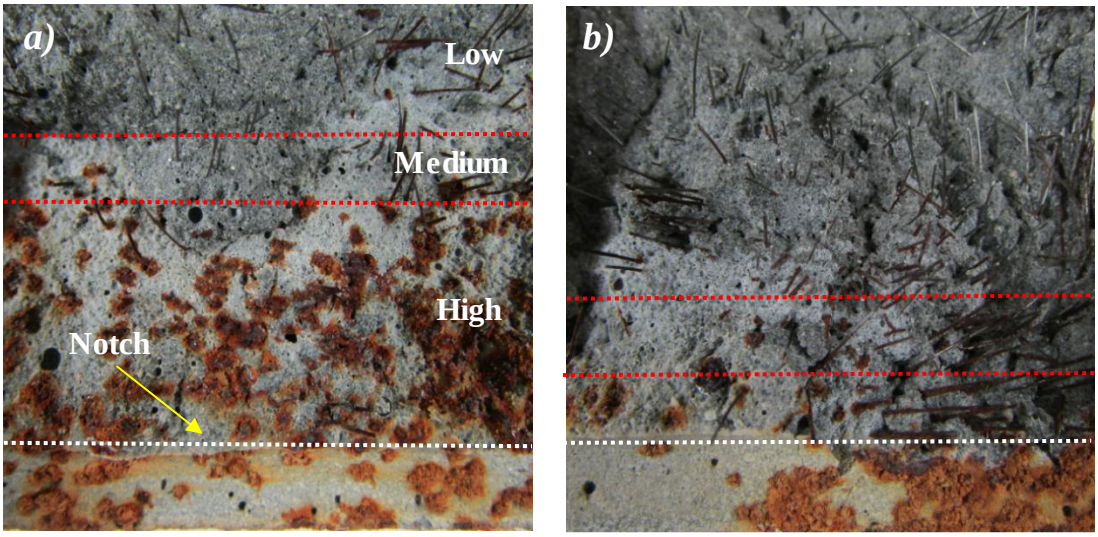

Figure 6.5 – Degree of fibre corrosion for specimens with crack width 0.35 mm at 65 cycles: fibre contents of a) 90 kg/m^3 and b) 190 kg/m^3.

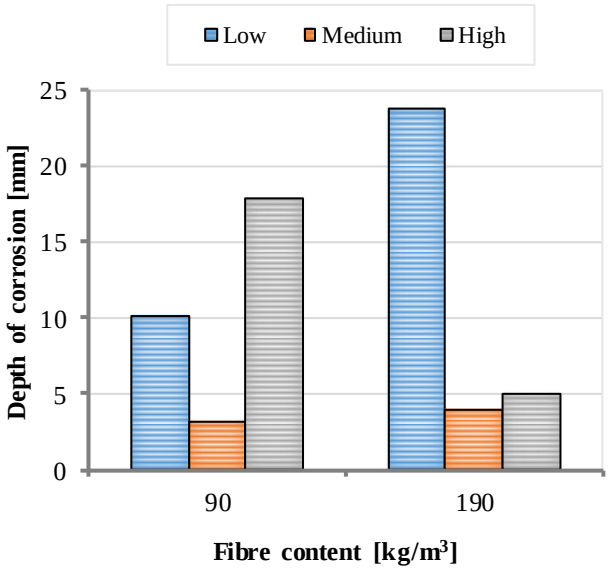

Figure 6.6 – Average depth for each level of corrosion in specimens with 65 wetting and drying cycles and crack width of 0.35 mm: fibre contents of with 90 and 190 kg/m^3.

The results reveal that specimens with 90 kg/m^3 of fibre present a bigger depth affected by high level of corrosion while specimens with 190 kg/m^3 present bigger depth with low level of corrosion. As described in the previous section, mixes with smaller fibre contents (90 kg/m^3) allow higher chloride penetration into the cracks over cycles. Furthermore, the chloride ions have to attack a smaller number of fibres, leading to a higher proportion of chlorides ions available to each fibre. Both factors lead to a more severe corrosion process of individual fibres in mixes with smaller fibre content.

Figure 6.7 shows the level and depth of corrosion of specimens crack widths of 0.05 and 0.50 mm (both containing 90 kg/m^3 at 35 cycles). The average values of the depth of each level of corrosion are presented in Figure 6.8.

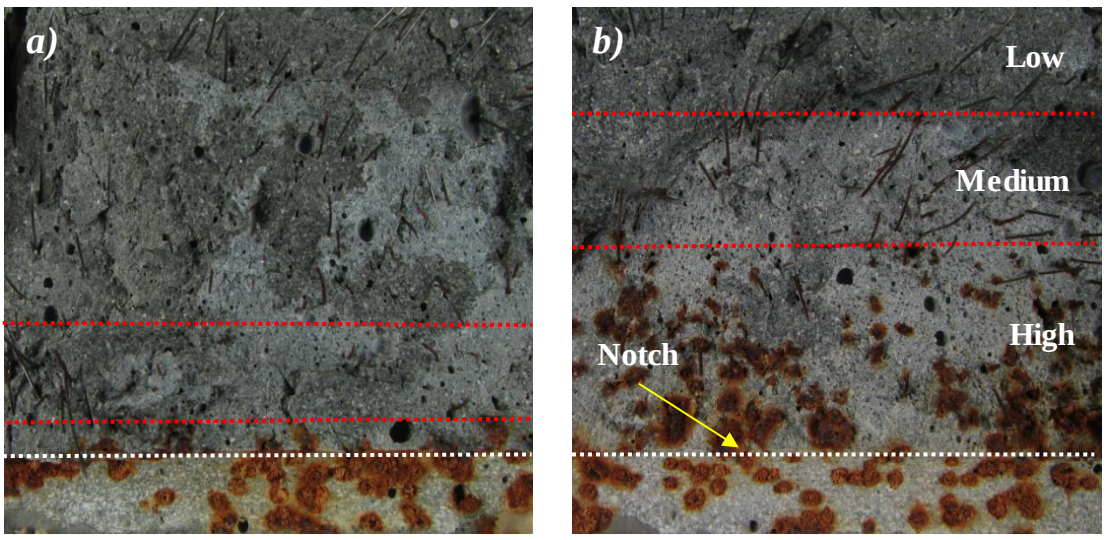

Figure 6.7 – Degree of fibre corrosion for specimens with 90 kg/m^3 at 35 cycles: crack widths of a) 0.05 mm and b) 0.50 mm.

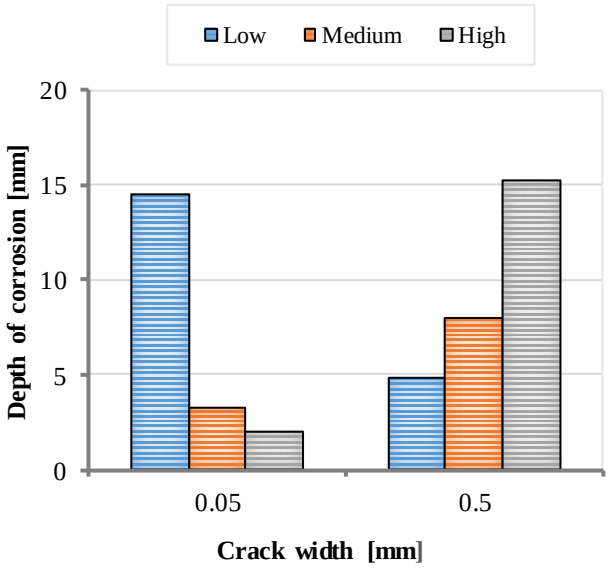

Figure 6.8 – Average depth for each level of corrosion in specimens with 35 cycles and 90 kg/m^3 of fibre: crack widths a) 0.05 mm and b) 0.50 mm.

Figure 6.7 shows that the surface of the crack width of 0.05 mm presents a negligible depth of high corrosion while the crack of 0.50 mm presents significant portion of the crack surface with a high level of corrosion. As expected, the bigger the crack width, the bigger the penetration of salt solution and oxygen over the cycles. This confirms that the crack width plays a key role and is the most important parameter in the evolution of the fibres corrosion. Narrow cracks limit the potential entrance of chlorides, reducing the degradation of the fibres along the crack.

The effect of the number of cycles on the corrosion is analysed for specimens with 35 and 95 cycles. The depth and level of corrosion are illustrated in Figure 6.9 for the samples with 140 kg/m^3 of fibre and crack width of 0.50 mm. Additionally, the average values of depth of corrosion relative to each level of corrosion are plotted in Figure 6.10. These figures reveal that the number of cycles increase the depth of cracked section affected by high level of corrosion. As expected, the increase in the concentration of chlorides over he cycles favours the corrosion process.

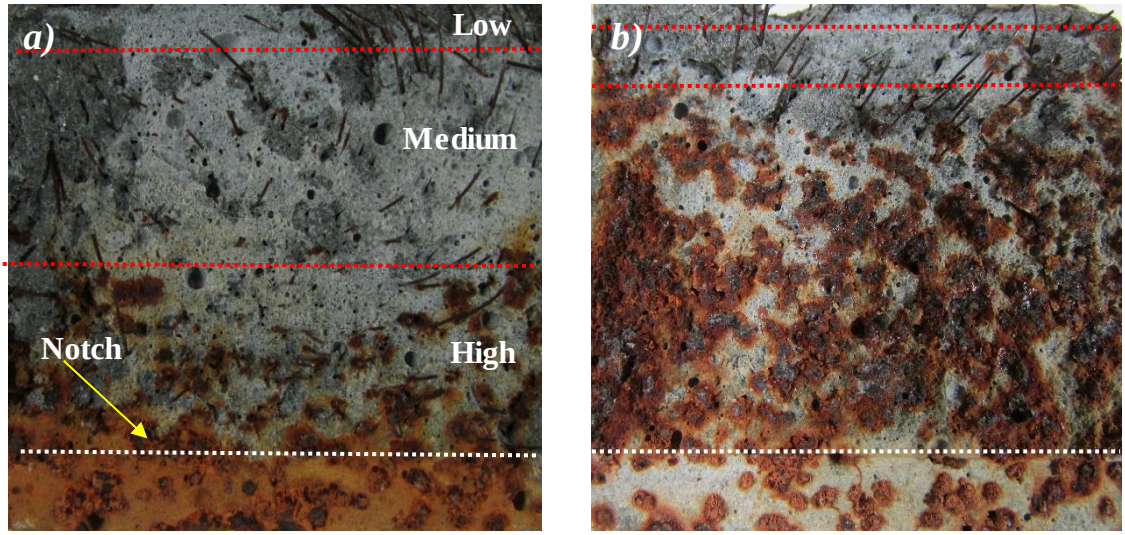

Figure 6.9 – Degree of fibre corrosion for specimens with 140 kg/m^3 of fibre and crack width 0.50 mm: cycles a) 35 and b) 95.

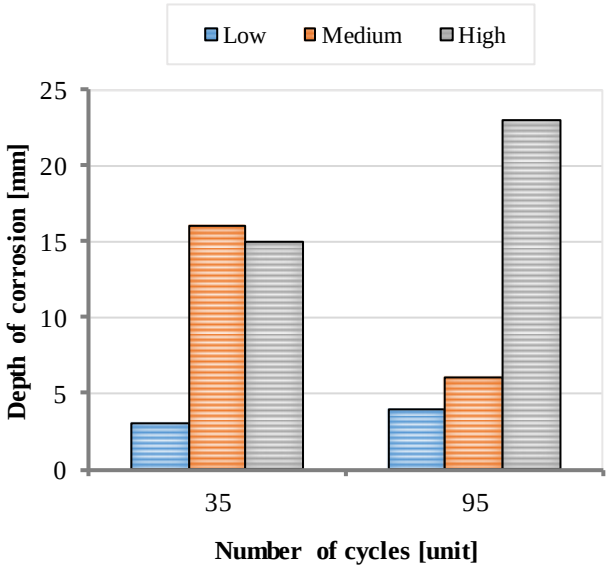

Figure 6.10 – Average depth for each level of corrosion in specimens with 140 kg/m^3 of fibre and crack width 0.50 mm: cycles a) 35 and b) 95.

6.4. HIGH CORROSION IN CRACKS

The high level of corrosion of the steel fibres in cracks may affect their crack bridging capacity since most of the fibre cross section is compromised. For further analysis of the effects of corrosion in the structural behaviour of HPSFRCC subjected to wet-dry cycles, the depth and rate of high corrosion in cracked section are analysed. Figure 6.11 illustrates the evolution of the depth and rate of high corrosion for the samples with 90, 140 and 190 kg/m^3 of fibre, at 5, 35, 65, 95 and 125 cycles (20, 140, 260, 380 and 500 days, respectively) and for crack widths of 0.05, 0.20. 0.35 and 0.50 mm.

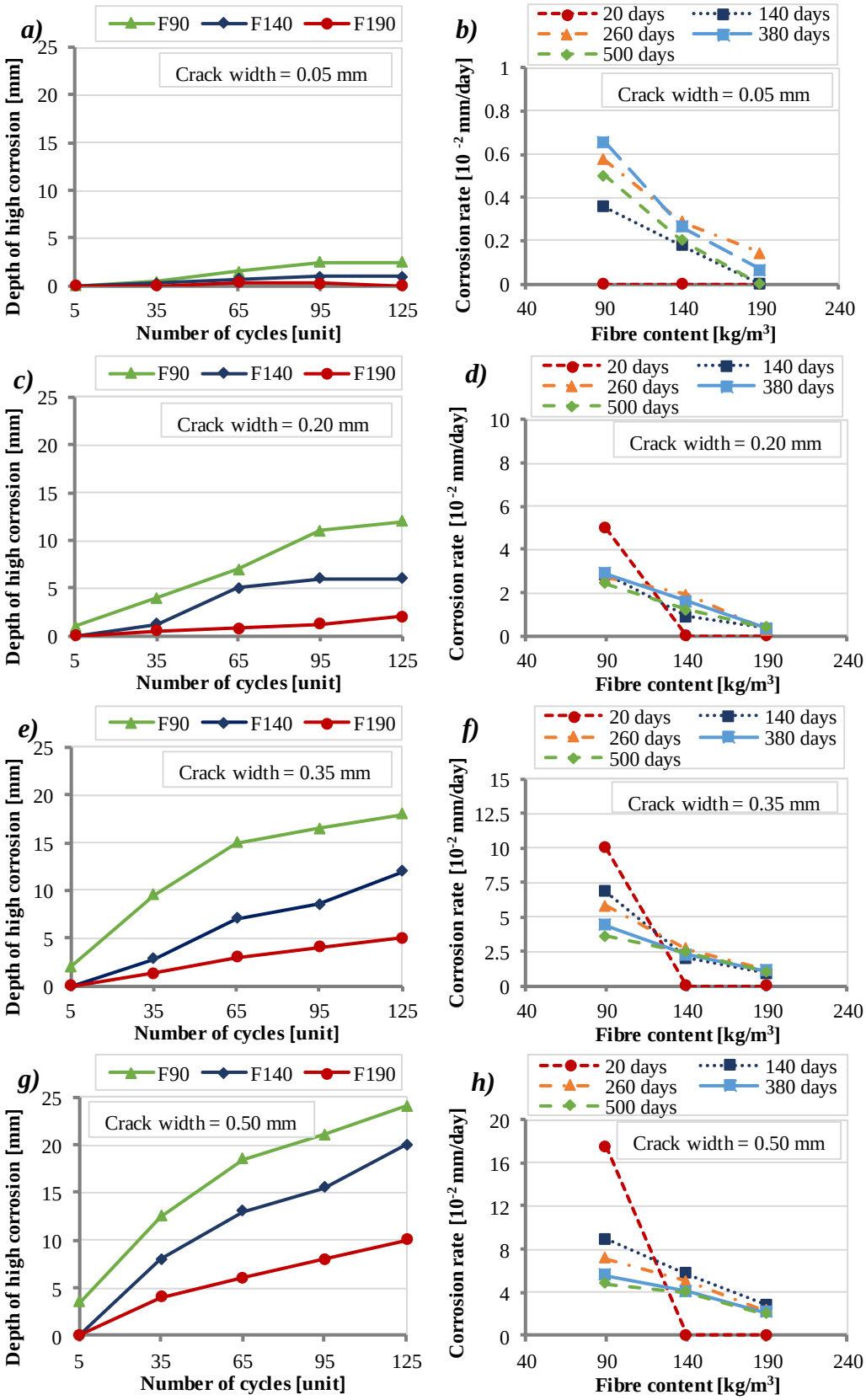

Figure 6.11 – High corrosion in cracks: a) depth of high corrosion and b) high corrosion rate.

Figure 6.11 reveals that the increment of the crack width increase significantly the high level of corrosion over time. Wider cracks lead to greater depths of high level of

corrosion. The higher crack width studied (0.50 mm) presented the greatest values of severe damage of the fibres, which may reduce strongly the crack bridging capacity during the pull-out. Parts of the fibre embedded into the matrix are completely damaged by corrosion, potentially compromising the mechanisms of transference of stress between fibre and matrix. The results show that the high corrosion rate increases significantly over the cycles with the increment of the crack width. In the case of the fibres studied, corrosion evolves fast due to the small cross sectional area of the fibre.

In the case of the crack of 0.05 mm, the increment tends to a stability and with negligible values due to the smaller ingress of chlorides, water and oxygen. In the case of wider cracks (0.20, 0.35 and 0.50 mm), no sign of reduction of the high corrosion rate is observed under accelerated exposure over cycles. Such outcome may indicate that the crack openings controlling the entry and the concentrations of corrosive substances lead to a continue damage of the fibres relative to the availability of iron.

6.5. MICROANALYSIS OF THE CRACKED SURFACE

In order to evaluate the effects of the chlorides throughout the cycles in the cracked specimens, a scanning electron microscopy with EDS was carried out after the mechanical tests. Results obtained in the EDS spectra are represented as the relative intensities of each element, placed above each image. The peaks considered for measurement of Ca, Si, Fe Na, Al, Cl, O and K correspond to the energies of 3.6, 1.8, 6.3, 0.9, 1.5, 2.7 and 3.4 keV, respectively.

The evolution of the corrosion of the fibres in cracked section is performed for 5 and 125 cycles. In addition to that, the interface between fibre-matrix, the surface of the fibre, the phases deposited on the surface of the fibre, the holes of the fibres pull-out, the distribution of oxides in the matrix and the damage of fibre-matrix interface were analysed at 0, 35, 65 and 95 cycles.

6.5.1. Microanalysis of the corrosion products

Figure 6.12 shows SEM images of the fibres from the cracks at 5 and 125 cycles. A general overview reveals a significant level of degradation of the fibre over cycles. At 5 cycles (see Figure 6.12-a and b), the fibre presents almost the original cross section and products of corrosion are formed along the surface. As observed by Dauberschmidt (2006) (see Section 5.5.1), the chloride induced corrosion in cold-draw steel fibre initiates in the micro-flaws of the fibre surface. These imperfections extend along the length of the fibre, where the passive film is not so stable, facilitating the formation of pits of corrosion. The presence of the products of corrosion along the micro-flaws is clearly observed.

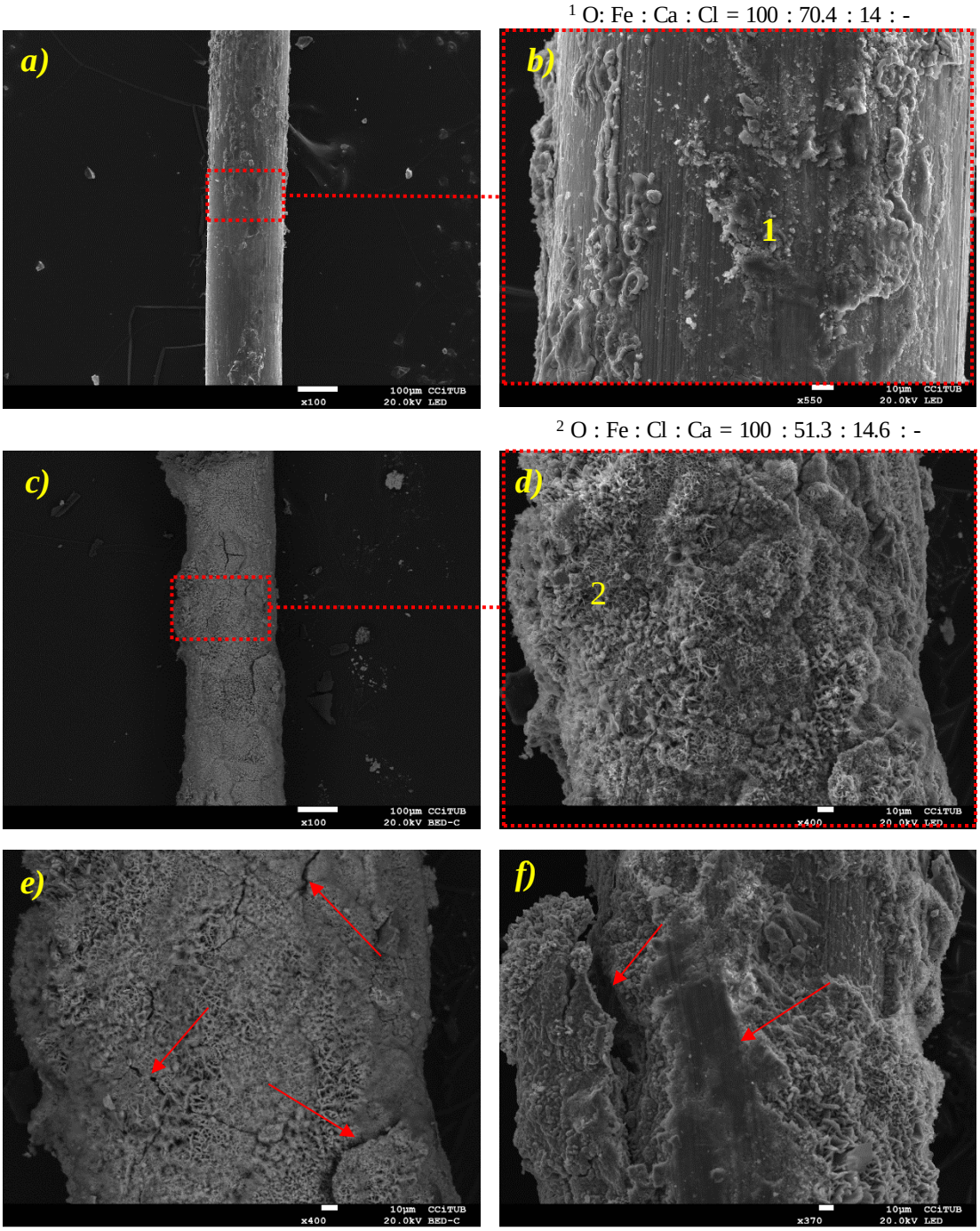

Figure 6.12 – SEM images of the fibre: a) at 5 cycles, b) detail of corrosion at 5 cycles, c) at 125 cycles, d) detail of corrosion at 125 cycles, e) detail of cracks of rust film at 125 cycles and f) detail of detached corrosion film at 125 cycles.

The analysis reveals the presence of products of the matrix (calcium hydroxide) at fibre surface. It may be a consequence of the good bond between fibre and matrix. After the pull-out, the fibre keeps its original diameter slightly increased by the corrosion. A slight level of corrosion might enhance the bond of the ITZ. According to Granju and Balouch (2005), the small deposition of corrosion products makes the external surface of the fibres rougher, creating additional resistance to slippage.

The microanalyses in Figure 6.12-c and d show a very severe corrosion generalized in all surface, forming a homogeneous film of iron oxides and hydroxides after 125 cycles. The surface is covered by a significant volume of products of corrosion that increase the cross section of the fibre. This is observed along the whole length, including the part embedded in the matrix. Such result may indicate that the microcell and macrocell corrosion is formed along the fibre length embedded in the matrix and crossing the cracks.

The rust layer formed at the surface of the fibre after 125 cycles (see Figure 6.12-e) presents high exfoliation. According to de la Fuente (2016), the corrosion film tends to exfoliate and become partly or completely detached from the base substrate, which may be composed of multiple rust phases (see Figure 6.12-f).

6.5.2. Microanalysis of the fibre – matrix interface

The microanalysis of the fibre-matrix ITZ at 0, 35, 65 and 95 cycles are presented in Figure 6.13. The results indicate that over the cycles, the corrosion also damages the fibre-matrix ITZ with potentially detrimental consequences for the bond strength.

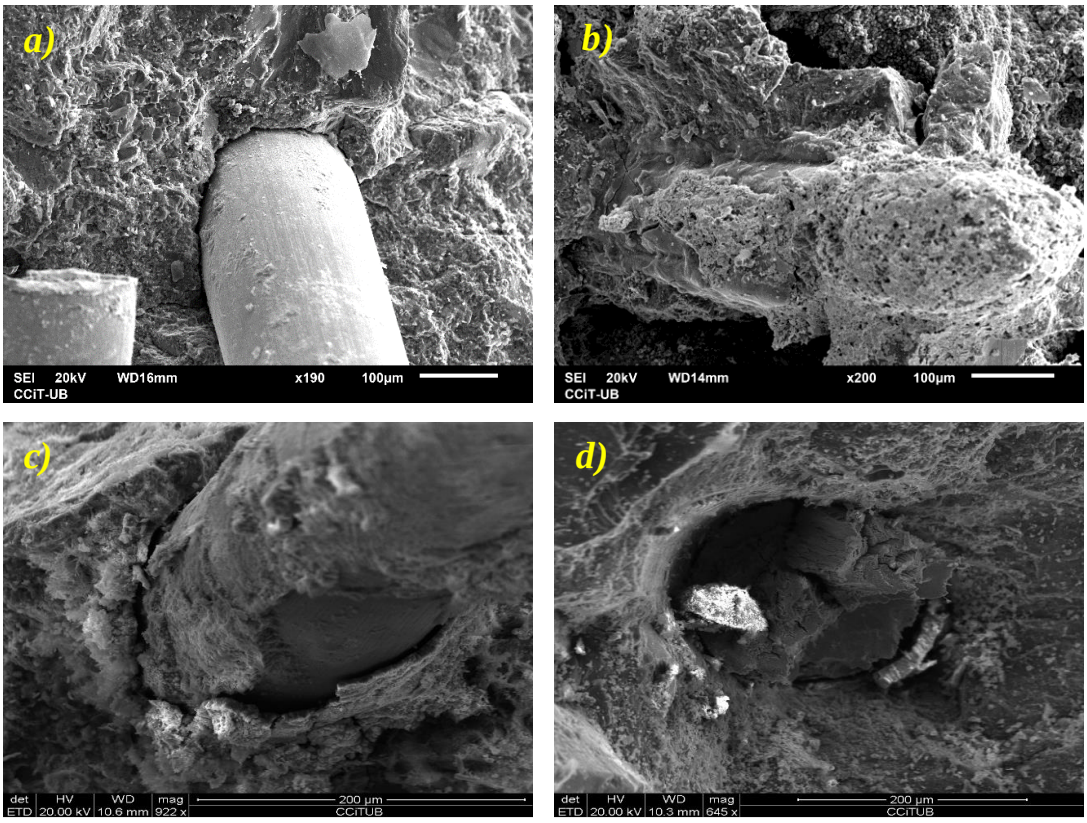

Figure 6.13 – SEM images of the fibre – matrix ITZ: at a) 0, b) 35, c) 65 and d) 95 cycles.

The microanalysis of the interface fibre-matrix at 0 cycles (see Figure 6.13-a), indicates that the region presents a morphology similar to that of the bulk matrix. The use of micro silica and of large amount of cement enhanced the microstructural properties of

the bulk matrix and ITZ. Besides that, the diameter of the micro-steel fibres (0.2 mm) is of the same order of magnitude of the aggregates, producing a good packing density of all components of the mixes.

The microstructure of the ITZ with 35 cycles (see Figure 6.13-b) shows significant presence of iron oxides and hydroxides. The analysis may indicate that the corrosion of the fibre reduces its cross sectional area and the ferrous oxides generated spread into the pores of the ITZ, which could justify an enhancement of the fibre-matrix bond. The SEM image at 65 cycles (see Figure 6.13-c) show that iron oxides and hydroxides dominate the ITZ. The significant amount of products of corrosion around the fibre might cause a reduction of bond strength and embrittlement of the ITZ, leading to reduced post-peak behaviour. At 95 cycles (see Figure 6.13-d) the corrosion has affected the whole cross section of the fibre, possibly eliminating its capacity to bridge the crack.

6.5.3. Microanalysis of the fibre surface

The microanalysis of the fibre surface presented in Figure 6.14 corresponds to 0, 35, 65 and 95 wetting-drying cycles. The pictures highlight a significant level of fibre degradation in the cracked section. Notice that the loss of cross sectional area of the fibres is directly related to the increment of number cycles.

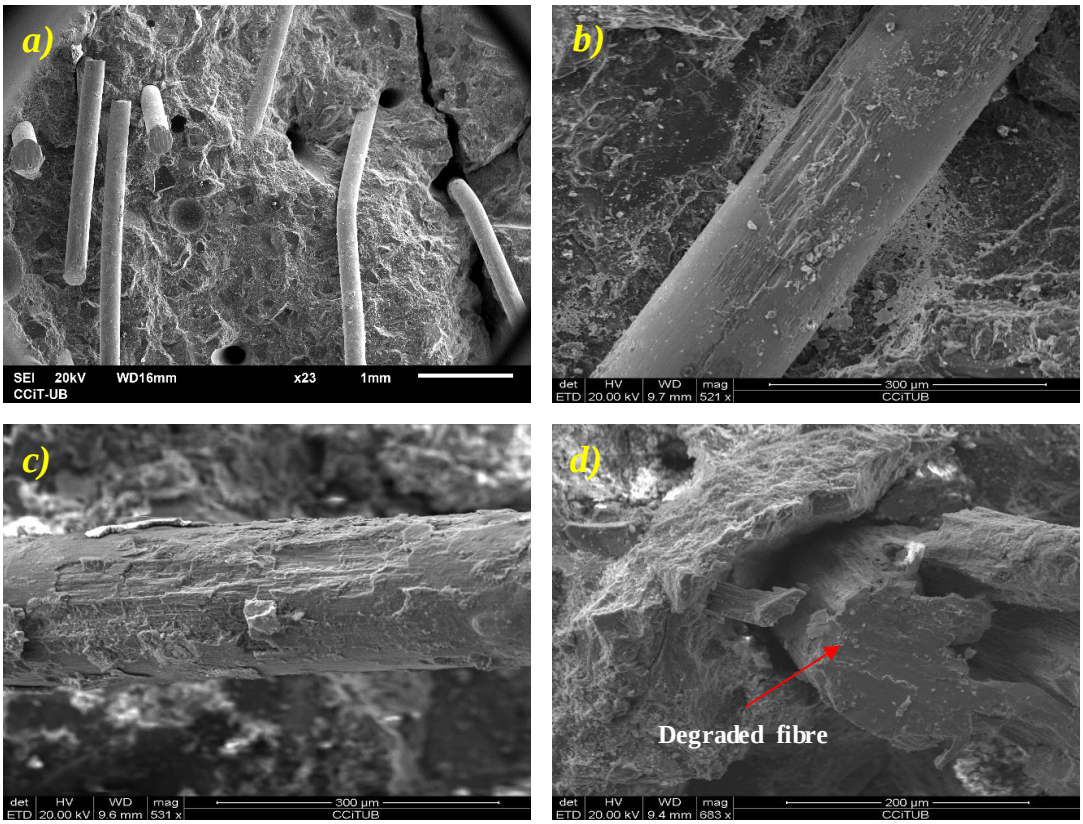

Figure 6.14 – SEM images of the fibre surface: a) 0, b) 35, c) 65 and d) 95 cycles.

Figure 6.14-a reveals that at 0 cycle (before the attack), steel fibres present a smooth surface with no sign of degradation. At 35 cycles (see Figure 6.14-b), the fibre presents a degraded surface with irregular and deep grooves indicating the reduction of the cross sectional area. A significant level of degradation is observed in the fibre surface at 65 cycles (see Figure 6.14-c) and corrosion products peel off of the fibre surface. At 95 cycles (Figure 6.14-d), the fibre is fully corroded and only rusted steel remains.

6.5.4. Microanalysis of phases deposited on the fibre surface

Figure 6.15 presents the SEM images of phases deposited on the fibre surface with 0, 35, 65 and 95 cycles. A general overview of the analysis reveals that the presence of chlorides induced an increment in the amount of products of corrosion at the fibre surface.

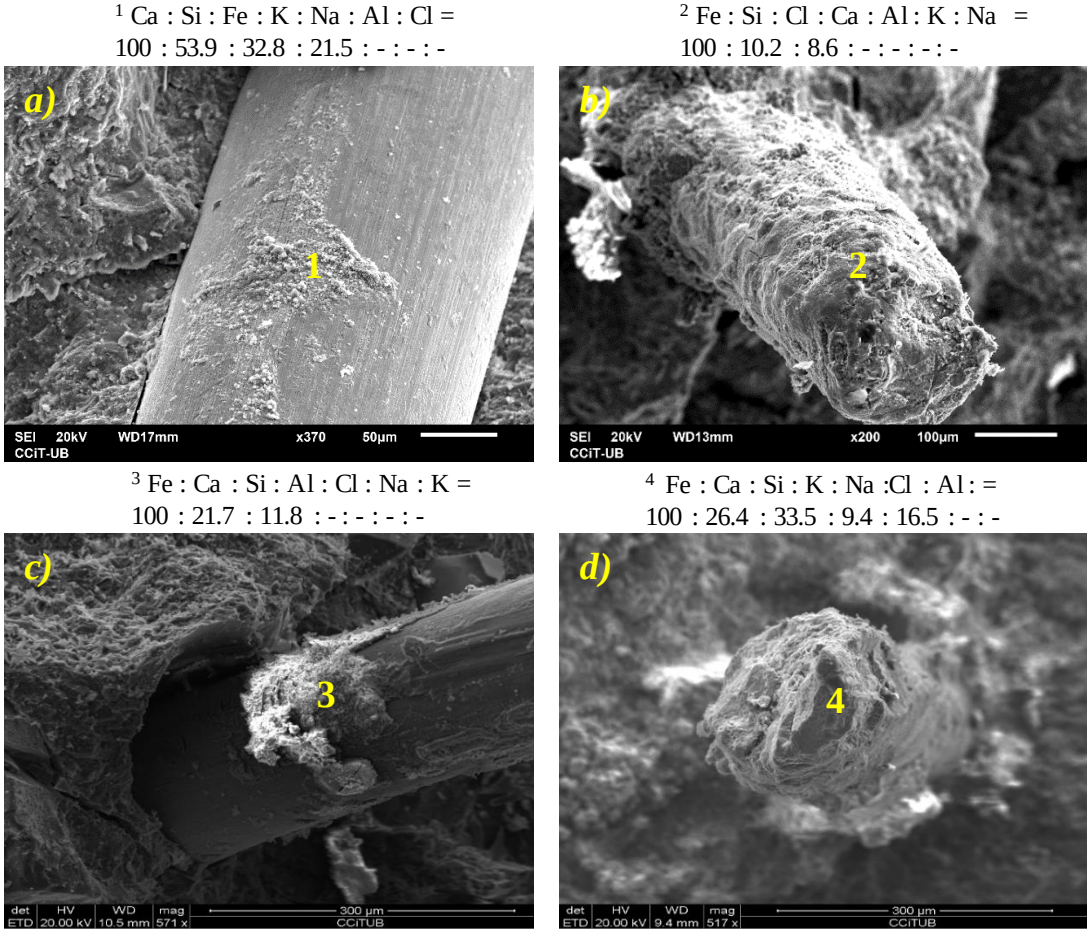

Figure 6.15 – SEM images of phases deposited on the fibre surface: a) 0, b) 35, c) 65 and d) 95 cycles.

The SEM image of the fibre at 0 cycle (see Figure 6.15-a) shows mainly C-S-H and portlandite deposited on the fibre surface. At 35 cycles, (Figure 6.15-b) a significant presence of iron oxides and a low content of hydration products deposited on the fibre surface are identified in the EDS results. At 65 cycles, the analysis shows that a large amount of products of corrosion over fibre the surface (see Figure 6.15-c). After 95 cycles (see Figure 6.15-d) almost only iron oxides and hydroxides appear on the fibre surface.

6.5.5. Microanalysis of fibre pull-out holes

Figure 6.16 shows the holes after fibre pull-out at 0, 35, 65 and 95 cycles. The evolution of fibre corrosion over the cycles is observed by the reduction of the size and change in the shape of the fibre pull-out holes.

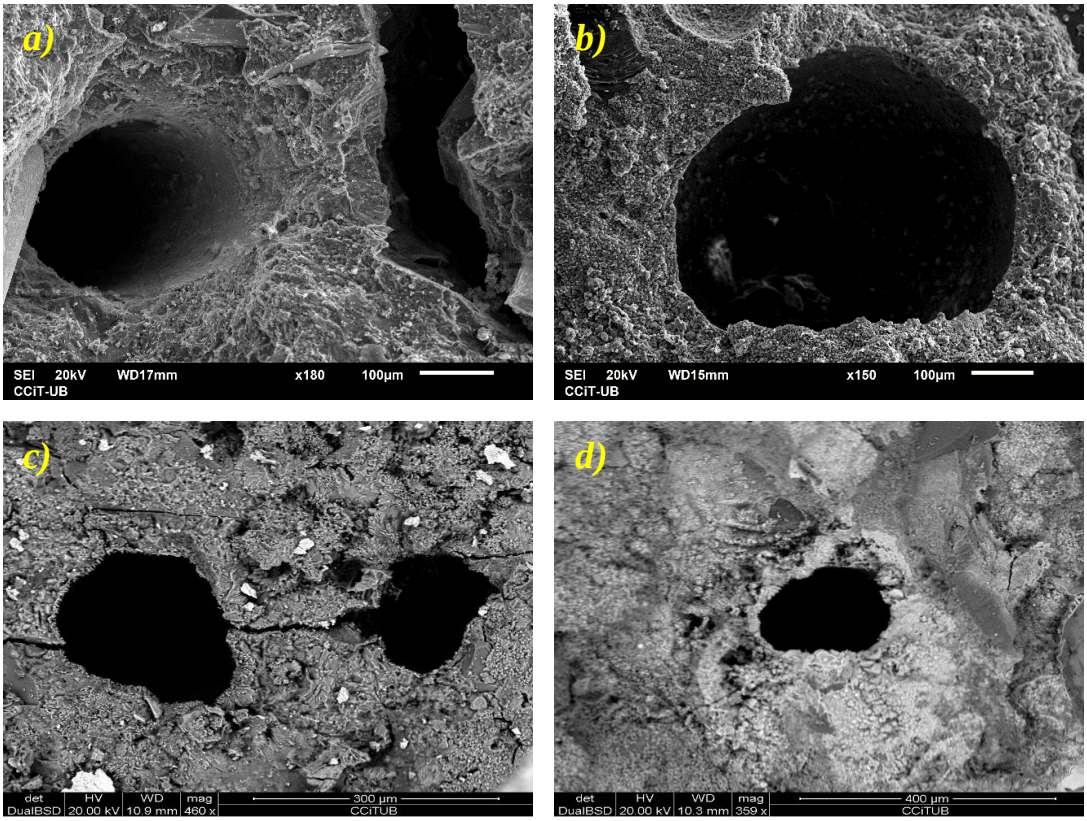

Figure 6.16 – SEM images of fibre pull-out holes: a) 0, b) 35, c) 65 and d) 95 cycles.

The microanalysis at 0 cycles (see Figure 6.16-a) reveals that the hole from the fibre pull-out can be observed with the original shape produced by the fibre and with no sign of reduction of the diameter. The hole presents a smooth, uniform and compact surface with few crystals deposited. At 35 cycles (see Figure 6.16-b), a reduction in the diameter of the hole can be observed. It may be attributed to the loss of cross sectional area of the fibre due to the corrosion. A consequent deposition of iron oxides is also observed in the border of the hole.

At 65 cycles (see Figure 6.16-c) a significant reduction of the diameter of the holes is observed, which may be attributed to the increase of chlorides exposure in the cracked area which produced further degradation of the fibre. The region presents a high amount of iron oxides. At 95 cycles (see Figure 6.16-d), the greatest reduction of the size of the hole is observed.

6.5.6. Microanalysis of the distribution of iron oxide in the matrix

Figure 6.17 shows the analysis of the distribution of iron oxide in the surface of the cracks at 0, 35, 65 and 95 cycles. The analysis shows a significant presence of products of corrosion (iron oxides and hydroxides) deposited in the matrix as the number of cycles increases.

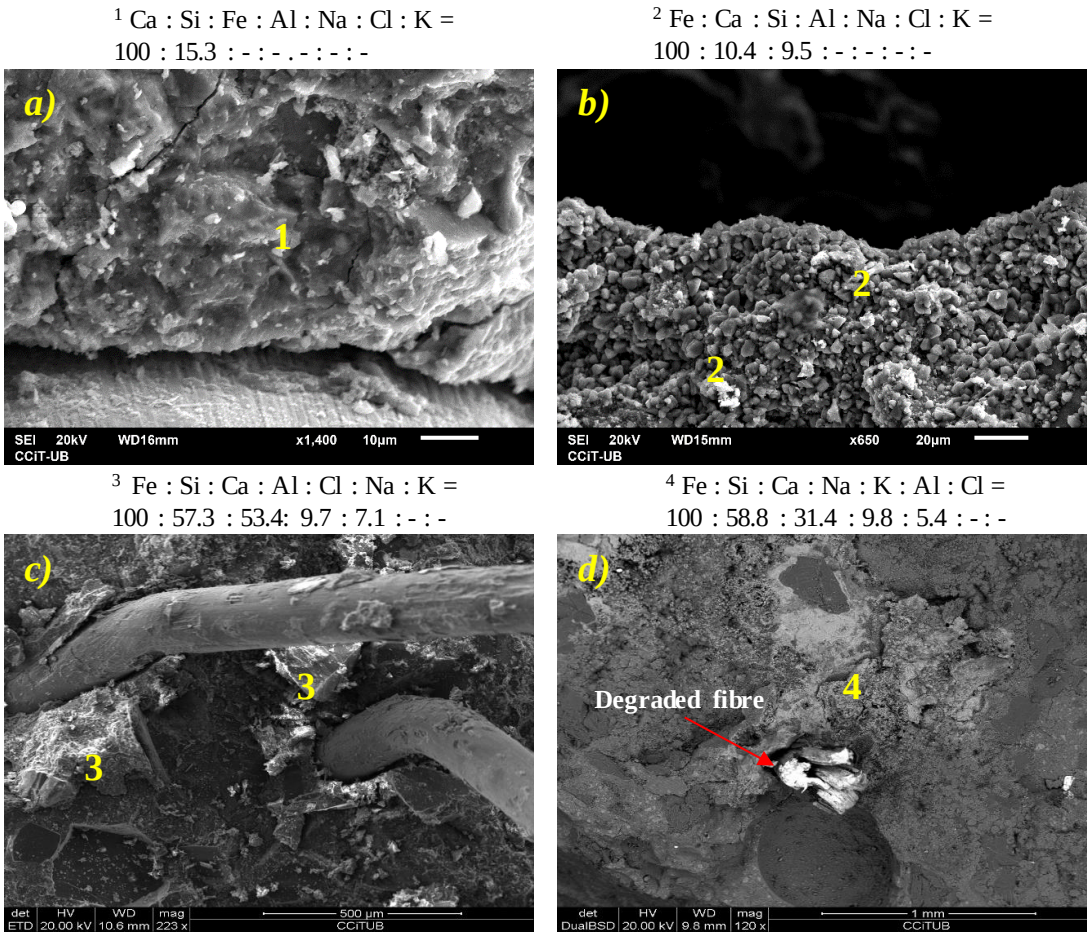

Figure 6.17 – SEM images of distribution of iron oxide in the matrix: a) 0, b) 35, c) 65 and d) 95 cycles.

The analysis reveals that at 0 cycles (see Figure 6.17-a), no sign of iron oxides can be noticed in crack surface. The microstructure presents a dense matrix mainly composed by hydration products with a major predominance of C-S-H and with a good bond between the different components. At 35 cycles (see Figure 6.17-b), the presence of iron oxides can be observed specially in the areas close to the steel fibres or the fibre pull-out holes. As the corrosion progresses, products of corrosion are deposited in the ITZ and region surrounding the fibres filling the pores or laying at the surface.

The SEM image at 65 cycles (see Figure 6.17-c) presents an increment of the presence of iron oxides distributed in the matrix close to the corroded fibres. At 95 cycles (see Figure 6.17-d), a large amount of iron oxides is found in the bulk matrix.

6.6. CONCLUDING REMARKS

Chapter 6 presented the analysis of chlorides corrosion in cracked section and its effects in the degradation of the fibre and the crack surface. The following conclusions may be derived from the results:

- The crack width has a great influence in the depth of ingress of chlorides in cracked section. In narrow cracks the higher concentration of chlorides is observed in the region close the crack mouth while in wider cracks a high chloride content is distributed over the crack surface. The studies conducted here suggest a limited chloride penetration that tend to reach stability over the cycles for specimens with crack width of 0.05 mm. Other specimens with bigger crack widths showed significant chloride penetration and signs of damage.

- The concentration and the depth of penetration of the chlorides into the crack reduce with the increase of the fibre content. The bigger number of fibre in the cross section increase the tortuosity of the path that chloride has to take to enter the crack. Corrosion products fill part of the space left, further increasing the tortuosity and limiting the entrance of chlorides. Moreover, a bigger number of fibres retain the chloride ions, hindering their penetration.

- A smaller level of corrosion of individual fibres is observed as the fibre content of the mix increases. In addition to the smaller penetration of chlorides mentioned previously, the bigger number of fibres implies that less chloride ions are available to enable the corrosion of each fibre. Consequently, the level of damage to individual fibres is reduced.

- The microanalysis indicates that fibres crossing the cracks are greatly affected by corrosion, showing deposition of corrosion products and an increase in diameter that affects the ITZ. In more advanced stages of corrosion, the whole cross section of the fibre is compromised.

7. CORROSION IN CRACKED SECTION - MECHANICAL BEHAVIOUR

7.1. INTRODUCTION

Results from Chapter 6 suggest that the presence of cracks in HPSFRCC specimens may accelerate fibre damage under aggressive environment. According to Marcos- Meson *et al*. (2018), inconsistences regarding the consideration of the steel fibres for SFRC exposed to chlorides suggest a limited understanding of the mechanisms governing chloride-induced corrosion on steel fibres and its effects on the mechanical behaviour of SFRC. This is particularly relevant for HPSFRCC specimens presenting cracks. Abbas (2014) reported that fibres crossing hairline cracks ($w \leq 0.2$ mm) presented limited level of corrosion followed by negligible reductions of the residual tensile strength. Serna and Arango (2008) observed that specimens with narrow cracks ($0.5 \text{ mm} \geq w > 0.2 \text{ mm}$) under wet-dry cycles with chlorides showed high level of corrosion, considerable loss of fibres cross-sectional area and reductions of the residual response.

An extensive experimental programme was conducted to provide deeper insight about the consequences of chloride-induced corrosion in cracked HPSFRCC specimens in the mechanical response of the fibres bridging the cracks. The influence of fibre content, crack width and total number of cycles exposure were assessed. The **general objective** of this chapter is to provide a deeper insight in the phenomenon and its mechanical consequences through the analysis of the results from the experimental programme. The following **specific objectives** are defined:

- Study the influence of fibre content and crack width in terms of the Load-CMOD curves, the residual flexural strength (f_{R1}, and f_{R3}) and of the absorbed energy;
- Analyse the evolution of these parameters depending on the number of wet-dry cycles;
- Identify the mechanisms affecting the structural performance of pre-cracked HPSFRCC specimens subjected to chloride cycles.

Section 7.2 presents a brief explanation of the variables of the experimental programme. Subsequently, sections 7.3 and 7.4 analyse respectively the influence of the fibre content and of the crack width in the results from 3-point bending tests. Section 7.5

discusses the evolution of the mechanical performance with the cycles. Finally, section 7.6 summarizes the main conclusions derived from the study.

7.2. VARIABLES STUDIED

Figure 7. illustrates the variables studied in the programme. Given the great number of experimental data and the similarities of the tendencies observed, only the main results are presented and discussed in this chapter. The complete data of all tests performed on pre-cracked specimens are presented in Appendix A. For more details about the experimental programme consult Chapter 3.

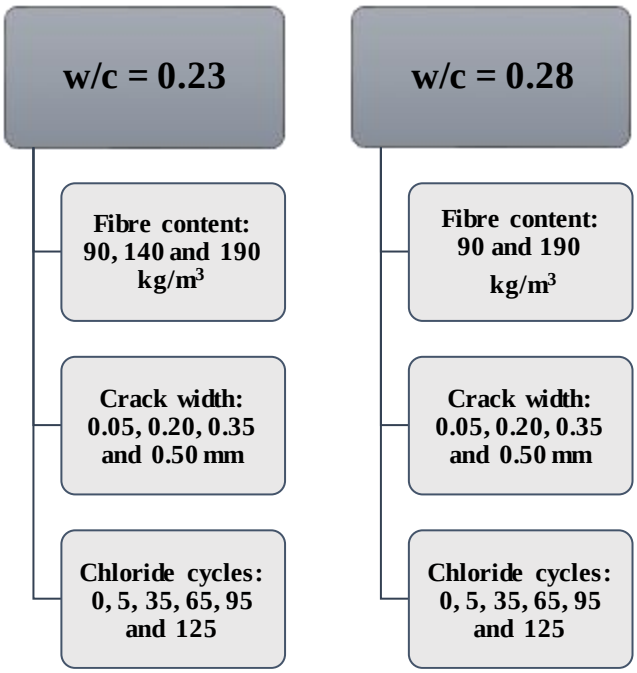

Figure 7.1 – Variables studied in the specific experimental programme.

7.3. ANALYSIS OF THE INFLUENCE OF FIBRE CONTENT

7.3.1. Load – CMOD curves

Figure 7.2 shows the average load-CMOD curves obtained for fibre contents of 90, 140 and 190 kg/m^3 with pre-crack width of 0.50 mm and water/cement ratio (w/c) of 0.23. To avoid repetitions, only curves corresponding to cycles 0 (before attack), 35, 65 and 95 cycles are presented. Notice that the CMOD of 0 is equivalent to the pre-crack width. All curves show a similar shape regardless of the variable studied. In the initial stage of the test, the load increases rapidly for small increments of CMOD. Once a peak is reached, the load diminishes with a pronounced increment of CMOD.

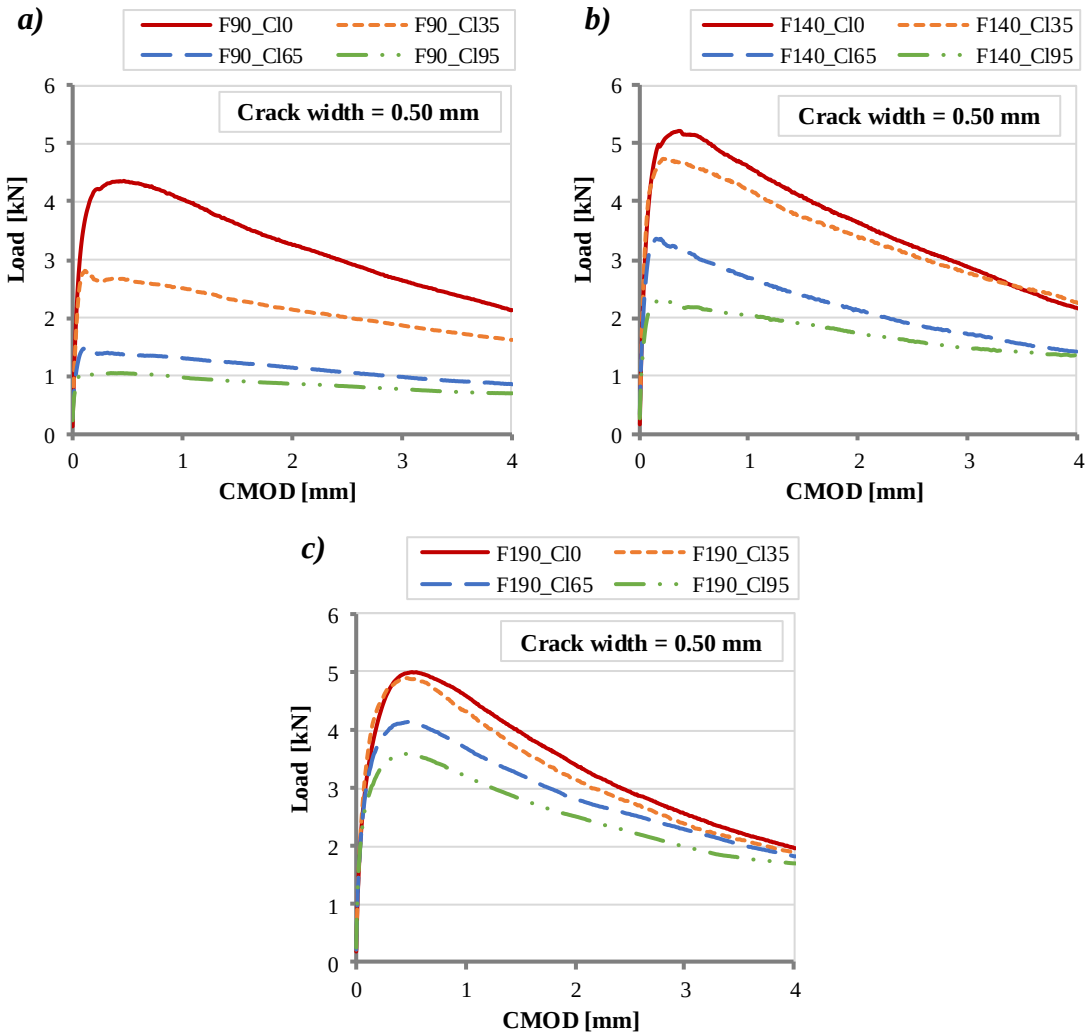

Figure 7.2 – Influence of fibre content in load-CMOD curves for specimens with crack width of 0.50 mm: a) 90 kg/m^3, b) 140 kg/m^3 and c) 190 kg/m^3 of fibre.

The influence of corrosion in the mechanical response becomes more evident with the cycles as a result of the enhanced degradation of the fibres. In general, the reduction in flexural resistant capacity is more evident for the pre-peak stage of the curve than for the post-peak stage. This is particularly evident for mixes with 90 kg/m^3 that present a post-peak reduction before the attack (cycle 0) that disappears for more advanced cycles. The contribution of the fibres to the residual strength after cracking comes from the pull-out resistance (Nordström 2005). Until the peak load, the pull-out resistance is mainly provided by the fibre-matrix bond through the ITZ. After the peak load, the response is increasingly governed by the sliding or breakage of fibres.

The more pronounced reduction of the pre-peak stage over the cycles may be a consequence of the faster reduction of the bond at the ITZ caused by the corrosion process, which was also observed in the analysis from Chapter 6. In the post-peak stage, bigger CMOD activate fibres located in the inner part of the cross-section, which require a bigger number of cycles to be affected. Another possible explanation is that to change significantly the post-peak response, fibres must start to break instead of sliding, which

requires more advanced levels of corrosion. Both explanations justify the effect of corrosion over the cycles are less noticeable in the post-peak stage of the curve.

The reduction in the maximum load becomes more evident as the fibre content decreases. Studies from Chapter 6 revealed that specimens with smallest fibre content (90 kg/m^3) presented the greatest depth affected by high levels of corrosion over the cycles, forming a porous layer of iron oxides and hydroxides at the ITZ that could compromise fibre-matrix bond. The smaller number of fibres led to a higher chloride availability per single fibre, thus accelerating their degradation. Conversely, specimens with the biggest fibre content displayed the smaller cross-section depth affected by high levels of corrosion. This explains why the drop in peak load becomes more evident as the fibre content decreases.

7.3.2. Residual flexural strength (f_{R1} and f_{R3})

Figure 7.3 shows the influence of fibre content in the average residual flexural tensile strengths f_{R1} and f_{R3} measured at cycles 0, 35, 65 and 95 in specimens with a pre-crack width of 0.50 mm and w/c equal to 0.23. Figure 7.3 also shows the relative results considering the respective strength at 0 cycles (100%) for each fibre content. Notice that residual strengths for mixes with 190 kg/m^3 of fibres tested at cycle 0 were strangely low in comparison with other mixes at cycle 0. This may be attributed to the scatter or problems during the production or testing of these specimens.

The results confirm that the fibre content has a major influence on the effect of corrosion in f_{R1} and f_{R3} - related with contribution provided by the fibres in the post-peak stage. Mixes with the lowest fibre content (90 kg/m^3) lead to the biggest reduction of resistant capacity over the cycles (see Figure 7.3-a). This reflects the rapid corrosion over the cycles that reduce the contribution of the fibres. The fact that smaller number of fibres are present not only accelerates the corrosion process but also increase its impact since there are less fibres left to pick up the bridging capacity. Conversely, the absolute values for the specimens with 190 kg/m^3 of fibre reduces more gradually over the cycles (see Figure 7.3-c). In additional to the smallest level of corrosion of each individual fibre, the cross-section counts with a bigger number of fibres that can maintain the bridging capacity.

These findings are also observed in the analysis of the relative residual flexural strengths (see Figure 7.3-b and Figure 7.3-d for f_{R1} and f_{R3}, respectively). Notice that the relative drop in the resistant capacity over the cycles is several times bigger for mixes with lower fibre content. Interestingly, the relative reduction in resistant capacity over the cycles is similar for f_{R1} and f_{R3}, which indicates that similar mechanisms govern the residual response of the fibres for such crack openings (mainly fibre-matrix slip or fibre breakage).

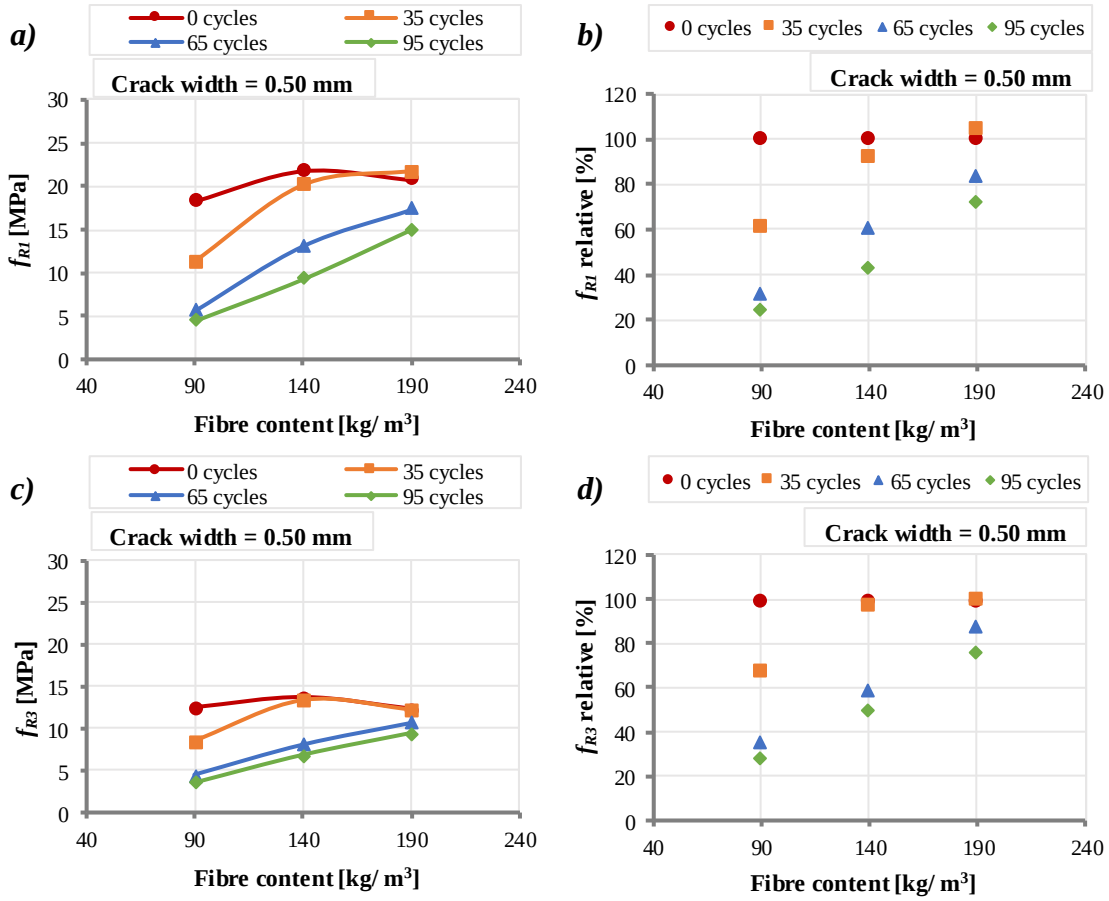

Figure 7.3 – Influence of fibre content in the residual flexural strengths: a) absolute and b) relative values for f_{R1} and c) absolute and d) relative values for f_{R3}.

7.3.3. Absorbed energy

The influence of the corrosion in the absolute and relative values of the energy absorption capacity is presented in Figure 7.4. For the study, specimens with three fibre content (90, 140 and 190 kg/m^3), pre-crack width of 0.50 mm, w/c of 0.23, at cycle 0, 35, 65 and 95 are considered. The relative values of the absorbed energy are related to the values of each fibre content at cycle 0 (considered 100%).

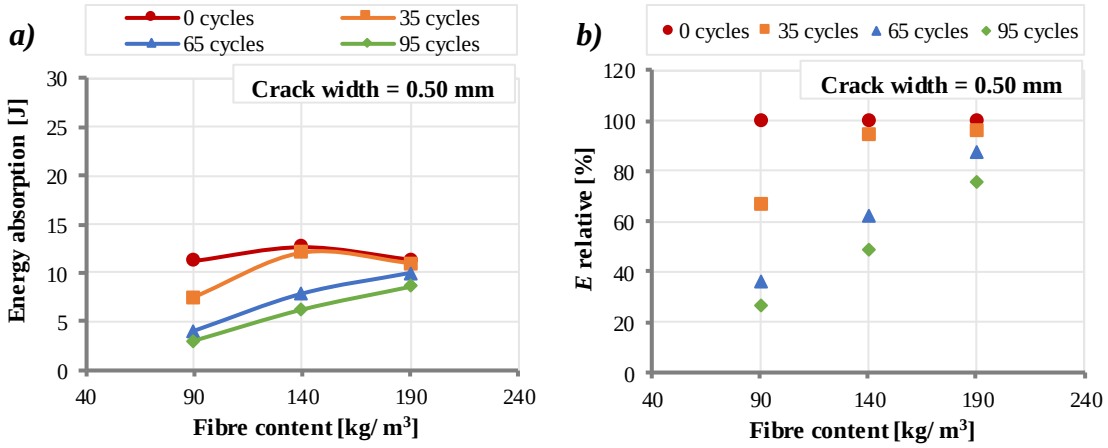

Figure 7.4 – Influence of the fibre content in the energy absorption: a) absolute and b) relative values.

The results reveal that the fibre corrosion over the cycles influence the absolute energy absorption values (see Figure 7.4-a). The degradation is more expressive for lower fibre content as it reduces strongly the cross-sectional area of the fibres as well as its structural contribution. The higher the level of corrosion, the higher the reduction of the fibres contribution in the post peak stage. Hence, a smaller enclosed area by the load-CMOD curve, which defines the energy absorption capacity is observed as lower residual loads occurs at larger deflections. Analogously to the described in previous sections for the peak load and residual strengths, the decrease in the energy absorbed over the cycles becomes more evident as the fibre content decreases.

7.4. ANALYSIS OF THE INFLUENCE OF CRACK WIDTH

7.4.1. Load-CMOD curves

In order to study the influence of the pre-crack width on the corrosion in pre-cracked HPSFRCC specimens, the load-CMOD curves obtained for the pre-crack widths of 0.05, 0.20 and 0.35 mm are presented in Figure 7.5. Given the similarity in the trend, only the curves corresponding to the mix with 90 kg/m^3 of fibre, w/c of 0.23 and cycle 0, 35, 95 and 125 are presented here.

All curves present a similar shape. In the first cycles, mixes with pre-crack widths of 0.05 mm and 0.20 mm present an increase in the whole load-CMOD curve after in the first cycles. A possible explanation for this behaviour could be that such specimens present a low level of corrosion whose effect is offset by a strength due to the additional hydration during the wetting stage. Furthermore, according to Granju and Balouch (2005), fibres with low level of corrosion may be surrounded by a thin layer of iron oxides and hydroxides that enhance the bond and further friction with the cementitious matrix. Consequently, contribution of fibres subjected to a low corrosion level could contribute to the mechanical performance.

Since the evolution of the damage is slower for specimens with pre-crack width of 0.05 mm, this favourable effect should be observed for a bigger number of cycles than in mixes with pre-crack width of 0.20 mm. In fact, the latter shows smaller increases of the curve in comparison with the former at cycle 35. As the corrosion progresses, the damage of the fibres and of the ITZ compromises their resistant capacity, leading ultimately to a reduction of the curves. Notice that mixes with pre-crack width of 0.35 mm show reductions for all cycles assessed, suggesting a fast evolution of the damage enabled by a more accelerated chloride penetration in the cracks. The analysis also shows that corrosion occurred in all crack widths tested, possibly due to the severe accelerated testing conditions used. Consequently, results from the specific experimental programme do not enable the assessment of a limit crack width below which corrosion of steel fibres does not initiate.

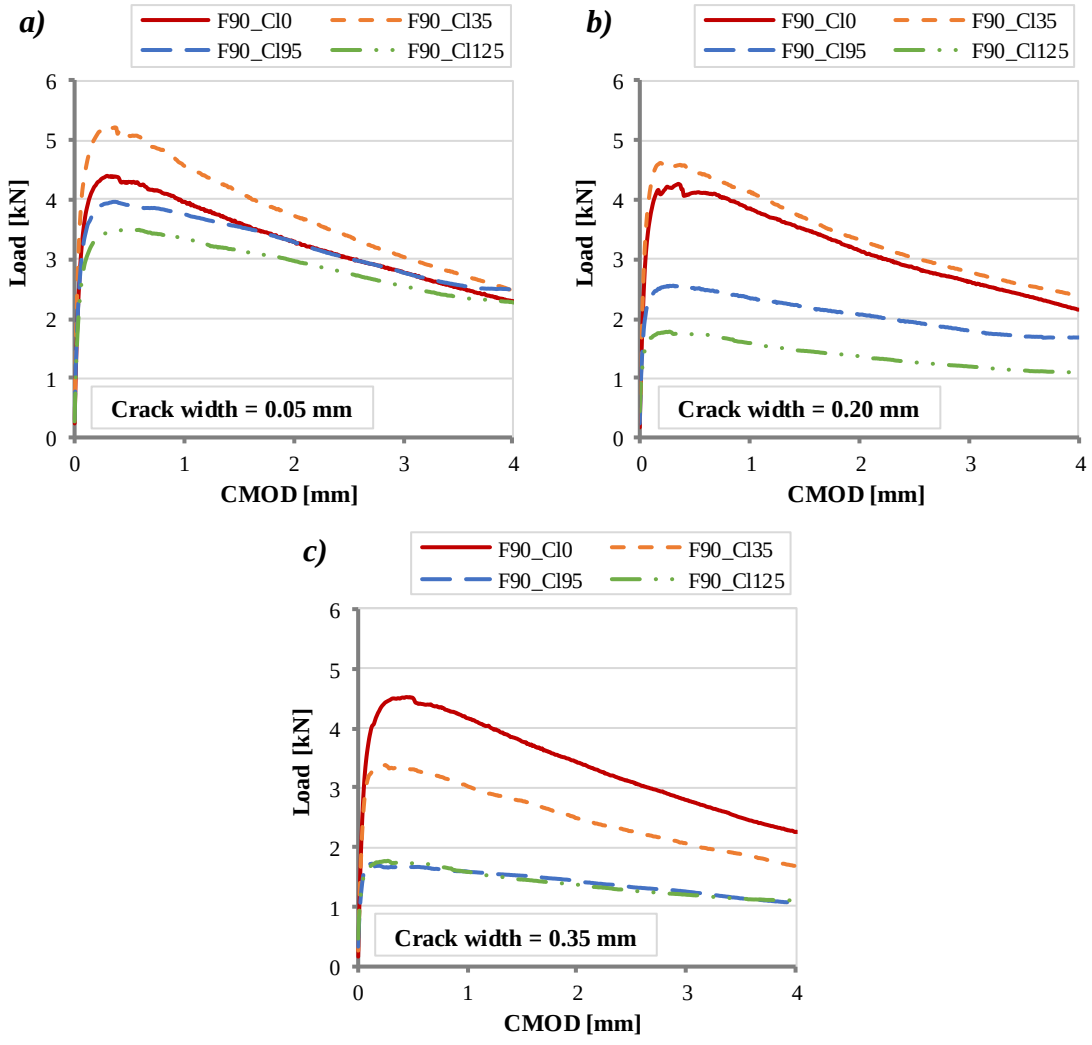

Figure 7.5 – Load-CMOD curves for specimens with pre-crack width of a) 0.05, b) 0.20 and c) 0.35 mm.

7.4.2. Residual flexural strength (f_{R1} and f_{R3})

The effects of the corrosion in the average residual flexural tensile strengths f_{R1} and f_{R3} associated to 90 kg/m^3 of fibre and w/c of 0.23 are presented in Figure 7.6. The study corresponds to the crack widths of 0.05, 0.20 and 0.35 mm at 0, 35, 95 and 125 cycles. Additionally, the relative values related to the crack width of 0.05 mm (considered 100%) are presented for the cracks of 0.20 and 0.35 mm.

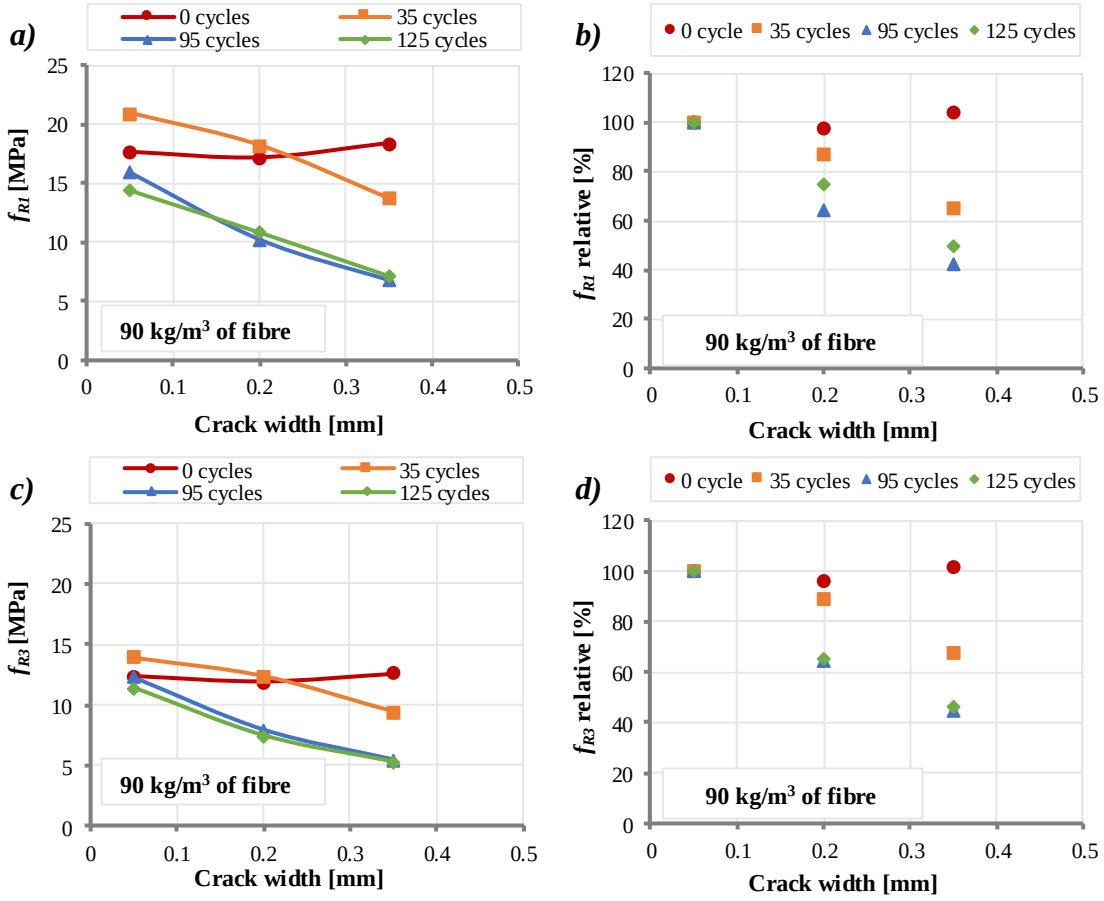

Figure 7.6 – Influence of the pre-crack width in the residual flexural strengths: a) absolute and b) relative values for f_{R1} and c) absolute and d) relative values for f_{R3}.

Similar trends are observed for f_{R1} and f_{R3} (see Figure 7.6-b and Figure 7.6-d, respectively). In general, the absolute values of f_{R1} and f_{R3} in Figure 7.6-a and Figure 7.6-c, respectively, indicate that the crack width is an important factor governing the degradation of the fibres bridging the cracks, affecting significantly the residual tensile behaviour. According to Šavija (2014), crack opening is the parameter which has received the most attention when it comes to research on chloride ingress and corrosion in cracked concrete.

Differently from what occurs with the crack of 0.05 mm, the corrosion presents a strong effect over the cycles for the specimens with crack widths of 0.20 and 0.35 mm. Such results are expected since larger crack widths favour higher ingress of chlorides,

water and oxygen throughout the cycles. In this case, the decrease in the ductile behaviour of the fibres is more evident due to a considerable loss of diameter produced by corrosion, which facilitates the fibre pull-out. As explained in Chapter 06, the increment in the crack width leads to increased depth affected by severe corrosion, causing fibres to slip or even break at lower load levels. The results also suggest that the crack width of 0.05 mm may be the only permissible situation if compared to the larger cracks widths studied (0.20 and 0.35 mm), although a reduction in residual tensile strength is also observed.

7.4.3. Absorbed energy

Figure 7.7 summarizes the absolute and absorbed energy for specimens with pre-crack widths of 0.05, 0.20 and 0.35 mm. Only samples with 90 kg/m^3 of fibres and w/c of 0.23 are depicted. The relative values of absorbed energy for the pre-crack widths of 0.20 and 0.35 are also included in the graphs in terms of percentage with regards to the crack width of 0.05 mm (100%).

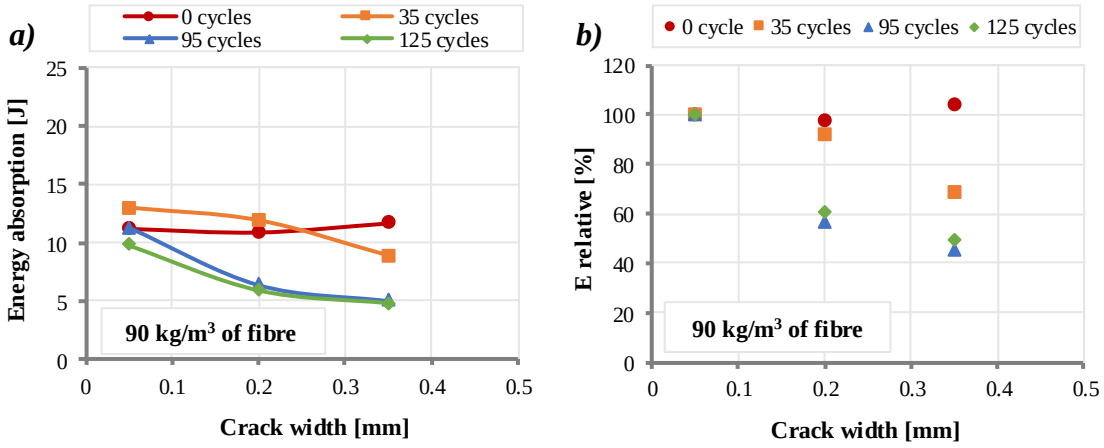

Figure 7.7 – Influence of the crack width in the energy absorption: a) absolute values of *E* and b) relative values of *E*.

The absolute absorbed energy (see Figure 7.7-a) are strongly influenced by the corrosion of fibres over the cycles. Greatest reductions are associated with the largest pre-cracks (0.20 and 0.35 mm), whereas for the pre-crack of 0.05 mm slight decreases are noticed. Such outcome may be attributed to the limited level of damage due to chlorides in the case of the smallest crack width of 0.05mm. Since the latter leads to lower corrosion due to the limited opening, a bigger enclosed area below the load-CMOD curve is observed.

An increment of absolute energy absorption is observed for the crack of 0.05 mm at an initial level of corrosive process if compared to the corresponding values of samples without chloride attacks. This behaviour may be influenced by the expansion of the fibre diameter due to the products of corrosion formed at their surface, which enhances the frictional forces during the pull-out. Reductions are observed as the ferrous oxides formed are porous and starts to be detached form fibres surface, reducing its cross-sectional area.

For larger crack widths (0.20 and 0.35 mm), the degradation is faster and the values of absolute energy absorption diminish more rapidly.

7.5. ANALYSIS OF THE INFLUENCE OF NUMBER OF CYCLES

7.5.1. Residual flexural strength (f_{R1} and f_{R3})

Figure 7.8 shows the absolute and relative flexural tensile strengths f_{R1} and f_{R3} for specimens with 90 kg/m^3 of fibre and w/c equal to 0.23. The analysis corresponds to the crack widths of 0.05, 0.35 and 0.50 mm at 0, 65, 95 and 125 cycles. Additionally, the relative results considering the respective strengths are presented at 0 cycles (100%) for the other cycles studied.

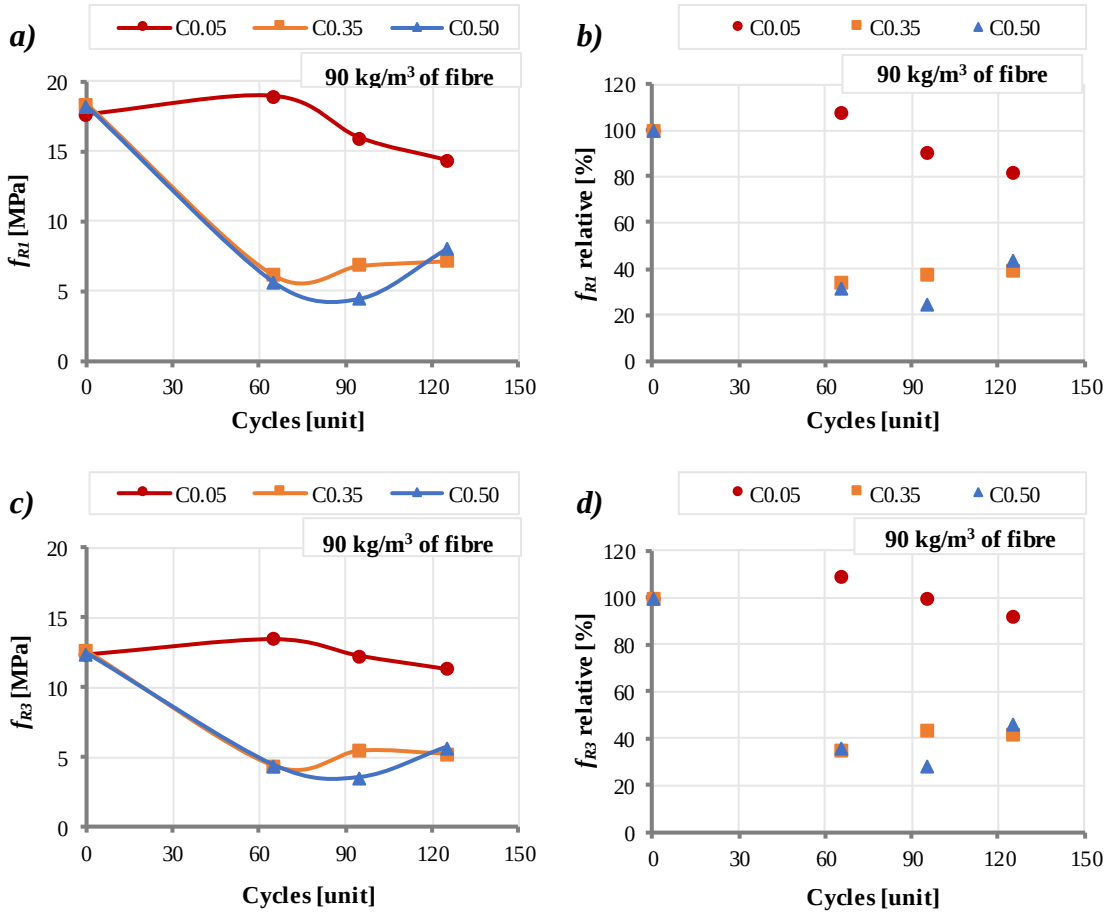

Figure 7.8 – Influence of the number of cycles in the residual flexural strengths: a) absolute and b) relative values for f_{R1} and c) absolute and d) relative values for f_{R3}.

The tendencies in Figure 7.8-a and Figure 7.8-c indicate that the number of cycles also influences greatly the ductility provided by the fibres. Initially, at 35 cycles the specimens with pre-crack of 0.05 mm presents higher residual flexural strengths f_{R1} and f_{R3} than at 0 cycles. This behaviour was already reported by Mangat and Gurusamy (1987). According to the authors, the trend of initial gain in flexural strength followed by a gradual loss in strength is evident for marine shower cured SFRC prisms.

As the number of cycles increases to 65, 95 and 125 cycles, the average absolute values of f_{R1} and f_{R3}, in general, are smaller if compared to the values at 0 cycles. This outcome suggests that the flexural response of the fibres is related to the number of cycles. As corrosion increases over cycles, the fibres present increasing loss of cross-sectional area, thus justifying the reduction of residual load values.

7.5.2. Absorbed energy

Figure 7.9 shows the influence of the cycles on the absolute and relative values of absorbed energy. For the analysis, samples with 90 kg/m^3 of fibres, w/c of 0.23 and crack widths of 0.05, 0.35 and 0.50 mm are considered. The graphs also show the relative values of absorbed energy at 65, 95 and 125 cycles related to 0 cycles (considered 100%).

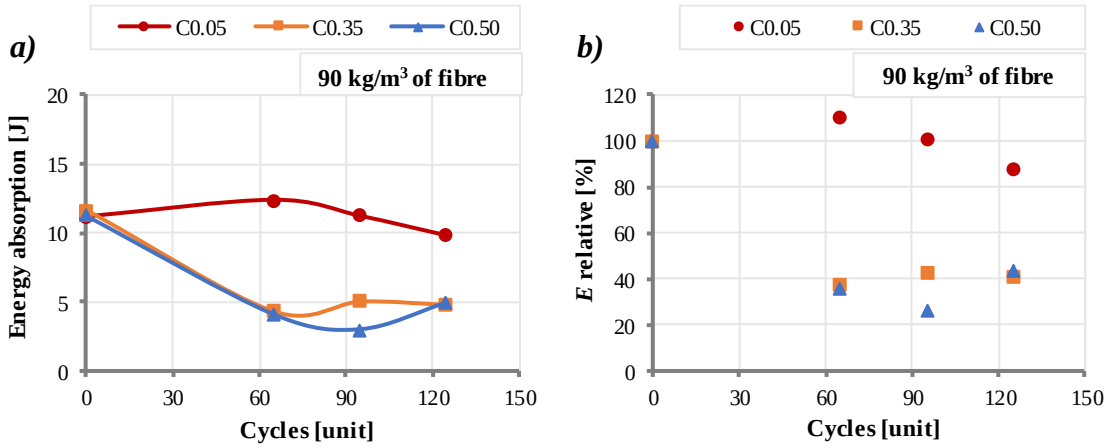

Figure 7.9 – Influence of number of cycles in the energy absorption: a) energy absorption absolute and b) energy absorption relative to 0 cycles.

The results in Figure 7.9 reveal a similar trend described for the residual flexural strength with a significant reduction of absorbed energy reducing with the cycles except for specimens with crack widths of 0.05 mm that until cycle 95 maintained similar energy. Other crack openings showed a more abrupt reduction of energy absorbed over the cycles. This can be explained by the increment of the level of corrosion of the fibres crossing the cracked section and consequent reduction of their diameter. Such outcome was also reported by Tran *et al*. (2015) regarding pre-cracked strain hardening-SFRCs under wet-dry cycles with chlorides. The authors observed a clear reduction in the mechanical performance due to the high level of fibres corrosion.

7.6. CONCLUDING REMARKS

Chapter 7 presented the mechanical results of the specific experimental programme involving pre-cracked HPSFRCCs prisms over chloride cycles regarding the influence the three main variables studied: fibre content, crack width and number of cycles. The following conclusions may be derived from the results:

- The analysis in general indicate that the main parameters studied (fibre content, crack width and number of cycles) influence the repercussion of the corrosion process in the crack-bridging capacity of the steel fibres and the performance of specimens.

- The mechanical performance of the specimens with smallest fibre content (90 kg/m^3) is strongly affected by the corrosion whereas specimens with the highest content (190 kg/m^3) present limited level of degradation of mechanical performance over the cycles. Such outcome is expected since lower fibre contents imply smaller amount of iron available in the cracks, which leads to a bigger depth of corrosion.

- The crack width shows the highest influence in the effect of corrosion on the mechanical performance in comparison with other variables. Larger crack widths allow higher penetration of chlorides and consequently increased fibres degradation over the cycles. Under the accelerated testing conditions, a reduction in the residual tensile strength was observed almost for all crack openings studied.

- The only exception is found for specimens with crack widths of 0.05 that show slight increase or no reduction up to cycle 95, depending on the parameter analysed. At a small number of cycles, low level of corrosion may lead to an increment of bearing capacity. As the number of cycles increases, higher corrosion along the cracked section ultimately leads to reductions in the post-peak behaviour over time.

8. ANALYTICAL MODEL

8.1. INTRODUCTION

Chapter 7 revealed that the corrosion leads to reduced structural performance of the fibres in pre-cracked HPSFRCC subjected to wet-dry cycles with chlorides. The corrosion process of real structural elements when subjected to aggressive environment could have adverse consequences both on the overall safety of the structure and on the predicted performance. In this context, the results obtained in previous chapters may be considered with the aim to modify the procedure of design of real structures prone to this type of aggressive environment.

The Model Code 2010 (MC2010) defines constitutive laws for the design of fibre reinforced concrete for structural applications. At the ultimate limit state (ULS), the contribution of the fibres can partially or totally substitute the traditional reinforcement. In the case of traditional reinforced concrete structures, the durability is satisfied in standard conditions by defining a minimum concrete cover to the reinforcement, a maximum w/c and a minimum cement content. Provisions for steel fibre reinforced concrete are unclear in the code.

Nordström (2005) suggests that the structural design of steel fibre reinforced concrete structure has to estimate the likely crack width expected and the environmental exposure and design service life. According to Nordström (2005), traditional service life criteria are not valid for steel fibre corrosion in cracks, and the service life prediction should be based on an acceptable reduction of a load-bearing capacity. A criterion for the consideration of contribution of fibres in the residual tensile strength may be a reduction in this contribution according to the fibres reduced diameter by corrosion with no acceptance of brittle failures of fibres. The designer can compensate the loss in load-bearing capacity due to corrosion by increasing the amount of fibres.

In this sense, the development of a simplified procedure to assess the long-term structural repercussion of the corrosion over the ULS capacity of steel fibre reinforced concrete may be of great interest. The **general objective** of this chapter is to propose a simplified model considering the effects of corrosion for the design HPSFRCCs member in the ULS. The following **specific objectives** are defined:

- Define the theoretical basis of the model that accounts for the influence of crack width, fibre content and number of chloride cycles in the residual tensile response of steel fibres;

- Correlate the results of the bending tests and the visual analysis (level and depth of corrosion in cracked section) to determine the values of the damage parameters;

- Propose parameters of corrosion damage that could be introduced in the design of HPSFRCCs structural elements in the ULS when subjected to chloride exposure.

Section 8.2 shows a brief explanation regarding the theoretical basic aspects for FRC design are presented. Subsequently, section 8.3 includes the application of theory to the experimental data provided by the 3-point bending tests and visual analysis of the cracked cross section, considering the influence of the main variable studied. Finally, section 8.4 summarizes the main conclusions of the study.

8.2. THEORETICAL BASIC ASPECTS FOR FRC DESIGN

8.2.1. Design of FRC in the ULS

According to di Prisco *et al*. (2009), ULS in bending is reached when one of the following conditions is obtained:

- Attainment of the maximum compressive strain in the FRC, ε_{cu};

- Attainment of the maximum tensile strain in the steel (if present), ε_{su};

- Attainment of the maximum tensile strain in the FRC, ε_{Fu};

The design axial force (N_{Sd}) and the ultimate bending moment (M_{Rd}) can be evaluated by means of the translation and rotation equilibrium equations. The fundamental hypotheses for ULS analysis of FRC sections are:

- Sections remain plane;

- Perfect bond conditions exist between steel bars and surrounding concrete;

- The tensile stresses in FRC are derived from the design stress-strain relationship;

- For the compressive stresses, the equations used for plain concrete can also be applied for FRC: of the maximum compressive strain in the FRC, ε_{cu};

In addition to that, for ULS, partial safety factors are also recommended. Figure 8.1 illustrates the bending moment resistance at ULS with longitudinal reinforcement, with the additional contribution of the fibre.

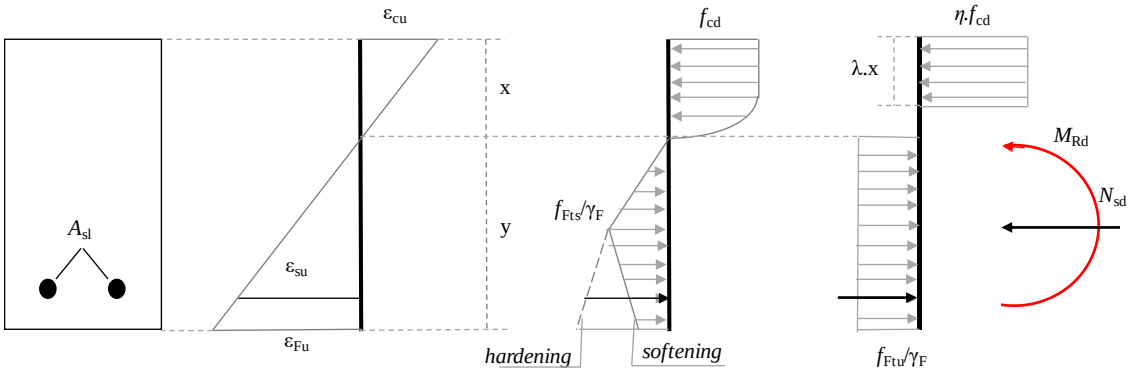

Figure 8.1 – ULS with the use of the simplified stress-strain relationship for ULS (di Prisco *et al*. 2009).

In the case of structural elements with fibre reinforcement and without traditional bars reinforcement under bending, a rigid-plastic response may be assumed to calculate both the compressive and post-cracking tensile response of the FRC element. The rigid plastic model identifies a unique reference value, f_{Ftu}, based on the ultimate behaviour, assuming w_u =CMOD$_3$. Furthermore, for HPSFRCCs, due to the high flexural response, simplified considerations can be adopted under combined tensile-flexural or compressive-flexural forces, with the simplified equation (8.1) in the ULS. In this case, the compressive force is concentrated at the top fibre of the cross-section.

$$y = h \tag{8.1}$$

Figure 8.2 shows the simplified models adopted to calculate the ultimate strength in uniaxial tension (f_{Ftu}) by means of a rigid-plastic model and the residual nominal bending strength (f_{R3}), for FRC and HPFRC in ULS.

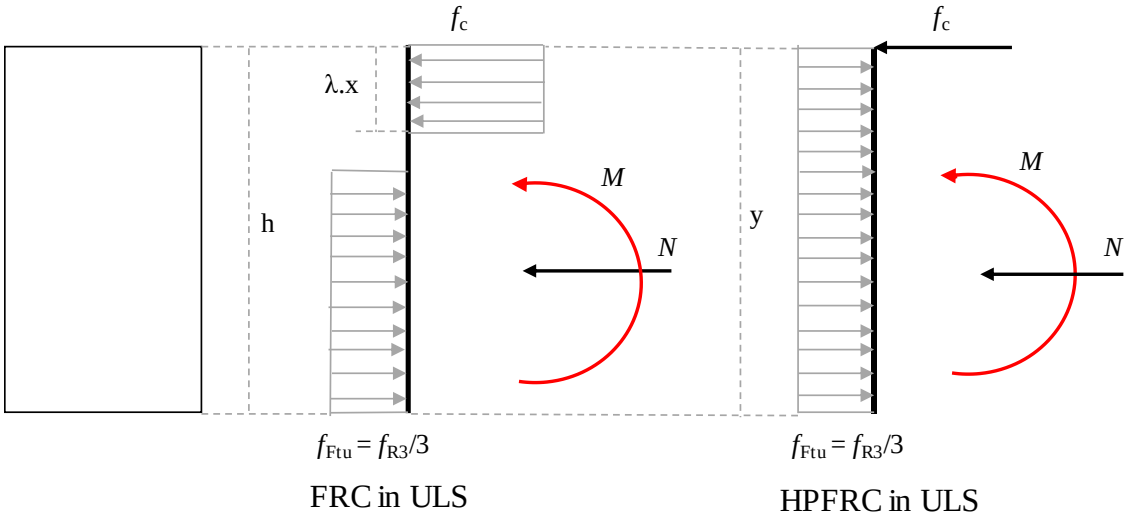

Figure 8.2 – Simplified model for FRC and HPFRC in ULS (adapted from di Prisco *et al*. 2009).

8.2.2. Simplified design of corroded HPSFRC in ULS

In order to simplify the structural design of corroded HPSFRC members in ULS, two main parameters are defined: the values for depth of corrosion (h_{cor}) and the parameter (α), which estimate a reduction in the residual strength due to corrosion in comparison with the uncorroded cross-section. The rectangular block of the ultimate strength in tension (f_{Ftu}) is reduced over the depth of corrosion in the cross section by α. Figure 8.3 illustrates the simplified model proposed for corroded HPSFRC in ULS.

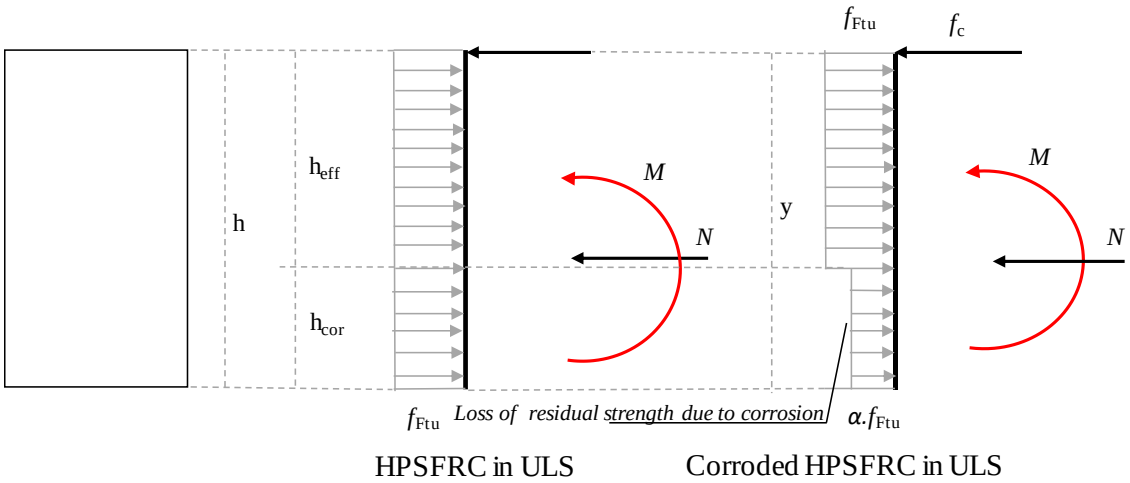

Figure 8.3 – Simplified model for corroded HPFRC in ULS.

8.2.3. Values of depth of corrosion (h_{cor})

The depth of corrosion is determined by the results of the visual analysis of the corroded cracked section performed in the specific experimental programme (see section 6.3). For the simplified model, the level of medium and high corrosion are considered for the depth of corrosion (h_{cor}). The height with non-corroded fibres or with low level of corrosion is considered as effective depth (h_{eff}) that has not been yet significantly compromised by corrosion. Figure 8.4 illustrates the depth of corrosion in the cracked cross section of the HPSFRCC prisms tested. To perform the 3-point bending test the prisms were notched and the height of the notch is not considered for total height of the cross-section.

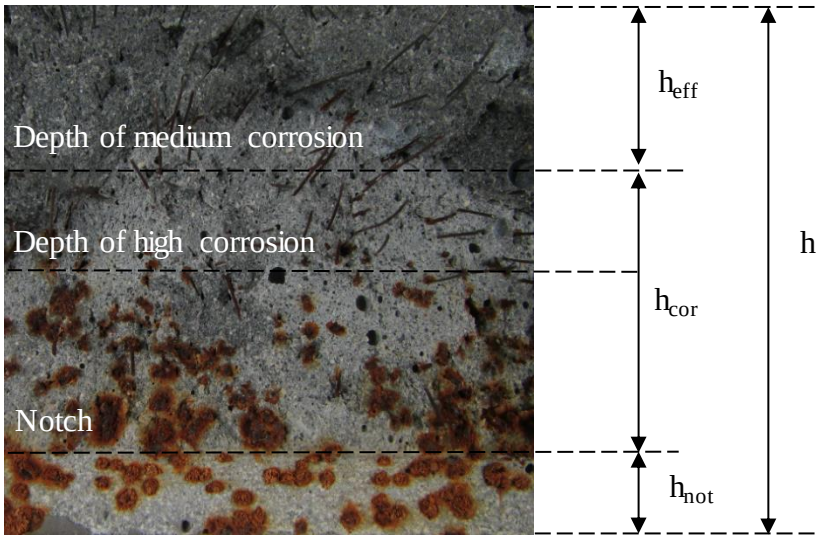

Figure 8.4 – Depth of corrosion in the cracked cross section of HPSFRCC specimen.

Figure 8.5 shows the curves that relate depth of corrosion (h_{cor}) and the number of chloride cycles 5, 35, 65, 95 and 125 related to the pre-crack widths studied (0.05, 0.20. 0.35 and 0.50 mm) and to the fibre contents of 90, 140 and 190 kg/m^3. Crack width is considered the most important factor that influences the chloride transport at the pre-cracked concrete (Gu *et al*. 2015). Such outcome is observed in the results from the curves (see Figure 8.5). The values of the depth of corrosion (h_{cor}) is greater as the crack width is larger. The level of severe (high and medium) corrosion increases throughout the cycles. According to Djerbi *et al*. (2008), cracks in concrete may act as flow channels for aggressive ions as chlorides, accelerating the rate of chloride ingress and hence the onset of corrosion.

The fibre content influences the level and depth of corrosion in fibres bridging the cracks (see section 6.3). From the curves it is noticed that the fibre content also controls the depth and level of corrosion. The samples with smaller amount of fibre (90 kg/m^3) present the greater depth of severe corrosion. On the contrary, for the specimens with 190 kg/m^3 of fibre, the depth of severe corrosion (h_{cor}) is reduced due to the amount of iron close to the crack mouth available to be corroded.

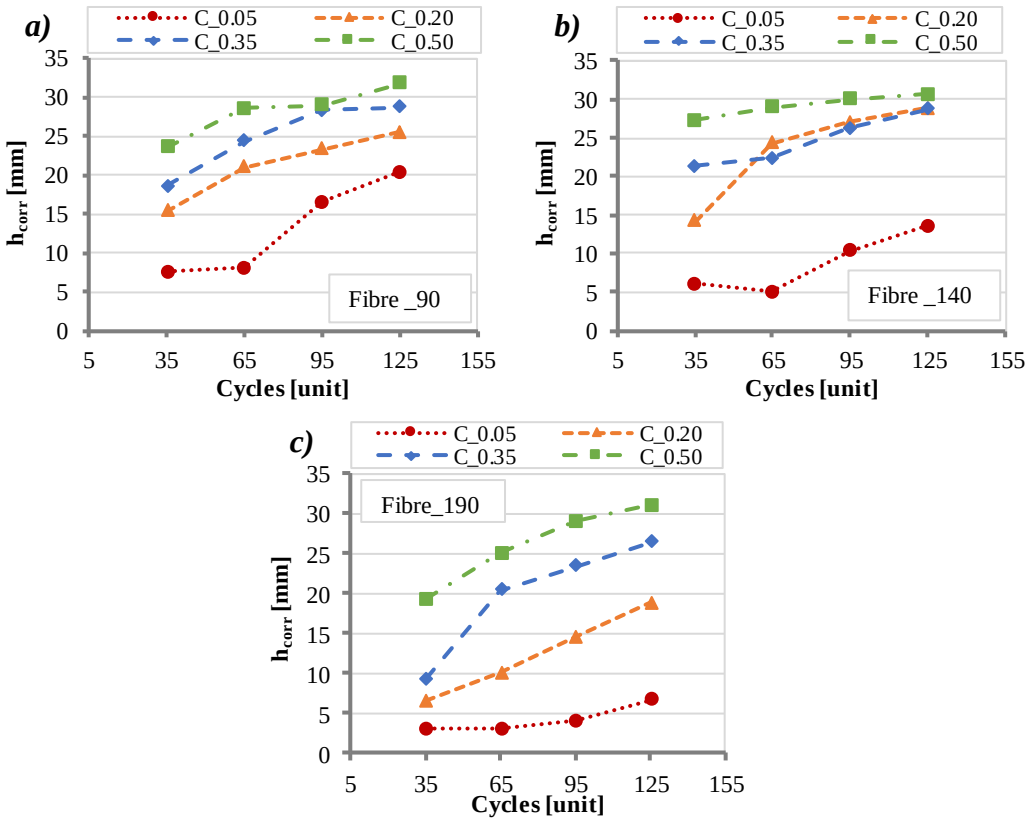

Figure 8.5 – Depth of corrosion (h_{cor}) – number of chloride cycles: a) 90 kg/m^3 of fibre, b) 140 kg/m^3 of fibre and c) 190 kg/m^3 of fibre.

Figure 8.6 shows the curves with the average values of depth of corrosion (h_{cor}) against the number of chloride cycles (5, 35, 65, 95 and 125) depending on the fibre content or pre-crack width. Since the influence of the matrix is small in this phenomenon dominated by the crack width, these curves should be valid also for other compositions. Consequently, these curves may be taken as a reference to estimate the depth of severe corrosion if no specific result is available.

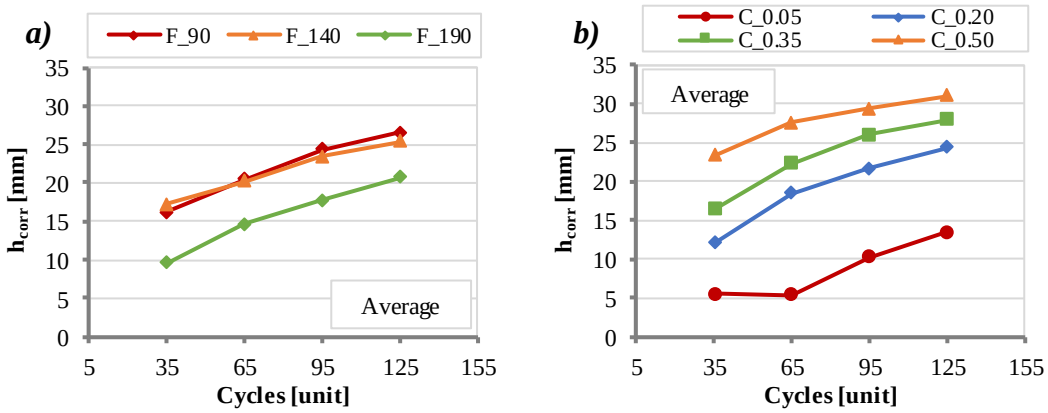

Figure 8.6 – Average values of depth of corrosion (h_{cor}) – number of chloride cycles, considering: a) fibre content and b) pre-crack width.

8.2.4. Derivation of alpha value

The alpha value can be found by solving the equation of the internal and external moment considering equilibrium of the cross-section. The external moment is due to the bending moment caused by the loading at midspan. The internal moment is due to the bending moment caused by the tensile stresses in the member.

External work

M_{ext} is the bending moment due to external loading. The load applied (F_c) at CMOD 2.5 mm (ULS) that equals the reaction of the supports multiplied by the lever arm, which for this case is to the centre of the member (equation (8.2)).

$$M_{ext} = \frac{F_c}{2} \cdot \frac{1}{2} = \frac{F_c \cdot l}{4} \tag{8.2}$$

The force in a cross-section of an element subjected to chloride corrosion can be split into the corroded section contribution and the non-corroded section contribution. The main parameters for the calculation of the internal moment (M_{int}) are: internal forces due to the non-corroded section (f_{eff}), internal force due to the corroded section (f_{cor}), height of the cross-section without corrosion (h_{eff}) and height of the cross-section with corrosion (h_{cor}). The summation of the internal moments due to each of these sections gives the total internal moment (M_{int}) shown in equation (8.3). The calculation of the force due to both parts (corroded and non-corroded) is obtained by means of the equations (8.4) and (8.5). At this stage the alpha value is introduced and the residual tensile strength of the corroded section is an unknown value.

$$M_{\text{int}} = \left(f_{eff} \cdot \frac{h_{eff}}{2} \right) + \left(f_{cor} \cdot \left(h_{eff} + \frac{h_{cor}}{2} \right) \right) \tag{8.3}$$

$$f_{eff} = f_{Ftud} \cdot h_{eff} \cdot b \tag{8.4}$$

$$f_{cor} = \alpha \cdot f_{Ftud} \cdot h_{cor} \cdot b \tag{8.5}$$

Calculating f_{Ftud}

The calculation of the ultimate residual tensile strength of a member (f_{Ftud}) may be derived for an uncorroded section by assessing the tensile stresses in the non-corroded member (σ) with the use of the equation (8.6).

$$\sigma = f_{Ftud} \cdot b \cdot h = \frac{M_{ext}}{\left(\frac{h}{2}\right)} \tag{8.6}$$

The rearrangement of the equation (8.6) in terms of f_{Ftud} and with the substitution of the M_{ext} from the equation (8.2), is presented in equation (8.7).

$$f_{Ftud} = \frac{F_c \cdot l}{2 \cdot b \cdot h^2} \tag{8.7}$$

Equating internal and external moments

Solving the equality of equations (8.2) and (8.3), and substituting f_{cor} and f_{eff}, lead to the expression in the equation (8.8). Dividing both sides of the equation (8.8) by b.f_{Ftud}, gives the expression (8.9).

$$\frac{F_c \cdot l}{4} = \left(\left(f_{Ftud} \cdot h_{eff} \cdot b\right) \cdot \frac{h_{eff}}{2}\right) + \left(\left(\alpha \cdot f_{Ftud} \cdot h_{cor} \cdot b\right) \cdot \left(h_{eff} + \frac{h_{cor}}{2}\right)\right) \tag{8.8}$$

$$\frac{F_c \cdot l}{4 \cdot b \cdot f_{Ftud}} = \frac{h_{eff}^2}{2} + \alpha \cdot h_{cor} \cdot \left(h_{eff} + \frac{h_{cor}}{2}\right) \tag{8.9}$$

In equation (8.10), the equation (8.9) is rearranged for the assessment of alpha.

$$\alpha = \frac{\frac{F_c \cdot l}{4 \cdot b \cdot f_{Ftud}} - \frac{h_{eff}^2}{2}}{h_{cor} \cdot \left(h_{eff} + \frac{h_{cor}}{2}\right)} \tag{8.10}$$

Substituting in the equation (8.10), the f_{Ftud} from equation (8.7) gives the equation (8.11).

$$\alpha = \frac{\frac{F_c \cdot l}{4 \cdot b \cdot \left(\frac{F_c \cdot l}{2 \cdot b \cdot h^2}\right)} - \frac{h_{eff}^2}{2}}{h_{cor} \cdot \left(h_{eff} + \frac{h_{cor}}{2}\right)} \tag{8.11}$$

Equation (8.11) may be used to calculate the alpha for all member with distinct properties. The values considered are the ultimate residual tensile strength at CMOD of 2.5 mm.

Given the great number of experimental data and the similarities of the tendencies observed, only the main results are presented and discussed in this chapter. Notice that the variables and results herein analysed involve the main mechanisms of chloride corrosion and its effects on the mechanical behaviour of the HPSFRCCs studied.

8.3. APPLICATION OF THEORY TO THE EXPERIMENTAL DATA

The parameter of damage (alpha value) obtained by means of the formulations in the previous section is a generic value which applies to any member property or dimension. It is applied to the data collected in the specific experimental programme by imputing the average parameters (i.e. level and depth of corrosion) into the formula. Since these parameters differ for each set of specimens, the alpha values also change.

8.3.1. Results of alpha values

Table 8.1 presents the alpha values obtained by means the simplified model. The values correspond to the specimens. The calculation considered the ultimate residual tensile strength at CMOD of 2.5 mm and the depth of corrosion (h_{cor}) presented in section 8.2.3.

Table 8.1 – Alpha values.

Mix design	Pre-cracking [mm]	Number of cycles			
		35	**65**	**95**	**125**
F90	0.05	1	1.0000	1	0.9176
	0.2	1	0.9802	0.6798	0.6376
	0.35	0.7302	**0.3491**	0.4313	0.4116
	0.5	0.6775	0.3586	0.2772	**0.4447**
F140	0.05	1	0.8635	0.9425	0.8482
	0.2	0.8950	0.5460	0.6887	0.7117
	0.35	0.8388	0.4929	0.4946	0.5416
	0.5	**0.9523**	0.5930	0.4976	0.4108
F190	0.05	**0.7271**	**0.6562**	0.7257	0.6682
	0.2	1	0.9235	0.7015	0.6315
	0.35	0.8625	0.8895	0.7248	0.6568
	0.5	0.9447	0.8673	0.7669	**0.9798**

Table 8.1 shows the all alpha values calculated, categorised by mix, the crack width and the number of chloride cycles. The values represent a factor of the original strength and therefore range from 1-0. A value of 1 represents no change in the contribution of a section which may occur in the section of a matrix without corrosion. A value of zero represents a complete loss in the contribution of the fibres in the area affected by corrosion, which can be observed in the case of completely corroded fibres.

Alpha values bigger than 1 may occur at lower levels of corrosion, as the residual tensile strength increase due to the enhanced bond between the fibre and the cementitious matrix (see Chapter 7). However, for design purposes, such results may be discarded and considered equal to 1 to be on the safe side and not to count on a positive contribution of the corrosion. The values in bold in Table 8.1 are considered outliers as they do not fit the general trend (alpha values should decrease with the cycles and should also decrease for an increased crack width).

The graph in Figure 8.7 presents the alpha values for the cycles 35, 65, 95 and 125. The values consider the pre-crack widths of 0.05, 0.20, 0.35 and 0.50 mm, and the fibre contents of 90, 140 and 190 Kg/m^3 for all members tested.

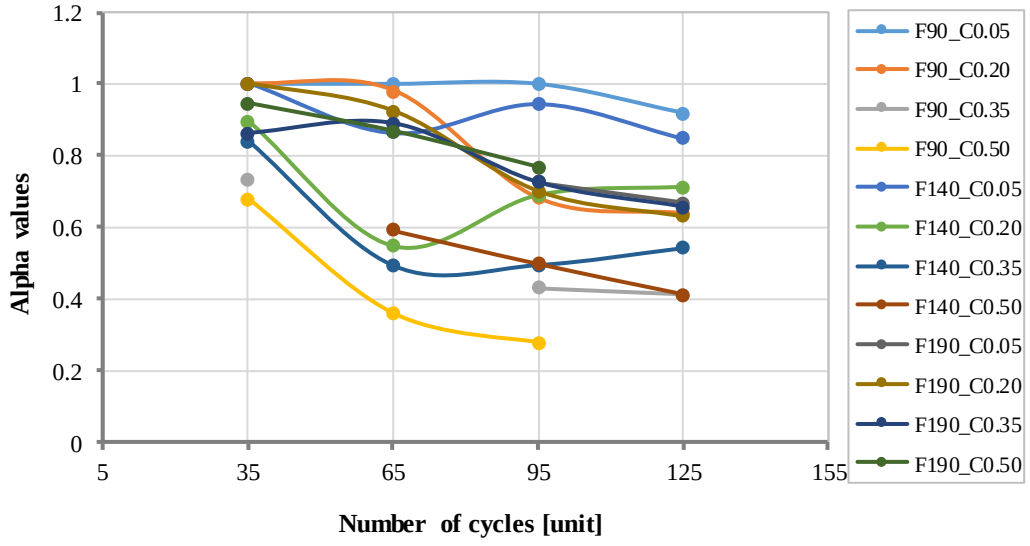

Figure 8.7 – Average alpha values per mix and pre-crack width.

There is clear a tendency showing a reduction in the alpha values for an increased number of cycles. The curves show almost the same trend, excluding the outliers, highlighted in Figure 8.7. From the results, the residual contribution of the corroded fibres in the cross section decreases over the cycles. Such outcome may be a consequence of the partial or complete loss of the fibre cross-sectional due to severe corrosion. This facilitates the mechanisms of debonding and pull-out in the cracked section, leading to smaller alpha values. In order to better visualize this behaviour, the overall average alpha values are plotted against the number of cycles in Figure 8.8.

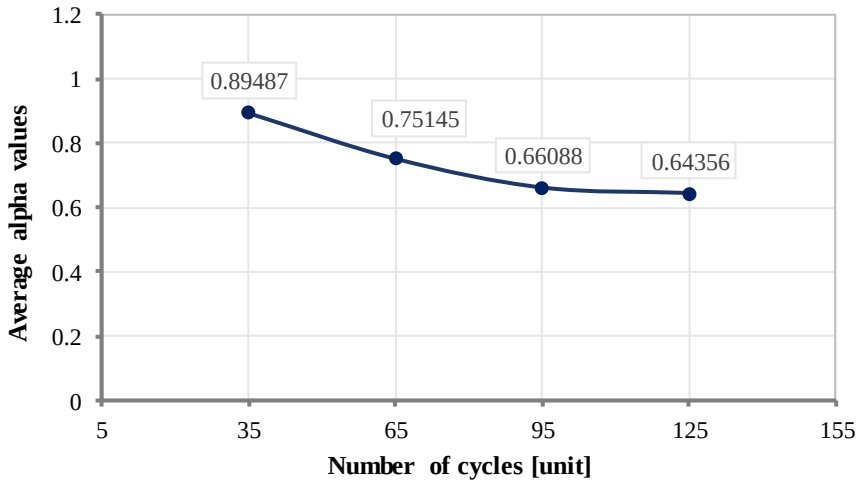

Figure 8.8 – Average alpha values for all number of chloride cycles.

Alpha multiplied by f_{Ftud} represents the strength of the corroded part of the cross-section. Notice that the reduction of the residual flexural capacity of the cross-section might come from the reduction of alpha or the increase in the depth of corrosion, as illustrated in Figure 8.9.

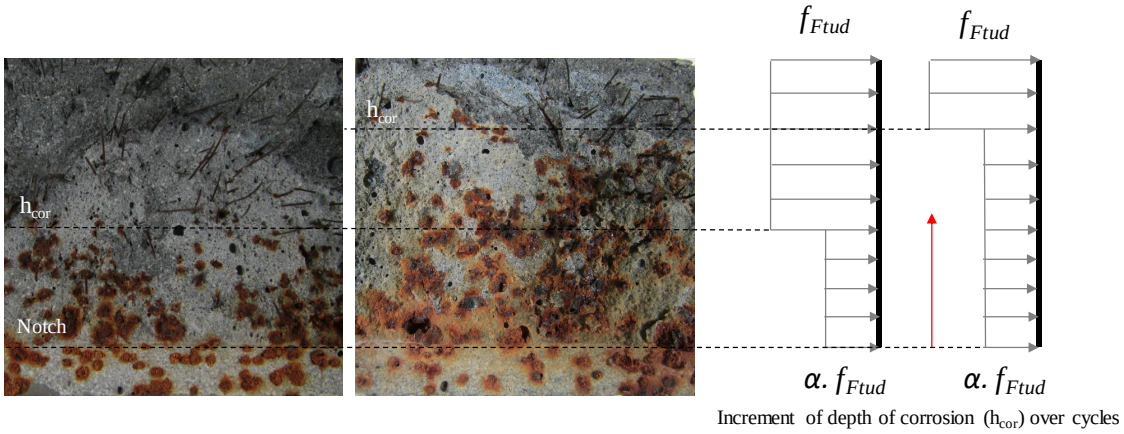

Figure 8.9 – Increment of depth of corrosion over cycles.

From Chapter 6, no sign of stabilization in the corrosion process was detected. Therefore, even though the depth of corrosion reached the full cross-section in some cases, the resistant capacity still diminished because of the increase in the degradation of the fibres, leading to a reduction of alpha. This demonstrates that the model proposed is capable of representing the phenomenon observed during the accelerated tests.

8.3.2. Effects of variable member properties on the alpha value

As discussed in Chapter 6, three main variables are considered in the tests: pre-crack width, fibre content and chloride cycles. A change in any of these variables will

affect alpha. The following sections analyse how a change in these variables affect the alpha values.

Pre-crack width

Figure 8.10 presents the average alpha values against the pre-crack widths studied (0.05, 0.20,0.35 and 0.50 mm). The values correspond to the average alpha values for the three fibre contents (90, 140 and 190 kg/m^3).

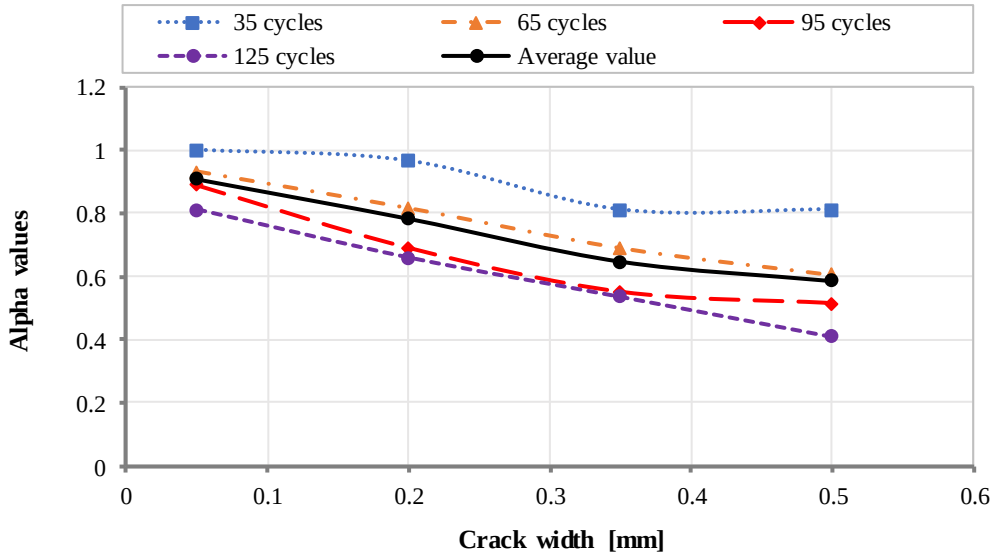

Figure 8.10 – Influence of the pre-crack width in the alpha values.

The graph shows that the crack width plays a key role on the reduction of the resistant capacity. The tendency of the curves reveals that larger pre-crack widths lead to smaller alpha values over the cycles. A plausive explanation for such outcome could be the influence of the crack opening on the control of the ingress of deleterious substances, such as chlorides ions. Besides that, the cracks allow the penetration of humidity and oxygen over cycles, favouring the onset of the corrosion process.

The narrow crack opening (0.05 mm) presents the smallest reductions in the structural performance of the fibres, with the highest alpha values. Such results are expected since hairline cracks allow a very limited penetration of salt solution and oxygen, leading to reduced degradation of fibres. In addition to that, the mechanism of chloride ions diffusion along the crack occurs slowly for thinner cracks. Consequently, reduced depth of penetration and concentration of free chloride ions are observed in the crack.

The alpha values in the case of wider cracks is smaller in comparison to the hairline crack width, indicating a reduction of the resistant capacity as the crack opening increases. Such outcome may be explained by the increment of the amount of salt solution and oxygen over cycles that produce more severe damage of the fibres. The larger crack

(0.50 mm) presented the greatest reductions in the alpha values as the level of severe corrosion was the most significant of all cases studied.

The corrosion in micro steel fibres do not induce significant corrosion propagation, as fibres do not present the continuity found in steel rebar and are randomly distributed in the matrix. In spite of that, the presence of cracks may lead to a considerable reduction in the structural contribution of the fibres bridging the cracks. From the results of alpha values considering the influence of crack width, it is clear that the limitation of a crack opening should also be applied to HPSFRCC with structural responsibility.

Fibre content

The influence of the fibre content in the variation of the alpha values is illustrated in Figure 8.11. The average alpha values are related to the four crack widths studied (0.05, 0.20, 0.35 and 0.50 mm).

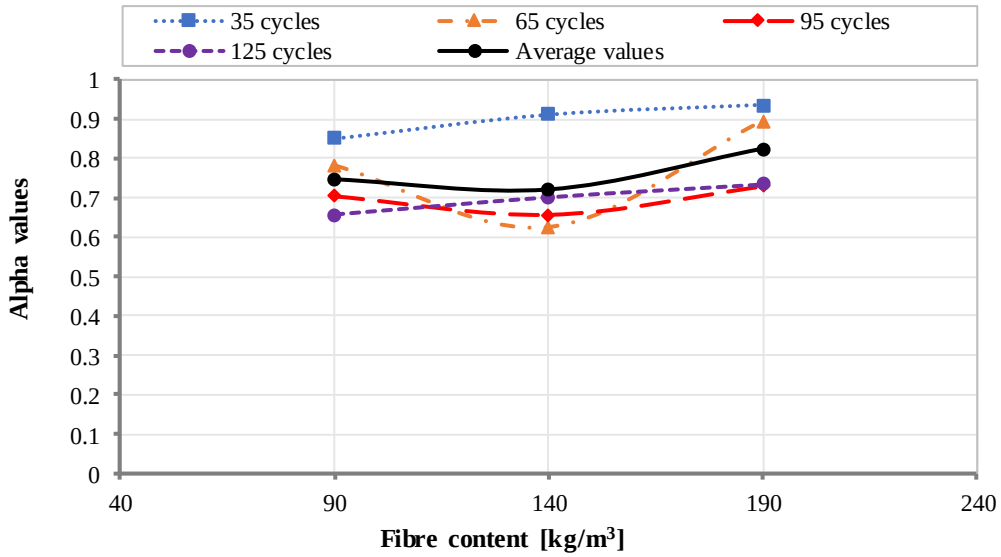

Figure 8.11 – Influence of the fibre content in the alpha values.

A general overview of the results in Figure 8.11, reveals that the fibre content influences the alpha values. In spite of a level of scatter in the data, the tendency of the curves indicates that smaller fibre content leads to lower alpha values whereas for greater fibre content, values are higher. This behaviour may suggest that the depth and level of corrosion along the crack also depends on the number of fibres subjected to corrosion. The differences in the fibre content into the crack may lead to distinct concentration of chloride ions, humidity and oxygen into the cracks.

Greater depth of severe corrosion was observed from the visual analysis in Chapter 6 for specimens with the smallest fibre content (90 kg/m^3). Such outcome may be attributed to the lower amount of iron from the fibres to be corroded into the cracks. It should be pointed that the fibres bridging the cracks are directly in contact with the salt solution and oxygen. By contrast, higher alpha values can be detected for the highest fibre

content analysed (190 kg/m^3). This result may be a consequence of the more limited depth and level of severe corrosion due to a more significant presence of fibres crossing the cracks. In this case the fibres might act as a barrier controlling the ingress of salt solution and oxygen.

Chloride cycles

Figure 8.12 shows the alpha values against the number of cycles considering the average for the fibre contents of 90, 140 and 190 kg/m^3.

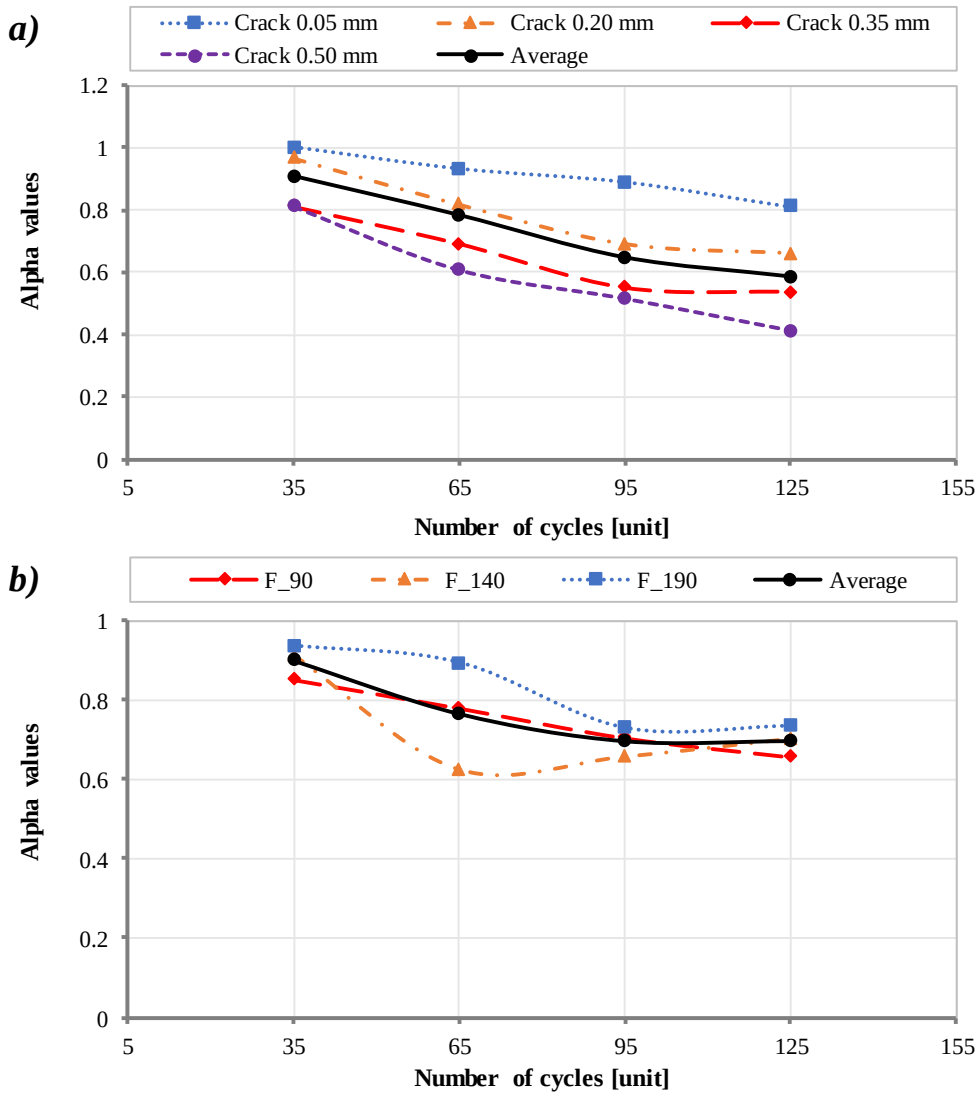

Figure 8.12 – Influence of the number of cycles in the alpha values for different a) crack-widths and b) fibre contents.

8.4. CONCLUDING REMARKS

Chapter 8 presented a simplified analytical model to predict the effects of fibres corrosion on the residual tensile strength of a HPSFRCCs member in ULS, as well as, a damage parameter (α) according to the experimental data. The model proposed to consider the influence of the corrosion in the design is capable of reproducing the behaviour observed in the experimental programme. It is also compatible with the design philosophy proposed in the most recent codes and guidelines. Notice that the model is not an attempt to make accurate estimations of structure durability or its performance in service. It has been presented just to give a reference for considering the corrosion in cracks in the design stage.

The following conclusions may be derived from the study conducted:

- The alpha value indicates the reduction in the residual tensile strength of the corroded part of a HPSFRCC cross-section. It may be used to estimate the residual tensile response of a HPSFRCC member exposed to chlorides, providing an estimation of the effects of fibres corrosion in the structural behaviour in ULS. The alpha value may be a suitable parameter of damage to be introduced in codes and guidelines for the structural design of fibre reinforced elements.

- The assessment of the influence of fibre content in the level of fibres corrosion over time allowed obtaining alpha values which consider this variable. In this procedure, the results of alpha values suggest that the increment of fibre content limits severe corrosion over the cycles.

- A clear trend on the reduction of the alpha values is identified as the crack width increases. This outcome is associated with the influence of the cracks in the corrosion process of fibres and consequently reduction of its structural performance. Wider cracks lead to increased degradation and reduced alpha values.

- The alpha value reduces linearly with increment of the number of cycles. No sign of corrosion stabilization over time in the cracked cross-sections is noticed.

9. CONCLUSIONS AND FUTURE PERSPECTIVES

9.1. GENERAL CONCLUSIONS

The vast possibility of field applications in civil engineering of HPSFRCCs, including under severe environment conditions led to an increment of research regarding the durability of these materials. However, several aspects still require further research. For that reason, this doctoral thesis was proposed, focussing on 4 specific issues: the assessment of the influence of chloride corrosion in uncracked HPSFRCCs under constant exposure; the study of the main mechanisms that govern the chloride corrosion in pre-cracked and uncracked HPSFRCCs under cyclic exposure; the analysis of the impact of chlorides on the surface aspect and on the mechanical behaviour and, finally, the proposal of a simplified model to predict the effects of chloride corrosion on the residual response of cracked HPSFRCCs.

Regarding the first subject, results demonstrated that the presence of chlorides in the HPSFRCC mixes produced surface corrosion and only limited reduction on the mechanical behaviour due to fibres corrosion. The outcomes of the second subject represent a contribution to the comprehension of the governing mechanisms of chloride-induced corrosion of HPSFRCC under long-term cyclic exposure. In the case of uncracked section, the wetting and drying chloride cycles favoured the corrosion of fibres in the region close to the surface for all specimens tested. The main cause of this outcome is the ingress of salt solution and oxygen throughout the cycles into the superficial pores of the samples. For cracked section, the chloride cycles led to significant corrosion of fibres bridging the cracks. The degree of corrosion was affected by the crack width and fibre content. Furthermore, different levels of corrosion were observed along the cracked section, decreasing from the crack.

The third subject entails an advance in experimental data regarding the influence of chloride-induced corrosion on the surface aspect and on the mechanical response. The uncracked section is more affected by the effects of chlorides on the aesthetic aspect, due to the surface corrosion with almost no reduction of the residual response, whereas in the case of pre-cracked samples, the corrosion presented a significant impact on the residual tensile strength.

In the fourth subject, a simplified model was proposed to consider the influence of corrosion on the typical design procedure of HPSFRCC in the ULS. According to the

model, useful parameters of corrosion-induced damage is proposed for the design, emulating the reduction in the residual tensile strength due to the corrosion.

9.2. SPECIFIC CONCLUSIONS

Several specific objectives are proposed in Chapter 1 for each of the subjects studied. In response to these specific objectives, the contributions made are described in detail in the chapters of this doctoral thesis. With the aim of providing a general overview of the contributions, the main specific conclusions of each subject addressed in this thesis are presented here.

Preliminary experimental programme

- The chlorides added to the mix induced a damage related to the superficial aspect. The corrosion was limited to the fibres close to the surface, producing a very thin layer of products of corrosion on the surface. The corrosion process was observed at both curing condition being influenced by the amount of water and oxygen from the laboratory exposure.

- The fibre content remarkably influences the level of surface corrosion in HPSFRCCs. The specimens with lower fibre contents (40 and 80 kg/m^3) presented expressive increment of corrosion spots in the first curing condition (with higher level of humidity). In the case of the samples with higher fibre contents (120 and 160 kg/m^3), a slower deposition of corrosion spots was observed over time, increasing in both curing conditions. Such outcome may be attributed to the presence of more fibres at the layer close to the surface, so that the surface corrosion still progresses in the second curing condition (at later ages).

- The results from the flexural test suggest that the fibre corrosion has little influence in the structural response of uncracked HPSFRCC specimens, even when chlorides are included in the composition.

Specific experimental programme uncracked section

- A level of surface corrosion was observed in all uncracked HPSFRCC specimens tested. Until 35 cycles, an increment in the area of the surface of samples with corrosion products deposited was observed. Then, the stabilization detected may be attributed to the reduction of the fibres to be corroded and the leaching of the corrosion products in the superficial layer of the specimen.

- Over cycles the superficial corrosion mechanism may be may be distinguished in three main phases: induction, acceleration and deceleration. Initially, the chloride ions ingress into the pores of a thin superficial layer leading to the onset of

corrosion. The acceleration of corrosion occurs due to an increment in chloride concentration close to the surface. Finally, the corrosion process reduces as the fibres in the surface layer are totally consumed.

- The flexural strength of the uncracked HPSFRCC specimens was not reduced even with the superficial corrosion observed. Such outcome reveals that the absence of cracks and the dense matrix avoid deeper corrosion and consequently reductions in the structural performance of fibres.

- The long-term chloride cycles revealed a level of damage on the surface aspect for uncracked HPSFRCC prisms whereas no significant effect of corrosion on the mechanical behaviour is noticed. Moreover, the mechanisms of surface corrosion limited to the fibres localized in a very thin very layer close to the surface can be easily explained by means of a conceptual model proposed.

Specific experimental programme pre-cracked section

- The crack width has a significant influence in the depth of ingress of chlorides in cracked HPSFRCC specimens. The concentration of chlorides is higher close to the crack mouth in the case of narrow cracks whereas for wider cracks the chlorides are distributed over the crack walls. From the results, the ingress of chlorides is limited for hairline crack (0.05 mm) and an expressive chloride penetration for specimens with wider crack widths is detected.

- The visual analysis of the cracked section revealed that the fibre content influences the level of corrosion of the fibres bridging the cracks. Higher fibre content limits the penetration of chlorides mainly due to the increment of the amount of corrosion products and the bigger quantity of fibres crossing the cracks.

- Lower level of damage due to corrosion is noticed in individual fibres in the case of high fibre content. Such outcome is expected since the great amount of iron to be corroded in the crack combined with the limited chloride ingress lead to reduced corrosion of each fibre.

- The microanalysis conducted suggests that the cross-sectional area of fibres is greatly reduced as a consequence of corrosion process. Additionally, the ITZ fibre-matrix is compromised with the increment of products of corrosion generated. A reduction and a complete loss of cross section of fibres is also observed over cycles.

- The results reveal that the structural behaviour of fibres bridging the cracks is affected by the corrosion process which is controlled by the main parameters studied: fibre content, crack width and number of chloride cycles.

- Specimens with smaller fibre content (90 kg/m^3) present reduced mechanical response whereas for the specimens with the highest fibre content (190 kg/m^3) the repercussion on the mechanical response has no significant influence. It may be attributed to the previously mentioned higher level of fibres degradation due to corrosion for samples with lower fibre content.

- In general, the crack width presents the major influence on the corrosion process and consequently on its effects on the structural performance if compared to the other variables studied: fibre content and number of cycles. This behaviour is specially observed for larger cracks due to the increased level of fibres corrosion over time. In the case of specimens with crack width of 0.05 mm, the lower level of corrosion may lead to increment or decrease on the residual behaviour depending on the variable considered.

Simplified model

- The curves of the depth of high and medium corrosion over cycles, considering the crack width and the fibre content may be a useful tool for the design of HPSFRCCs in ULS under chloride exposure. The values indicate that depth of severe damage due to corrosion which may be introduced in the structural design.

- An analytical formulation was proposed to estimate the reduction on the residual tensile strength due to corrosion. The simplified model proposed may be easily implemented in current design codes to account for the influence of the corrosion in the ULS.

- The parameter of corrosion damage (alpha value) obtained by means of the simplified model may provide an initial assessment of the reduction in the residual response in ULS considering the main variables studied: fibre content, crack width and number of chloride cycles.

- The alpha values reduce significantly as the crack width increases. This outcome suggests that the crack width control the corrosion process of fibres and consequently the reduction of the residual performance. Wider cracks lead to increased degradation and smaller alpha values.

9.3. FUTURE PERSPECTIVES

Despite the contributions reported in the previous section, further research on the topics covered in this doctoral thesis are required. For that reason, several suggestions for future research and experimental programmes are proposed below.

Preliminary experimental programme

- The study regarding the surface corrosion was focussed on the high carbon cold-drawn wire steel fibre distributed into the cementitious matrix. The analysis of the corrosion mechanisms of other types the steel fibres is needed.

- This study considered HPSFRCC specimens with three different fibre contents. In this regard, it might be interesting to analyse the effect of corrosion in mixes of high and ultra-high performance cementitious composites with higher steel fibre contents.

- Models to predict the formation surface corrosion taking account the main mechanisms involved in the corrosion process of HPSFRCC, the transport and the precipitation of corrosion products at the surface should be proposed.

Specific experimental programme pre-cracked section

- The study performed detected the significant influence of the crack width on the corrosion process of steel fibres in HPSFRCCs. Further research is required to investigate critical crack width to ensure the integrity of these structures under long-term severe chloride exposure.

- Regarding the long-term durability, research focussing on the influence of other parameters such as type of fibre, quality of cementitious matrix and different field exposure conditions should be conducted.

- The study concerning the effects of corrosion on the flexural response of HPSFRCC was limited in terms of dimensions of the prisms. Hence, bigger dimensions should be tested in order to investigate the influence of the dimension on the corrosion. Furthermore, numerical simulation to estimate the effects of corrosion in real scale HPSFRCC structures should be conducted.

Simplified model

- A numerical simulation to predict the ingress of chlorides and its effects on the depth and level of corrosion of HPSFRCC should be developed.

- The analytical model developed here is an initial estimation of the reduction on the residual response of HPSFRCC members at ULS. Further research should be conducted in order to propose models considering the structural design at serviceability limit state (SLS).

- The study proposed a model taking into account experimental data of accelerated chloride corrosion at laboratory conditions. Further refinement of the model correlating the accelerated exposure with field exposure data should be conducted.

- The effects of corrosion on the pull-out of individual fibres should be further studied both experimentally and numerically.

10. REFERENCES

Abbas, S. *Structural and durability performance of precast segmental tunnel linings*. Doctoral Thesis, University of Western Ontario, Ontario, 2014.

Abbas, S., Soliman, A.M. and Nehdi, M.L. Chloride ion penetration in reinforced concrete and steel fiber-reinforced concrete precast tunnel lining segments. *ACI Materials Journal*, 2014, vol.111, no. 6, p. 613-621.

AENOR. UNE-EN 1097-6:2001. Ensayos para determinar las propiedades mecánicas y físicas de los áridos. Parte 6: Determinación de la densidad de partículas y la absorción de agua. Asociación Española de Normalización y Certificación, Madrid, 2001.

AENOR. UNE-EN 12350-5:2009. Ensayos de hormigón fresco. Parte 5: Ensayo de la mesa de sacudidas. Asociación Española de Normalización y Certificación, Madrid, 2009.

AENOR. UNE-EN 196-1:2005. Métodos de ensayo de cementos. Parte 1: Determinación de resistencias mecánicas. Asociación Española de Normalización y Certificación, Madrid, 2005.

Aitcin, P.–C., Laplante, P. and Palme, Y.L. The use of fibre reinforced concrete for highway rehabilitation. *Report no. 231, Canada National Research Council, Industrial Materials Research Institute*, Boucherville, Quebec, 1985.

Alizade, E., Jandaghi Alaee, F. and Zabihi, S. Effects of steel fiber corrosion on mechanical properties of steel fiber reinforced concrete. *Asian Journal of Civil Engineering*, 2016, vol. 17, no. 2, p. 147-158.

Aljeboury, A. *Applicability of ultra-high performance fibre concrete in structures*. Master Thesis, Delft University of Technology, Delft, 2005.

Anandan, S., Manoharan, S.V. and Sengottian, T. Corrosion effects on the strength properties of steel fibre reinforced concrete containing slag and corrosion inhibitor. *International Journal of Corrosion*, 2014, vol. 2014, p. 1-7.

Andrade, C. Calculation of chloride diffusion coefficients in concrete from ionic migration measurements. *Cement and Concrete Research*, 1993, vol. 23, no. 3, p. 724-742.

Angst, U. *Chloride induced reinforcement corrosion in concrete: concept of critical chloride content – methods and mechanisms*. Doctoral Thesis, Norwegian University of Science and Technology, Trondheim, 2011.

Balouch, S.U., Forth, J.P. and Granju, J. –L. Surface corrosion of steel fibre reinforced concrete. *Cement and Concrete Research*, 2010, vol. 40, no. 3, p. 410-414.

Barros, J.A.O., Lourenço, L.A.P., Soltanzadeh, F. and Taheri, M. Steel fibre reinforced concrete for elements failing in bending and in shear. *European Journal of Environmental and Civil Engineering*, 2014, vol. 18, no. 1, p. 33-65.

Batson, G.B. Strength of steel fiber concrete in adverse environments, *Special Report M-218 Construction Engineering Research Laboratory*, Champaign, Illinois, US, June 1977.

Bentur, A. and Mindess, S. *Fibre reinforced cementitious composites*. 2nd Edition ed. Abingdon, UK: Taylor & Francis Group, 2007.

Bentur, A., Diamond, S. and Mindess, S. The microstructure of the steel fibre-cement interface. *Journal of Materials Science*, 1985, vol. 20, n. 10, p. 3610-3620.

Bentur, A., Wu, S.T., Banthia, N., Baggott, R., Hansen, W., Katz, A., Leung, C.K.Y., Li, V.C., Mobasher, B., Naaman, A.E., Robertson, R., Soroushian, P., Stang, H. and Taerwe, L.R. Fiber-matrix interfaces. *In 2º High performance Fiber Reinforced Cement composites* - RILEM, Ann Arbor, MI, June 11-14 1995, NaamanReinhardt Eds, p. 149-192.

Bernard, E.S. Durability of cracked fibre reinforced shotcrete, Shotcrete: More Engineering Developments, In Bernard. *Proceedings of the 2º International Conference on Engineering Developments in Shotcrete*, Cairns, Australia, October, Taylor and Francis Group, 2004.

Berrocal, C.G. *Corrosion of steel bars in fibre reinforced concrete: corrosion mechanisms and structural performance*. Doctoral Thesis, Chalmers University of Technology, Göteborg, 2017.

Berrocal, C.G., Löfgren, I, Lundgren, K. and Tang, L. Corrosion initiation in cracked fibre reinforced concrete: influence of crack width, fibre type and loading conditions. *Corrosion Science*, 2015, vol.98, p. 128-139.

Bertolini, L., Elsener, B., Pedeferri, P., Redaelli, E. and Polder, R. B. *Corrosion of steel in concrete: prevention, diagnosis, repair*. 2nd Edition ed. Weinheim: John Wiley & Sons, 2013.

Blagojević, A. *The influence of cracks on the durability and service life of reinforced concrete structures in relation to chloride-induced corrosion: a look from a different perspective.* Doctoral Thesis, Delft University of Technology, Delft, 2016.

Blanco, A. *Characterization and modelling of SFRC elements*. Doctoral Thesis, Universitat Politècnica de Catalunya, Barcelona, 2013.

Blokland, G.van. *Verbreding van viaducten in beton van reactief poeder*. Master Thesis, Delft University of Technology, Delft, 1997.

Blunt, J.D. *The effect of fiber reinforcement on the corrosion controlled degradation of reinforced concrete flexure elements*. Master Thesis, University of California, Berkeley, 2008.

Brandt, A.M. Fibre reinforced cement-based (FRC) composites after over 40 years of development in building and civil engineering. *Composite Structures*, 2008, vol. 86, n. 1-3, p. 3-9.

Brommfield, J.P. *Corrosion of steel in concrete – understanding, investigation and repair*. 2nd Edition ed. London and New York: Taylor & Francis Group, 2007.

Carrillo, J., Cárdenas Pulido, J. and Aperador, W. Flexural mechanical properties of steel fiber reinforced concrete under corrosive environments. *Revista Ingeniería de Construcción*, 2017, vol.32, no. 2, p. 59-72.

Cavalaro, S.H.P. and Aguado, A. Intrinsic scatter of FRC: an alternative philosophy to estimate characteristic values. *Materials and Structures*, 2015, vol. 48, n. 11, p. 3537-3555.

Cavalaro, S.H.P., López, R., Torrents, J.M. and Aguado, A. Improved assessment of fibre content and orientation with inductive method in SFRC. *Materials and Structures*, 2015, vol.48, no. 6, p. 1859-1873.

Cavalaro, S.H.P., López-Carreño, R., Torrents, J.M., Aguado, A. and Juan-García, P. Assessment of fibre content and 3D profile in cylindrical SFRC specimens. *Materials and Structures*, 2016, vol.49, no. 6, p. 577-595.

Chen, D. and Mahadevan, S. Chloride-induced reinforcement corrosion and concrete cracking simulation. *Cement & Concrete Composites*, 2008, vol. 30, p. 227-238.

Corinaldesi, V. and Moriconi, G. Durable fiber reinforced self-compacting concrete. C*ement and Concrete Research*, 2004, vol. 34, n. 2, p. 249-254.

CPH. Instrucción del Hormigón Estructural EHE-08, Ministerio de fomento, Madrid, 2008.

Dauberschmidt, C. *Untersuchungen zu den korrosionsmechanismen von stahlfasern in chloridhaltigem beton*. Doctoral Thesis, Munich University, Munich, 2006.

Davenport, A.J., Oblonsky, L.J., Ryan, M.P. and Toney, M.F. The structure of the passive film that forms on iron in aqueous environments. *Journal of The Electrochemical Society*, 2000, vol. 147, no. 6, 2162-2173.

de la Fuente, D., Díaz, I., Alcántara, j., Chico, B., Simancas, J., Llorente, I., García-Delgado, A., Jiménez, J.A., Adeva, P. and Morcillo, M. Corrosion mechanisms of mild steel in chloride-rich atmospheres. *Materials and Corrosion*, 2016, vol. 67, no. 3, p. 227-238.

di Prisco, M., Plizzari, G. and Vandewalle L. Fibre reinforced concrete: new design perspectives. *Materials and Structures*, 2009, vol.42, n. 9, p. 1261-1281.

Djerbi, A., Bonnet, S., Khelidj, A. and Baroghel-bouny, V. Influence of traversing crack on chloride diffusion into concrete. *Cement and Concrete Research*, 2008, vol. 38, p. 877-883.

Dogan, E. and Krstulovic-Opara, N. Seismic retrofit with continuous slurry-infiltrated mat concrete jackets, *ACI Structural Journal*, vol. 100, no. 6, p. 713-722.

Dousti, A., Shekarchi, M., Alizadeh, R. and Taheri-Motlagh, A. Binding of externally supplied chlorides in micro silica concrete under field exposure conditions. *Cement and Concrete Composites*, 2011, vol. 33, no. 10, p. 1071-1079.

Ferrara, L., Fratesi, R., Signorini, S. and Sonzogni, F. Durability of steel fibre-reinforced concrete precast elements: experiments and proposal of design recommendations. *In Proceedings of the 6º International RILEM Symposium on Fibre-Reinforced Concrete. (BEFIF 2004)*, Varenna, Italy, September 20-22 2004, di PriscoFelicettiPlizzari Eds.

fib. Model Code 2010, International Federation for structural Concrete, Laussane, 2010.

Figueiredo, A.D. *Concreto com fibras de aço*. Boletim Técnico da Escola Politécnica da Universidade de São Paulo, ISSN 0103-9830, BT/PCC/260, São Paulo, 2000.

Figueiredo, E.P. and Meira, G. *Corrosión de armadura das estructuras de hormigón*. Boletín Técnico da Asociación Latinoamericana de Control de Calidad, Patología y Recuperación de la Construcción - ALCONPAT, Mérida, México, 2013.

Frazão, C., Camões, A., Barros, J. and Gonçalves, D. Durability of steel fiber reinforced self-compacting concrete. *Construction and Building Materials*, 2015, vol. 80, p. 155-166.

Ghods, P. *Multi-scale investigation of the formation and breakdown of passive films on carbon steel rebar in concrete*. Doctoral Thesis, Carleton University, Ottawa, 2010.

Graeff, A.G., Pilakoutas, K., Lynsdale, C. and Neocleous, K. Corrosion durability of recycled steel fibre reinforced concrete. *Intersections/Intersectii*, 2009, vol.6, no. 7, p. 77-89.

Granju, J.–L. and Balouch, S. U. Corrosion of steel fibre reinforced concrete from the cracks. *Cement and Concrete Research*, 2005, vol. 35, no. 3, p. 572-577.

Gu, C-p., Ye, G. and Sun, W. A review of the chloride transport properties of cracked concrete: experiments and simulations. *Journal of Zhejiang University-SCIENCE A*, 2015, vol.16, no. 2, p.81-92.

Guerrini, G.L. Applications of high-performance-fiber-reinforced cement-based composites. *Composite Materials*, 2000, vol. 7, n. 2-3, p. 195-207.

Habel, K., Viviani, M., Denarié E. and Brühwiler, E. Development of the mechanical properties of an ultra-high performance fiber reinforced concrete (UHPFRC). *Cement and Concrete Research*, 2006, vol. 36, n.7, 1362-1370.

Hannant, D.J. Additional data on fibre corrosion in cracked beams and theoretical treatment of the effect of fibre corrosion on beam load capacity. *In Proceedings of the International RILEM Symposium on Fibre-Reinforced Cement and Concrete*, London, England, September 1975.

Hansen, E.J.deP., Ekman, T. and Hansen, K.K. Durability of cracked fibre reinforced concrete structures exposed to chlorides, *In 8º International Conference on Durability of Building Materials and Components (8DBCM)*, NRC Research Press, Vancouver, Canada, May 30 June 3 1999, LacasseVanier Eds., p. 280-289.

Heusler, K.E. and Fischer, L. Kinetics of pit initiation at passive iron. *Materials and Corrosion*, 1976, vol. 27, n. 8, p. 551.

Hobbs, D.W. Concrete deterioration: causes, diagnosis, and minimising risk. *International Materials Reviews*, 2001, vol. 46, n. 3, p. 117-144.

Hoff, G.C. Durability of fiber reinforced concrete in a severe marine environment. Concrete Durability. *In Proceedings of Katharine and Bryant Mather International Symposium, ACI Special Publication*, 100-55, 1987, p. 997-1042.

Holschemacher, K., Mueller, T. and Ribakov, Y. Effect of steel fibres on mechanical properties of high-strength concrete. *Materials and Design*, 2010, vol. 31, p. 2604-2615.

Homma, D., Mihashi, H. and Nishiwaki, T. Self-healing capability of fibre reinforced cementitious composites. *Journal of Advanced Concrete Technology*, 2009, vol. 7, no. 2, p. 217-228.

Hong, K. *Cyclic wetting and drying and its effects on chloride ingress in concrete*. Master Thesis, University of Toronto, Toronto, 1998.

Hooton, R.D. and McGrath P.F. Issues related to recent developments in service life specifications for concrete structures. *In Proceedings of the International RILEM Workshop: Chloride Penetration into Concrete*, Paris, 1995, p. 388-397.

http://www.marketresearchstore.com. Concrete fiber market (synthetic fiber, glass fiber, steel fiber, basalt fiber and others) market for construction, road industry, Industrial, Mining and other applications: global industry perspective, comprehensive analysis and forecast, 2014-2020. http://www.marketresearchstore.com (accessed July 5, 2018).

Jaffer, S.J. and Hansson, C.M. The influence of cracks on chloride-induced corrosion of steel in ordinary Portland cement and high performance concretes subjected to different loading conditions. *Corrosion Science,* 2008, vol. 50, no. 12, p. 3343-3355.

Jayalakshmi, M. and Muralidharan, V.S. Empirical and deterministic models of pitting corrosion – an overview. *Corrosion Reviews*, 1996, vol. 14, n.3-4, p. 375-402.

Kesner, K.E. and Billington, S.L. Tension, compression and cyclic testing of engineered cementitious composite materials. *Technical Report, MCEER-04-0002*, Cornell University, New York, 2004.

Kim, B., Boyd., A.J. and Lee, J.-Y. Durability performance of fiber-reinforced concrete in severe environments. *Journal of Composite Materials*, 2011, vol. 45, no. 23, p.2379-2389.

Kim, K. and Parra-Montesinos, G. Behavior of HPFRCC low-rise walls subjected to displacement reversals. *In Proceedings of the 4º International RILEM Workshop on High Performance Fiber Reinforced Cement Composites (HPFRCC 4)*, Ann Arbor, Michigan, June 15-18 2003, NaamanReinhardt Eds.

King, M.R. and Adler, A.J. The practical specification of steel fibre reinforced concrete (SFRC) for tunnel linings, *In Proceedings of the Underground Construction Conference*, London, England, 2001.

Kitowski, C.J. and Wheat, H. G. Effects of chlorides on reinforcing steel exposed to simulated concrete solutions. *Materials Science & Engineering Database*, 1997, vol. 53, no. 3, p. 216.225.

Klein, N.S. and Aguado, A. Concreto de ultra-alta desempenho com fibras para produção de painéis pré-fabricados. *In Proceedings of the 52º Congresso Brasileiro do Concreto: Novas Tecnologias do Concreto para o Desenvolvimento Sustentável*, Fortaleza, Brazil, October 2010, p.1-13.

Kosa, K. and Naaman, A.E. Corrosion of steel fiber reinforced concrete, *ACI Materials Journal*, 1990, vol. 87, no. 1, p. 27-37.

Lambrechts, A., Nemegeer, D. Vanbrabant, J and Stang, H. Durability of steel fibre reinforced concrete, *In Proceedings of the 6º CANMET/ACI Durability of concrete Conference SP212*, Michigan, USA, 2003.

Lankard, D.R. and Walker, A.J. Status report on laboratory and field investigations of the durability of WIRAND concrete exposed to various service environments. *Battelle Development Corporation, Columbus Laboratory*, Columbus, Ohio, June 28 1978.

Lee, H., Cody, R.D., Cody, A.M. and Spry, P.G. Effects of various deicing chemicals on pavement concrete deterioration. *In Mid-Continent Transportation Symposium*, Iowa State University, Ames, IA, 2000.

Levi, S.M. and Helene, P. Durability of recycled aggregates concrete: a safe way to sustainable development. *Cement and Concrete Research*, 2004, vol. 34, no. 11, p. 1975-1980.

Löfgren, I. *Fibre-reinforced concrete for industrial construction – a fracture mechanics approach to material testing and structural analysis*. Doctoral Thesis, Chalmers University of Technology, Göteborg, 2005.

Macdonald, D.D. Passivity – the key to our metals-based civilization. *Pure and Applied Chemistry*, 1999, vol. 71, no. 6, p. 951-978.

Macdonald, D.D. The point defect model for the passive state. *Journal of The Electrochemical Society*, 1992, vol. 139, no. 12, p. 3434-3449.

Mangat, P. S. and Gurusamy, K. Permissible crack widths in steel fibre reinforced marine concrete. *Materials and Structures*, 1987d, vol. 20, p. 338-347.

Mangat, P.S. and Gurusamy, K. Chloride diffusion in steel fibre reinforced marine concrete. *Cement and Concrete Research*, 1987c, vol. 17, p. 385-396.

Mangat, P.S. and Gurusamy, K. Corrosion resistance of steel fibres in concrete under marine exposure. *Cement and Concrete Research*, 1988, vol. 18, p. 44-54.

Mangat, P.S. and Gurusamy, K. Long-term properties of steel fibre reinforced marine concrete. *Materials and Structures*, 1987b, vol. 20, p. 273-282.

Mangat, P.S. and Gurusamy, K. Pore fluid composition under marine exposure of steel fibre reinforced concrete. *Cement and Concrete Research*, 1987a, vol. 17, p. 734-742.

Mangat, P.S. and Molloy, B. T. Size effect of reinforcement on corrosion initiation. *In Proceedings of the 5º International RILEM Symposium on Fibre-Reinforced Cement Composites (BEFIF 5)*, France, September 13-15 2000, RossiChanvillard Eds.

Mansfeld, F. Recording and analysis of AC impedance data for corrosion studies: background and methods of analysis, *Corrosion*, 1981, vol. 37, p. 301-307.

Mantegazza, G. and Gatti, A. Aspects of durability of fiber reinforced concrete: workability and stress-corrosion. *In Proceedings of the 6º International RILEM Symposium on Fibre-Reinforced Concrete. (BEFIF 2004)*, Varenna, Italy, September 20-22 2004, di PriscoFelicettiPlizzari Eds.

Marcos-Meson, V., Michel, A., Solgaard, A., Fischer, G., Edvardsen, C. and Skovhus, T. L. Corrosion resistance of steel fibre reinforced concrete – a literature review. *Cement and Concrete Research*, 2018, vol. 103, p.1-20.

Marković, I. *High-performance hybrid-fibre concrete – development and utilisation*. Doctoral Thesis, Delft University of Technology, Delft, 2006.

Morse, D.C. and Williamson, G.R. Corrosion behaviour of steel fibrous concrete, Technical *Report M-217 Construction Engineering Research Laboratory*, Champaign, Illinois, US, May 1977.

Murphy, O.J. Spectroscopic characterization of the passive film on iron before and after exposure to chloride ion. *Electrochemistry in Transition*, Edition ed. New York: Plenum Press, 1992, p. 521-545.

Naaman, A.E. and Reinhardt, H. W. Characterization of high performance fiber reinforced cement composites – HPFRCC. *In Proceedings of the 2º International RILEM Workshop on High Performance Fiber Reinforced Cement Composites (HPFRCC 2)*, Ann Arbor, Michigan, June 11-14 1995, NaamanReinhardt Eds.

Naaman, A.E. High performance fiber reinforced cement composites: classification and applications. *In CBM-CI International Workshop, Karashi, Pakistan*, 2007.

Nagayama, M. and Cohen, M. The anodic oxidation of iron in a neutral solution. *Journal of The Electrochemical Society*, 1962, vol. 109, no. 9, p. 781-790.

Nemegeer, D. Vanbrabant, J and Stang, H. Brite Euram program on steel fibre concrete. Subtask: Durability of steel fibre reinforced concrete, *In International RILEM Workshop Test Methods Steelfibre Reinforced Concrete, RILEM Publications SARL, Bochum, Germany, 2003, p. 47-66.*

Nemegeer, D. Vanbrabant, J and Stang, H. Brite Euram Project BRPR-CT98-0813. Final report on durability of steel fibre reinforced concrete, *In Subtask 5.1 Durability of SFRC,* Copenhagen, Denmark, 2000.

Neville, A. Chloride attack of reinforced concrete: an overview. *Materials and Structures*, 1995, vol. 28, no. 176, p.63-70.

Nishimura, R. and Sato, N. Potential-pH diagram of composition/structure of passive films on iron. *Journal of the Japan Institute of Metals*. 1983, vol.47, p. 1086-1093.

Nordström, E. *Durability of sprayed concrete: steel fibre corrosion in cracks*. Doctoral Thesis, Luleå University of Technology, Luleå, 2005.

Nordström, E. *Steel fibre corrosion in cracks: durability of sprayed concrete*. Licentiate Thesis, Luleå University of Technology, Luleå, 2000.

NT BUILD 492:1999. Chloride migration coefficient from non-steady-state migration experiments, Nordtest, Espoo, Finland, 1999.

Odriozola, M.A.B. and Gutiérrez, P.A. Comparative study of different test methods for reinforced concrete durability assessment in marine environment. *Materials and Structures*, 2008, vol. 41, p. 527-541.

Ohtsuka, T. Passive oxide films on iron by in-situ detection of optical techniques. *In Progress in Corrosion Science and Engineering II*, Springer, USA, 2012, PyunLee Eds, p. 183-241.

Otieno, M. *Corrosion propagation in cracked and uncracked concrete*. Master Thesis, University of Cape Town, Cape Town, 2008.

Page, C.L. Microstructural features of interfaces in fibre cement composites. *Composites*, 1982, vol. 13, no.2, p. 140-144.

Parra-Montesinos, G.J. High-performance fiber-reinforced cement composites: an alternative for seismic design of structures, *ACI Structural Journal*, 2005, vol. 102, no. 5, p. 668-675.

Paul, S.C. *The role of cracks and chlorides in corrosion of reinforced strain hardening cement-based composite (R/SHCC)*. Doctoral Thesis, Stellenbosch University, Stellenbosch, 2015.

Plusquellec, G., Geiker, M. R., Lindgård, J., Duchesne, J., Fournier, B. and De Weerdt, K. Determination of the pH and the free alkali metal content in the pore solution of concrete: review and experimental comparison. *Cement and Concrete Research*, 2017, vol. 96, p. 13-26.

Poulsen, E. and Mejlbro, L. *Diffusion of chloride in concrete: theory and application*. Edition ed. London and New York: Taylor & Francis Group, 2005.

Pruckner, F. *Corrosion and protection of reinforcement in concrete measurements and interpretation*. Doctoral Thesis, University of Vienna, Vienna, 2001.

Rafiee, A. Computer modelling and investigation on the steel corrosion in cracked ultra high performance concrete. *Structural Materials and Engineering Series*. Edition ed. Kassel; Kassel University Press, 2012.

Ramachandran, V.S. Possible states of chloride in the hydration of tricalcium silicate in the presence of calcium chloride. *Matériaux et Construction*, 1971, vol. 4, no. 1, p. 3-12.

Reineck, K-H. HPC hot-water tanks for the seasonal storage of solar heat. *In Proceedings of the 6º International Symposium on the Utilization of High Strength/ High Performance Concrete*, Leipzig, Germany, June 16-20 2002.

Richardson, M. G. *Fundamentals of durable reinforced concrete*. Edition ed. London and New York: Taylor & Francis Group, 2003.

Rider, R.G. and Heidersbach, R.H. The effects of sea water on the structural properties of metal-fiber reinforced concrete. *In Proceedings of the Offshore Technology Conference*, Houston, Texas, May 8-11 1978.

Rodriguez, O.G. *Influence of cracks on chloride ingress into concrete*. Doctoral Thesis, University of Toronto, Toronto, 2001.

Roque, R.P.E., Kim, N., Kim, B. and Loop, G. *Durability of fiber-reinforced concrete in Florida environments*. UF Project No. 00050493, Florida, USA, July 2009.

Sadeghy-Pouya, H., Ganjian, E. Claisse, P. and Muthuramalingam, K. Corrosion durability of high performance steel fibre reinforced concrete. *In Proceedings of the 3º International Conference on Sustainable Construction Materials and Technology*, Kyoto, Japan, August 18-21 2013.

Sato, N.A Theory for breakdown of anodic oxide films on metals. *Electrochimica Acta*, 1971, vol.16, p. 1683-1692.

Šavija, B. *Experimental and numerical investigation of chloride ingress in cracked concrete*. Doctoral Thesis, Delft University of Technology, Delft, 2014.

Schiessl, P. and Raupach, M. Laboratory studies and calculations on the influence of crack width on chloride-induced corrosion of steel in concrete. *ACI Materials Journal*, 1997, vol. 94, no. 1, p. 56-61.

Schiessl, P. and Weydert, R. Korrosion von stahlfasern in gerissenem und ungerissenem stahlfaserbeton. *Kurzberichte Aus Der Bauforsch*, 1998, vol. 39, p. 331-336.

Schnütgen, B. Design of precast steel fibre reinforced garages. *In Proceedings of the International RILEM workshop on Test and Design Methods for Steelfibre Reinforced Concrete*, 2003, Bochum, Germany, SchnütgenVandewalle Eds., 153-159.

Schroeder, V. and Devine, T.M. Surface enhanced raman spectroscopy study of the galvanostatic reduction of the passive film on iron. *Journal of The Electrochemical Society*, 1999, vol. 146, no. 11, 4061-4070.

Schupack, M. Durability of SFRC exposed to severe environments. *In Proceedings of the Steel Fiber Concrete*, US-Sweden Joint Seminar (NSF-STU), Stockolm, June 3-5 1985.

Serna, P. and Arango, S.E. Evolution of the flexural behaviour of precracked SFRC in marine environment. *In Proceedings of the 7º International RILEM Symposium on Fibre-Reinforced Concrete: Design and Applications (BEFIF 2008)*, RILEM Publications SARL, Chennai, India, September 2008.

Solgaard, A.O.S. *Corrosion of reinforcement bars in steel fibre reinforced concrete structures*. Doctoral Thesis, Technical University of Denmark, Denmark, 2013.

Strehblow, H.–H. Breakdown of passivity and localized corrosion: Theoretical concepts and fundamental experimental results. *Werkstoffe und Korrosion*, 1984, vol.35, p. 437-448.

Swartzlow, R.J. *Missouri Historical Review*, Columbia, Mo. 1, 1934.

Szklarska-Smialowska, Z. Pitting corrosion of metals. *In NACE*, Houston, Texas, 1986, p. 347.

Thoft-Christensen, P. Corrosion crack based assessment of the life-cycle reliability of concrete structures. *In Proceedings of ICOSSAR 01*, California, USA, June 2001.

Toutanji, H.A. Properties of polypropylene fiber reinforced silica fume expansive-cement concrete. *Construction and Building Materials*, 1999, vol. 13, no. 171-177.

Trüb, M. *Numerical Modeling of high performance fiber reinforced cementitious composites*. Doctoral Thesis, Swiss Federal Institute of Technology, Zürich, 2011.

Van den Hurk, M. *Slender box girders and/or less stirrups by applying HSC or HSFRC*. Master Thesis, Delft University of Technology, Delft, 2014.

Walter, R., Stang, H., Gimsing, N.J. and Olesen, J.F. High performance composite bridge decks using SC FRC, *In Proceedings of the 4º International RILEM Workshop on High Performance Fiber Reinforced Cement Composites (HPFRCC 4)*, Ann Arbor, Michigan, June 15-18 2003, NaamanReinhardt Eds.

Weydert, R. and Schiessl, P. Corrosion of steel fibres in cracked and uncracked steel fibre reinforced concrete, *In IBAC 61*, 1996, p. 1310-1315.

Weydert, R. and Schiessl, P. Korrosion von stahlfasern in gerissenem und ungerissenem stahlfaserbeton. *Abschlussbericht*, Edition ed. Bergisch Gladbach, Germany: Technische Hochscule Aachen, 1998.

Win, P.P., Watanabe, M. and Machida, A. Penetration profile of chloride ion in cracked reinforced concrete. *Cement and Concrete Research*, 2004, vol. 34, no. p. 1073-1079.

Xia, Z. and Naaman, A.E. Behavior and modelling of infill fiber-reinforced concrete damper element for steel-concrete shear wall. *ACI Structural Journal*, 2002, vol. 99, no. 6, p. 727-739.

Yoon, J.K. and Billington, S. L. Experimental and numerical studies of precast unbonded post-tensioned bridge columns with engineered cementitious composites. *Research Report 02-03*, 2002, Cornell University, Ithaca, N. Y.

APPENDIX A. SUPLEMENTARY EXPERIMENTAL DATA

This appendix includes the data corresponding to the 3-point bending tests performed on the pre-cracked specimens of the specific experimental programme.

Figure A. 1, Figure A. 2 and Figure A. 3 present the average Load-CMOD curves obtained for fibre content of 90, 140 and 190 kg/m^3, respectively. The curves correspond to pre-crack widths of 0.05, 0.20, 0.35 and 0.50 mm, w/c of 0.23, at 0, 5, 35, 65, 95 and 125 cycles.

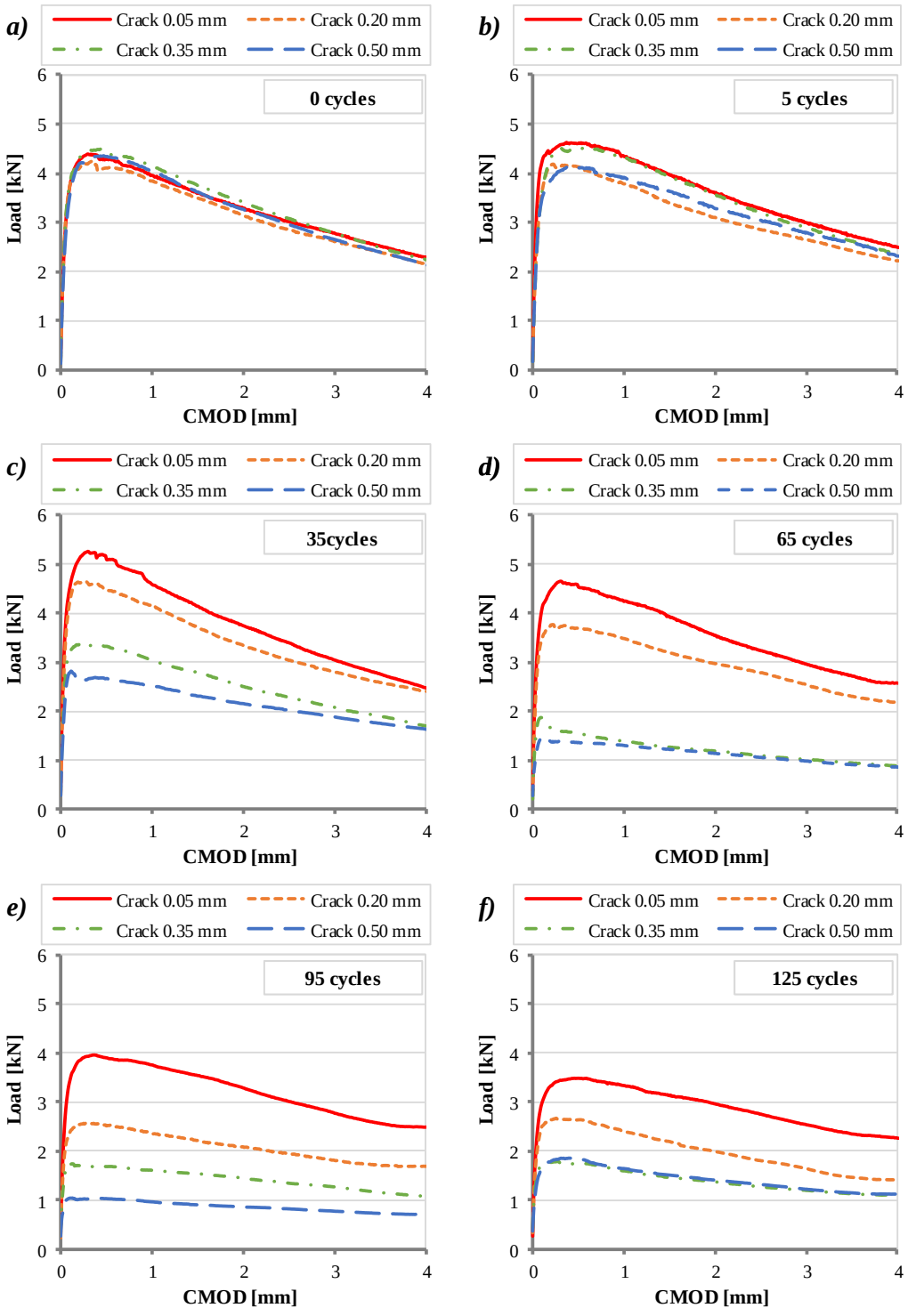

Figure A. 1 – Load-CMOD curves for specimens with 90kg/m^3 of fibre, w/c of 0.23, pre-crack widths of 0.05, 0.20, 0.35 and 0.50 mm at cycles: a) 0, b) 5, c) 35, d) 65, e) 95 and f) 125.

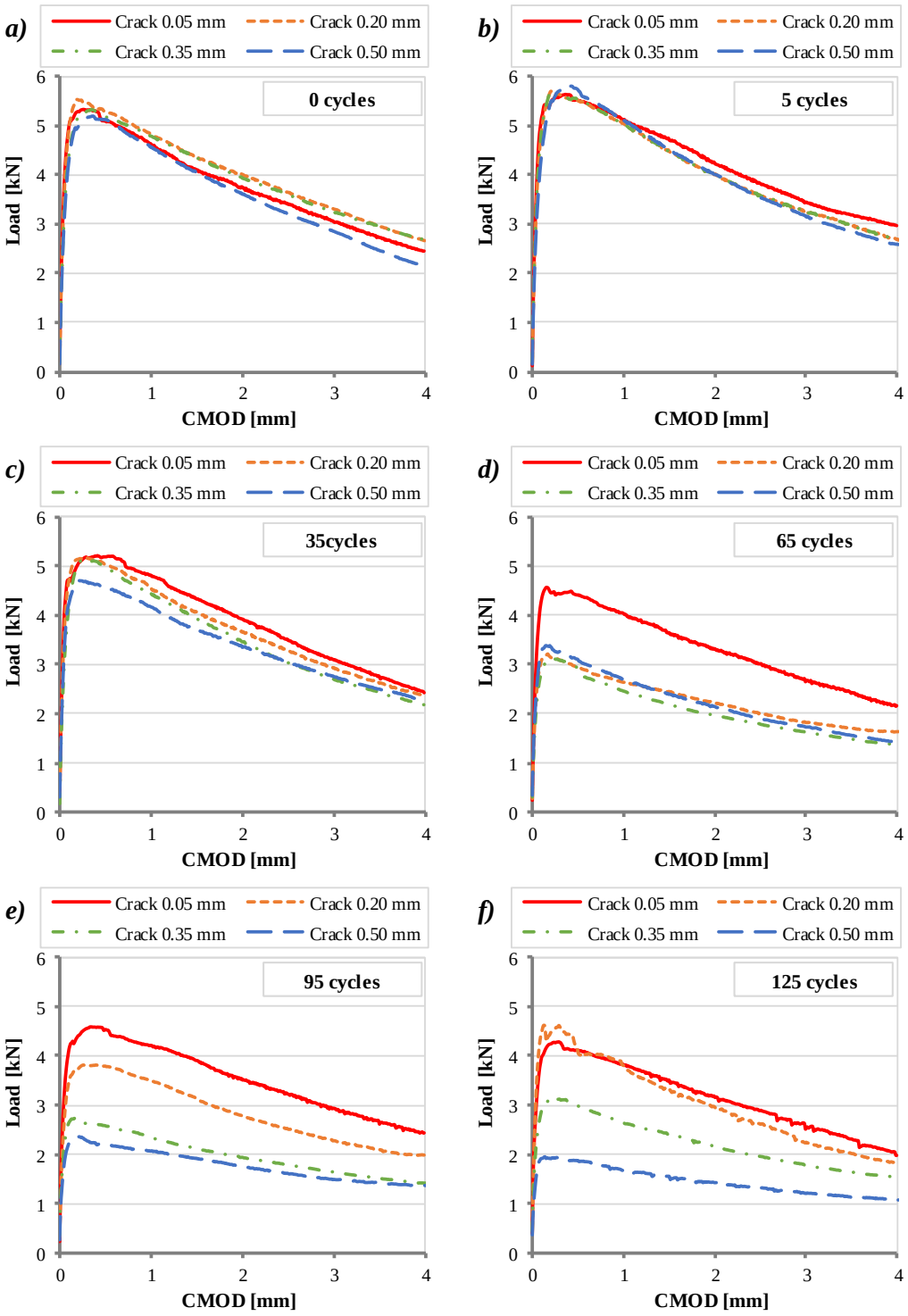

Figure A. 2 – Load-CMOD curves for specimens with 140kg/m^3 of fibre, w/c of 0.23, pre-crack widths of 0.05, 0.20, 0.35 and 0.50 mm at cycles: a) 0, b) 5, c) 35, d) 65, e) 95 and f) 125.

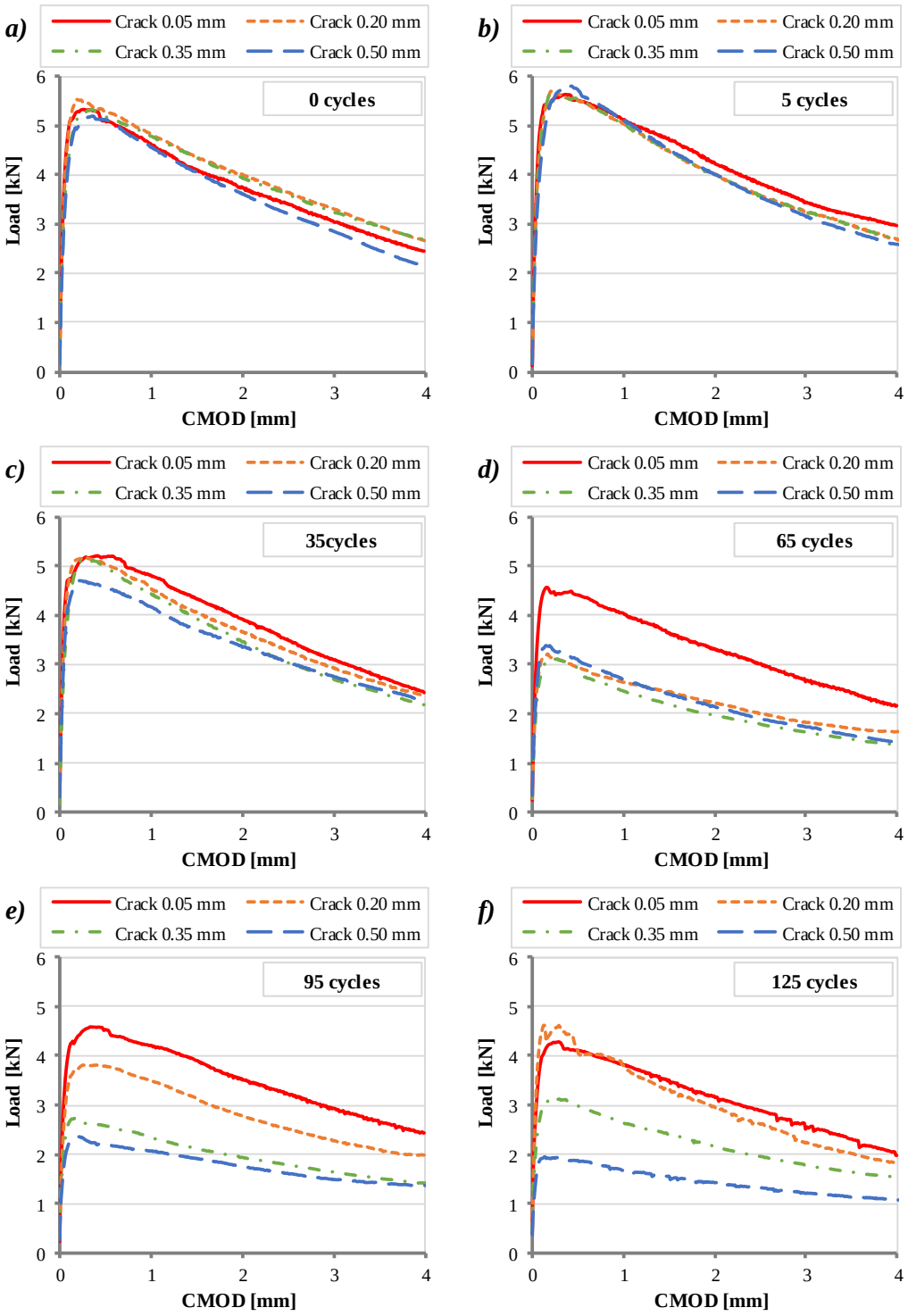

Figure A. 3 – Load-CMOD curves for specimens with 190kg/m^3 of fibre, w/c of 0.23, pre-crack widths of 0.05, 0.20, 0.35 and 0.50 mm at cycles: a) 0, b) 5, c) 35, d) 65, e) 95 and f) 125.

Figure A. 4 shows the average Load-CMOD curves obtained for 90 kg/m^3. The curves correspond to pre-crack widths of 0.05, 0.20, 0.35 and 0.50 mm, w/c of 0.28, at 0, 5, 35, 65, 95 and 125 cycles.

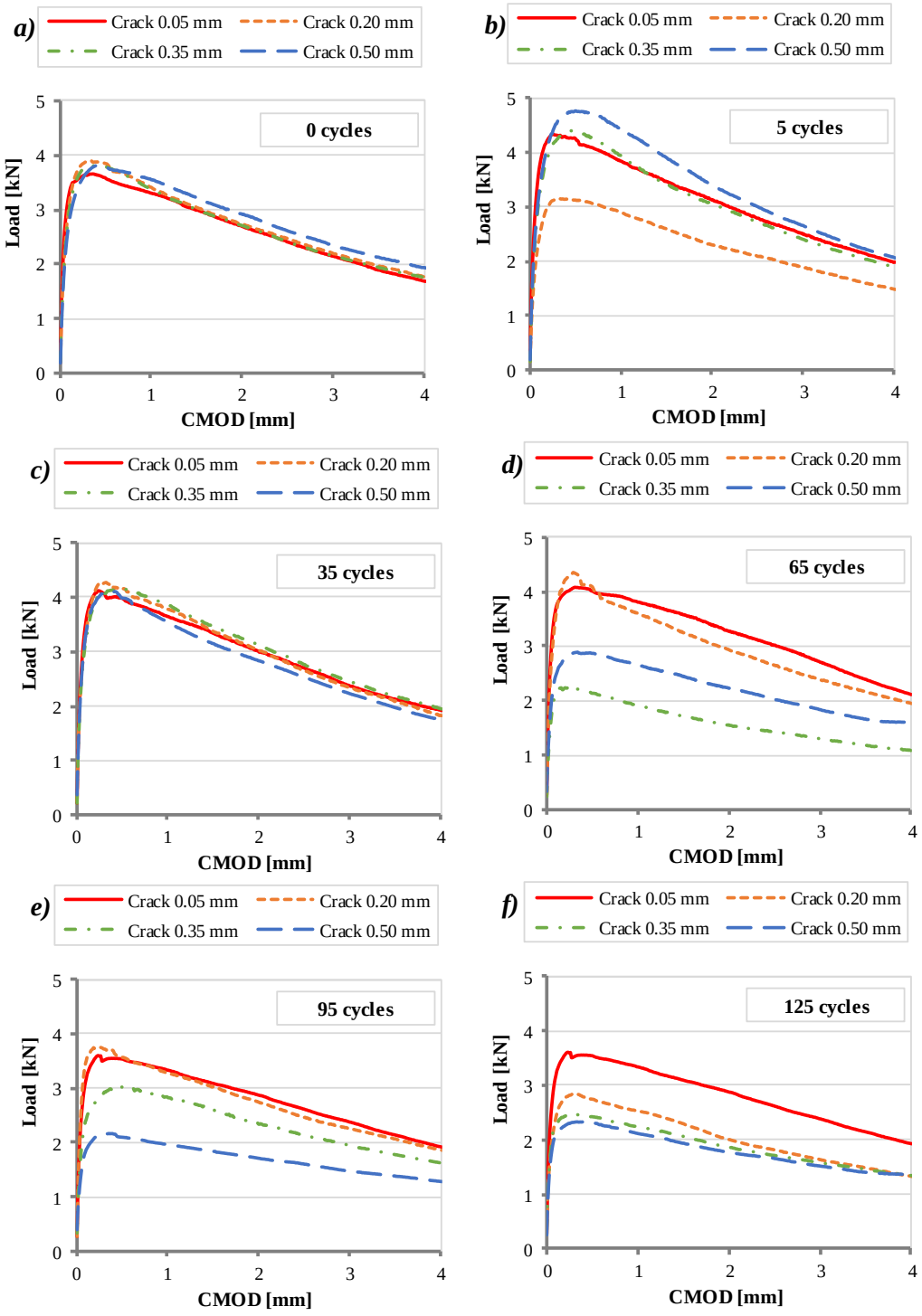

Figure A. 4 – Load-CMOD curves for specimens with 90 kg/m^3 of fibre, w/c of 0.28, pre-crack widths of 0.05, 0.20, 0.35 and 0.50 mm at cycles: a) 0, b) 5, c) 35, d) 65, e) 95 and f) 125.

In Figure A. 5, the average Load-CMOD curves obtained for 190 kg/m^3 are presented. The curves correspond to pre-crack widths of 0.05, 0.20, 0.35 and 0.50 mm, w/c of 0.28, at 65 and 95 cycles.

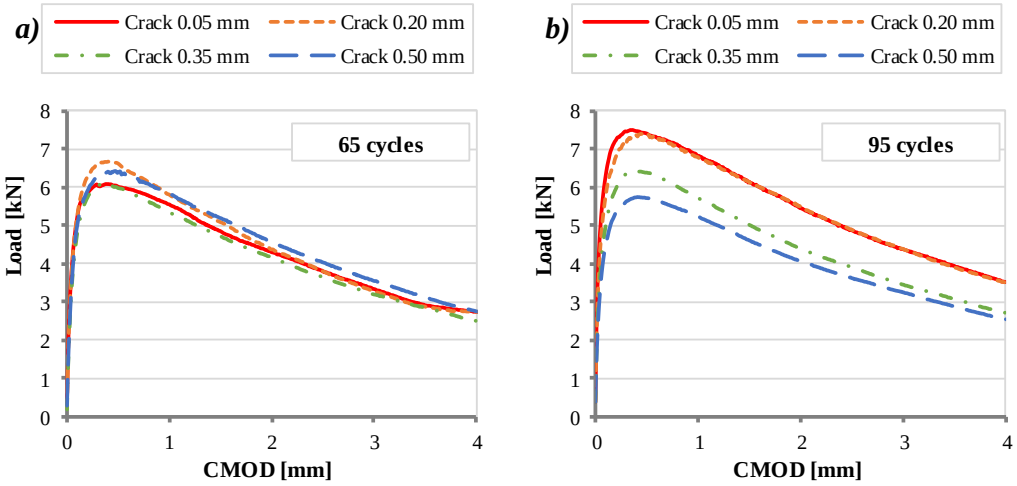

Figure A. 5 – Load-CMOD curves for specimens with 190kg/m^3 of fibre, w/c of 0.28, pre-crack widths of 0.05, 0.20, 0.35 and 0.50 mm at cycles : a) 65 and b) 95.

PUBLICATION

The publication developed during the PhD research period is presented subsequently:

Vieira, M.M., Cavalaro, P.H.P. and Aguado, A. Influence of chloride corrosion on the surface aspect of steel fibre reinforced cementitious composites. *In Proceedings of the 3º International Workshop ACI-fib-RILEM on Fibre Reinforced Concrete: from Design to Structural Applications,* Desenzano, Italia, June 27-30 2018, PlizzariMinelli Eds.